Optical sensory and motor mapping of mouse dorsal cortex

THÈSE N^O 9012 (2018)

PAR

Matthieu Pierre AUFFRET

EPFL

ÉCOLE POLYTECHNIQUE
FÉDÉRALE DE LAUSANNE

Suisse
2018

Acknowledgements

The completion of this work would not have been possible without the support of all these persons.

First, I would like to thank my PhD supervisor, Prof. Carl Petersen, for all his support in my research every day, his guidelines and his feedbacks. I was really happy to share these five years with him for all the nice scientific discussions and for all the trust he has placed in me.

I would also like to thank all the members of my jury for accepting to review my work. Starting by my co-supervisor Prof. Rolf Gruetter, who advised me a lot during the first year of my PhD. I also would like to thank the president of my jury, Prof. Carmen Sandi, the external experts Prof. Alan Carleton and Prof. Bruno Weber and the internal expert Prof. Brian McCabe.

I would like to thank all the members of the lab for the nice scientific discussions, the teaching of the techniques and the great time we had all together: Alexandros Kyriakatos, Sami El-Boustani, Johannes Mayrhofer, Semihcan Sermet, Célia Gasselin, Vahid Esmaeili, Angeliki Vavladeli, Pierre Le Merre, Xander Houbaert, Georgios Foustoukos, Varun Sreenivasan, Sylvain Crochet, Tanya Sippy, Eloise Charrière, Anastasiia Oryshchuk and Nathalie Just. I would like to thank the students that helped me during my projects up to the publication Nicolas Hankov, Veronica Ravano and Giulia Rossi. It was a great pleasure to work with you.

I would like to thank my parents, Annie and Alain, without which all this would not have been possible, for their support at all times and for always believing in me. I would like to thank my dad to have made me discover the EPFL. I would like to thank my mom for all the logistic support. I would like to thank also my sister Claire for her kind presence, even from far away, you are always very very close.

I would like to thank all my friends around the world. I would address a special thank to Idrees and Emilien for all the amazing discussions and projects that we had and we will have. I would like to thank all the family of the brotherhood la Bout de Boisière. I would like to thank my friends from the Hammers and Rod of the Colère du Panda for the amazing moments playing music, laughing and travelling around the world. I would like to thank my skiing buddys Robin Brad Pittet and le Gros Benji. I would like to thank Phiphi, Juju and Maxou for all the journey that has been made since our first experiments in high school… I would like to thank l'équipe des 3 Petits Chats. I would like to thank my bushcraft friend, who was the first guy I met in EPFL, Gaspard.

Finally, I would like to thank Sylwia for sharing my joys and frustrations during this journey.

Lausanne, le 7 Septembre 2018

Abstract

Throughout species, including mice and humans, we all have to make decisions to fulfill our fundamentals needs: eat, drink, explore, communicate, reproduce... To make those decisions, we have to collect informations from the surrounding world and to process them with our nervous system. The neocortex is the most distinctive feature of the brain as it is the substrate of high cognitive functions. One commonly used model to study the brain is the mouse. Mice can be genetically modified to express fluorescent reporters, or optogenetic actuators in their neurons. The questions I ask in this thesis are where and when specific sensory information is processed in the mouse cortex, and where and when these signals are integrated to generate to a motor command.

First, I developed a protocol to get reliable sensory maps from wide-field optical intrinsic signal imaging. Mice undergo a surgical procedure to get a relatively transparent view of the left dorsal cortex. Then I sequentially repetitively stimulated different parts of the body of anesthetized mice to map the cortical sensory representation of each stimulated organ. I also successfully imaged optogenetically evoked responses by combining optogenetic experiment with wide-field optical intrinsic signal imaging.

Second, I found the coordinates of the tongue/jaw primary sensory cortex tjS1 and of the tongue/jaw primary motor cortex tjM1. While I was mechanically stimulating tongue and jaw in anesthetized Thy1-GCaMP6f mice, I imaged the calcium signals evoked in the left cortical hemisphere with a wide-field fluorescence macroscope.

Third, I recorded cortical activity of behaving mice performing a 2-whisker discrimination task with the wide-field calcium imaging technique. There was a large difference between hit and miss trials. The amplitude of the responses in S1, S2, M1 and M2 were decreasing over the days of training. The earliest difference between hit and miss response occurred in S1 and S2 after 100 ms. Then the signals converged toward M2 where the amplitude of the response was amplified to lead to a lick command.

Finally, I optogenetically stimulated the cortex of awake mice and I measured the evoked whisker movements to obtain whisker motor maps. I found that almost the entire cortex can evoke whisker movement. The earliest evoked movement occurred when S1 was stimulated, the contralateral whisker had a prolonged retraction. Then the ipsilateral whisker started large rhythmic protractions. When M1 was stimulated, it triggered the most protracted whisker movement of rhythmic protractions. The largest oscillating protraction was observed when the parietal association area (PtA) was stimulated.

These data suggest that neuronal information needed to perform even simple tasks requires distributed cortical areas to process sensory inputs, like passive whisker deflection or optogenetic stimulation, and in return generate motor outputs, like licking or whisking. Future experiments must investigate the complex neuronal circuits connecting specific cell-types in various cortical regions using wide-field calcium imaging and combine it with optogenetic manipulations of this network at specific times and brain regions.

Keywords

Résumé

Dans toutes les espèces, y compris chez la souris et chez l'Homme, nous devons tous prendre des décisions pour répondre à nos besoins fondamentaux : manger, boire, explorer, communiquer, se reproduire... Pour prendre toutes ces décisions, nous devons recueillir des informations du monde qui nous entoure pour ensuite les traiter avec notre système nerveux. Le néocortex est un élément spécifique du cerveau, car il est le substrat des fonctions cognitives. Un des modèles couramment utilisés pour étudier le cerveau est la souris. Les souris peuvent être génétiquement modifiées pour exprimer des rapporteurs fluorescents ou des actionneurs optogénétiques dans les neurones qui les expriment. Les questions que je soulève dans cette thèse sont où et quand ces informations sensorielles sont traitées par le cortex chez la souris, et où et quand ces signaux sont intégrés pour ensuite générer une commande motrice.

Tout d'abord, j'ai développé un protocole pour obtenir des cartes sensorielles fiables à partir de l'imagerie du signal optique intrinsèque à large champ. Les souris subissent une intervention chirurgicale pour permettre une vue transparente du cortex dorsal gauche. J'ai ensuite stimulé séquentiellement et répétitivement différentes parties du corps de la souris après avoir été préalablement anesthésiée. Cela a permis d'obtenir une cartographie sensorielle dans le cortex pour chacun des organes stimulés. J'ai également réussi à imager des réponses provoquées par stimulation optogénétique en combinant cette technique avec de l'imagerie optique de signal intrinsèque à large champ.

Deuxièmement, j'ai trouvé les coordonnées du cortex sensoriel primaire de la langue/mâchoire tjS1 et du cortex moteur primaire de la langue/mâchoire tjM1. J'ai obtenu des images de signaux calciques provoqués par la stimulation de la langue et de la moustache chez des souris Thy1-GCaMP6f anesthésiées.

Troisièmement, j'ai enregistré l'activité corticale de souris effectuant une tâche de discrimination entre 2 vibrisses avec la technique d'imagerie calcium à large champ. J'ai découvert une différence importante entre les hits et les rejets corrects. L'amplitude des réponses dans S1, S2, M1 et M2 diminue au cours des jours d'entrainement. La différence qui apparaît le plus tôt entre la réponse des hits et la réponse des miss se produit dans S1 et S2 après 100 ms. Puis les signaux convergent vers M2 où l'amplitude de la réponse est amplifiée pour générer une commande de léchage.

Enfin, j'ai stimulé optogénétiquement le cortex de souris éveillées et j'ai mesuré les mouvements des moustaches générés par ces stimulations afin d'obtenir la carte motrice de la vibrisse. J'ai découvert que quasiment tout le cortex peut provoquer un mouvement des moustaches. Le mouvement qui survient le plus tôt est lorsque S1 est stimulé, la moustache controlatérale se rétracte longuement. Alors que la vibrisse ipsilatérale fait de grands mouvements de protractions rythmiques. Quand on stimule M1, les vibrisses bougent le plus en avant et de manière rythmique. Les mouvements d'oscillation les plus importants sont observés lorsque la région du cortex pariétal associatif (PtA) est stimulée.

Ces données suggèrent que l'information neuronale nécessaire à l'exécution de tâches simples recrute des régions corticales distribuées à travers tout le cortex afin de traiter les inputs sensoriels, comme par exemple la stimulation passive d'une vibrisse ou une stimulation optogénétique du cerveau, ce qui génère en retour des outputs moteurs, comme

le léchage ou le mouvement des vibrisses. Les expériences futures pourraient étudier des circuits neuronaux complexes reliant des types de cellules spécifiques dans diverses régions corticales à l'aide de l'imagerie calcique à large champ et la combiner avec des manipulations optogénétiques du réseau neuronal à des moments et des régions spécifiques du cerveau.

Mots-clés

# Contents

1. Introduction

1.1. Neocortex

Neuroscience is the only science field where we have to use the subject of our research as a tool to investigate it: the brain. It could be seen as an intrinsic investigation. The brain has a highly structured anatomy, both at macroscopical and microscopical scale, and function. The neocortex is the most recent brain structure that developed in the mammalian brain (Herculano-Houzel 2009; Rakic 2009). The neocortex is considered as the substrate of higher-order cognitive functions such as sensory perception, generation of motor commands (Lodato and Arlotta 2015), learning, decision making, spatial reasoning, consciousness and language (Rakic 2009). The human brain is outstanding among all mammalian brains, as it is the most cognitively able, the largest-than-expected from body size with the most overdeveloped cerebral cortex that constitutes over 80% of the brain mass, and contains approximately 86 billion neurons (- 2012). Although the brain represents only 2% of the body weight, it consumes about 20% of the oxygen and 25% of the total body glucose utilization to work (Weber and Barros 2015). The wiring of the brain network has been optimised by placing the cell bodies close to each other to facilitate fast communication in the grey matter while having the output myelinated axons joined together in the white matter to enhance the speed of the neural information and thus reacting appropriately and rapidly to the surrounding environment. Sensorimotor interactions between sensory inputs coming from the sensors at the periphery and motor outputs toward the muscles to react adequately to the environment is called behavior. One of the most complex behavior is to learn how to speak where the auditory system is involved in speech perception and the motor system plays a role in production of the sound making words and associate them to create a sentence (Hickok, Houde, and Rong 2011). This behavior that is used by humans everyday requires multiple brain areas that need to coordinate in order to make coherent percepts and actions. To simplify the problems and get closer to the mechanisms underlying brain function, researchers tend to use other models with less complex cognitive capacity (Toda and Platt 2015; Huttunen, Adams, and Platt 2017). One of the models extensively used in neuroscience is the mouse. The mouse brain can be a powerful tool for unravelling the mystery of human mental disorders, learning, decision making and all the basic fundamental theories that rule this system. Mice can perform simple behavior tasks that still involve complex neural circuits with distributed areas to process and integrate sensorimotor information by the neocortex. Mice can be engineered to express genetically-encoded reporters that can be used to image the neural activity with high temporal and spatial resolution. Mice can also be genetically modified to express an opsin in specific neurons, which, when light is pointed toward them, can activate those neurons with a great precision and this technique is called "optogenetics". My thesis will be trying to address the question of what brain areas are involved in a tactile discrimination reported by a simple motor action and trying to define an extended optical sensory and motor map of the dorsal neocortex of the mouse.

The neocortex contains both excitatory (~80%) and inhibitory (~20%) neurons (Noback et al. 2005). These two categories of neurons are defined by the effect of their activity upon their postsynaptic targets. Neurons are connected by synapses where they release neurotransmitters. The nature of the neurotransmitter determines if the neuron will

have an excitatory (increasing probability to generate action potentials, e.g. glutamate) or inhibitory (decreasing probability to get an electrical response, e.g. GABA) effect on the postsynaptic neuron. These neurons are not uniformly distributed in the neocortex. Indeed, the cortex is organised into six layers, which can be distinguished by cell-types, density and connectivity (figure 1.1). Usually, sensory signals enter the cortex in layer 4, the internal granular layer, which is the main input layer for thalamocortical projections (Woolsey and Van der Loos 1970; Lefort et al. 2009). It contains a large proportion of stellate or granular cells. As it is more an input layer, it is almost not present in motor cortex. Then the signal projects to layer 2/3, intracortical afferents and efferents, either within the same hemisphere or commissural (Petersen and Crochet 2013). The layer 2, the external granular layer, composed mainly of pyramidal and stellate neurons and the layer 3, the external pyramidal layer, containing mainly pyramidal cells and interneurons are usually pooled together as one layer, called layer 2/3, as it is difficult to distinguish it anatomically and structurally and the two layers are intricate. Layer 1, the molecular layer, is the most superficial layer and is characterized by a paucity of neuronal cell bodies, instead constituted mainly of bundles of traversing axons (e.g. feedbacks from motor cortex) making synaptic connections with apical dendritic tufts from deeper pyramidal neurons and various types of inhibitory neurons. Layer 5, the internal pyramidal layer, is mostly the output layer. It contains large pyramidal neurons with long axons leaving the cortex and running down to subcortical structures (such as the basal ganglia, thalamus, striatum or brain stem for voluntary motor control). Layer 6, the polymorphic or multiform layer, is the deepest cortical layer and it is also more an output layer strongly innervating the thalamus. It is composed of some large pyramidal neurons and many small multiform neurons. It establishes a reciprocal interconnection between the cortex and the thalamus.
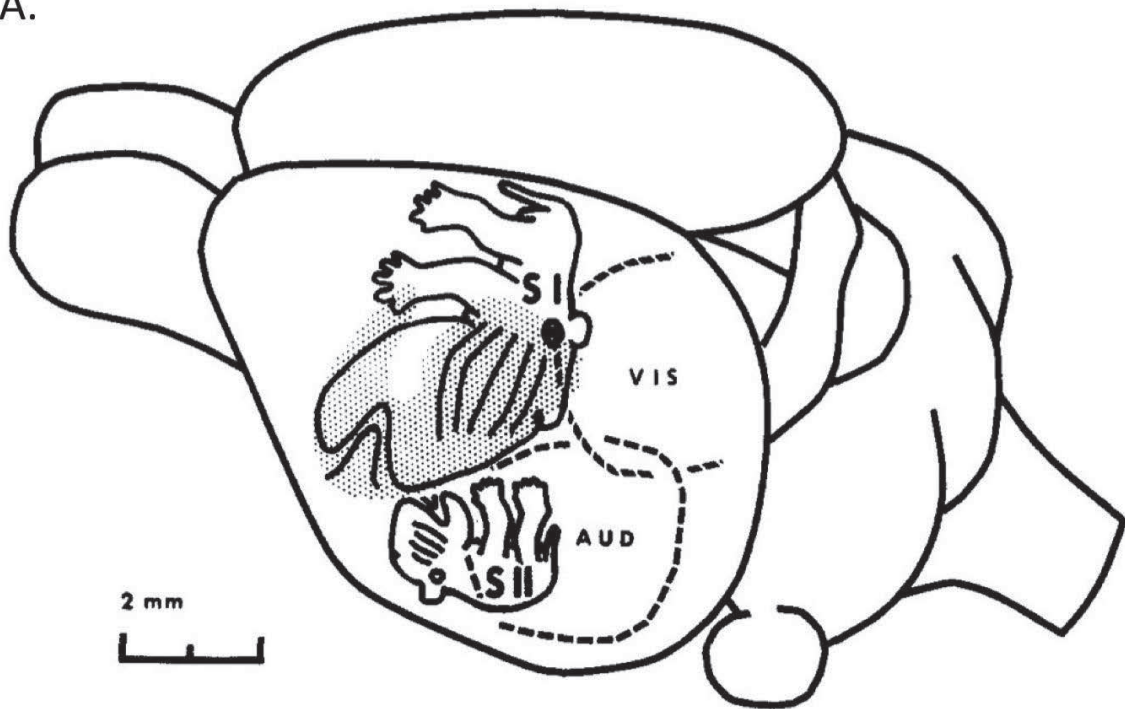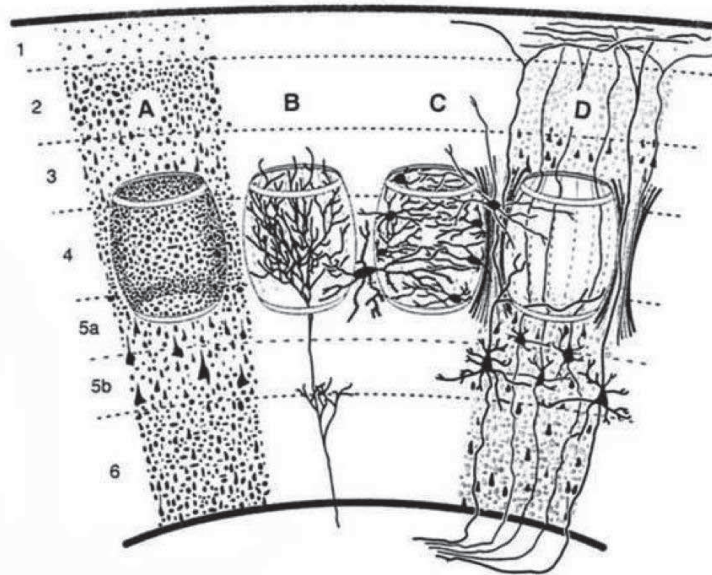
Figure 1.1. The barrel cortex
A. Historically-important diagram of the mouse brain to show the whole-body sensory representation in the dorsal neocortex. Barrel cortex (the whisker primary somatosensory cortex) has a large representation in the cortex meaning that whiskers are highly sensitive tactile organs. Interestingly, there is a mirror representation of the mouse somatotopy S1 in the secondary sensory cortex S2 (somatotopic mirror representation not correct in this representation). Figure reproduced from (Woolsey and Van der Loos 1970).
B. Schematic representation of a barrel illustrating the three-dimensional appearance of the multi-cellular cortical cytoarchitectonic unit of the whisker primary somatosensory cortex.

The drawing is a detail from a 17th century etching after Bruegel's painting "Fair of St. George's Day". Figure reproduced from (Woolsey and Van der Loos 1970).
C. Cytoarchitecture of neurons in the barrel cortex. a: distribution of neuronal somata as observed with Nissl staining. b: afferent axonal projection from the ventral posteromedial nucleus (VPM) of the thalamus ends primarily in a barrel located in layer 4. c: morphology of barrel spiny stellate neurons, cell bodies in the walls of the barrel and the dendrites projecting toward the center. d: apical dendrites of infragranular (mainly layer 5 cells) and axons of supragranular pyramidal neurons pass preferentially through the barrel wall and septum. Figure reproduced from (Paxinos 2014).

1.2. Sensory perception

The brains of all vertebrates have sensory systems that process information from receptors of the skin, the eyes, the ears, the mouth and the nose in order to guide their motor behavior and avoid damage (Kaas 2015). Each of the five senses have a sensory representation in the cortex that is functionally and anatomically highly specialized to process the very different sensory inputs coming from the environment. For somatosensation, the inputs come from receptors at the surface of the skin that respond to touch, vibration, temperature, humidity or tissue damage. There are also receptors deeper in the muscles or the joints that give information about movement and limb position, called proprioception. The eyes have specific receptors for light at the surface of the retina. The photoreceptive cells are the cones, encoding for colors, and the rods, sensitive to low light intensity. The ears of mammals are important for auditory perception using the cochlear system and for the sense of balance and spatial orientation to coordinate movements with the vestibular system. The tongue is the organ of the sense of taste. Sensorimotor processing related to the tongue plays an important role, especially in behavioral studies with mice. Most mammals have their sensory and motor areas separated where the sensory cortices are usually posterior (or caudal) and the motor cortex is more frontal (or rostral). In mice, sensory and motor cortices overlap for the hindlimb area. Motor areas can also receive inputs from sensory cortex and use this information to guide motor cortex outputs that produce appropriate behavior.

Whisker system: from periphery to neocortex

To interact with our environment, we continuously collect a lot of information (light, sounds, touch, tastes or odors) with our senses that send electrical signals generated by the sensors at the boundary of the outside world and our body to our brain. In my thesis, I will focus on the tactile sensory system. Mice can probe the outside world by moving their whiskers providing information about the location, shape and texture of the objects touched (Hutson and Masterton 1986; Carvell and Simons 1990; O'Connor, Clack, et al. 2010). The whiskers are tactile arrays of long hairs on the snout of the rodent. Mice actively protract and retract their vibrissae in large back and forth sweeping movements at high frequencies (8-10 Hz), while navigating into their environment (P. Gao, Bermejo, and Zeigler 2001; Berg and Kleinfeld 2003b). Since mice are nocturnal burrowing animals, they developed this whisking strategy to compensate the poor visual acuity to navigate in narrow underground tunnels.

Upon passive or active whisker deflection, the tactile information is transferred from mechano-gated ion channels of the follicles to the trigeminal nuclei of the brain stem through the infraorbital branch of the trigeminal ganglion, with one trigeminal ganglion neuron targeting one single follicle (figure 1.2) (Zucker and Welker 1969). Once in the brain stem, the trigeminal ganglion cells make excitatory glutamatergic synapses with neurons of the principal trigeminal nucleus (Pr5) (Veinante and Deschênes 1999) and spinal trigeminal nuclei (Sp5). Tactile information from each whisker is organized in topographic maner called barrellettes. There is one-to-one correspondence for follicle-to-barrelette (Feldmeyer 2012). The principal trigeminal nucleus neurons project to the contralateral side of the thalamus, to the ventral posterior medial nucleus (VPM), in the 'lemniscal' pathway. Some neurons in Sp5 project to the posterior medial nucleus (POm) in the 'paralemniscal' pathway. In the VPM, the incoming axons are somatotopically organized in anatomical structures termed 'barreloids'. The neurons located in one barreloid are strongly activated by deflection of the principal whisker and weakly by the neighbouring whiskers (Simons and Carvell 1989; M. E. Diamond et al. 1992). The sensory information then travels from VPM to principally layer 4 of the primary somatosensory cortex wS1. Axons from the VPM project into the corresponding discrete anatomical and functional structure, called a 'barrel' (due to its shape that looks like a barrel) (Woolsey and Van der Loos 1970). Cytochrome oxidase staining gives a clear image of the barrel anatomy in tangential sections. This one-to-one mapping of the whisker pad is kept all along the sensory path until the layer 4 of the cortex where the somatotopy is organised in defined cortical columns (C. Welker 1971). The axons projecting from POm mainly end in layer 5A and other travel through the septal region of layer 4 to reach layer 1. A cortical column is a structure perpendicular to the brain surface containing cells with the same tuning for a certain salient receptive field characteristic and delimited by a structural border. Because of this well conserved somatotopic organization, the whisker system is a extensively used model in neuroscience to characterize evoked sensory information in the brain from a well-controlled stimulus at the periphery.
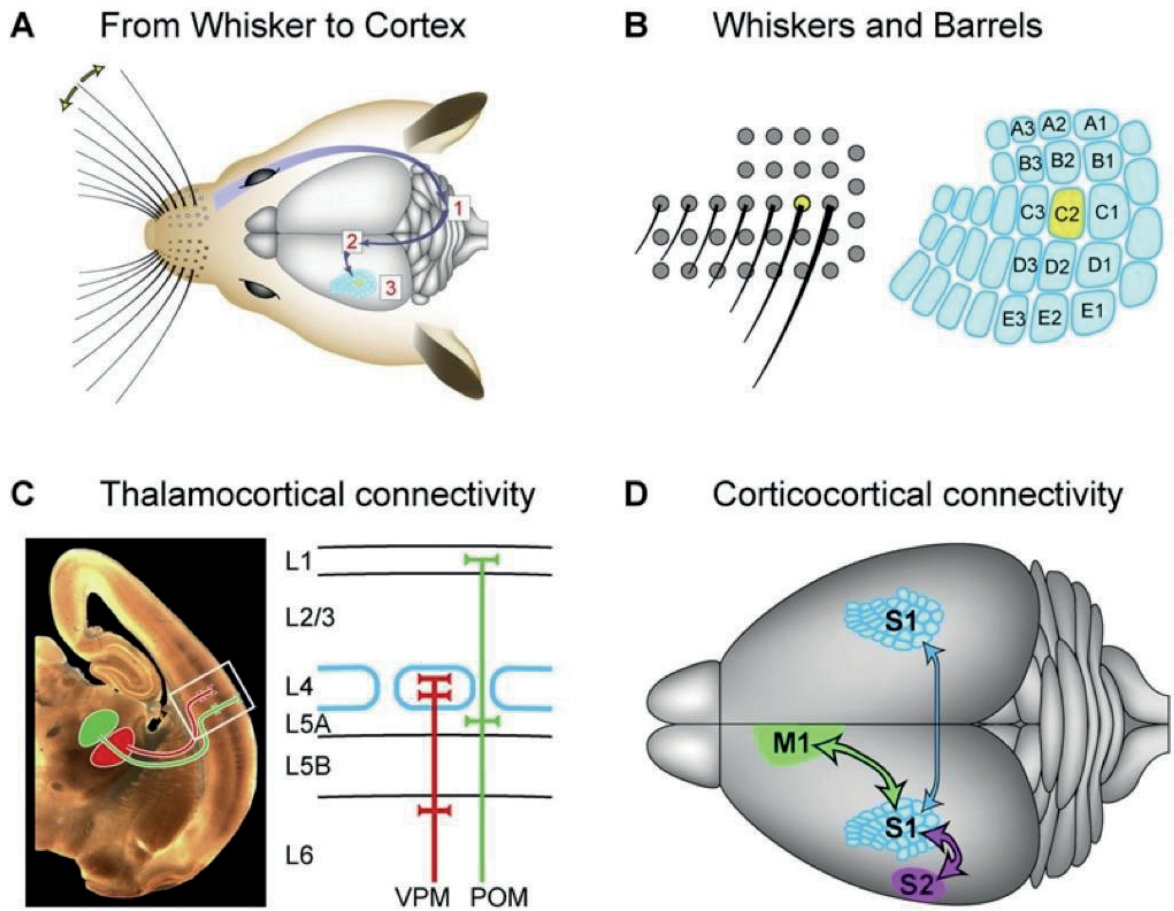
Figure 1.2. Synaptic pathways for the sensory perception of a whisker stimulation from the periphery to the barrel cortex in rodents.

A. A whisker deflection evokes action potentials in sensory neurons of the trigeminal nerve, which release glutamate at a first synapse in the brain stem (1). The brain stem neurons relay sensory information to the thalamus (2), where a second glutamatergic synapse activates thalamocortical neurons projecting to the layer 4 of whisker primary somatosensory cortex (3).

B. The layout of whisker follicles (left, only C-row whiskers shown) on the snout has a one-to-one representation in the whisker primary somatosensory cortex. This structure in rodents is highly conserved and the layout is similar between rats and mice. There are anatomical structures called "barrels" in layer 4 of the primary somatosensory neocortex. Whisker pad nomenclature uses capital letters for the rows and numbers for the arcs.

C. Representation of the two important parallel thalamocortical pathways for signaling whisker sensory information to the barrel cortex: one originating from VPM projecting layer 4 (in the barrel) and layer 6 and the other originating from POM projecting to layer 1 and to layer 5A.

D. Neurons in the whisker primary somatosensory cortex are directly reciprocally connected to other cortical areas through long-range glutamatergic corticocortical synapses. The primary somatosensory cortex wS1 is connected with the secondary somatosensory cortex S2 and the primary motor cortex M1 of the same hemisphere. The primary somatosensory cortex wS1 also sends callosal projections to S1 of the other hemisphere but to a lesser extent. Figure reproduced from (Petersen 2007).

Forepaw tactile sensory pathway

Mice use their forepaws to grab and actively sense the surrounding environment. They can detect complex features like shape, temperature and texture of the objects. At the periphery, the mechanical friction of the skin can transduce electrical action potentials by myelinated or unmyelinated sensory afferents: Aα, Aβ, Aδ and C fibers (Roudaut et al. 2012; Olson et al. 2016). The afferent neurons make a first synapse in the dorsal horn of the spinal cord. The axon of the tract cells crosses over (decussates) to the other side of the spinal cord via the anterior white commissure, and to the anterolateral corner of the spinal cord. The axon travels along the spinal cord to the rostral ventromedial medulla of the brainstem. The neuron makes a synapse with a third-order neuron in several nuclei of the thalamus, like the ventral posterolateral nucleus (VPL), which also transmits sensory information from the hind-limbs and trunk. The thalamus relays the sensory signal to the corresponding primary somatosensory part of the forepaw cortex (fpS1).

Auditory pathway

Mice can transduce sounds from the exterior into electrical signals using their cochlea located into their inner ear. The hair cells in the organ of Corti of the cochlea are tuned to certain sound frequencies by their location in the cochlea, due to the degree of stiffness in the basilar membrane. Thousands of hair cells sense the motion evoked by a specific sound via their stereocilia, and convert the mechanical displacement into electrical signals that are transduced to many thousands of nerve cells via neurotransmitters. From the cochlea the auditory nerve travels to the cochlear nucleus (CN) of the brainstem. The secondary auditory neurons in the CN decussate and send their ascendant axons to the superior olivary complex (SO). The SO plays an important role to detect the interaural level and time difference used for sound localization. Third-order neurons of the SO send axons to the inferior colliculus (IC) of the midbrain, which is important for binaural information processing and auditory information integration. Fourth-order neurons projects to the medial geniculate nucleus (MGN) of the thalamus, where auditory information is filtered before it is transmitted to the cortex. Fifth-order MGN neurons make synapse with neurons of the primary auditory cortex (A1). The learning and memory of vocalizations likely occur in A1 (Charitidi and Canlon 2010; Asaba et al. 2014).

Visual pathway

Mice can detect light arriving to their eyes and the retina transforms the photons into electrical signals used to detect the different features of the objects around, like their size, shape, color and distance. The retina consists of several layers of neurons interconnected by synapses. It has two types of photoreceptor cells: rods and cones. Rods are very sensitive to light and function mainly in dim nocturne light condition by providing black-and-white vision. Cones function in bright daylight for the perception of colors. After initial transformation of the photon light by the opsins of photoreceptor cells of the retina to electrical signal, visually evoked signals are transmitted by retinal ganglion cells (RGCs) that are the main output cell type in the retina. The majority of axons of the RGCs project to the

contralateral hemisphere after crossing at the optic chiasm. The percentage of ipsilateral and contralateral projections varies between species with the location of the eyes on their head. In mice, RGCs neurons project either to a thalamic structure called the lateral geniculate nucleus (LGN) or to a midbrain structure named superior colliculus (SC). The LGN is a structure located in the dorsal lateral section of the thalamus. The LGN provides the main source of visual input to the cortex, while the SC is involved in multisensory coordination of fast response actions (Zhao, Liu, and Cang 2014). The LGN directly projects to the primary visual cortex (V1) (Grubb and Thompson 2003). The LGN is organized retinotopically: neurons in neighbouring regions of LGN respond to stimuli in neighbouring regions of the visual field. Like for LGN, V1 is also organized retinotopically (Wang and Burkhalter 2007).

1.3. Motor command

Motor control is a complex mechanism that involves different cortical structures. There are two classical methods used to localise motor areas: i) functionally by stimulating one cortical area and observing if it can evoke movement of the corresponding muscular organ at the periphery or ii) by disrupting the motor cortex and observing if it produces motor outcomes. In addition, some studies define motor cortex anatomically by following the frontally-projecting axons from the primary sensory area. Several studies in rodents using microelectrodes found that movements could be evoked by stimulating many different parts of the neocortex, including M1 and S1 (Hall and Lindholm 1974; Gioanni and Lamarche 1985; Neafsey et al. 1986; Brecht, Krauss, et al. 2004; Haiss and Schwarz 2005; Ferezou et al. 2007). In the motor cortex, there is only a very minor layer 4 and motor cortex is thus also called the medial agranular cortex (AGm) (Smith and Alloway 2013). Motor maps obtained by surface stimulation or intracortical microstimulation showed that forelimb and hindlimb are bordering and sometimes overlapping with their S1 representations. The motor representations of the head, whiskers and eyes are further apart from their sensory representations and are located more frontal and medial (figure 1.3).
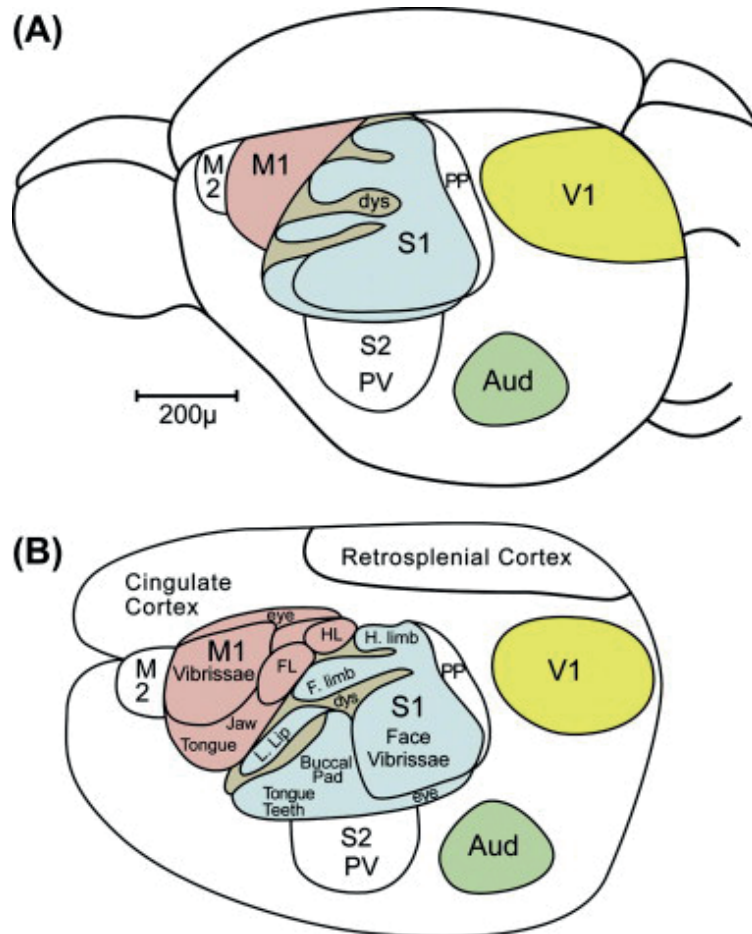
Figure 1.3. Anatomical and functional organisation of the motor cortex in rodents.
A. Primary (M1) and secondary (M2) motor cortical areas are located in frontal agranular cortex. Primary (S1) and dysgranular somatosensory cortex also have motor functions.
B. Enlarged view of mouse neocortex after it has been separated from the rest of the brain and flattened so that the cortex of the medial wall of the hemisphere is visible. In the primary motor cortex M1 there is a mirror motor functional representation of the somatotopy present in primary sensory cortex S1.
Figure reproduced from (Young, Stepniewska, and Kaas 2012).

Whisker system: from cortex to periphery

Mice use their whiskers to explore their close environment. They actively move their whiskers back and forth in large sweeping movements to get complex information about the objects around them. These rapid protraction and retraction movements are called whisking. To get this high-precision and complex sensory information, mice need to move their whiskers and integrate the signals from all the whiskers that were touching or not the object. By sampling the surrounding they can determine different features: shape, texture and location of the objects (Kleinfeld and Deschênes 2011). In rats two types of movements can be evoked by electrical stimulation in two distinct regions of the cortex (Haiss and Schwarz 2005). When the anterolateral region of wM1 is stimulated (the retraction-face region), it drives a prolonged retraction of the contralateral whisker, whereas when the posteromedial region (called the rhythmic whisking region), it generates a rhythmic whisker protraction.

Similar results were reproduced in mice (Ferezou et al. 2007; Matyas et al. 2010). Remarkably, when the primary somatosensory cortex wS1 is silenced by pharmacological inactivation, stimulation of wM1 evokes only rhythmic protraction, regardless of the precise M1 region stimulated. It implies that retraction is controlled by the interaction with wS1. Another study showed that when wM1 is optogenetically inhibited, it can promote whisker movement by disinhibiting contralateral whisker movements and leading to contralateral whisker protraction (Ebbesen et al. 2017). On the other hand, when layer 5 neurons of wM1 are stimulated, it generates phase locked rhythmic whisker movements, whereas when layer 6 neurons were stimulated, there is a trial-to-trial variability with different whisk cycles (Brecht, Schneider, et al. 2004).

The primary motor cortex wM1 makes cortico-cortical connections with the primary and secondary somatosensory cortices (wS1 and S2) and with the wM1 of the contralateral hemisphere. The main projection to wM1 originates from wS1 (Chakrabarti and Alloway 2006; Aronoff et al. 2010). This is the main source of tactile sensory feedback response going to wM1. This connection between wS1 and wM1 is reciprocal with projecting axons from layer 2/3 and layer 5a (Sato and Svoboda 2010; Mao et al. 2011; Petreanu et al. 2012). The S2 cortex projects to M2 with axonal terminals intermingled with those arising from wS1 projecting to wM1, making two parallel pathways (Colechio and Alloway 2009). Projections coming from posterior parietal cortex (PPC) terminate in AGm (Colechio and Alloway 2009). Also, both wM1 of the two hemispheres are strongly interconnected with each other, this might be why there is such an important coordination of the bilateral whiskers (much more than the limbs that move more independently and have less bilateral interconnections) (Colechio and Alloway 2009).

Primary whisker motor cortex also has afferent and efferent connectivity with various thalamic nuclei (Cicirata et al. 1986). In particular, it has been observed that wM1 and POm have reciprocal connections that are important in the motor gating of ascending sensory feedback information via the paralemniscal pathway (Urbain and Deschênes 2007).

In addition, primary whisker motor cortex wM1 projects to other subcortical structures such as the cerebellum, the striatum, the claustrum and the brainstem. By injecting rabies virus in the muscles revealed the existence of direct cortico-motoneuron projections (Sreenivasan et al. 2015). The role of these direct connections are still not clear as after unilateral lesion of wM1, rats could recover almost normal kinematic profiles of whisking (Puhong Gao et al. 2003). Several brainstem regions receive axonal projections from wM1 and in turn send axons to the facial motoneurons in the snout. It was found that intermediate reticular formation (IRt) has a central pattern generator (CPG) which can generate rhythmic whisking movements and it also receives projections from the contralateral wM1 (Takatoh et al. 2013).

In the snout of the rodents, the whiskers are moved by two antagonist muscles for protraction and retraction: intrinsic and extrinsic (nasolabialis and maxillolabialis) muscles (Haidarliu et al. 2010). The retraction movements of the whiskers are executed by the extrinsic muscles, which are located at the surface outside of the whisker pad. On the other hand, whisker protraction movements are made by intrinsic muscles, which are part of the whisker pad. They are attached to the base of the follicle and can pivot the whisker to protract. During rhythmic whisking movements, both the intrinsic and extrinsic group muscles are active. Electromyography (EMG) recordings in the whisker pad showed that the rhythmic

activation of this antagonist group of muscles is out of phase (Berg and Kleinfeld 2003a; Hill et al. 2008).

1.4. Wide-field optical techniques

Intrinsic optical imaging

In 1977, Jöbsis measured blood and tissue oxygenation changes in the brain of a cat using near-infrared light (Jöbsis 1977). Since then, optical intrinsic signal imaging has become a tool commonly used to map cortical activity and to investigate brain function and organization (A. Grinvald et al. 1986; R. D. Frostig et al. 1990; Ts'o et al. 1990). It is possible to image intrinsic signals through the skull of the mouse and get an evoked response regardless the mouse line. The mouse is typically lightly anesthetized to get reliable signals. These intrinsic optical signals are in part induced by spiking of neurons and subthreshold synaptic activity giving an indication of the local neuronal activity in the brain. When the neurons are active, they require energy which is mainly used to generate action potentials and in synaptic transmission, followed by neurotransmitter uptake later by the surrounding astrocytes. Astrocytes are glial cells in the brain, that get their name based on their "star-shape". Indeed, although the brain makes about 2% of the body weight in humans, it consumes up to 25% of the total metabolic energy (Weber and Barros 2015). This explains the importance of neurovascular coupling, as the brain does not have a large energy reserve (figure 1.4).

The nature of the intrinsic optical signal has been proposed to vary with time from the stimulus onset (Cynthia H. Chen-Bee et al. 2007, 2010). Usually, right after stimulus neurotransmitters are released by the synapses (in the order of ms) leading to rapid light scattering. The increase in neuronal activity provokes a brief decrease in oxyhemoglobin (HbO) and thus a relative increase in deoxyhemoglobin (HbR). The metabolic demand is counterbalanced by an increase in local perfusion of the brain called the hemodynamic response. To compensate this local diminution of glucose and oxygen in the blood, there is an increase in the cerebral blood flow leading to an increase of both oxyhemoglobin and cerebral blood volume. It is this part of the response that is detected and quantified by BOLD fMRI. Then it takes 5 to 10 sec for the signal to fall back to baseline after the stimulus offset. Therefore, it is important to interleave stimulus and no stimulus trials separated by long intertrial intervals. The stimuli are thus separated by tens of seconds depending on total trial time (including baseline and postimulus periods).
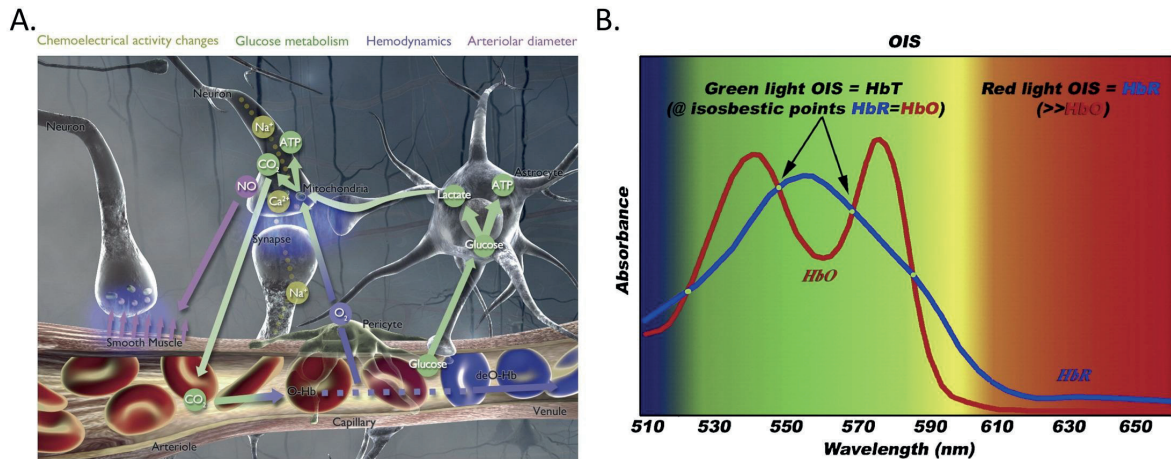
Figure 1.4. Sources of intrinsic optical signals.

A. Neurovascular coupling maintains metabolic homeostasis of the brain with microvessels travelling nearby activated neurons. Information jumps from one neuron to the next neuron through synapses where presynaptic neurons release neurotransmitters. Astrocytes extensive endfoot around blood vessels take-up the glucose from the blood and transform the glucose into lactate (glucose is first transformed to pyruvate and then converted into lactate during anaerobic glycolysis). The lactate is transported to the connected neuronal synapses. Also, there is an uptake of O_2 to generate energy by the mitochondria located in the active neuronal synapses. There is an adaption of the cerebral blood flow to the demand of glucose uptake, which overcompensates local oxyhemoglobin (HbO) and leads to a relative decrease in deoxyhemoglobin (HbR).

B. In the visible light spectrum, hemoglobin is the major source of light absorption for IOS imaging, whereas in the near infrared, IOS imaging is dominated by light scattering of the neuronal swelling. In the green light spectrum, the absorption of the total-hemoglobin HbT is high as both HbO and HbR are high. In the red light spectrum, light absorption is mainly due to HbR concentration changes as HbO absorbance is very low.

Figure reproduced from (Prakash et al. 2009).

This technique was extensively used to investigate the mapping of functional organisation of the cortex. It was used to demonstrate that iso-orientation stimuli of the cat visual cortex are arranged in pinwheel-like structures (Bonhoeffer and Grinvald 1991; Schuett, Bonhoeffer, and Hübener 2002).

Wide-field calcium imaging

Optical microscopy is one of the key tools that permits biologists to observe living organisms. The technology of microscopy kept improving spatial resolution since its invention in the 17th century. Now it is possible to image behaving mice down to the cellular resolution and even subcellular resolution with spine imaging (Svoboda and Yasuda 2006). In this thesis I will stay at macroscale resolution in order to characterize the cortical signal dynamics during mapping or behavioral experiments. By using a tandem lens macroscope (Ratzlaff &

Grinvald), with two lenses face-to-face in front of the camera, they could image one hemisphere of the dorsal neocortex of an adult mouse.

Historically neuroscientists were using another wide-field functional imaging technique by applying fluorescent voltage-sensitive dyes (VSDs) on top of the brain of the animal after a craniotomy. This imaging technique has a high spatial resolution (~50 μm for population recordings) and very high temporal resolution (~1 ms). As the top of the cortex is stained with VSD, the dye binds to the plasma membrane of all types of cells: neurons (both excitatory and inhibitory) and glial cells. Glial cells have less contribution on VSD signals because of their lower electrical activity compared to neurons. So VSD signals is mostly due to the average voltage change generated by neuronal depolarization or hyperpolarization evoked by local activity of the cortex. In neurons, the surface of the soma is several orders of magnitude smaller than the surface of its axon and dendrites. So, the neuron somata have a minor contribution on the VSD signal change. VSD was used to study the evoked response following a passive stimulation of the whisker in the mouse cortex (Ferezou et al. 2007). As this technique is invasive and requires a large craniotomy to have a good access to the cortical surface it is complicated to perform longitudinal studies and investigate learning and plasticity in behaving mice but it was performed during the last day of training in expert mice (Kyriakatos et al. 2017).

It is possible to image calcium signals over long training periods to see the evolution of the activity of a large part of the cortical neural network with high temporal and spatial resolution. This experiment is now possible because of the emergence of mouse lines that express genetically encoded calcium indicators (GECI) throughout the entire brain of the mouse in specific neuronal population. GECIs are fluorescent proteins (usually derived from GFP) that can respond to the binding of Ca^{2+} ions by changing their conformation. GCaMP is one of the most commonly used and it was developed by Junichi Nakai (Nakai, Ohkura, and Imoto 2001). GCaMP is a construct made from a fusion of green fluorescent protein (GFP), calmodulin and M13, a peptide sequence from myosin light chain kinase. Calmodulin (CaM) is a calcium-binding messenger protein expressed in all eukaryotic cells and involved in calcium signal transduction pathway (figure 1.5) (Stevens 1983). One challenge with calcium imaging is to understand the ontology of the measured signal, especially the link between the global wide-field GCaMP response and the response of single neurons (Stevens 1983; Seidemann et al. 2016). The relationship is not easy to predict as calcium signals can result from a mixture of two distinct cellular responses: spikes or synaptic potentials in dendrites. Measurements in single neurons have described that the somatic GCaMP signal is dominated by action potential firing (Helmchen and Denk 2005). Calcium signals recorded with high-affinity indicators like GCaMP6f can estimate spike dynamics produced by each action potential, as each action potential (AP) is associated to a rather stereotypical somatic calcium influx resulting to a characteristic elementary calcium transient (Lütcke et al. 2013). In wide-field recordings, it is possible that the spike-to-calcium non-linearities observed in single neurons are averaged out when pooling all together the heterogeneous responses leading to wide-field calcium responses that correlates with the sum of all the local spiking activity. On the other hand, wide-field voltage sensitive dye (VSD) imaging measures the locally pooled membrane potential. Because of the nonlinearity between membrane potential variations and spiking activity in single neurons (Priebe and Ferster 2008), there is a difference in VSD and Ca^{2+} response in regions where there is subthreshold activity, which can affect the sensitivity of GCaMP in some low contrast response experiments. Both techniques measure different aspects of neuronal population activity.

Calcium imaging technique has several advantages compared to other wide-field imaging techniques in behaving mice. GCaMP is expressed genetically in some mouse lines throughout the whole brain, meaning that mice can be imaged through their transparent skull over several days and with stable fluorescent signal. Intrinsic optical signal imaging has the same advantage as it does not need special surgery and it can be performed in any mouse line, but the signal is not as fast as calcium signals and intrinsic signals are difficult to detect reliably in awake animals. Although, the temporal resolution of GCaMP is not as good as VSD, GCaMP signal amplitude is nearly an order of magnitude larger than VSD and intrinsic signal (Seidemann et al. 2016). Also, VSD imaging requires very invasive surgical procedures, meaning that it has to be acute experiments preventing longitudinal studies during learning of a task, and moreover, the animal still needs to recover from the painful surgery and still perform well. For all those reasons, calcium signal imaging is until now one of the best techniques to study wide-field cortical signal dynamics in behaving mice with a high temporal and spatial resolution. Progressively, some transgenic voltage-sensor mice are available and will be another interesting tool to investigate wide-field neuronal processing of the sensorimotor interactions in behaving mice (Akemann et al. 2012; Empson et al. 2015).
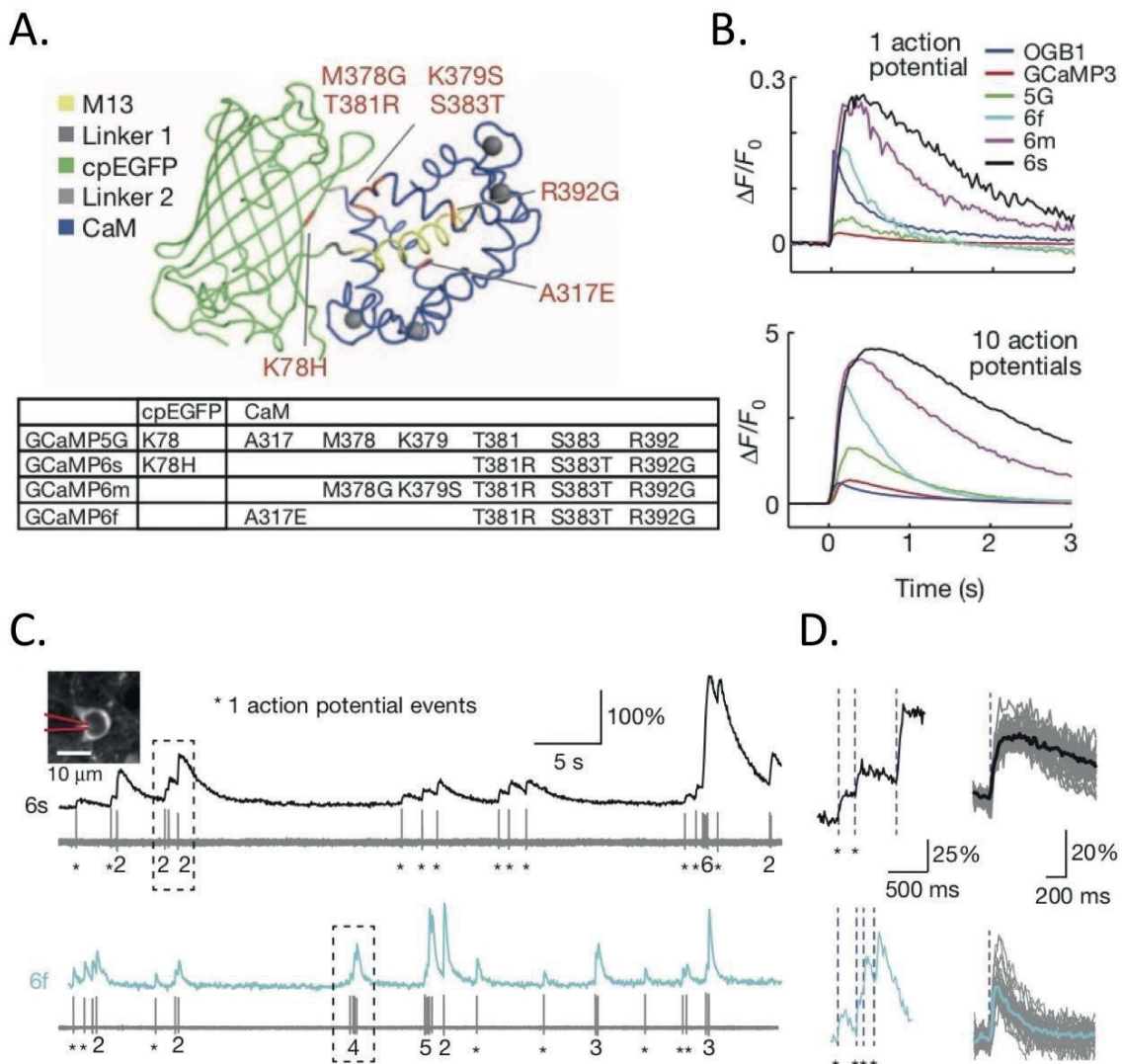
Figure 1.5. Functional evoked fluorescence change of GCaMP6 compared to electrophysiological recording of the same neurons in the mouse visual cortex.

A. GCaMP structural conformation and mutations in different GCaMP variants relative to GCaMP5G.

B. In vitro responses averaged across multiple neurons for GCaMP3, GCaMP5G, GCaMP6f, GCaMP6m, GCaMP6s, and OGB1-AM. Top, fluorescence changes in response to 1 action potential. Bottom, fluorescence changes in response to 10 action potentials.

C. Simultaneous fluorescence dynamics and spikes in a GCaMP6s (top) and a GCaMP6f (bottom) expressing neuron. The number of spikes for each burst is indicated below the trace (single spikes are indicated by asterisks).

Top left inset, image of a GCaMP6s-expressing neuron with the recording pipette in red.

D. On the left of the panel there is a zoomed-in view of bursts of action potentials for both GCaMP6s and GCaMP6f.

On the left of the panel there is the fluorescence change and the average fluorescence change (in bold) in response to one action potential for both GCaMP6s and GCaMP6f.

Figure reproduced from (T.-W. Chen et al. 2013).

Optogenetic mapping

To map the motor cortex, many studies used stimulation with microelectrodes (Hall and Lindholm 1974; Gioanni and Lamarche 1985; Brecht, Krauss, et al. 2004). Even though those maps were reproducible, this brain stimulation method suffers from some limitations. This method stimulates the cell bodies close to the electrode, but it can also stimulate traveling axons passing through the region, reducing the spatial resolution of the obtained map. Also, this technique is not selective for one type of neuron or for a subpopulation of neurons. It would not be possible to inhibit brain areas. It is not well suited for longitudinal studies where it would require to stimulate the same area for several days with similar electrophysiological parameters. For all those reasons, in the last decade, optogenetic methods have attracted great interest for mapping and inhibition experiments. Viruses and mice have been engineered to express light-sensitive ion channels and transporters at the membrane surface of genetically modified neurons. This technique uses light to control cells activity by changing the conformation of some optogenetic actuators like channelrhodopsins (ChRs). ChRs are light-gated cation-selective channels located in the cell membrane that open with specific light to depolarize the cell. The first idea of controlling selectively neural activity with light within subtype of neurons was evoked by Crick in 1999 (Crick 1999). After some success in drosophila (Zemelman et al. 2002; Lima and Miesenböck 2005), the first demonstration of a single-component optogenetic system in cultured mammalian neurons was performed in Deisseroth's laboratory (Boyden et al. 2005). Channelrhodopsin-2 (ChR2) is a non-selective cation channel that response to blue light (Nagel et al. 2003). This is a powerful tool that can reach a single cell spatial resolution (using electroporation for example) and a temporal resolution on the order of milliseconds (Lim et al. 2013).
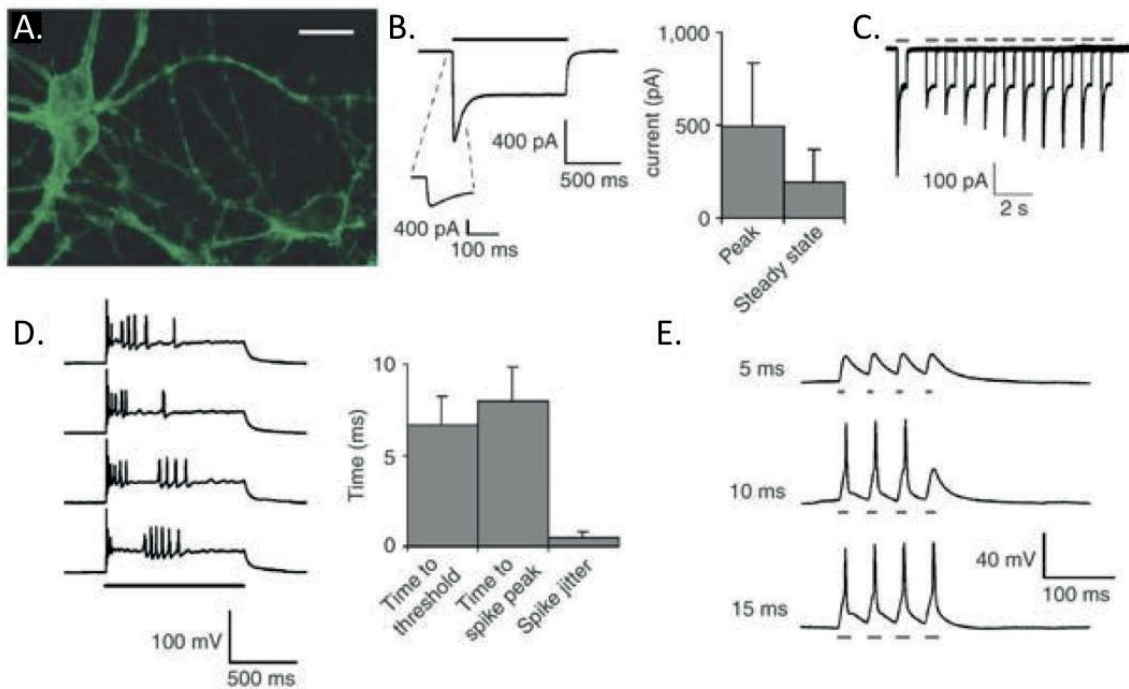
Figure 1.6. Spiking evoked by blue light (GFP excitation wavelength) in neurons expressing channelrhodopsin-2 (ChR2).
A. Hippocampal neurons expressing ChR2-YFP (scale bar 30 μm).
B. Left, inward current in voltage-clamped neuron evoked by 1 s blue light (indicated by black bar).
Right, population data (mean ± s.d. n = 18).
Inset, expanded initial phase of the current transient.
C. Overlay of 10 current traces recorded from a hippocampal neuron illuminated with pairs of 0.5 s light pulses (indicated by gray bars), separated by intervals varying from 1 to 10 s. D. Left, voltage traces showing membrane depolarization and spikes in a current-clamped hippocampal neuron (left) evoked by 1 s periods of light (gray bar).
Right, electrophysiological properties of the first spike elicited (n = 10): latency to spike threshold, latency to spike peak, and jitter of spike time.
E. Voltage traces in response to brief light pulse series, with light pulses (gray bars) lasting 5 ms (top), 10 ms (middle) or 15 ms (bottom).
Figure reproduced from (Boyden et al. 2005).

Mouse behavior

Mice can be trained to perform simple tasks. Usually, one stimulus or a sequence of stimuli are delivered to the mouse, then the mouse has to respond to this stimulus by a motor action and it gets a reward if the action was correct or a punishment if it was not the expected answer. The Go-NoGo paradigm is often used in head-fixed rodents (Stüttgen and Schwarz 2008). During this type of behavior, the mouse has to be engaged in the task to generate a motor command, otherwise it ignores the stimulus and the mouse does not perform. In order to assess if miss trials are due to demotivation of the mouse or the mouse did not perceive the stimulus, we have to do some psychometric tests, to define the perception threshold

(Busse et al. 2011; N. Takahashi et al. 2016; Aoki et al. 2017). In other types of tasks, where there is no passive stimulation (e.g. deflection of the whiskers, visual pattern shades, sound delivered, odor diffusion…) the mouse has to move its whiskers or its forepaws to probe the nature of the stimulus and discriminate between stimuli or simply the presence or the absence of an object (Arabzadeh, Zorzin, and Diamond 2005; O'Connor et al. 2013; Makino et al. 2017; Hasegawa et al. 2017; Helmchen, Gilad, and Chen 2018). During simple whisker detection tasks, as well as whisker discrimination tasks, primary somatosensory cortex has a causal role in the neural network to perform in this task (Krupa et al. 2001; Sachidhanandam et al. 2013). Different parts of the network were studied with various techniques to address the sequence of events in this detection task (Kyriakatos et al. 2017; Yamashita and Petersen 2016). Sensory cortex is not necessarily required in all detection behaviors like in unconditioned reflexes (Sprague 1996; Yeomans et al. 2002). In this thesis, I will focus more on discrimination between two salient whisker stimuli to attract the attention of the mice and to avoid pure conditioned learning, hoping that a large part of the cortex is recruited to perform this task (El-Boustani et al., *manuscript in preparation*).

In order to have a more independent measure of the mouse performance, without questioning the engagement of the animal in the task, mice undergo two alternative forced choice behaviors (Mathew E. Diamond and Arabzadeh 2013; T.-W. Chen et al. 2017). In contrast, in the Go-NoGo task, it is impossible to distinguish a lack of motivation or a lapse of attention. Also, in head restrained mouse behavior, this multi motor response behavior requires high precise licking movement that recruits frontal area to trigger correct liking (e.g. anterior lateral motor cortex, secondary motor cortex).

All these behaviors study the complex neural networks that are involved in sensory processing, sensorimotor integration, motor learning and decision making. It can be studied at different cellular levels with various time precision and spatial resolution. In this thesis, we will try to decode what the cortex is doing during a two-whisker discrimination task.

1.5. General aims of the PhD thesis

The aim of this thesis is to further understanding of cortical sensorimotor maps, and to investigate processing of information upon well-defined stimulation perturbing the cortical network. I also wanted to characterize the networks involved in simple decision making. To achieve those aims and get a global representation of the cortical network, I did four sets of independent experiments.

In chapter 2, I developed a method to reliably get optical intrinsic signal images that allowed whole body sensory mapping. I also combined this with optogenetic stimulation during functional mapping. This could be a potentially very interesting way to get motor maps by targeting blue light on the previously mapped sensory areas.

In chapter 3, I mapped the sensory and the frontal cortical areas activated upon tongue and jaw stimulation using wide-field calcium imaging in anesthetized mice. Presumably, the frontal areas correspond to the primary motor cortex of tongue and jaw, similar to how these regions have been defined in the whisker system (Ferezou et al. 2007).

In chapter 4, I imaged with a high temporal resolution the left dorsal cortex of mice performing a two-whisker discrimination task. I described the cortico-cortical sensorimotor processing occurring in layer 2/3 by characterising the calcium dynamics generated by the sensory integration and decision making of a performing mouse.

In chapter 5, I obtained an unbiased optogenetic motor map of the bilateral C2 whisker. I stimulated the left hemisphere in ChR2 mouse and observed the evoked movement of the whiskers at the periphery by filming the mouse face at high temporal resolution.

2.   Wide-field intrinsic optical signal imaging for sensory mapping

Author contributions

Matthieu Auffret and Carl Petersen designed the project. Matthieu Auffret wrote the manuscript. Matthieu Auffret wrote the MATLAB script for data acquisition. Matthieu Auffret carried out all experiments and analyzed data.

2.1.   Introduction to signal origin: light absorption and scattering measurement

Intrinsic optical signal imaging (IOS) is a functional brain mapping technique with a time resolution in the range of ~0.1-10 s and a spatial resolution of ~10^{-4} m that can resolve one barrel in the mouse primary somatosensory cortex wS1 (A. Grinvald et al. 1986; Cannestra et al. 1996). IOS has become an imaging technique of fundamental importance in neuroscience able to map changes in light reflectance from the illuminated brain of many species in response to sensory stimulation (Ron D. Frostig and Chen-Bee, n.d.; Amiram Grinvald et al. 2015; Roe 2009). The source of the optical intrinsic signal likely originates in a combination of local vascular changes, metabolic activity and changes in brain-tissue light-scattering. Blood is a major contributor to light absorption in the brain, and, in general, increases in neural activity correlate with increases in cerebral blood volume (CBV) and cerebral blood flow (CBF). Local metabolic changes influence the ratio of oxy- and deoxy-hemoglobin, which have very different absorption spectra (Eaton et al. 1978; Dubova, Ya. Khairullina, and Shumilina 1982). The relative contributions of the different underlying components of intrinsic optical signals depend on the wavelength of the illumination light used (Malonek and Grinvald 1996). With green-yellow light illumination (from ~500 to ~600 nm), total-hemoglobin (HbT) and cerebral blood volume (CBV) are the dominant source of the intrinsic signal. With red light illumination (from ~600 to ~700 nm), IOS preferentially infers the deoxyhemoglobin (HbR). With near infrared light illumination spectrum (from ~700 to ~800 nm), the intrinsic optical signal is dominated by light scattering caused by swelling of intracellular compartments, and perhaps fusion of secretory vesicles with presynaptic membranes during exocytosis (Prakash et al. 2009).

The intrinsic optical signal imaging method can be performed through the intact skull of mice and thus the same region of cortex can be imaged over several weeks for longitudinal functional studies for plasticity assessment (Frostig, Chen-Bee, and Polley 2002). Furthermore, this endogenous optical signal does not require functional activity indicators (e.g. GCaMP) and can thus be performed across various mouse strains to correlate with different techniques during simultaneous recording comparison. However, the amplitude of the intrinsic signals is about one order of magnitude smaller than genetically encoded

calcium indicators like GCaMP3 (Vanni and Murphy 2014) or GCaMP6 (see chapter 3 and 4) (Juavinett et al. 2017; Morone et al. 2017; Ma et al. 2016; C. H. Chen-Bee et al. 2000; Vincis et al. 2015).

2.2. Materials and methods

Animal preparation and surgery

All experiments were carried out in accordance with protocols approved by the Swiss Federal Veterinary Office. In this study we used four transgenic mice (two male and two female, age ~3 months) expressing ChR2 under the Thy1 promoter: mouse strain name B6.Cg-Tg(Thy1-COP4/EYFP)18Gfng/J, JAX mouse number 07612, RRID: IMSR_JAX:007612 (Arenkiel et al. 2007).

We used an intact skull preparation with implantation of an aluminium head-holder to restrain movement. First, the mouse was anesthetized under deep isoflurane. Second, an intraperitoneal injection of 300 µl carprofen (0.5 mg/ml) was administered to the mouse for analgesia. Then, the animal was placed on a stereotaxic frame and the mouse was held tight by a nose clamp. To locally anesthetized the mouse, small drops of lidocaine/bupivacaine was injected below the head skin. Some cream (Pharma Medica AG, Switzerland, Roggwil, VITA-POS) was applied on the eyes of the mouse to prevent drying of the eyes during anesthesia. Once the animal was deeply anesthetized, a small incision of the head skin was done by cutting with scissors and a piece of skin was removed. The skull was cleaned with Ringer solution. The surrounding tissues were disinfected with betadine. After drying the skull, we removed the epithelial tissue on top of the bone by scratching the mouse skull with a scalpel blade. We detached and pushed down the muscles around the skull in order to have a larger optical access to the brain surface and to have a good bond for the glue later. When the skull was clean, we verified that the midline was aligned to the stereotaxic frame and that Bregma (anatomical point on the skull at which the coronal suture is intersected perpendicularly by the sagittal suture) and Lambda (anatomical point of meeting of the sagittal and the lambdoid suture) were at the same height. Next, the implant was glued using cyanoacrylic Loctite glue 401. For a better reproducibility of the experiments, the implant was always put at the same location regarding to Bregma (2.5 mm anterior and 1.5 lateral to Bregma). Once the glue was dry, we made a small chamber of transparent dental acrylic cement (Jet Repair Acrylic) (Guo, Hires, et al. 2014) on the implant and around the dorsal cortex on the bone (above the olfactory bulb, the side of somatomotor cortex, somatosensory cortex, auditory cortex, visual cortex, retrospinal area and anterior cingulate area) to consolidate the whole construct. Finally, to make the surface even, uniform and transparent, a thin layer of Loctite glue 401 applied to the surface. After the surgery, the mouse was put back in its home cage with a bottle of water mixed with ibuprofen, diluted 100x (Algifor Dolo Junior 100mg/5ml 200 ml, Vifor Consumer Health SA). This procedure for implantation of the mouse skull gave a solid, stable and transparent view of the dorsal neocortex for several weeks. All whiskers were trimmed except for the contralateral A1, C2 and D1 whiskers.

Mouse physiology

IOS is a metabolism-based hemodynamic signal and the amplitude of the signal is strongly influenced by animal physiology. It is therefore critical to keep physiological parameters of mice constant during the image acquisition. Mice were lightly anesthetized with ~0.5% isoflurane. If the anesthesia was too deep, intrinsic signals of the mouse vanished and if the anesthesia was lowered, movement-related artefacts dominated. The body temperature of the mouse was maintained at 37°C by a closed-loop system constituted of a heating pad regulated by feedback from a body-temperature probe.

Camera specs and image frame rate

Images were acquired at 10 Hz (corresponding to an exposure time of 100 ms) with 8.7 × 8.7-mm field of view and a detector of 1024 × 1024 pixels (Photon Focus, Lachen, Switzerland, MV-D1024E-40). As the signal is relatively slow, the time resolution was not increased, in order to favor image resolution instead with longer exposure time. The camera detector was a CMOS active pixel (APS) of 12-bit well depth chip that allowed a high sensitivity signal detection of light absorption. It is important to use a high bit depth camera since the measured evoked response comes from a very small modulation of the signal detected, on the order of 10^{-4} (Cynthia H. Chen-Bee et al. 2010). It would be impossible to detect signals in single pairs of frames using a 8-bit camera as it has only 256 grey levels. Since a 12-bit camera has 4096 levels of grey, it was the lowest sensitivity allowing detection of 1 ‰ signal change without averaging several stimulation trials. As CMOS camera chips have a given quantum efficiency (that corresponds to the ratio of photons reaching the sensor converted into electrons) the level of noise of the sensor depends on both the shot noise (which is the number of photons arriving randomly to the sensor) and the temporal dark noise or read noise (which is the inaccuracy into the readout of the voltmeter measuring the generated electrons by the light). The camera used need to have a good signal-to-noise ratio, meaning good quantum efficiency with good well-depth to encode the analog signal into a precise digital output, to resolve the small changes in signal amplitude. The camera was mounted on a stereo microscope (Leica, Wetzlar, Germany, MZ9.5)), which gave the ability to easily change the field of view and the image resolution.

Continuous light excitation

In order to overlay from what region of the dorsal cortex the evoked response arised, a first image of the cortical surface was acquired with green light using a 530 nm fiber-coupled LED (Thorlabs, Newton, New Jersey, USA, M530F2). The green LED was coupled to a Ø1000 μm fiber optic, 0.39 NA, (Thorlabs, Newton, New Jersey, USA, M35L02). For functional imaging, the cortical surface was continuously illuminated with bright red light using a 625 nm fiber-coupled LED (Thorlabs, Newton, New Jersey, USA, M625F2). Since the signal changes measured were very small (in order of 10^{-4}), a very stable light was needed to reduce the noise coming from the illumination. LEDs can provide this very stable illumination over the time. The light intensity should be sufficient to bring signal close to

saturation (~50%) of the camera sensor, where their sensitivity is the highest (and thus the recording noise the lowest) to detect those small changes. Also, as the signal detected was a light absorption and scattering meaning a local decrease in the collected light, it was important to be close to saturation to be able to detect those small decreases in the light intensity.

Mechanical stimulation of mouse peripheral somatosensory system

During functional imaging, different body-parts were mechanically stimulated sequentially by a long glass capillary tube attached to a piezoelectric-element bender (PI Ceramic GmbH, Lederhose, Germany, PICMA Bender PL127.10) (figure 2.1). After trimming of the other whiskers, the remaining right whisker was inserted into the glass tube. The paradigm used was a succession of stim trials and no stim trials of 10 s each separated by a minimum of 5 s intertrial interval. The stimulation was a oscillation of 10 Hz (filtered rectangular pulses) that started after a 4 s baseline period and lasted for 4 s followed by a 2 s of post-stimulus period. In this study, the A1, C2 and D1 whiskers were sequentially stimulated to map the whisker somatotopy in the mouse barrel cortex.

Also, the right forepaw and the right hindpaw were sequentially stimulated by tapping the inside or the outside of paw and fingers with the glass capillary tube. The middle of the tail of the animal and the lip were stimulated with the same piezo system and the same paradigm of 4 sec 10 Hz stimulation.

The piezoelectric element was activated by a computer via a digital-to-analog converter which outputs were filtered and amplified by an external amplifier. The analog outputs to the piezo were filtered to decrease the click-sound that the piezo would make, which would lead to an activation of the auditory cortex. The triggering of the image frame was controlled by the same PCi card (National Instruments, Austin, Texas, USA) that delivered TTL pulses to the camera. The stimulation and the image acquisition were precisely synchronized to correlate the cortical evoked response with the given stimulus at the periphery of the mouse.

As the evoked responses were small changes from baseline activity, it was necessary to average many trials to obtain an obvious response (from 20 to 30 stim trials), since signal-to-noise ratio should increase ideally in proportion to the square root of the number of measurements ($n^{1/2}$).

Visual stimuli

A green LED (and also in some other experiments a blue LED) was put around a black opaque tube to shield the light. The tube extremity was brought around the right eye of the mouse. Visual stimuli to the right eye were delivered by flashing the LED at 10 Hz for 4 sec. Very small amount of light could evoke a response in V1 as the eye is a very sensitive organ.

Auditory stimuli

Two types of auditory stimuli were delivered. One purely auditory was created by increasing the current given to the piezoelectric element. The displacement of the piezo increased in amplitude and made click-sounds at 10 Hz for 4 sec close to the right ear of the mouse. Another one was both tactile and auditory, as the glass tube was moved on the pinna of the right ear of the mouse. By tapping the ear of the mouse, this created both a tactile stimulus and an auditory stimulus as the friction on the ear made noise. Auditory stimuli were delivered by click-sound pulses at 10 Hz for 4 sec.
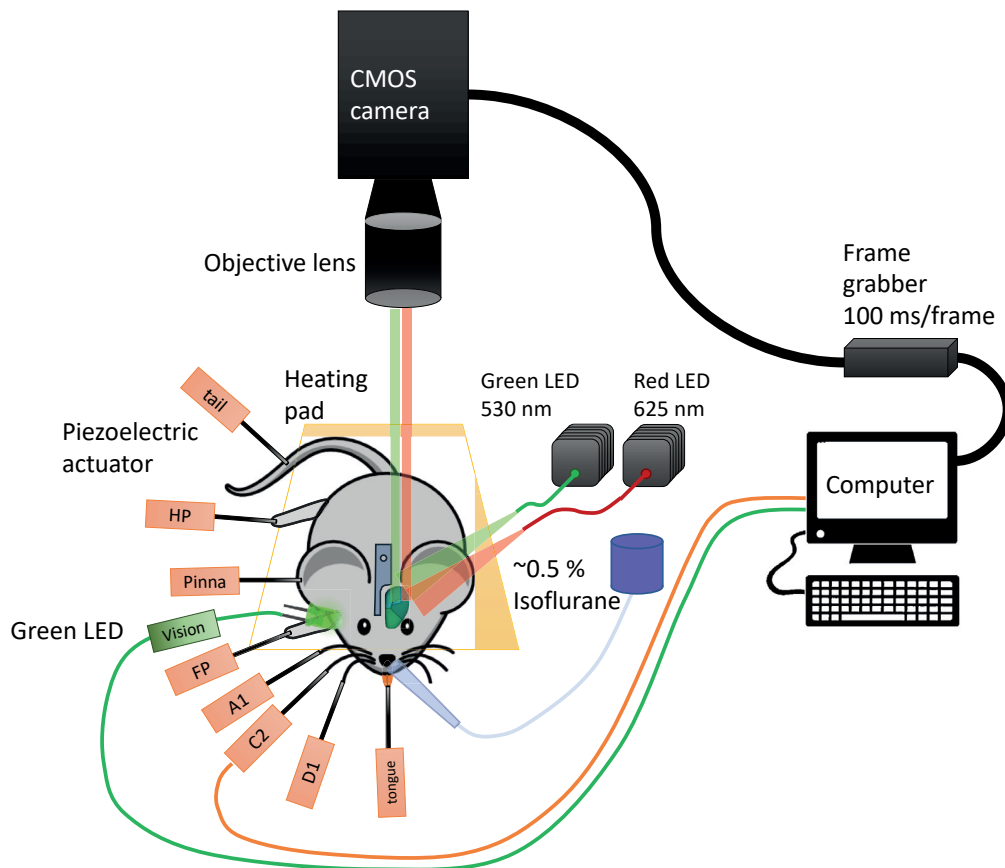

Figure 2.1. Scheme of the set-up used for intrinsic optical signal (IOS) imaging.

The implanted mouse was anesthetized with ~0.5% isoflurane. The mouse was kept at 37°C with heating pad and a body temperature probe feedback system. Left hemisphere of the dorsal neocortex was made transparent by using cyanoacrylic glue preparation. The top of the brain was illuminated by either green or red optic fiber coupled-LED. The light was collected by a highly sensitive 1024 × 1024 pixels CMOS camera through a stereo microscope with adjustable magnification. Different right body parts were mechanically stimulated by a piezoelectric actuator: whisker (A1, C2 or D1), tongue, forepaw (FP), hindpaw (HP), tail, or pinna of the ear. The eye was stimulated by a green or blue LED placed in a black tube close to the right eye to shield the stimulus light. The stimulus was a 10 Hz square pulse train of 4 s duration. Both the frame trigger and the stimulus outputs were delivered and synchronized by a PCI board of one computer.

Optogenetic stimulation

A blue light pulse at 10 Hz for 1 s duration was delivered on top of the cortex with a Ø1000 µm optic fiber (Thorlabs, M71L02) using a fiber-coupled LED at 470 nm (Thorlabs, M470F3).

Analytical procedure to process IOS images

During image acquisition, a repetition of 20 to 30 interleaved stim and no stim trials was performed.

First step of the image processing was to separately average the trials for each condition (stim and no stim) and for each stimulated body part. Then a baseline was calculated by averaging all the frames of the 4 s prior to the stimulus. Finally, a ΔR/R was computed by using the following formula:

$$\Delta R/R(i,j,t) \ = \ \frac{R(i,j,t) - R_0(i,j)}{R_0(i,j)}$$

The image plotted in figure 2.2. was an average of all the frames after stimulus onset divided by baseline - 1.

The second step consisted of smoothing the obtained averaged raw image with a Gaussian filter to remove the high frequency spatial noise. Usually, for an image of 1024 × 1024 pixels, a sigma of 10 and a filter size of 100 × 100 pixels were used for the Gaussian filter. This mathematical method could decrease the overall noise of the averaged image.

The third step was selecting a region of interest (ROI) around the targeted sensory area in order to detect the local minimum of the image. Indeed, in some cases, some artifacts at the boundaries of the image or in neighboring places were observed, preventing the primary sensory response to be a global minimum in the processed image. Those artifacts could come from micromovement of the mouse or blood vessels or could be due to spontaneous activity emerging from the physiology of the mouse (anesthesia depth, secondary satellite areas).

The fourth step was an evaluation of the amplitude and width of the evoked signal decrease in the sensory cortex. We selected an area centered on the targeted cortical area and we projected and averaged on one dimension the image along each x and y axis to get a 1D-vector. This vector was the average amplitude for either column or row of the selected area (meaning that the dimension of this vector goes along pixel counter, not time as sometimes for 1D-vectors).

The fifth step consisted of selecting a closer ROI centered on the evoked response and averaging those pixels for every frame such that a single averaged value was obtained per frame. This vector reflected the time course of the evoked response. A slow decrease of the signal was observed after the 4 sec baseline.

The sixth step was to plot the vector along time by changing frame number by time (multiplied by the frame rate, which was 100 ms).

The seventh and last step was to overlay the contour plot, corresponding to the 5% percentile value of the image, with the anatomical green image. The pattern of the blood vessels could be used to identify the center of the stimulated sensory cortex.

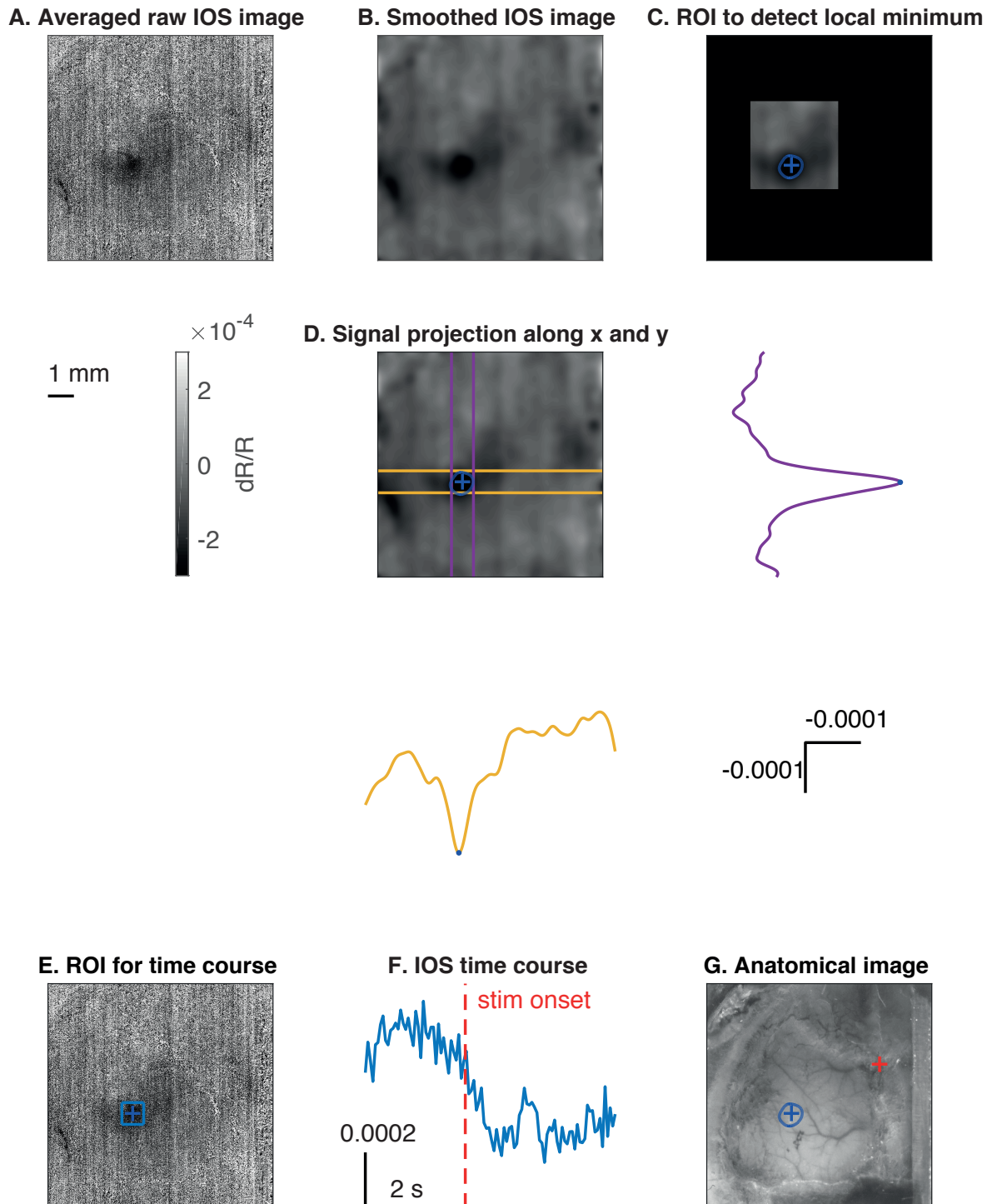# Methods for intrinsic optical signal (IOS) image processisng

A. Averaged raw IOS image

B. Smoothed IOS image

C. ROI to detect local minimum

1 mm

$\times 10^{-4}$

2

0

dR/R

-2

D. Signal projection along x and y

-0.0001

-0.0001

E. ROI for time course

F. IOS time course

stim onset

0.0002

2 s

G. Anatomical image

Figure 2.2. Procedure for image processing of intrinsic optical signal (IOS) images.

A. Stim trials were first averaged. A baseline was computed by averaging the period before the stimulus onset. This baseline image was then subtracted to the entire movie pixel by pixel. This baseline image was finally divided to compute ΔR/R. ΔR/R was averaged along the entire stim period and was plotted on panel A.

B. The averaged ΔR/R image was smoothed using a Gaussian filter to eliminate the high frequency spatial component of the image.

36

C. A region of interest (ROI) was drawn around the activated region to find the local minimum of the collected light reflection from the cortex. A contour was plotted using the 5% percentile of the signal, meaning that 10 % of the pixels of the image are below this value.

D. The projection along either x or y axis were computed in a region around the local minimum found. This showed the signal spatial profile with a Gaussian shape decrease of the signal.

E. Another ROI was drawn on the activated region of 100 × 100 pixels to evaluate the time course of intrinsic signal along the 10 sec trial.

F. Representation of the time course of the averaged intrinsic signal within the ROI along the trial. After 4 sec of baseline period, a 4 sec stimulus was delivered to the mouse and a 2 sec post-stimulus period followed.

G. Overlay of the contour obtained in panel C, on the anatomical green image of the skull surface with the vasculature pattern and the Bregma (represented with a red cross).

2.3. Results

Whole body sensory map

In figure 2.3, the whole body sensory map for each mouse was obtained by computing the contour of the different evoked responses and overlaid on the anatomical image of the vasculature. The contour corresponded to the 1% percentile of the minimal pixel values. Bregma position was located 1.9 mm frontal and 3.4 mm medial to the C2 whisker representation in wS1. The same color code was used for all the 4 maps.

The summary sensory map of all four mice was computed by aligning all the brains on C2 wS1 reponse. The alignment was performed by simple translation of the different images. For sake of clarity, only the minimum value for each body part was represented with a cross. There was a small variability in the center of the evoked response in the different mice.

Whole body sensory map using wide-field intrinsic optical signal (IOS) imaging (n=4)
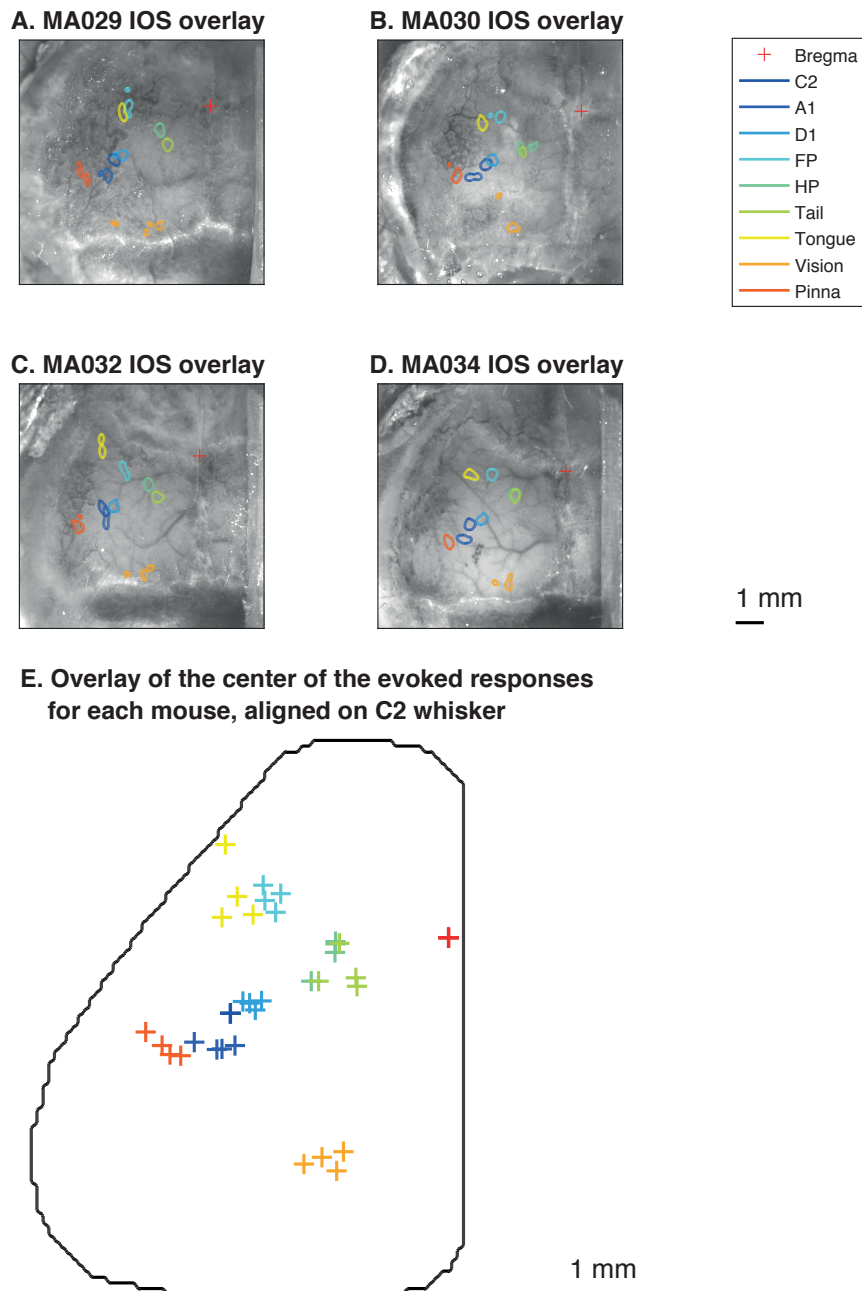

A. MA029 IOS overlay

B. MA030 IOS overlay

Legend:
- + Bregma
- C2
- A1
- D1
- FP
- HP
- Tail
- Tongue
- Vision
- Pinna

C. MA032 IOS overlay

D. MA034 IOS overlay

1 mm

E. Overlay of the center of the evoked responses for each mouse, aligned on C2 whisker

1 mm

Figure 2.3. Whole body sensory map using wide-field intrinsic optical signal (IOS) imaging.

A-D. Sensory map for 4 different mice. 3 different right whiskers were sequentially stimulated: A1, C2 and D1, right forepaw (FP), right hindpaw (HP), tail, tongue and the pinna of the right ear were mechanically stimulated at 10 Hz using a piezoelectric actuator. Light flashes pointed toward the right eye were used to deliver visual stimuli. After performing the image processing described in figure 2.2, contours of all the sensory evoked responses were computed for each mouse and overlaid on the green anatomical image of the corresponding mouse dorsal cortex. Bregma was represented with a red cross.

E. An overlay of all the mice sensory evoked responses was represented by a cross located where the minimal response was found. The sensory maps were all aligned on C2 response (dark blue cross). Bregma was represented with a red cross.

Quantification of primary sensory cortical regions

In order to quantify the location of whisker primary sensory cortex wS1 (for C2, A1 and D1), of forepaw, hindpaw, tail and tongue primary sensory cortex, of primary visual cortex and primary auditory cortex we first estimated Bregma location using the green anatomical image. We placed Bregma at the junction of the sagittal suture (midline) and the coronal suture. The distance between Bregma and the reported maxima of figure 2.3 was calculated using the spatial resolution of 118 × 118 µm.

Mouse name	C2 ML | AP	A1 ML | AP	D1 ML | AP	FP ML | AP	HP ML | AP	Tail ML | AP	Tongue ML | AP	Vision ML | AP	Pinna ML | AP
MA029	3.42 | -1.93	3.62 |- 2.47	3.13 | -1.78	2.92 | -0.01	1.84 | -0.86	1.53 |- 1.40	3.08 | -0.45	1.82 | -4.30	4.69 | -2.21
MA030	3.12 | -1.85	3.66 | -2.28	2.93 | -1.67	2.60 | -0.15	1.91 | -1.36	1.80 | -1.36	3.25 | -0.41	2.02 | -4.11	4.14 | -2.33
MA032	3.39 | -1.86	3.27 | -2.35	2.97 | -1.81	2.66 | -0.35	1.77 | -0.95	1.44 | -1.46	3.42 | 0.67	1.64 | -3.94	4.25 | -2.48
MA034	3.37 | -2.08	3.50 | -2.61	2.91 | -1.89	2.62 | -0.28	1.80 | -1.03	1.74 | -1.03	3.27 | -0.32	2.00 | -4.24	4.12 | -2.71
Average	**3.31 | -1.93**	**3.51 | -2.43**	**2.98 | -1.79**	**2.70 | -0.20**	**1.83 | -1.05**	**1.63 | -1.31**	**3.25 | -0.13**	**1.87 | -4.15**	**4.30 | -2.43**
Std	**0.11 | 0.09**	**0.15 | 0.13**	**0.09 | 0.08**	**0.13 | 0.13**	**0.05 | 0.19**	**0.15 | 0.17**	**0.12 | 0.46**	**0.15 | 0.14**	**0.23 | 0.19**

Table 2.1. Coordinates of the cortical region for each individual mouse and the average location.
The number on the left corresponds to mediolateral axis and the number of the right corresponds to anteroposterior axis distance (in mm) from Bregma.

On average, C2 whisker primary somatosensory cortex wS1 is 3.31 ± 0.11 mm lateral to Bregma, -1.93 ± 0.09 mm posterior to Bregma. A1 whisker primary sensory cortex wS1 is 3.51 ± 0.15 mm lateral to Bregma, -2.43 ± 0.13 mm anterior to Bregma. D1 whisker primary sensory cortex wS1 is 2.98 ± 0.09 mm lateral to Bregma, -1.79 ± 0.08 mm anterior to Bregma. FP primary sensory cortex fpS1 is 2.70 ± 0.13 mm lateral to Bregma, -0.20 ± 0.13 mm anterior to Bregma. HP primary sensory cortex hpS1 is 1.83 ± 0.05 mm lateral to Bregma, -1.05 ± 0.19 mm anterior to Bregma. Tail primary sensory cortex tS1 is 1.63 ± 0.15 mm lateral to Bregma, -1.31 ± 0.17 mm anterior to Bregma. Tongue primary sensory cortex tjS1 is 3.25 ± 0.12 mm lateral to Bregma, -0.13 ± 0.46 mm anterior to Bregma. Primary visual cortex V1 is 1.87 ± 0.15 mm lateral to Bregma, -4.15 ± 0.14 mm anterior to Bregma. Primary auditory cortex A1 is 4.30 ± 0.23 mm lateral to Bregma, -2.43 ± 0.19 mm anterior to Bregma.

Signal along time in primary sensory cortex

The figure 2.4 showed that the signal measured was a decreased response. There is a latency of 725 ± 150 ms (corresponding to the time when the signal passes through the threshold of 4 times the standard deviation of the baseline period). This was a relatively slow response. As mentioned in the introduction (chapter 1.1.4) intrinsic signal comes from slow mechanisms of local physiological changes of the vasculature that occurs much slower than the neuronal response. This is why a delay of the response was always observed.

The intrinsic signal was noisy along the time mainly because of the artifact of the heartbeat and of the small physiological changes that were occuring and provoking micro movements of the brain. For all those reasons, we had to average over several trials to have a robust and reproducible evoked response.

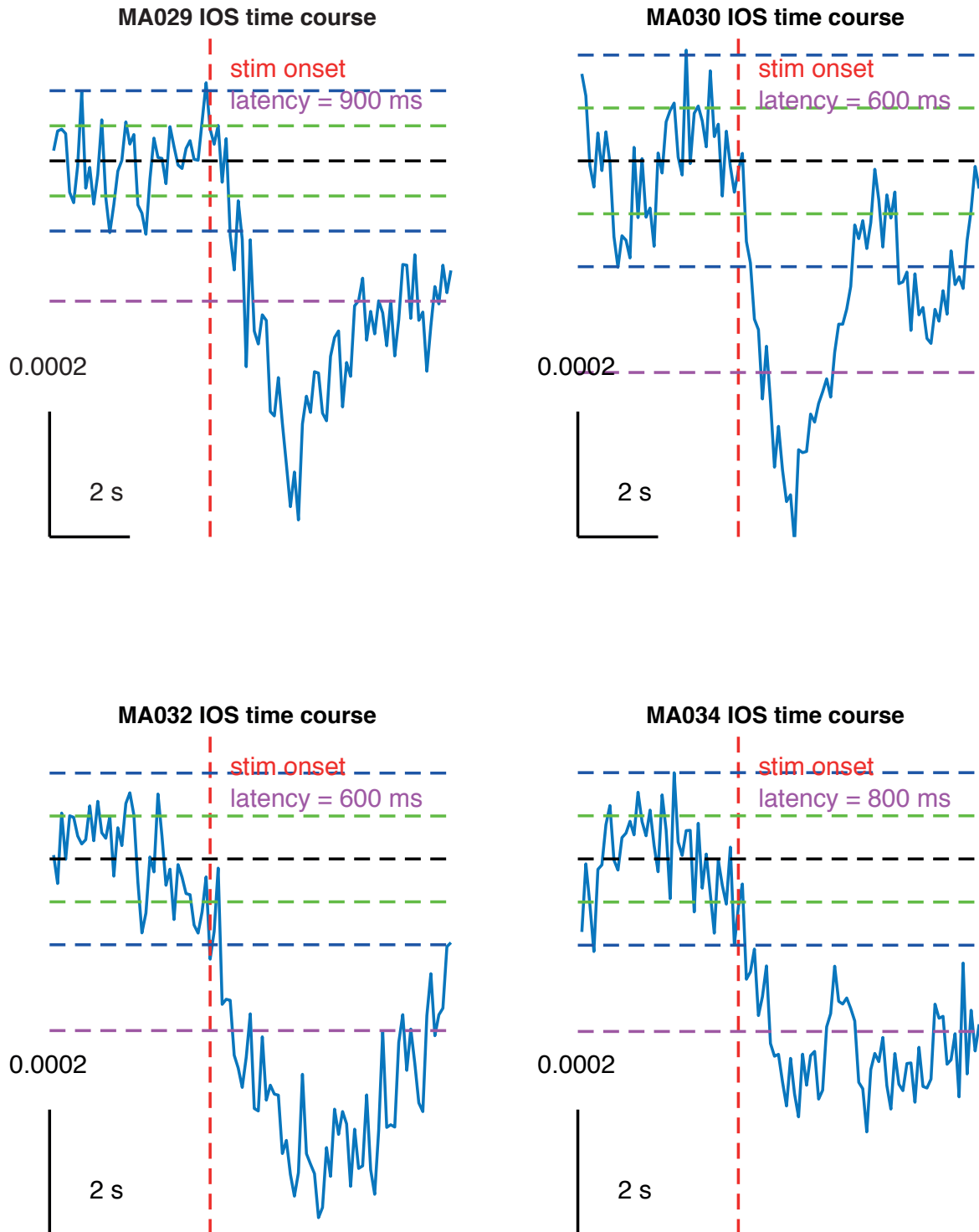## Latency of intrinsic optical signal (IOS) for C2 stim

Figure. 2.4. Latency of the intrinsic signal for C2 stim trials.

The latency was corresponding to the frame when the signal passed below the threshold of 4 times the standard deviation of the baseline (4 s prestimulus time window).

Connectivity of the intrinsic signal

The intrinsic signal evoked propagation depends on the functional organisation of the stimulated cortex, and the number of cortical columns and layers recruited. The spread of the signal results from the functional representation of the specific stimulus. It depends on the topographical nature of cortical organization. More precisely, it relies on somatotopy for tactile stimuli, retinotopy for visual and tonotopy for auditory stimuli. To address this fundamental question, it is important to have a well defined stimulus: e.g. single whisker deflections for the barrel cortex, single color illumination for the visual cortex or pure tone stimulation for the auditory cortex. The spatial extent of the signal from the peak location (e.g. center of the stimulated cortical barrel) constitutes the cortical activity propagation. It largely depends on the physiology of the animal (if the animal is not deeply anesthetized, not in hypoxia, the body temperature) and the strength of the stimulus. It is also affected by the size of the receptive field of the cortical neurons and the number of recruited neurons. All these different parameters affects the amount of activated cortex by a point-like stimulation. The signal decrease observed has a Gaussian like shape centered of the peak location and is called the cortical point-spread (Ron D. Frostig and Chen-Bee, n.d.; Polley, Chen-Bee, and Frostig 1999). This is why, it is usually prefered to give the peak location of the signal as the spread of the signal can be affected on the physiology of the mouse (biological noise), the stimulation strength, frequency and direction, the sensitivity of the camera (electrical noise) and the image processing (level of the contours for example) (see figure 2.3.E).

An optogenetic stimulation of the cortex should signal to multiple downstream brain regions, which could evoke intrinsic optical signals. When wS1 was stimulated by blue light, the contralateral wS1 of the right hemisphere was activated as well as frontal parts of the cortex as wM1. This showed that intrinsic optical signal imaging is sufficiently sensitive to measure evoked signals in projecting parts of the cortex provided that the activation is strong enough to recruit a hemodynamic response in the secondarily activated regions see (figure 2.5).

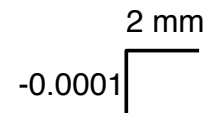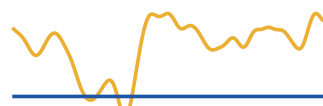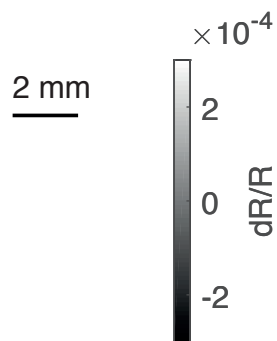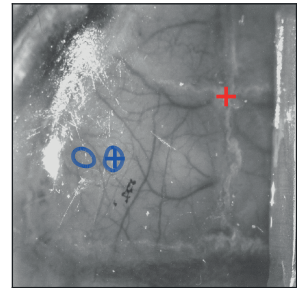# Propagation of the intrinsic signal in secondary cortical regions
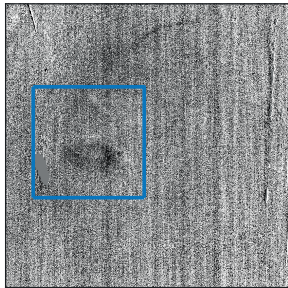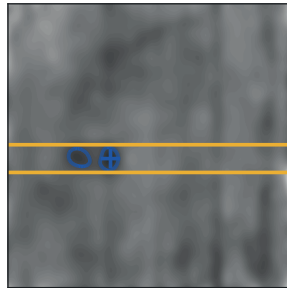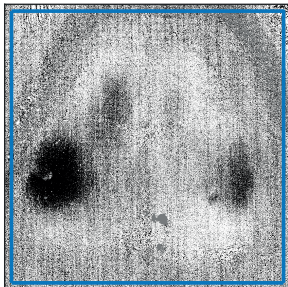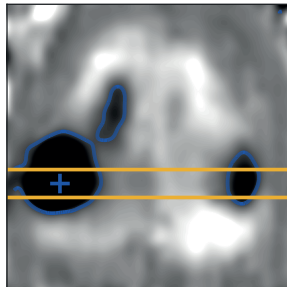
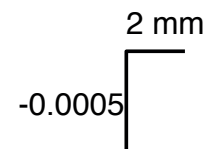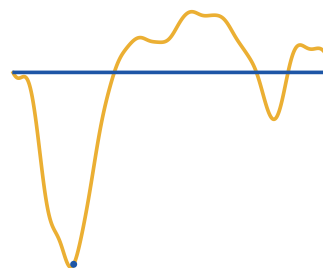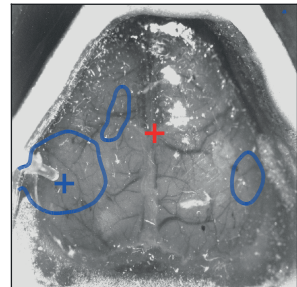**Figure 2.5. Intrinsic optical signal images showing how the intrinsic signal propagated in secondary cortical regions.**
A. Intrinsic optical signal images were acquired during stimulation of C2 whisker at 10 Hz for 4 s. An averaged ΔR/R image of the stim trials was computed and a ROI was placed on the image around the activated regions.

B. The averaged ΔR/R image obtained was smoothed using a Gaussian filter to eliminate the high frequency spatial component of the image. A contour of the 5% percentile of the signal was plotted around the local minimum located in wS1. The second spot lateral to wS1 corresponded to wS2. The projection of the signal showed a minimum value on wS1 and a second local minimum on wS2.

C. An overlay of the contours on the green anatomical image with the vasculature pattern confirmed that the signal corresponded to wS1 and wS2.

D. Intrinsic optical signal images were acquired during optogenetic stimulation of wS1 cortex at 10 Hz for 1 s of Thy1-ChR2-YFP mouse. An averaged ΔR/R image of the stim trials was computed and a ROI was placed on the image around the activated regions, corresponding to the entire brain.

E. The averaged ΔR/R image obtained was smoothed using a Gaussian filter to eliminate the high frequency spatial component of the image. A contour of the 10% percentile of the signal was plotted around the local minimum located in wS1. The contralateral wS1 of the right hemisphere was activated by the optogenetic stimulation and also ipsilateral wM1 was activated. The projection of the signal showed a large minimum value on left wS1 and a second local minimum located on right wS1 (contralateral to the stimulation).

F. An overlay of the contours on the green anatomical image with the vasculature pattern confirmed that the signal corresponded to both left and right wS1 and wM1 of the ipsilateral frontal part of the cortex.

2.4. Discussion

In the laboratory, intrinsic optical imaging was used to map whisker primary somatosensory cortex wS1 but not only. Indeed, it was possible to map secondary areas like wS2 and also tongue jaw motor cortex tjM1. If the animal was in perfect physiological condition, with a very transparent preparation (sometimes also through a chronically implanted cranial window used for two-photon imaging) and with a strong and repetitive sensory stimulation, it was possible to obtain secondary cortical regions. For wS2, there were some evidence showing that there are some direct parallel thalamocortical projections toward wS1 and wS2. This technique of mapping secondary areas worked only for well separated cortical regions like for the whisker system where wS1, wS2 and wM1 are sufficiently far apart.

Optogenetic stimulation could evoke long range activation of different part of the cortex, even in the other hemisphere. This method could be used to investigate cortical connectivity maps in the mouse cortex. Alternative methods, like combining optogenetic with GCaMP imaging requires a very complicated light pathway to collect emission light of the fluorophore used while blocking both excitation of the indicator and excitation and emission lights of the rhodopsin. Moreover, the crossing of mouse lines could be very tedious work that might need many mice to obtain the correct genetic construct.

This raised the question of what cortical layers contribute to the intrinsic signal? Some in vitro intrinsic cortical imaging experiments in primary somatosensory cortex (the upper and lower limb and trunk representations as well as the barrel field) showed that high-intensity deep layers stimulation and superficial layers responded differently. After stimulation of input

cortical layer 4 a rapid and large activation of superficial layers 2/3 (more narrow) and I (larger spread) propagated along the cortical column (Kohn et al. 2000). The repetitive activation of the input layer 4 could potentially propagate through cortico-cortical connections of superficial layers and generate secondary evoked intrinsic signals. In vivo wide-field imaging signal came from the sum of all the activated layers of a cortical column that provoked a metabolic response.

Intrinsic optical signal imaging is one of the technique measuring metabolic response evoked by the recruitment of a local neuronal population. Other methods are available to measure large scale parameters of the endogenous physiological response to neuronal activation in the brain. Functional magnetic resonance imaging fMRI measures BOLD signal, which comes from the hemodynamic response. The change in oxy and deoxy hemoglobin (that have different magnetic properties) can be detected by T2* contrast acquisition sequence. Functional imaging fMRI can record the entire brain activity but the spatial (~1 mm) and temporal (~1 s) resolutions are relatively poor compared to other electrophysiological techniques preventing this technique to resolve short and precise neural activity patterns. This method is well developed in human (noninvasive technique), monkey and rat research but the small size of the mouse brain makes it difficult to get images with a large SNR and thus reliable signals. Up until now, almost exclusively anesthetized mice were scanned (Guilfoyle et al. 2013; Jonckers et al. 2015; Niranjan et al. 2016; Bukhari et al. 2017).

Electroencephalography EEG measures difference of potential generated by brain activity between two electrodes placed at the surface of the scalp. This technique has a good temporal resolution (~1 kHz) but a poor image resolution (~1 mm). This method is also well developed in humans because it is not invasive, but only a few studies have been published in mice (Choi et al. 2009; Lee, Shin, and Choi 2009; Lee et al. 2011).

An alternative optical measurement of intrinsic signals in mice is the mitochondrial flavoprotein autofluorescence imaging (M. Takahashi et al. 2017; Ma et al. 2016; Chery et al. 2011). Interestingly, flavoprotein autofluorescence is often measured at wavelengths similar to GFP. The flavoproteins are mainly located in mitochondria due to their redox power used in cellular respiration to produce ATP for the neurons. The oxidation of the flavoproteins during aerobic metabolism is closely coupled to neuronal activation. The fluorescence of the flavoproteins changes with the neural activity evoked by sensory stimulation. The signal coming from the autofluorescence of the flavoproteins gives the ability to map the mouse brain with high spatial localisation without using any dyes or indicators in intact brains. Flavoprotein autofluorescence imaging has the advantage of being restricted to subcellular compartments and represents neuron's metabolism (and not glial). This relatively new technique could present a potential alternative to intrinsic optical imaging for sensory mapping of a large variety of mouse strains (Issa and Robert Husson 2009).

The ideal optical imaging technique would faithfully and reliably measure local neural activity for both spiking and subthreshold activity at cellular resolution without exogenous reporters in any mouse strains. As this method does not exist, intrinsic signal imaging tries to fulfil partially this role and presents a good alternative.

3. Tongue-jaw sensory and motor cortex mapping

Author contributions

Johannes Mayrhofer, Matthieu Auffret and Carl Petersen designed the project. Matthieu Auffret wrote the manuscript. Matthieu Auffret wrote the MATLAB script for data acquisition. Matthieu Auffret carried out all experiments and analyzed data.

3.1. Introduction

Whisker primary sensory and motor cortex

Mice are nocturnal animals. In complete darkness they use their whiskers to probe their environment and are able to extract tactile information on shapes and textures of the objects (Brecht 2007; Petersen 2007; Mathew E. Diamond et al. 2008; Bosman et al. 2011; Feldmeyer et al. 2013). Mice typically move their whiskers rhythmically back and forth at a frequency of about 10 Hz to probe the space in the vicinity of their snout (W. I. Welker 1964). Tactile information is actively acquired and processed in the cortex by interactions between sensory inputs and motor outputs. During active touch, the self-generated movements create direct inputs from whisker object contact to the somatosensory cortex that integrates those complex sensory signals, and in return refine the motor outputs by precise motor control. There is a close interaction between sensory and motor pathways (Kleinfeld, Ahissar, and Diamond 2006).

A brief whisker deflection generates an activation signal that first emerges in the whisker primary somatosensory cortex (namely the barrel cortex, wS1) and then spreads toward the whisker primary motor cortex (wM1). The spread of information between sensory and motor cortex can be regulated by behavior. In some trials a passively applied whisker stimulation can lead to self-generated whisker movements. This behavioral evoked response suggests that motor control plays an important role in tactile sensory perception integration coming from a close interaction between wS1 and wM1 (Ferezou et al. 2007).

Whisker movements can be evoked by directly stimulating the whisker primary motor cortex generating an oscillatory protraction of both ipsi and contralateral whiskers (Brecht, Schneider, et al. 2004; Haiss and Schwarz 2005; Sreenivasan et al. 2016; Auffret et al. 2018) or the barrel cortex generating a prolonged retraction of the contralateral whisker and a oscillatory protraction of the ipsilateral (Matyas et al. 2010; Sreenivasan et al. 2015; Auffret et al. 2018), whereas a stimulation of the whisker primary somatosensory cortex makes the mouse head turning toward the "supposed" object to explore it while retracting the whisker touching as a protective movement. Another study showed that whisker motor cortex activity suppresses contralateral whisking (Ebbesen et al. 2017). The internal sensorimotor reciprocal interactions make the mouse behave appropriately with the external world.

Tongue/jaw primary sensory and motor cortex

To be able to drink water, mice need to rapidly and repeatedly move their tongue into the water and back in their mouth, while opening and closing the jaw to collect water from the environment and to swallow the drop of water (Lin et al. 2013). They use their tongue to scoop water into their mouth. This repetitive movement is called 'licking'. Tongue and jaw muscles are innervated by motor neurons which are located in the hyperglosal nucleus. These neurons in turn are controlled by a network of neurons in the brainstem which form a central pattern generator. This natural behaviour of tongue/jaw motor action to drink liquids is accompanied by two sensory feedbacks: touch and taste. Touch sensory feedbacks allow the mouse to point its tongue in the right direction and take water to its mouth (Lin et al. 2013).

Electrical stimulation of the primary jaw motor area tjM1 in the rat cortex could evoke rhythmical jaw movements resembling of mastication (Sasamoto, Zhang, and Iwasaki 1990). The first movement evoked by stimulating tongue/jaw-related motor cortex is a jaw opening followed by high frequency (5-7 Hz) simple opening-closing movements of the jaw. Electromyography in the anterior digastric muscles of the rats showed time-locked signals to each stimulus pulse. Electrical stimulation in the ventral part of the insular cortex also evoked rhythmical jaw movements. In contrast, this movement started with a jaw closing movement. The movements of the jaw were large and complex at low frequency (3-4 Hz). The jaw was moving laterally or sagittally, depending on where the stimulation was. The activity in the anterior digastric muscles did not show the stimulus-locked component. Interestingly, ablation of one of these two areas did not affect the pattern of movement observed when stimulating the other remaining area, meaning that those two areas are working independently.

In mice, both optical (Ayling et al. 2009) and electrical microstimulation delivered in the anterior-lateral motor cortex ALM (2.0 mm lateral and 2.4 mm anterior to Bregma) can reliably evoke movements of the tongue, jaw and lip (Komiyama et al. 2010). In this study, they also injected a retrograde transsynaptic tracer expressing GFP in the mouse tongue of the mouse. Four days after injection, they found clusters of GFP-positive layer 5 pyramidal neurons bilaterally in the posterior-medial motor cortex PMM (1.2 mm lateral and 0.3 mm anterior to Bregma). These two distinct regions of the cortex ALM and PMM project to the brain stem where rhythmic licking is generated. Inactivation of one of this two areas impaired licking of the mice. Activity in both ALM and PMM is therefore required for voluntary licking.

Some ramping preparatory activity for licking was detected in ALM, suggesting that this cortical region might be playing an important role in decision making in mouse behavior or at least in motor planning and predicting a lick onest (Guo, Li, et al. 2014; T.-W. Chen et al. 2017; Svoboda and Li 2018).

As for whisker system, it seems that tongue/jaw sensorimotor cortex plays an important role in fine movement of the tongue and to start the oscillatory movement for licking that is then take over by the brain stem.

The goal of the work presented in this chapter is to map the sensory and motor parts of the cortex for tongue and jaw in anesthetized mice using wide-field calcium imaging.

3.2. Materials and methods

Animal preparation and surgery

All experiments were carried out in accordance with protocols approved by the Swiss Federal Veterinary Office. In this study we used five transgenic mice (two male and three female, age between 2 to 4 months) expressing GCaMP6f under the Thy1 promoter: mouse strain name C57BL/6J-Tg(Thy1-GCaMP6f)GP5.17Dkim/J, JAX mouse number 025393, RRID: IMSR_JAX:025393 (T.-W. Chen et al. 2013; Dana et al. 2014). This mouse line has a strong expression of GCaMP6f in cortical layers 2/3 and in layers 5 and 6 but a low expression in layer 4 (figure 3.1).

We used a transparent skull preparation in combination with an implantation of an aluminium bar to restrain head movement. Before any surgical intervention mice were deeply anesthetized with isoflurane (3% in pure oxygen, 1 L/min) and injected intraperitoneally with 300 µl of carprofen (0.5 mg/ml) for analgesia. After induction of anaesthesia isoflurane concentration was reduced to (1.5%). The temperature of the mice was maintained at 37°C by a heating pad controlled by a closed-loop system with a body temperature probe. Before scalping the mouse skin, a local injection of lidocaine/bupivacaine was done subcutaneously at the place of scalpel insertion. Once the skin above dorsal cortex was removed, the exposed tissue was disinfected by application of betadine. Afterwards the epithelium tissue on the skull was removed by scratching the bone surface with a scalpel blade. The bone was cleaned and residual bleedings were stopped with cotton tips and Ringer solution. Bregma and Lambda were aligned at the same height and along the anteroposterior axis using a stereotaxic frame. The skull was covered by a layer of cyanoacrylic glue (Loctite glue 401) before the implant was placed on the cleaned skull. The implant was always put at the same coordinates relative to Bregma (most anterior part of implant was at 2.5 mm anterior and 1.5 lateral on top of the right hemisphere). This allowed a good reproducibility on the location of the imaged left hemisphere with respect to the fixed camera (maybe give number here, SD of Bregma over mice). A second layer of cyanoacrylic glue was applied on the implant and the first layer of glue to homogenise the preparation. After one day of drying of the glue, the preparation gave a very transparent and stable view of the cortex below and stayed transparent for several weeks. After the surgery, the mouse was put back in its home cage and ibuprofen (Algifor Dolo Junior 100mg/5ml 200 ml, Vifor Consumer Health SA) was mixed in its drinking water, diluted 100x. Before imaging was started all whiskers were trimmed except the C2 right whiskers (the whiskers on the left side were kept intact). This procedure for implantation of the mouse skull gave a reliable, stable and transparent preparation of the dorsal neocortex for several weeks.
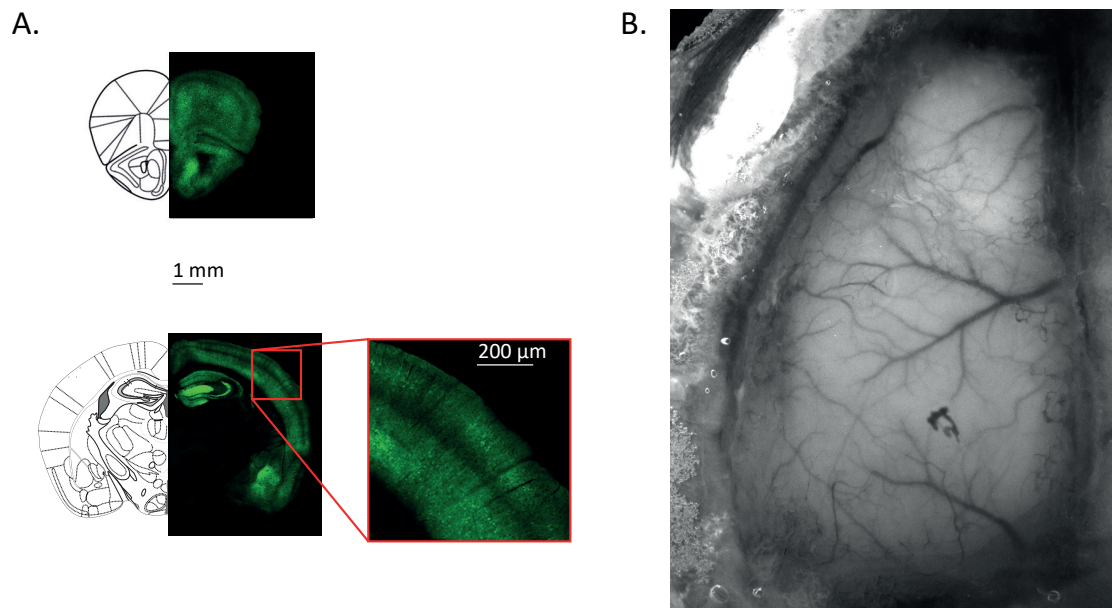
Figure 3.1. Transgenic mouse line Thy1-GCaMP6f expression

A. GCaMP6f fluorescence in fixed coronal slices of a Thy1-GCaMP6f mouse imaged at 16× magnification at two different anterior–posterior locations, ~2.10 mm frontal to Bregma (close to wM2, left image) and ~1.48 mm posterior to Bregma (center image) where we observed the barrel cortex structure of wS1. The images were downsampled 6 times which produced some averaging and smoothing of the slices resulting into an image resolution of 4.8 × 4.8 × 5 µm. Schematic drawings were adapted from Paxinos and Franklin (Paxinos and Franklin 2004). A zoomed-in version of the barrel cortex was displayed (right image). Layers 2/3, 5 and 6 pyramidal neurons and their dendritic arborizations extending to superficial layers were observed. Layer 4 had low GCaMP6f expression.

Images of the mouse were acquired using a custom-made whole-brain serial two-photon tomography system (Ragan et al. 2012; Amato et al. 2016; Han et al. 2018). The objective is a 16× (Nikon). Original image resolution is 0.8 × 0.8 µm for xy-plane and 5 µm for z-plane.

B. Image of the raw fluorescence 68 days after implantation showing how spatially uniform GCaMP6f signal was and how transparent and stable the prep was. We can also clearly distinguish the blood vessels on top of the cortex.

Tactile stimulation of C2 whisker and tongue

Mice were lightly anesthetized with ~0.5% isoflurane. The temperature of the mice was maintained at 37°C by a heating pad controlled by a closed-loop system with a body temperature probe. C2 whisker of the mice was placed into a small capillary tube attached to a piezoelectric actuator (PI Ceramic GmbH, Lederhose, Germany, PICMA Bender PL127.10) and stimulated by rostrocaudal oscillations of 25 Hz for 400 ms.

The tongue of the mice was pulled out of the their mouth with small tweezers. A glass capillary tube bounded to a piezoelectric actuator was tapping the tongue with the same oscillations for the whisker at 25 Hz for 400 ms. The Gaussian-shaped curve stimulation was

delivered by a digital-to-analog converter (National Instruments, Austin, Texas, USA) controlled by a custom written routine in Matlab.

Wide-field calcium imaging

Wide-field calcium imaging was performed on a custom-built setup. A narrow banded blue excitation light was produced by bandpass filtering 485 ± 20 nm the light coming from halogen lamp (Olympus, Japan) (figure 3.2). The excitation light was reflected using a long pass dichroic 495 nm cut-off wavelength and focused onto the cortical surface with a 50 mm camera lens (Nikon, Japan). Green fluorescence from GCaMP6f emission was collected via the same optical pathway, but passing the dichroic and filtered at 525 ± 50 nm, and focused onto the sensor of a high-speed MiCAM Ultima (Scimedia) camera via a 50 mm video lens (Navitar, Japan). This high-speed CMOS camera has a detector with 100 × 100 pixels. The resulting field of view was 10 × 10 mm, and therefore each pixel collected light from a cortical region of 100 × 100 µm. To collect an anatomical reference image for each imaging session the top of the transparent skull was illuminated with a fiber (M71L02 - Ø1000 µm, 0.48 NA, SMA-SMA Fiber Patch Cable, Thorlabs, USA) coupled green LED (530 nm, M530F2, Thorlabs, USA). Images were collected with 10 ms temporal resolution and analyzed offline using custom written routines in MATLAB (Mathworks, Natick, Massachusetts, USA).
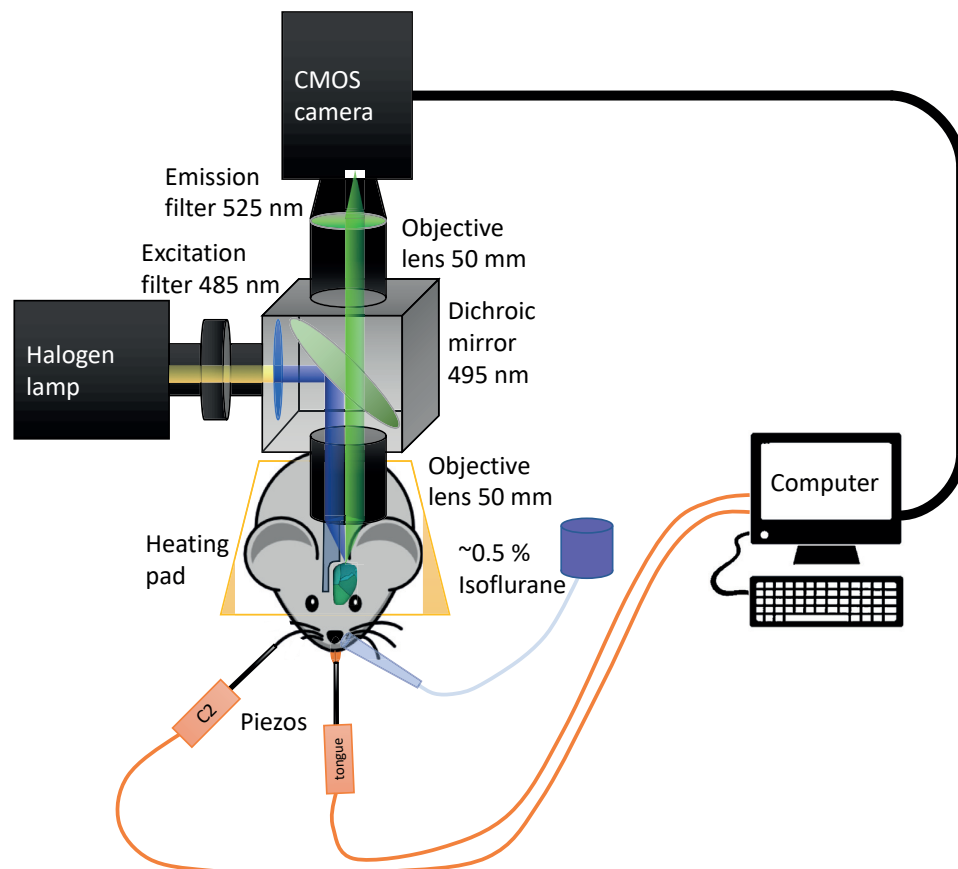

Figure 3.2. Experimental setup for whisker and tongue sensory-motor mapping

The left hemisphere of Thy1-GCaMP6f mice was continuously excited by 485 nm (± 20 nm width of excitation) blue light wide beam. The light was reflected by a longpass dichroic mirror at 495 nm through a 50 mm focal length camera lens to focus the beam on the whole cortical surface of the left hemisphere. The emitted green light was collected by the objective lens, passed through the dichroic mirror and was then filtered by a green filtering light at 525 ± 50 nm and focused onto a high-speed CMOS sensor camera by a second objective lens. The image frame rate of the camera was 10 ms/frame. Mice were anesthetized with ~0.5% isoflurane and maintained at 37°C with a heating pad. Either C2 whisker or tongue were stimulated by piezoelectric actuator with a 25 Hz Gaussian-shape of 400 ms duration.

Image processing

During image acquisition, a single trial consisted of 2 s prestimulus and 3.12 s poststimulus. For each stimulus condition 50 repetitions (trials) were acquired. The first step of the image processing was to average those trials for each stimulus condition to create an average movie F, where $F(i,j,t)$ indicates the fluorescence of single pixel (ith row, jth line) measured at time point t. Then a baseline image $F_0(i,j)$ was calculated by averaging 5 frames prior to the stimulus onset (-50 ms to 0 ms). Finally, a $\Delta F/F(i,j,t)$ was computed by using the following formula:

$$\Delta F/F(i,j,t) \; = \; \frac{F(i,j,t) - F_0(i,j)}{F_0(i,j)}$$

The second step consisted of averaging over the first 100 ms after the stimulus onset resulting in an image of the early evoked response. An image of the late evoked response was generated by averaging from 100 to 200 ms after stimulus onset.

The third step was to find regions of interest (ROI) centered on wS1 and tjS1. Those ROIs were obtained by finding the coordinates of the maximum amplitude in the early evoked response images for whisker and tongue stimulation, respectively. Then a mask was drawn on the late response images in the frontal motor cortex to detect the second local maximum which correspond to the center of wM1 and tjM1, respectively (see figure 3.3).

Finally, calcium signal time courses were extracted based on these ROI. The response latency was defined as the time the calcium activity took to cross 4 times standard deviation threshold measured from the baseline. The standard deviation of the signal was computed during the 2 sec before the stimulus onset.
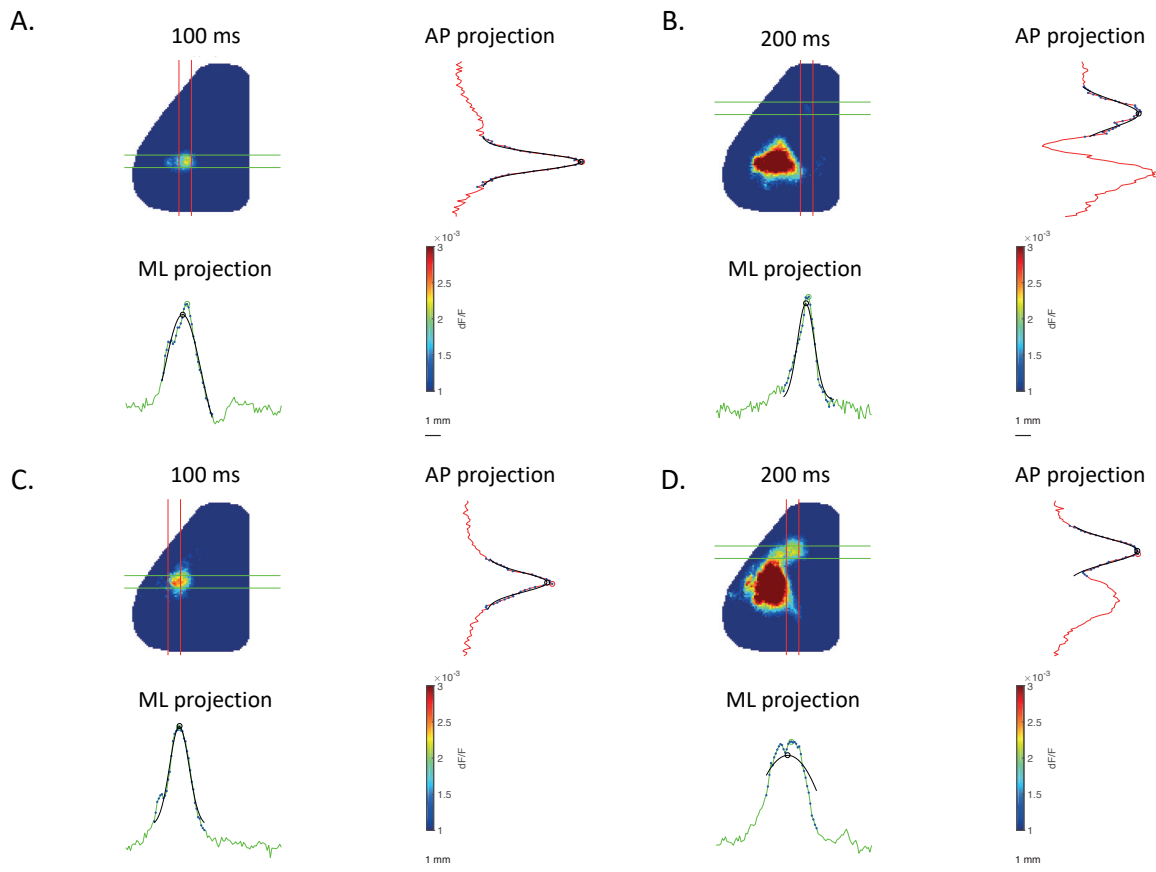
Figure 3.3. Method to find maximum for C2 whisker and tongue.

A. Mediolateral (ML) and anteroposterior (AP) signal projection centered on C2 primary somatosensory cortex wS1 of early image averaged from 0 to 100 ms.

B. Mediolateral (ML) and anteroposterior (AP) signal projection centered on C2 primary motor cortex wM1 of late image averaged from 100 to 200 ms.

C. Mediolateral (ML) and anteroposterior (AP) signal projection centered on tongue primary somatosensory cortex tjS1 of early image averaged from 0 to 100 ms.

D. Mediolateral (ML) and anteroposterior (AP) signal projection centered on tongue primary motor cortex tjM1 of late image averaged from 100 to 200 ms.

The maximum was found based on the Gaussian fit maximum curve for each condition.

3.3. Results

Response maps in individual mice evoked by whisker and tongue stimulation

Before each functional mapping experiment, a anatomical image of the mouse cortical surface was acquired to get the blood vessel pattern and Bregma as a reference location. An image of the left hemisphere of mouse MA076 is shown in the top left panel of figure 3.4. An example average GCaMP6f signal time course is presented for wS1 and wM1, as well as for tjS1 and tjM1 for whisker stimulation and tongue stimulation, respectively. An average fluorescent image of the early and late evoked response was displayed for individual mice

for both C2 stimulation and tongue stimulation. The early response was computed by averaging from 0 to 100 ms relative to stimulus onset and showed mainly a localized response in S1. Whereas, the late response (averaged from 100 to 200 ms) displayed a large and broad response in S1 and a smaller localized secondary response frontally in M1 (see figure 3.4 lower panels).

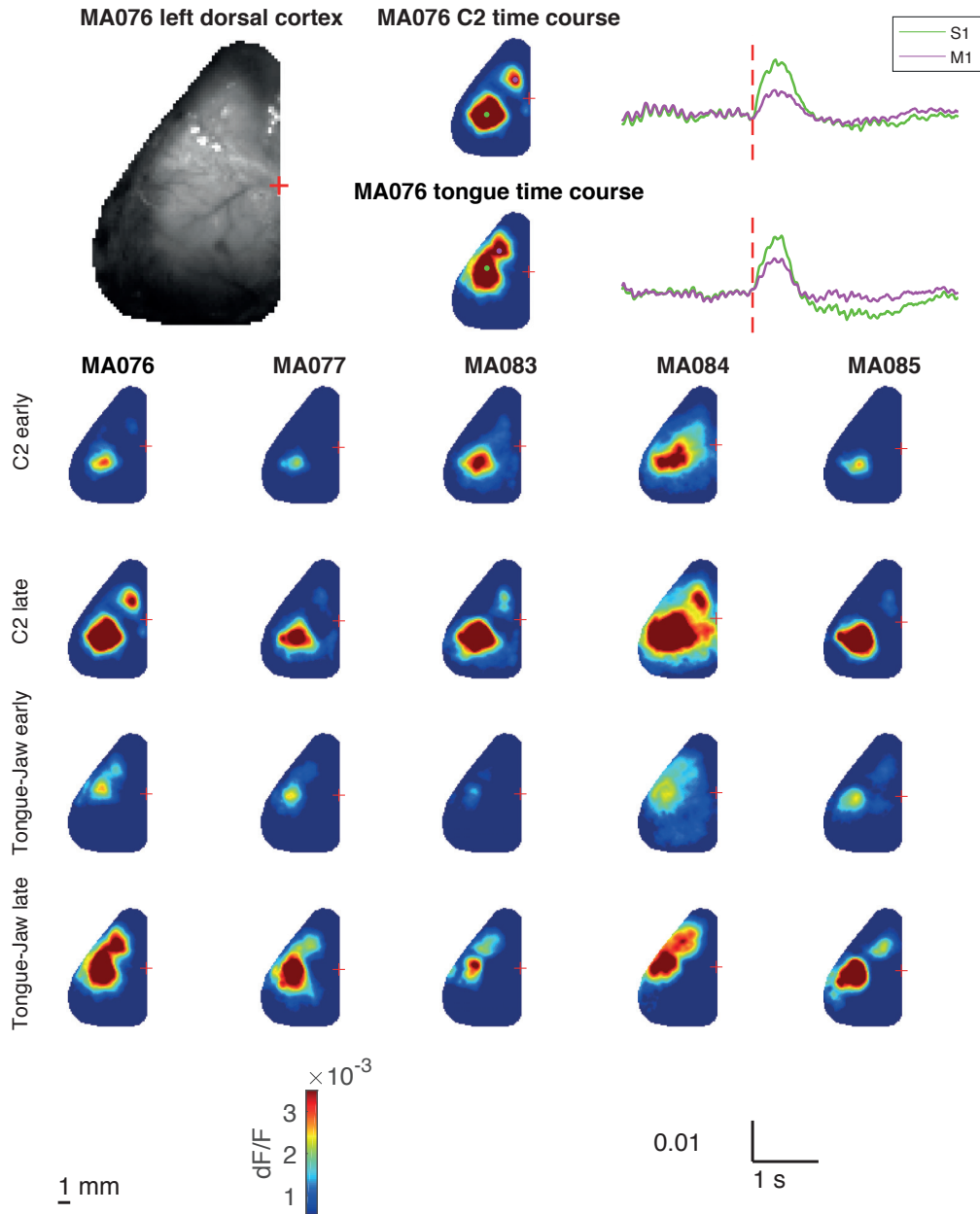Signal propagation from S1 to M1 during whisker or tongue stimulation in individual mice

Figure 3.4. Functional mapping of C2 whisker and tongue across different mice.
Top left panel: example anatomical green image for MA076.
Top right panel: example of late evoked response measured in anesthetized Thy-GCaMP6f mouse MA076. ROIs were drawn on S1 and M1 for both whisker and tongue stimulation image. The extracted curves from these ROIs are shown on the right. The red dashed line represents the stimulus onset.

On the lower panel the early and late average response to C2 and tongue stimulation for individual mice is displayed. Bregma position is represented by a red cross.

The latency of the evoked response was calculated for each extracted time course from the ROIs. For wS1 the latency of the signal was 66 ± 11 ms, for wM1 the latency was 183 ± 26 ms, for tjS1 the latency was 156 ± 103 ms and for tjM1 the latency was 238 ± 111 ms (see figure 3.5). The signal was first emerging in S1 and a second activation spot appeared in the M1 with a delay of 118 ± 22 ms for C2 whisker and 82 ± 118 ms for the tongue on average.
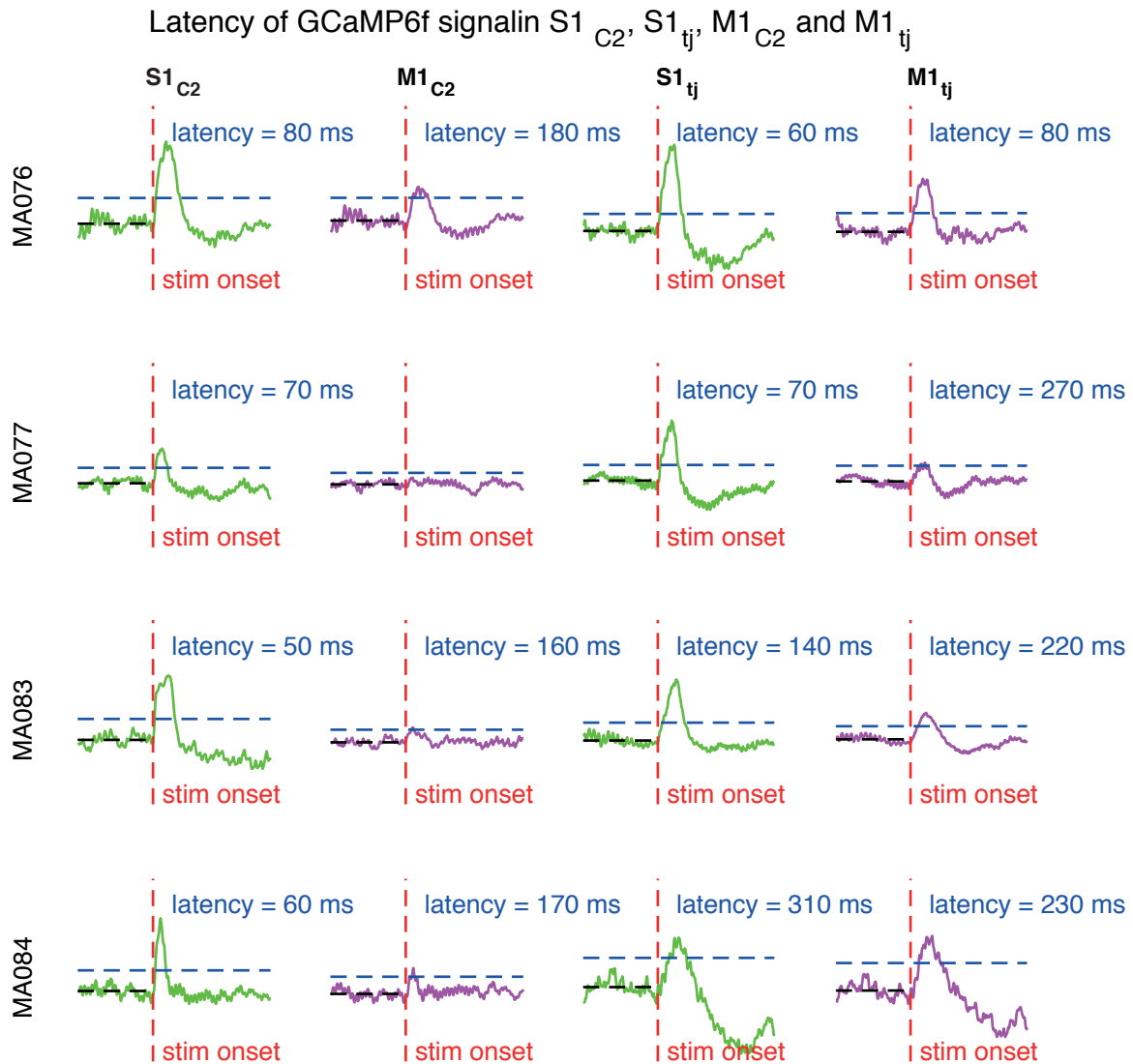

Figure 3.5. Latency of the sensory and motor response to C2 whisker and tongue stimulation.
Extracted time course from the wide-field calcium imaging during C2 whisker mapping and tongue mapping in anesthetized Thy1-GCaMP6f mice. The latency is the time when the curve passed the threshold of 4 times the standard deviation of the baseline (average of the baseline represented by the black dashed line). Stimulus onset is represented by the red dashed line. The curves are represented all on the same scale.

Grand average evoked response for whisker and tongue functional mapping centered on C2 wS1

A grand average evoked response was computed over all the mice (n=5) (figure 3.6). The images were all centered on C2 wS1 location. The late response of the average is displayed corresponding to an average from 100 to 200 ms. The green crosses represent S1 center response for each mouse and the magenta crosses are position on the center of M1 response of each mouse. S1 center corresponds to the coordinates of the global maximum of the early response (from 0 to 100 ms), whereas M1 center corresponds to the coordinates of the local maximum located in the motor cortex map of the late response map (see figure 3.3).

As wS1 and wM1 are far apart, it is easier to distinguish the responses in sensory and motor cortices. On the other hand, tjS1 and tjM1 are located closer so there is more a continuum of the response with two bridged local maxima.

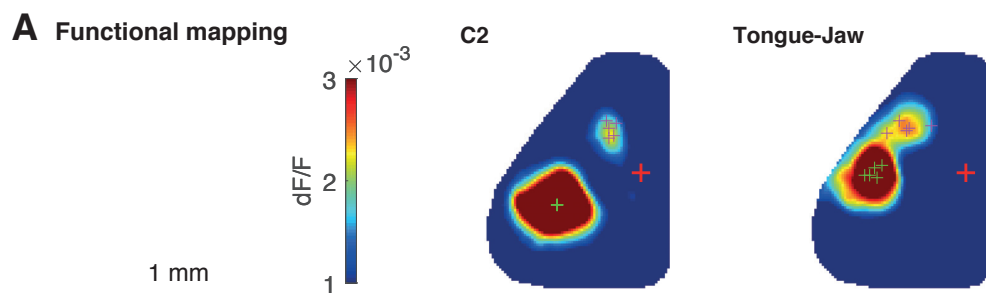Comparison of signal propagation from S1 to M1 during whisker or tongue stimulation (n=5)

Figure 3.6. Average of the C2 and tongue evoked responses over all the mice.
The fluorescent images show the late response (average from 100 to 200 ms) of C2 and tongue stimulation both centered on C2 wS1. Sensory cortex mapping is represented by the green crosses, and the projections for motor cortex mapping is represented by the magenta crosses. Bregma position is represented by a red cross.

Quantification of S1 and M1 locations for whisker and tongue

In order to quantify the location of whisker primary sensory cortex wS1, whisker primary motor cortex wM1, tongue/jaw primary sensory cortex tjS1 and tongue/jaw primary motor cortex tjM1 we first estimated Bregma location using the green anatomical image. We placed Bregma at the junction of the sagittal suture (midline) and the coronal suture. The distances between Bregma and the reported maxima of figure 3.6 were calculated with a spatial resolution of 100 × 100 μm.

Mouse name	wS1 ML | AP	wM1 ML | AP	tjS1 ML | AP	tjM1 ML | AP
MA076	3.44 | -1.32	1.25 | 1.49	3.56 | 0.49	2.57 | 1.83
MA077	3.37 | -1.39	1.26 | 1.67	3.57 | -0.20	2.41 | 1.81
MA083	3.47 | -1.11	1.41 | 1.84	3.86 | 0.27	2.96 | 1.85
MA084	3.46 | -1.25	1.26 | 1.25	3.91 | -0.09	2.64 | 1.83
MA085	3.70 | -1.59	1.12 | 1.33	3.91 | -0.51	1.61 | 1.62
Average	**3.49 | -1.33**	**1.26 | 1.52**	**3.76 | -0.01**	**2.44 | 1.79**
Std	**0.11 | 0.16**	**0.09 | 0.22**	**0.16 | 0.35**	**0.45 | 0.09**

Table 3.1. Coordinates of the cortical region for each individual mouse and the average location.
The number on the left corresponds to mediolateral axis and the number of the right corresponds to anteroposterior axis distance (in mm) from Bregma.

On average, C2 whisker primary somatosensory cortex wS1 is 3.49 ± 0.11 mm lateral to Bregma, -1.33 ± 0.16 mm posterior to Bregma. C2 whisker primary motor cortex wM1 is 1.26 ± 0.09 mm lateral to Bregma, 1.52 ± 0.22 mm anterior to Bregma. Tongue/jaw primary sensory cortex tjS1 is 3.76 ± 0.16 mm, -0.01 ± 0.35 mm, more or less at Bregma level. Tongue/jaw primary motor cortex tjM1 is 2.44 ± 0.45 mm lateral to Bregma, 1.79 ± 0.09 mm anterior to Bregma.

3.4. Discussion

In this chapter, I defined the area where tongue/jaw primary somatosensory cortex tjS1 as the first sensory evoked response and tongue/jaw primary motor cortex tjM1 as the secondary sensory evoked response after simple repetitive mechanical stimulation of the tongue in anesthetized mice. The second activation spots in motor cortex was comparable to what we obtained upon whisker stimulation in wM1. It seems to have a mirror reflection of the somatotopy observed in sensory cortex projecting to the motor cortex with a similar organisation and function.

But these results raised two questions. The first one, does the delayed evoked response emerges from direct projection from tjS1 or if it comes from other structures of the brain (like

motor parts of thalamus for example)? The second one can tjM1 described her evoke tongue or jaw movements when directly stimulated?

The variations in the evoked responses amplitudes might come mainly from the depth of anesthesia. Usually, presumably when the animal was in good physiological conditions (we would have to measure physiological parameters to be sure) there was a large response in S1 and a secondary response emerging later frontally in M1 region for both C2 and tongue. Anesthesia depth was most likely the main source of the noise in the evoked response of those mapping experiments. We did some awake whisker mapping experiments in TIGRE2.0-GCaMP6f mice (see chapter 4) and with a reliable response. Also, the C2 response in anesthetized mice was generally more reliable and easier to observe than tongue response. We should have a better control on the physiology of the animal by measuring parameters like heartbeat rate or blood oxygenation to assess the depth of anesthesia of the animal and have a direct feedback on the signal amplitude and the physiological state of the animal.

To address the question of direct innerval feedforward connection from tjS1 to tjM1, I should inject anterograde virus in tjS1. If direct traversing axons are projecting to tjM1 it would support the hypothesis of a monosynaptic pathway from tjS1 to tjM1. But I would still not be able conclude if this innervation is reciprocal from tjM1 to tjS1. So, we know that tjS1 activation can activate tjM1 but we cannot conclude on the feedback interaction from tjM1 to tjS1 as observed in the whysker system (Ferezou et al. 2007).

Also, based on both studies, the functional mapping and the viral injection, we would not know if the evoked activity is caused only by the feedforward activation form tjS1 to tjM1 or if this activity would be driven by subcortical structures or other cortical areas. To address the causal connectivity of tjS1 with tjM1, we should either inject a retrograde virus or rabies virus in tjM1 to see anatomically what brain areas directly project to tjM1.

To assess the functional connectivity, we could also inject muscimol in tjS1 for pharmacal inhibition, or use VGAT-ChR2 mice for optogenetic inhibition, and image the cortex with calcium imaging while inhibiting tjS1. If we do not see any activity in tjM1 anymore, it would mean that tjM1 is likely activated via tjS1.

Finally, to address the second question of whether tjM1 could induce tongue/jaw movements, we could optogenetically stimulate tjM1 in Thy1-ChR2-YFP mice to see if we could evoke movement of the jaw while stimulating directly tjM1, the same experiment that was done for whisker system (see chapter 5) (Auffret et al. 2018). This result would then be consistent with what was reported with microstimulation of the tongue/jaw motor cortex (Sasamoto, Zhang, and Iwasaki 1990; Avivi-Arber, Lee, and Sessle 2010; Komiyama et al. 2010).

4. Wide-field calcium imaging in layer 2/3 of mouse dorsal cortex during a 2-whisker discrimination task

Author contributions

Sami El-Boustani, Matthieu Auffret and Carl Petersen designed the project. Matthieu Auffret wrote the manuscript. Matthieu Auffret wrote the MATLAB script for data acquisition. Matthieu Auffret carried out all experiments. Matthieu Auffret and Sami El-Boustani analyzed data.

4.1. Introduction

Neural circuit in behaving mice

The cortical neural networks involved in the processing of relevant sensory information in order to generate a useful motor command is not completely understood. Perceptual decision making requires the optimisation of various parameters in order to minimize the errors and maximize the gain. In fact, the animal has to take into account the context in which this task is learned and to focus its attention on all the relevant stimuli in order to reach a good performance. So, the animal has to be motivated and engaged in the task. Even a simple behavior of tactile discrimination therefore requires to consider multiple complex parameters that are processed by many cortical areas. To understand the causality of the events in the mouse brain, one can use a simple behavior with well-defined events occuring in cascade in order to decompose the brain circuits involved between sensory and motor areas. Most likely, a complex neural circuit is used to take even simple decisions.

Multiple studies have previously addressed the question of where and when decision-making occurs in the cortex during mouse behavior, but with either good temporal and spatial resolution and poor overview of the all network (2-photon calcium imaging, patch recordings, extracellular recording) (Komiyama et al. 2010; Sachidhanandam et al. 2013; Yamashita and Petersen 2016; Le Merre et al. 2018; O'Connor, Peron, et al. 2010) or with good global view but poor temporal or spatial resolution (fMRI, EEG) (A. P. Harris et al. 2015; Chang et al. 2016; Yoshida et al. 2016) or in acute experiments preventing assessment of learning (VSD imaging) (Kyriakatos et al. 2017). To overcome all these problems, one promising solution is to use wide-field calcium imaging with the recent advances in mouse genetic lines (T.-W. Chen et al. 2017; Allen et al. 2017; Makino et al. 2017; Gilad et al. 2018). Indeed, with this technique, it is possible to image large-scale layer-specific or cell-type-specific cortical activity in behaving mice all along the learning of the task. This method benefits from a high signal-to-noise ratio. If combined with two-photon imaging it is possible to image the whole cortex and zoom in to see single cells activity.

We studied what happens in layer 2/3 of the dorsal cortex of mice that were trained to complete a task to get a reward. In the behavior developed by Dr. Sami El-Boustani in Carl Petersen's laboratory (El-Boustani et al., *manuscript in preparation*) thirsty mice learned to discriminate between two tactile stimuli: deflection of either the B2 or the C2 whisker. If the mouse licked a reward spout after the C2 whisker stimulation, the mouse was rewarded with a water drop, whereas if the mouse licked after B2 whisker stimulation the mouse was punished with 10 s timeout. Wide-field calcium imaging was carried out across days during the learning of the task. Thanks to this technique we could look at the dynamic of the changes in the signal along the learning of the task.

We found that in whisker sensory cortex S1/S2 the amplitude of the signal significantly decreased over the learning of the task in all mice. Also, the earliest difference between hit (C2 stimulation lick) and correct rejection catch (no stim no lick) trials was occurring in S1/S2 after 100 ms. Interestingly, the earliest difference in hit (C2 stimulation lick) and miss (C2 stimulation no lick) trials also occurred in S1/S2 after 100 ms. Then, the signals converged toward M2 after 200 ms where they were amplified. This might be caused by the direct projection from S2 to M2 and the indirect projection of wS1 to M2 through wM1. This would be where both sensory and motor informations are integrated and amplified by the cortex to trigger the decision to lick and send the motor command. Thus, some other differences might be taking place in deeper layer where the output signals are generated.

4.2. Materials and methods

Animal preparation and surgery

All experiments were carried out in accordance with protocols approved by the Swiss Federal Veterinary Office. In this study we used 11 GCaMP6f transgenic mice (five males and six females, age ~2 months) and 3 GAD67-GFP transgenic mice (three females, age ~2 months) (Tamamaki et al. 2003). The 11 mice expressing GCaMP6f were made through a genetic cross of TIGRE2.0-GCaMP6f Ai148(TIT2L-GC6f-ICL-tTA2) mice (JAX mouse stock number 030328, RRID: IMSR_JAX:030328) (T.-W. Chen et al. 2013; Daigle et al. 2018) with Rasgrf2-2A-dCre mice (JAX mouse stock number 000664, RRID: IMSR_JAX:022864)(J. A. Harris et al. 2014). Rasgrf2-2A-dCre mouse line holds an inducible system with the destabilized Cre (dCre) expressed under the control of the Rasgrf2 promoter which needs to be stabilized by injecting trimethoprim (TMP) to get expression. TMP (Sigma T7883) was reconstituted in dimethyl sulfoxide (DMSO, Sigma 34869) by mixing 100 mg of DMT in 1 ml of DMSO (100 mg/ml), freshly prepared for each experiment. For TMP induction, mice were given an intraperitoneal injection (250 µg TMP/g body weight) diluted in 0.9% saline solution for three consecutive days.
The Rasgrf2-2A-dCre crossed with TIGRE2.0-GCaMP6f mouse line has a very strong and specific expression in cortical layers 2/3 (figure 4.1).
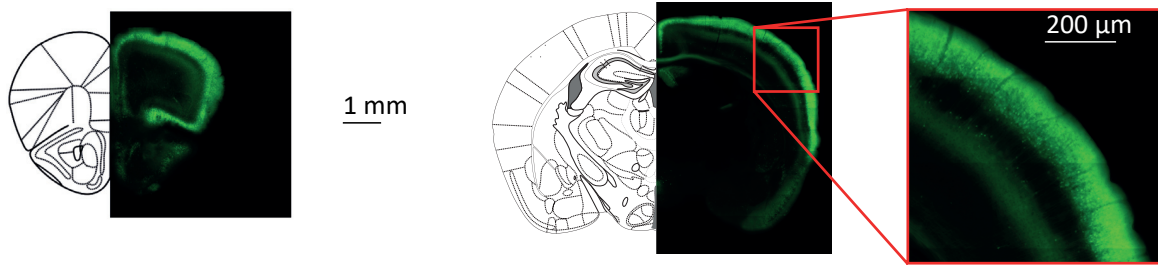
Figure 4.1. Transgenic mouse line Rasgrf2-2A-dCre × TIGRE2.0-GCaMP6f expression
GFP fluorescence in fixed coronal slices of Rasgrf2-2A-dCre × TIGRE2.0-GCaMP6f mouse were imaged at 4× magnification at two different anterior-posterior locations, ~2.22 mm frontal to Bregma (close to wM2, left image) and ~1.34 mm posterior to Bregma (center image). Schematic drawings were adapted from Paxinos and Franklin (2001). A zoomed-in version of the barrel cortex was acquired with a 10× magnification lens (right image).

We used an intact skull preparation where mice were implanted with a metal head-holder to prevent movements of the head. Mice were anesthetized under deep isoflurane and injected intraperitoneally with 300 µl carprofen (0.5 mg/ml) analgesic. Lidocaine/bupivacaine was the injected subcutaneously between the skin head and the bone of the skull. After scalping the mouse, we applied some betadine on the skull and the surrounding tissues for disinfection. The skull was then cleaned by using a scalpel blade. After alignment of the Bregma with Lambda, the skull was covered with a thin layer of cyanoacrylic glue (Loctite glue 401). The aluminium implant was always glued at the same location regarding to Bregma (2.5 mm anterior and 1.5 lateral to Bregma) in order to have approximately all brains oriented in the same position. A second layer of cyanoacrylic glue was applied on top of the implant and of the first layer. After this surgical procedure, the mouse was put back in its home cage with a bottle of water mixed with ibuprofen. All whiskers were trimmed except the B2 and C2 right whiskers (the whiskers on the left side were kept intact).

Wide-field calcium imaging macroscope

The GCaMP6f calcium indicator was excited with 485 ± 20 nm for blue light from a 100 W halogen lamp (Olympus) and reflected on a 45° oriented dichroic mirror of 495 nm cut-off wavelength. At the beginning of each session, the excitation light was adjusted to always have similar average fluorescence, corresponding to ~80% of saturation of the camera sensor. The blue excitation light was focused on the top of the dorsal cortex left hemisphere of the mouse through a 50 mm camera lens (Nikon). Green fluorescent light was collected by a high sensitive CMOS camera via the same optical path. The green light emitted by the cortical activation went through the same 50 mm camera lens through the longpass dichroic mirror, then through a green emission filter at 525 ± 50 nm and finally was focused on the high-speed MiCAM Ultima (Scimedia) camera detector by a 50 mm video lens (Navitar) (figure 4.2). This efficient imaging system (known as back to back tandem-lens epifluorescence macroscope) was developed by Grinvald (Ratzlaff and Grinvald 1991). With this configuration we had a field of view of 10 × 10 mm. The high-speed CMOS camera has a detector of 100 × 100 pixels giving a collected light from a cortical region of 100 × 100 µm spatial resolution. Images were acquired at 100 Hz leading to a 10 ms temporal resolution.

The images were analyzed offline using custom written routines in MATLAB (Mathworks, Natick, Massachusetts, USA).

Whole body sensory mapping

Wide-field calcium imaging experiments were carried out to map the sensory representations of multiple body parts. The sensory mapping was performed using 5 of the layer 2/3 × TIGRE2.0-GCaMP6f mice that were imaged during the 2-whisker discrimination task. Mice were lightly anesthetized under ~0.5% isoflurane. The body temperature of the mouse was maintained at 37°C by a heating pad linked to a feedback probe for the temperature. A first image of the top of the cortex vasculature and of the Bregma was acquired with a green fiber coupled LED at 530 nm (Thorlabs, M530F2). For functional mapping using GCaMP6f indicator, the illumination was changed to bright and steady light from halogen lamp filtered at 485 ± 20 nm for blue excitation light (Allen et al. 2017).

A first subset of body parts was sequentially mechanically stimulated with a glass capillary attached to a piezo-actuator. The stimulus was an oscillation of a gaussian shaped curve of 40 ms long repeated 10 times. Each trial consisted of a baseline period of 2 s followed by a 400 ms stimulation and a 2720 ms poststimulus period. The total trial duration was 5.12 s and the intertrial interval was from 4 to 5 s (randomly distributed). We began by stimulating the tongue after pulling it out of the mouth. Tactile stimuli were performed by tapping the tip of the tongue at 25 Hz. Then the jaw was stimulated by tapping the part below the mouth and dorsal to the lip. The right forepaw and right hindpaw were similarly stimulated by tapping with the glass tube. Right C2 whisker and right B2 whisker were sequentially inserted into the glass capillary and stimulated for 400 ms at 25 Hz. The visual stimuli were delivered to the right eye of the mouse by flashing green light with the 530 nm fiber-coupled LED used for anatomical imaging. So, to not get any artifact from the stimulus on the image, we had to shield the light with a black tube around the extremity of the optic fiber and placed very close to the mouse right eye. Very small amount of light was used. A 400 ms stimulation was delivered at 25 Hz. Finally, auditory stimuli were a beep sound that was generated from the PCI board of the computer at 5 kHz for 400 ms and played by small in-ear headphones on both side of the mouse head.

Behavior two-whisker discrimination task

A total of 21 mice (male and female; Rasgrf2-2A-dCre × TIGRE2.0-GCaMP6f; TIGRE2.0-GCaMP6f injected with viruses; GAD67-GFP mice) were trained in the discrimination task. All whiskers were trimmed on the right side except B2 and C2 whiskers. The first day or the first two days, mice were exposed to the same stimuli of either B2 or C2 whiskers without the licking spout in front of their mouth. The whiskers were inserted into a glass tube attached to a piezo-actuator. The stimuli were a repetition of 5 sine-shaped oscillations of 40 ms each leading to a stimulus of 200 ms long oscillating at 25 Hz. We called this an awake mapping day in naive mice to explore what is the signal without the licking motor command. The day before the start of the training, mice were water restricted to 1 ml of water/day. Their weight and general health status were then carefully monitored every day using a score sheet. The mice should not lose more than 80% of their weight before the water restriction. Mice were

trained daily with one session/day. The training started with some association trials during which the mice automatically got a reward of 5 µl of water after a Go-stimulus, in this case C2 stimulus, whether or not they were licking the water spout. With this association phase, mice were able to associate licking of the spout with water delivery as well as eventually stimulus with water reward. Only a subfraction of the trials had association and this was tuned by the experimenter on how well the mouse was licking to get the reward water drop. As soon as the mice made the link between licking and reward uptake, we stopped association trials. For some mice, we stopped association at during their first session after a few trials, sometimes it took some more trials or sessions to get there. Licks were detected by a piezoelectric sensor attached to the reward water spout. Whisker movements with their piezo stimulations and movements of the jaw and tongue were filmed filmed through a 50 mm video lens (Navitar) with a high-speed camera (Optronis) at 200 Hz under infrared light illumination. Ambient white noise at 80 dB was continuously played to mask any potential auditory cues generated by the setup (like the vibration of the piezo actuators for example) or external noise that could distract the mice. Behavioral control and behavioral data acquisition programs were carried out with custom-written computer routines using a National Instruments board interfaced through MATLAB (MathWorks).
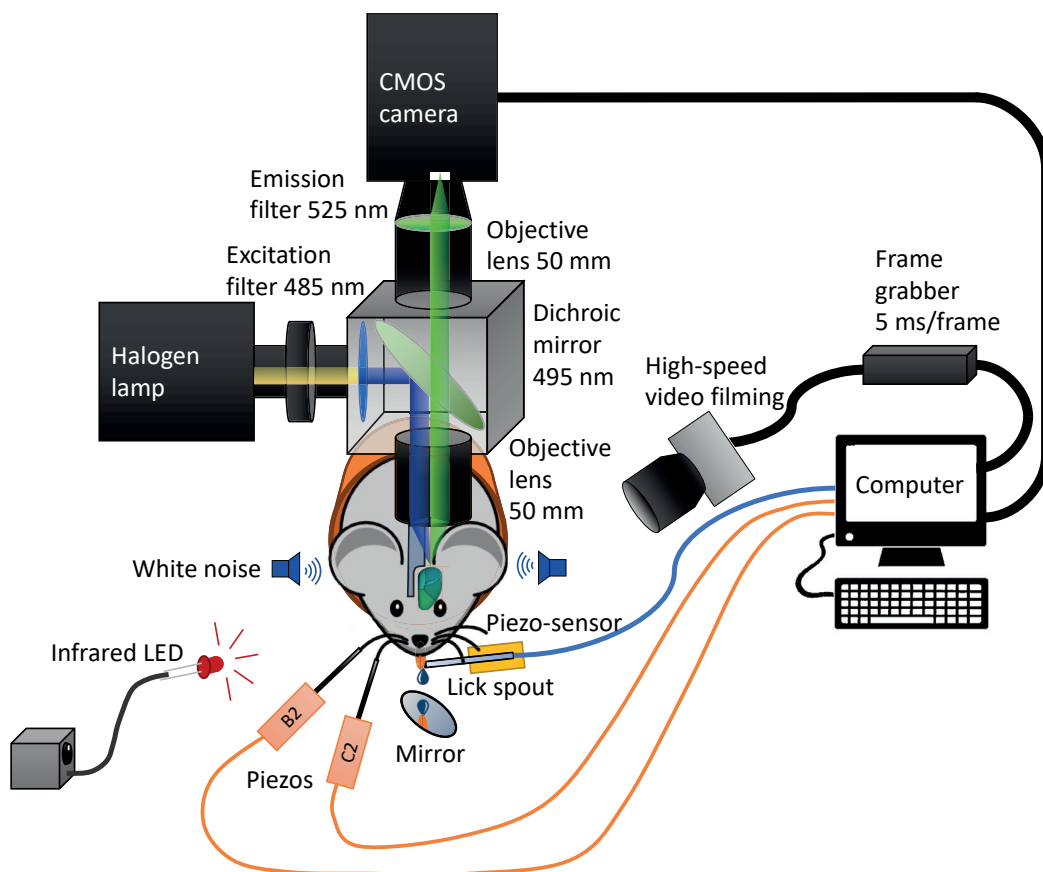

Figure 4.2. Experimental setup for the two-whisker discrimination task
The left hemisphere of Rasgrf2-2A-dCre × TIGRE2.0-GCaMP6f mice was continuously excited by 485 nm blue light. The light was reflected by a longpass dichroic mirror at 495 nm through a 50 mm focal length camera lens to focus the beam on the cortical surface of the left hemisphere. The emitted green light passed by the objective lens and though the dichroic mirror and was then filtered by a band pass emission filter at 525 nm and focused

onto a high-speed CMOS sensor camera by a second objective lens. The image frame rate of the camera was 10 ms/frame.

Either C2 whisker (Go signal) or B2 whisker (NoGo signal) or no whiskers (catch trials) were stimulated by piezoelectric actuators with a 200 ms long Gaussian-shape curve oscillating at 25 Hz delivered by a PCI board. The mouse had to lick a spout after C2 whisker stimulation to get a water drop reward.

Ambient continuous white noise was played in the background at 80 dB to mask any sounds that could be used as a cue by the mouse.

A behavioral camera was filming mouse whiskers and the two piezos as well as the mouth and the licking of the spout with a mirror at a frequency of 200 Hz, giving a time resolution of 5 ms/frame. The mouse face was illuminated by infrared LED light.

For the discrimination task, trials were 5.12 s long and separated by random inter-trial intervals ranging from 4 to 5 s. The trials started with a 2 s baseline period with no cues. If the mouse licked during this baseline period, the trial was still recorded by the wide-field camera but no stimulus was delivered to the whiskers. This was classified as early lick trials. If the mouse did not lick during this 2 s baseline window, three different events could occur by randomly selecting one with various probabilities changing based on the stage of learning of the task of the mice. Either a 200 ms stimulus was delivered to right C2 whisker or 200 ms stimulus of the right B2 whisker or no stimulus. Then if the mouse licked within the 2 s response window, the mouse was rewarded with a water drop of 5 µl if it was following a C2 whisker stimulation (Go trial) and was considered as a hit trial, whereas if the mouse did not lick it was considered as a miss trial. If the mouse licked after a B2 whisker stimulation (No Go trail), the mouse did not get reward and was punished with a 10 s timeout, this trial was considered as a false alarm stim trial, whereas if the mouse did not lick it was notified as a correct rejection stim trial. If the mouse licked after no stimulation (Catch trial) the mouse was not rewarded and it was counted as a false alarm catch trial, whereas if the mouse did not lick it was specified as a correct reject catch trial. This was to assess the rate of spontaneous licking of the mouse. The licks that occurred during the last 1.12 s of the trial and during the intertrial intervals were not rewarded.

	Lick	No lick
C2 whisker stimulation	**Hit** ⇒ *Reward*	**Miss**
B2 whisker stimulation	**False alarm stim** ⇒ *Timeout*	**Correct rejection stim**
No stimulation	**False alarm catch**	**Correct rejection catch**

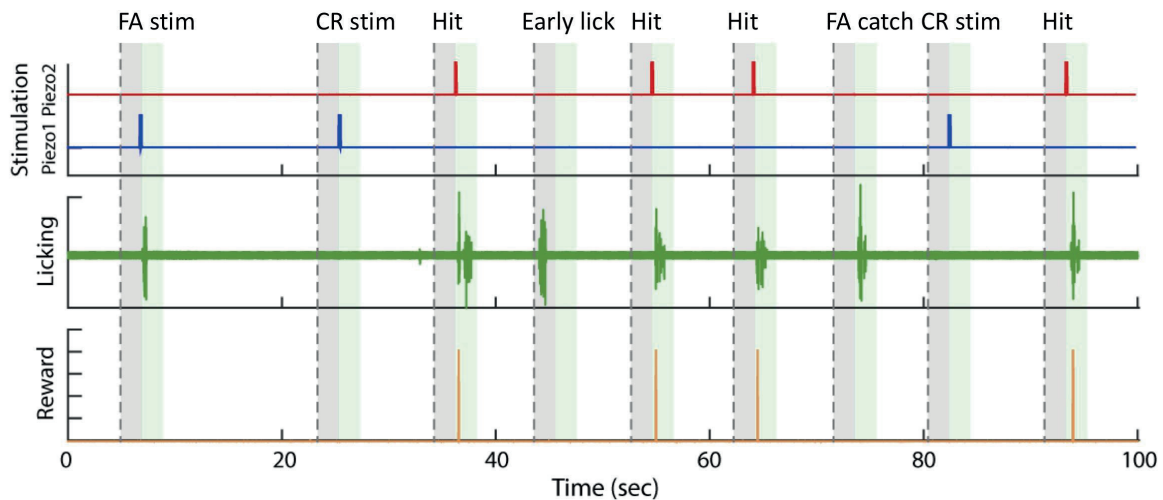*Table 4.1. Two-whisker discrimination behavioral conditions*

Figure 4.3. Two-whisker discrimination behavioral inputs (from the setup) and outputs (from the mouse)

Red trace corresponds to C2 stimulation of 200 ms oscillations at 25 Hz.

Blue trace corresponds to B2 stimulation of 200 ms oscillations at 25 Hz.

Green trace corresponds to lick signal recorded from the piezo-sensor of the water spout.

Orange trace corresponds to the reward valve opening, triggered by the crossing of a threshold of the piezo-sensor on the spout after a C2 whisker stimulation within the 2 s response window.

The trial start with a 2 s baseline window, followed by a 2 s response window and finished by 1.12 s of recording. The trials are separated by at least 4 to 5 s intertial time interval (up to 10 s if the mouse did a FA stim punished by a timeout).

Hit: when mouse licked after a C2 stimulation

Miss: when mouse did not lick after a C2 stimulation

FA stim: a false alarm when the mouse licked after a B2 stimulation

CR stim: a correct rejection when the mouse did not lick after a B2 stimulation

FA catch: a false alarm when the mouse spontaneously licked during the response window without any stimuli

CR catch: a correct rejection when the mouse did not lick during the response window without any stimuli
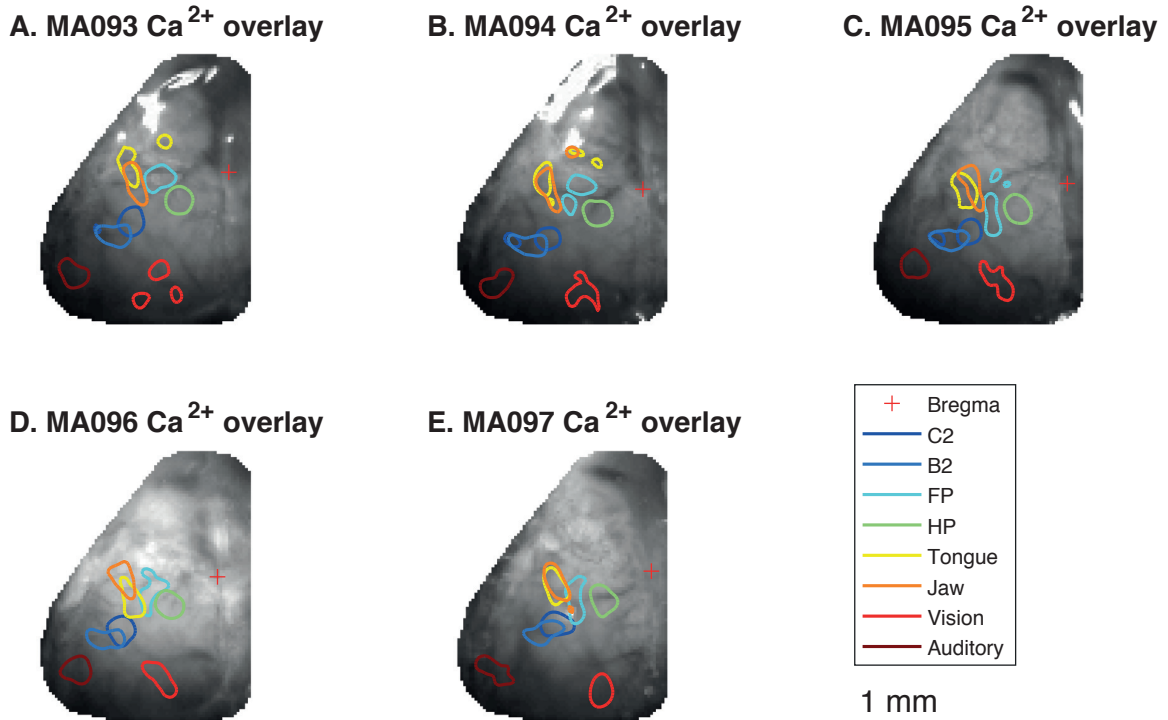
4.3. Results

Whole body sensory map

In figure 4.3, the cortical responses evoked by stimulating different body part at the periphery were acquired with wide-field calcium imaging. The contour of the responses were computed for all the activated sensory areas and corresponded to the 5% percentile of the maximal pixel values. All the contours were overlaid on the green image of the vasculature for each mouse. The Bregma was determined based on the green images at the junction of the coronal and sagittal sutures at the surface of the skull. The same color code was used for all the 6 maps.

The summary sensory map of all the mice was computed by aligning all the brains on Brema positions. The alignment was performed by simple translation of the different images. For sake of clarity, only the maximum value for each body part was represented with a cross.

Whole body sensory map using wide-field calcium imaging (n=5)

A. MA093 Ca^{2+} overlay   **B. MA094 Ca^{2+} overlay**   **C. MA095 Ca^{2+} overlay**

D. MA096 Ca^{2+} overlay   **E. MA097 Ca^{2+} overlay**

F. Overlay of the center of the evoked responses for each mouse, aligned on Bregma
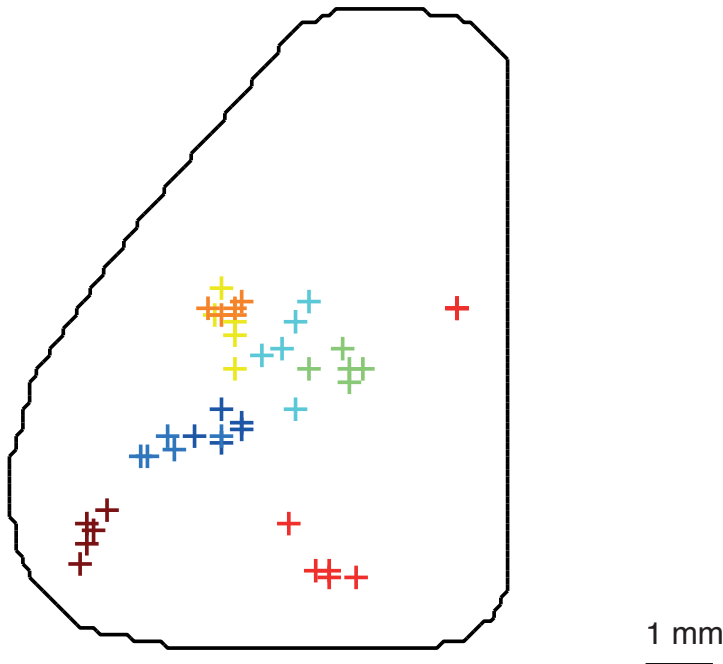

Figure 4.3. Body sensory map using wide-field calcium imaging.

A-E. Sensory map for 5 mice. Tongue and jaw were stimulated by mechanically tapping the surface with a glass tube attached to a piezoelectric element at 25 Hz for 400 ms. Right B2 and C2 whiskers were stimulated at 25 Hz for 400 ms after inserting the whisker into the glass capillary. Right forepaw (FP) and right hindpaw (HP) were also mechanically stimulated at 25 Hz for 400 ms using the piezoelectric actuator. Light flashes oscillating at 25 Hz pointed toward the right eye with a black tube shield were used to deliver visual stimuli. Auditory stimuli were delivered by a continuous beep sound at 5 kHz for 400 ms. The functional images were smoothed and contours were computed with a 5% percentile of the maximum pixels. The obtained contours were overlaid on the green anatomical image of the corresponding mouse dorsal cortex. Bregma was represented with a red cross.
F. An overlay of all the mice sensory evoked responses was represented by a cross centered on the maximal response. The sensory maps were all aligned on the Bregma location, represented by a red cross.

Quantification of primary sensory cortical regions

In order to quantify the location of whisker primary sensory cortex wS1 (for B2 and C2), of forepaw, hindpaw, tongue and jaw primary somatosensory cortex, of primary visual cortex and primary auditory cortex we first estimated Bregma location using the green anatomical image. We placed Bregma at the junction of the sagittal suture (midline) and the coronal suture at the surface of the skull. The distances between Bregma and the reported maxima of figure 4.3 were calculated using the spatial resolution of 100 × 100 µm.

Mouse name	C2 ML | AP	B2 ML | AP	FP ML | AP	HP ML | AP	Tongue ML | AP	Jaw ML | AP	Vision ML | AP	Auditory ML | AP
MA093	3.8 | -1.2	3.7 | -1.8	3.4 | -1.0	1.6 | -0.5	3.0 | 1.5	2.9 | 0.2	2.6 | -3.4	5.4 | -3.1
MA094	3.6 | -1.5	4.0 | -1.8	3.5 | -1.0	1.7 | -0.8	2.7 | 1.1	3.0 | 0.9	2.4 | -3.3	5.1 | -3.1
MA095	3.6 | -1.9	3.7 | -2.1	3.0 | -1.0	1.5 | -1.1	4.0 | -0.2	3.3 | 0.1	2.4 | -3.4	5.9 | -3.0
MA096	3.8 | -1.5	3.8 | -1.5	2.5 | -1.0	1.9 | -0.3	3.5 | -0.5	3.5 | 0.6	2.5 | -2.8	5.4 | -2.8
MA097	3.5 | -1.5	3.8 | -1.8	2.9 | -1.0	1.3 | -0.8	3.6 | -0.3	3.5 | 0.1	1.8 | -3.6	5.1 | -3.3
Average	3.66 | -1.52	3.80 | -1.80	3.06 | -1.00	1.60 | -0.70	3.36 | 0.32	3.24 | 0.38	2.34 | -3.30	5.38 | -3.06
Std	0.12 | 0.22	0.11 | 0.19	0.36 | 0.60	0.20 | 0.28	0.46 | 0.82	0.25 | 0.32	0.28 | 0.27	0.29 | 0.16

Table 4.1. Coordinates of the cortical region for each individual mouse and the average location. *ML: mediolateral axis, AP: anteroposterior axis*

Somatotopy of the barrel cortex in awake mapping experiment

Before starting the behavioral training for the 2-whisker discrimination task, each mouse was exposed to one or two days of awake B2 and C2 whisker mapping. The mouse was head-fixed with the implant on the transparent intact skull and either B2 or C2 was stimulated with a glass tube attached to a piezoelectric bender. There was no spout in front of the mouse.

This experiment provided a reference calcium activity of whisker stimuli in naive awake mice without generating a motor command in response to these stimuli. There was mainly a strong response in both wS1 and S2 with no strong activity in motor cortex. C2 responses in wS1 and S2 were further apart compared to B2 responses. Indeed, C2 wS1 is medial to B2 wS1 and as S2 is located lateral to wS1 the two blubs for S1 and S2 were closer for B2 than for C2. There was a clear somatotopy of S1 whisker primary somatosensory cortex (figure 4.4).

Somatotopy of wS1 for B2 and C2 whiskers in awake mice (average from 50 to 100 ms)
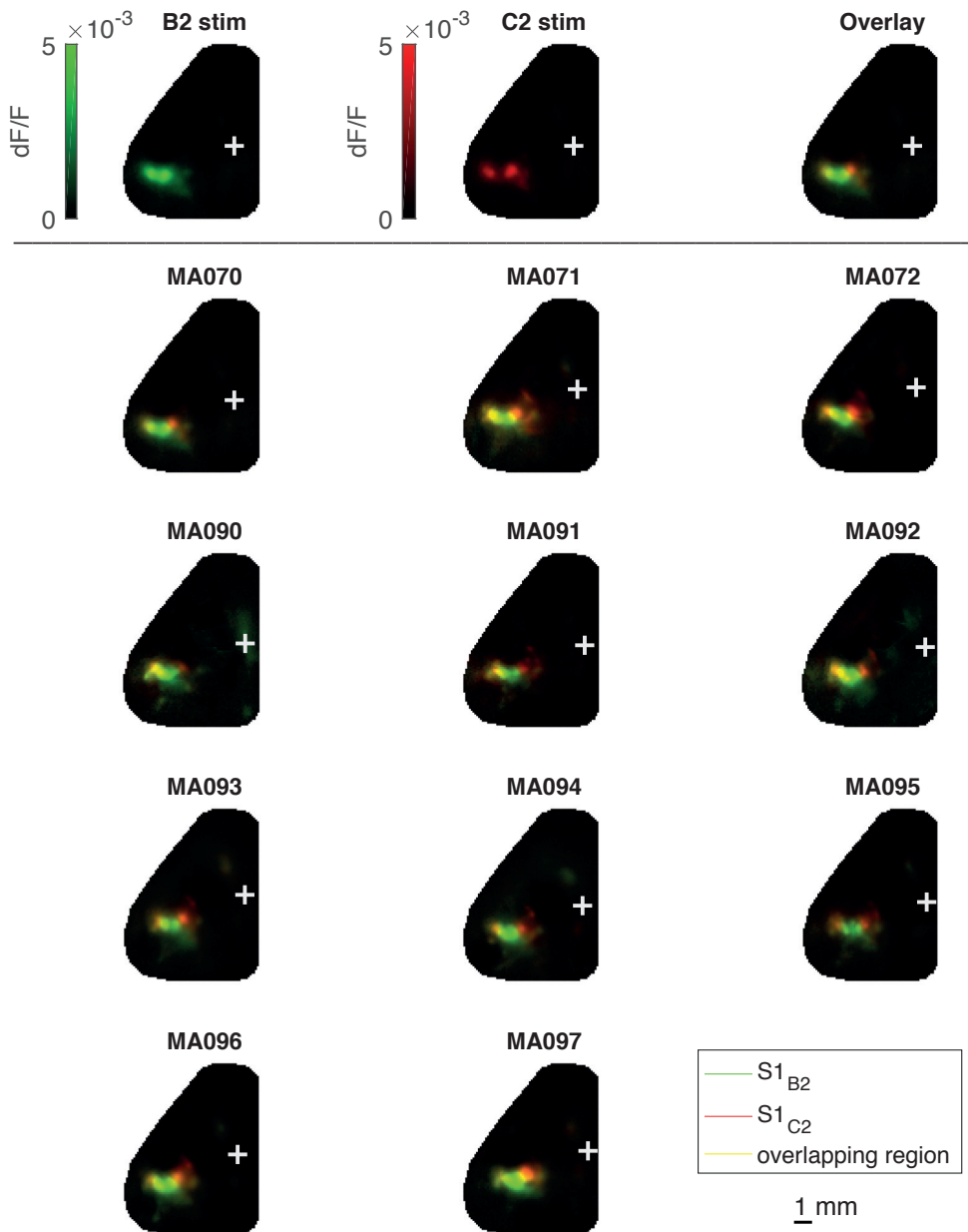
Figure 4.4. Whisker somatotopy for 11 mice.
The top panel is an example for mouse MA070 where the image in green represented the responses to B2 whisker stimulation and in red the responses for C2 whisker stimulation, and the last image was the overlay of those two images on the same color scale. Images are an average from 50 to 100 ms.

The bottom panel shows the images for each mouse averaged from 50 to 100 ms after B2 and C2 stimulation onset. The images were overlaid on the same maps where the yellow color reflected the overlap between B2 and C2 responses.
Bregma position is represented by a white cross.

We calculated the average of all the 11 mice by aligning them on C2 wS1 (figure 4.5). A early response, corresponding to an average from 50 to 100 ms and a late response, corresponding to 150 to 200 ms was calculated for this averaged map over all mice. Then after smoothing image, a contour plot for each individual mouse was computed for a contour level of 75% of each local maximum (S1/S2 for the early response and M1/M2 for the late response). The obtained contour plots were overlaid on the average early and late response.

Both early and late contours were displayed with two colors (blue for B2 and red for C2) on a mask by removing the sensory contour activations for the late responses. This showed a relatively clear distinct location between S1 and S2 for both B2 and C2 stimulation. This suggested that there was some somatotopy in wS1 (as known) and for S2 as well. Interestingly there is partially the same distribution of the response in M1 and M2 as for S1 and S2 where B2 responses were surrounded by C2 responses.
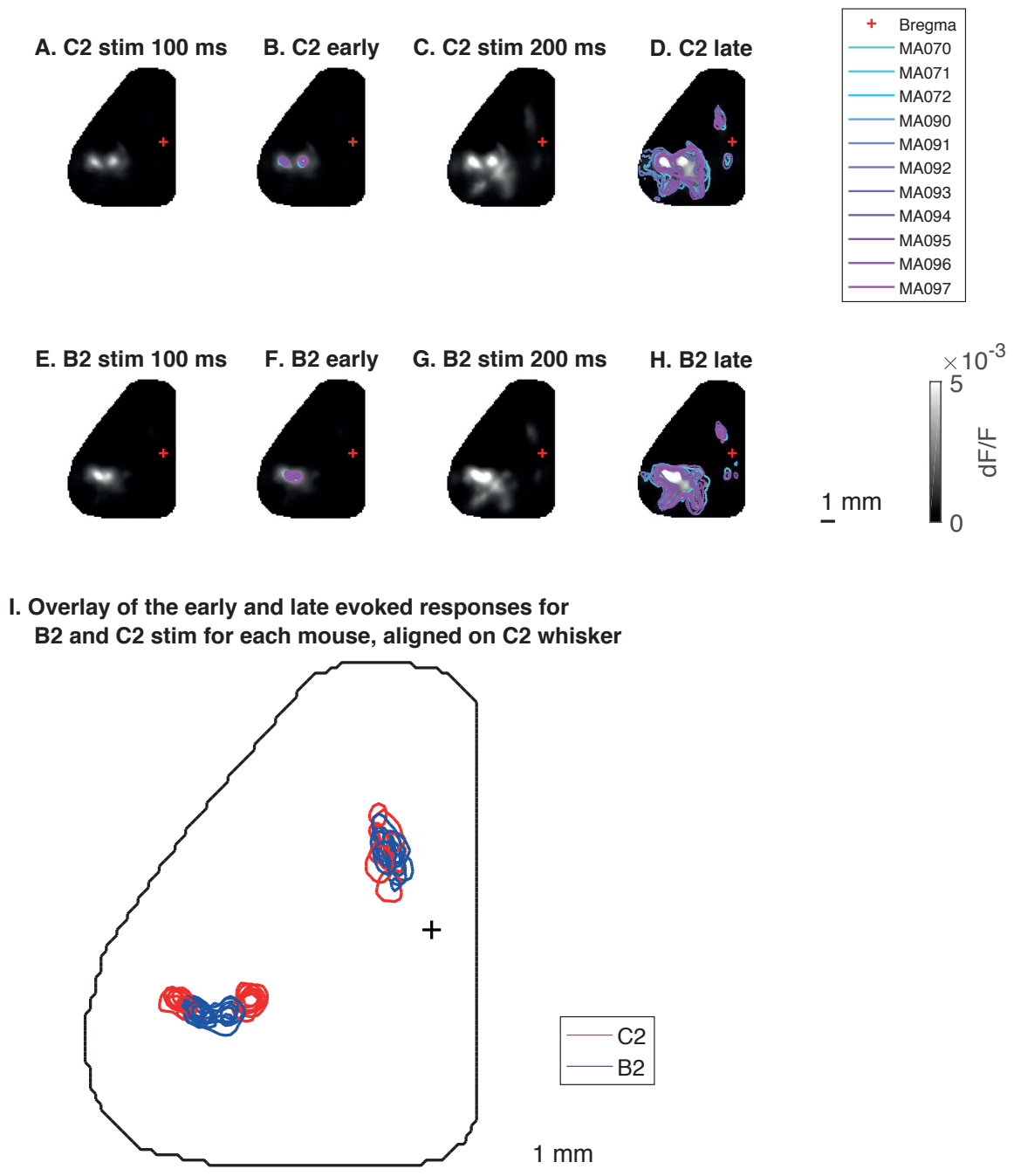
Somatotopy for B2 and C2 whiskers (n=11)

A. C2 stim 100 ms   B. C2 early   C. C2 stim 200 ms   D. C2 late

E. B2 stim 100 ms   F. B2 early   G. B2 stim 200 ms   H. B2 late

Legend:
- + Bregma
- MA070
- MA071
- MA072
- MA090
- MA091
- MA092
- MA093
- MA094
- MA095
- MA096
- MA097

$\times 10^{-3}$ dF/F (scale 0 to 5)

1 mm

I. Overlay of the early and late evoked responses for B2 and C2 stim for each mouse, aligned on C2 whisker

- C2 (red)
- B2 (blue)

1 mm

Figure 4.5. Average of early and late responses for all 11 mice aligned on C2 wS1
A and E. Average response from 50 to 100 ms for C2 and B2 stimulation.
B and F. Contour plots of the 11 mice overlaid on the average early response map for C2 and B2 stimulation. The contour level was at 75% of the maximum signal amplitude of the early response map of each individual mouse.
C and G. Average response from 150 to 200 ms for C2 and B2 stimulation.
D and H. Contour plots of the 11 mice overlaid on the average late response map for C2 and B2 stimulation. The contour level was at 75% of the maximum signal amplitude detected in motor cortex (M1/M2) of the late response map of each individual mouse.

Bregma position was represented by a red cross.
I. Overlay of contours for B2 (blue lines) and C2 (red lines) early responses and late responses where the sensory components have been removed.
Bregma position was represented by a black cross.

2-whisker discrimination mouse behavioral performances

Mice were trained for 13 to 17 days on the discrimination task. All along the training of the mice, they were exposed to the same stimuli of 200 ms at 25 Hz. The first few go trials (from one day to three days) we did some association where the reward water drop was automatically delivered. Once the mice understood that they had to lick the spout to get the reward, we stopped the association. During a first phase of the learning, the mice were more detecting all the stimulations, meaning that they were licking with almost the same probability for C2 (the go signal) and B2 (the no go signal) stimulation. As mice were punished by a 10 s timeout if they licked after B2 stimulation, they gradually learnt to restrain licking for B2 whisker. The mice started to discriminate for the two whiskers. Usually, the false alarm catch rate decreased slightly too or remained constant throughout the learning of the task (figure 4.6).

During an individual session, expert mice were typically licking intensively for the first 200 to 400 trials leading to a ~100% hit rate, ~100% false alarm stim rate and a high false alarm catch rate. Also, during this period, the mice had a large early lick rate, meaning that they were less exposed to stimuli as the stimulations were canceled for those trials. During this first phase, mice were impulsive because they were thirsty and motivated. Then the false alarm catch rate (nostim lick trials) usually started to decrease and detected all stimuli with a fast reaction time. During a second phase, the false alarm stim rate (B2 stim lick trials) gradually decreased and the mice started to discriminate between B2 and C2 whiskers. During this discrimination phase, the mice were less impulsive, still motivated to lick and focusing more on the nature of the stimulus. This usually led to the peak performance of the mouse. After this peak, a third phase started, when the mice lost motivation, they were less thirsty and progressively reduced licking and the reaction time increased. Usually, the false alarms were very low. For some sessions, the mice were starting licking more again for a short period of time and definitively stopped licking after. I was stopping the session after ~80 miss trials.

This behavior performance was assessed by calculating the average licking rate for each of the three conditions (C2 stimulation, B2 stimulation and no stimulus) over a sliding window of 80 trials. This represented a running average performance.

$$Lick\ rate\ = \frac{n_{lick}}{n_{lick}+n_{nolick}} \text{ for a given behavioral condition}$$

The overall performance of each individual mice was computed by averaging the lick rate for each of the three conditions across all trials.
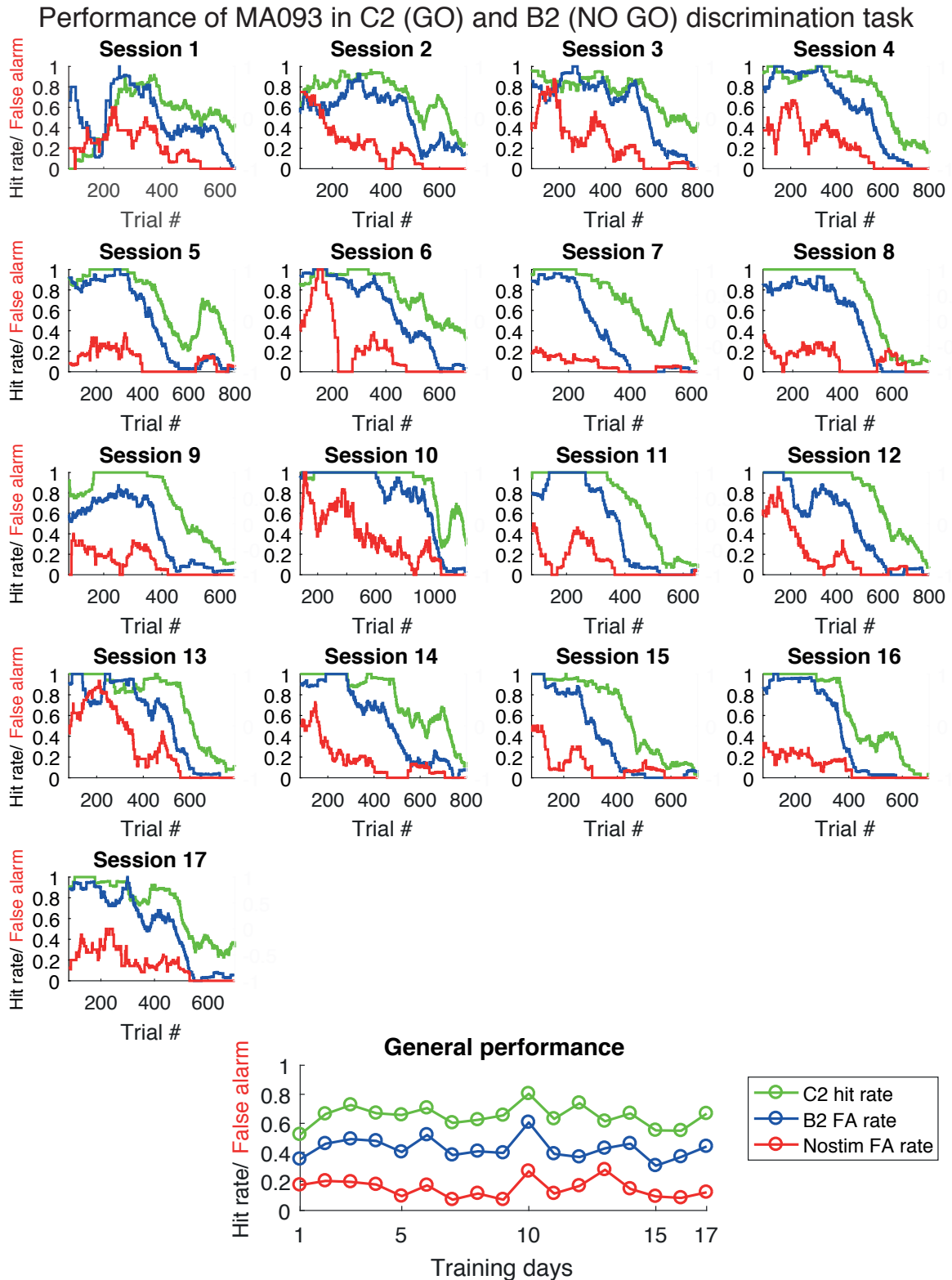
Figure 4.6. Evolution of the behavioral performance of the mouse MA093 over the training of 2-whisker discrimination task.

The graphs for each session were obtained by plotting the running average of the licking rate with a sliding window of 80 trials for each condition: C2 stimulation (hit rate in green), B2 stimulation (false alarm stim rate in blue), no stimulation (false alarm catch rate in red).

The general performance of the mouse was computed by averaging the lick rate for each behavioral condition: C2 stimulation (hit rate in green), B2 stimulation (false alarm stim rate in blue), no stimulation (false alarm catch rate in red).

The average performance over all mice that went through this 2-whisker discrimination task was computed (figure 4.7). On average, the hit rate was always above the false alarm stim rate. So the mice were able to discriminate relatively rapidly, already during the first 4 sessions between B2 and C2 whiskers. The stimulations of the whiskers were strong and well above their perception threshold. This might be a good reason why the mice understood rapidly the behavioral outcome difference (reward or timeout) between the two whiskers.
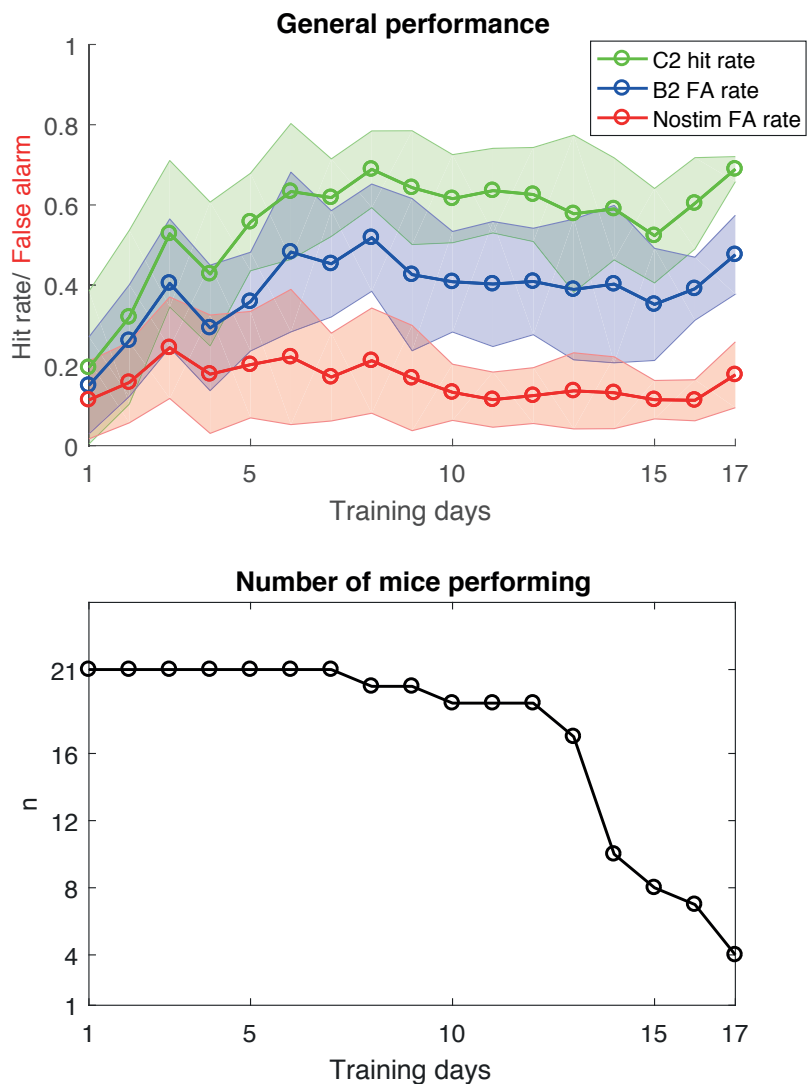
Figure 4.7. Average performance over all mice undergoing 2-whisker discrimination task.
The top panel shows the average performance over days for 21 mice during the first 7 days and down to 4 mice during the 17 days of training. The thick lines represent the averages of the performance and the shades around those lines represent the standard deviation.
The bottom panel shows the number of mice over days of training.

Single trial wide-field calcium imaging data

Based on the mapping days (see figure 4.4) we could define specific regions of interest for wS1 and S2 for both B2 and C2 whiskers. Those four ROIs for wS1 and S2 were centered on the two local maxima of the average dF/F early responses (from 50 to 100 ms) for either B2 or C2 stimulation during the mapping days specifically for each mouse.

Two other ROIs were defined in the motor cortex, wM1 and M2 based on their coordinates. The wM1 spot is located 1 mm anterior and 1 mm lateral to Bregma and the M2 spot is located 2 mm anterior and 1 mm lateral to Bregma.

There was an important trial to trial variability with some trials having rapid and large calcium waves in wS1 and S2 or in motor cortex with a dF/F exceeding 1.5% change and on the other hand in some other trials very low signal amplitude change below 0.5%. Nonetheless we reliably recorded signal increase in whisker sensory areas (the significance of the signal change in the cortex will be discussed later).

Also, there was a large signal oscillation at ~12 Hz that was due to the heartbeat artifact. Indeed, it corresponded to ~750 BPM which was in the physiological range in active awake mice (Kramer et al. 1993; Späni et al. 2003). This oscillatory signal was much reduced when averaged over several trials.

Signal amplitude for individual trials can go up to 3% change within the first 250 ms but when averaged, wide-field calcium imaging was more in the range of ~1% change. The signal is rising rapidly after whisker stimulation. Already 30 ms after stimulus onset some increase in signal was observed on average. This effect will be quantified later with statistical maps. The decay of the wide-field calcium signal was much longer to go back to baseline (in the order of a second).
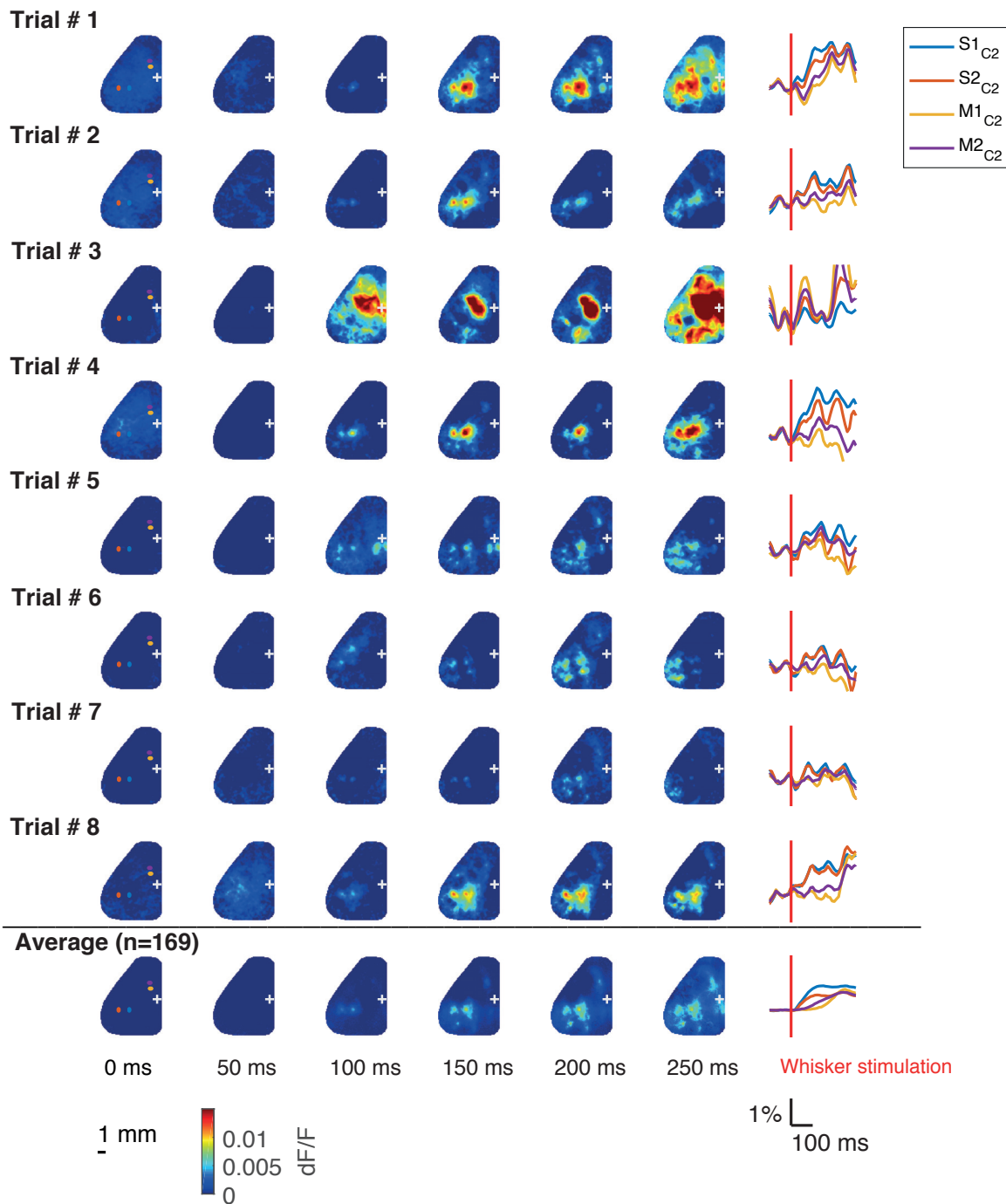
C2 stim lick responses for MA095

Figure 4.8.a. Example of dF/F maps and signal time course for single trials for one representative GCaMP6f mouse.

Single trial examples were selected for hit trials (licking after C2 stimulation). The maps on the first column are an average of 5 frames from -50 to 0 ms, on the second column an average from 0 to 50 ms, on the third column an average from 50 to 100 ms, on the fourth column an average from 100 to 150 ms, on the fifth column an average from 150 to 200 ms and on the last column an average from 200 to 250 ms. All the maps are represented on the same color scale.

The traces on the right side of the panel are the extracted from the ROIs drawn on the maps of the first column located in wS1, S2, wM1 and M2. The red vertical bar represents the time of the stimulus onset. The stimulus was an oscillation at 25 Hz for 200 ms.
The last row is an average of 169 hit trials. Bregma position was represented by a white cross.

GFP control

We imaged GFP mice in control experiments to test if the detected signal was coming from GCaMP6f fluorescence change or if the signal was dominated by intrinsic signal changes. To do so, we used three GAD67-GFP mice that overwent complete 2-whisker discrimination task training. Both signals came from GFP fluorescence but one should be functional (GCaMP6f should reflect calcium increases induced by neuronal activity) and the other should be structural (should not change with neuronal activity). We noticed that GAD67-GFP mice did not have any signal significant change in wS1 and S2 during the first 250 ms. The main changes in the collected fluorescence came from the superior sagittal sinus. These changes could be a mixture of motion artifact, and intrinsic signals coming from the blood flow changes due to the recruiting of neurons in cortical motor areas to trigger licking. The same signal oscillation at ~12 Hz was detected due to the heartbeat artifacts. On average the change in collected fluorescence was flat for the first 200 ms.
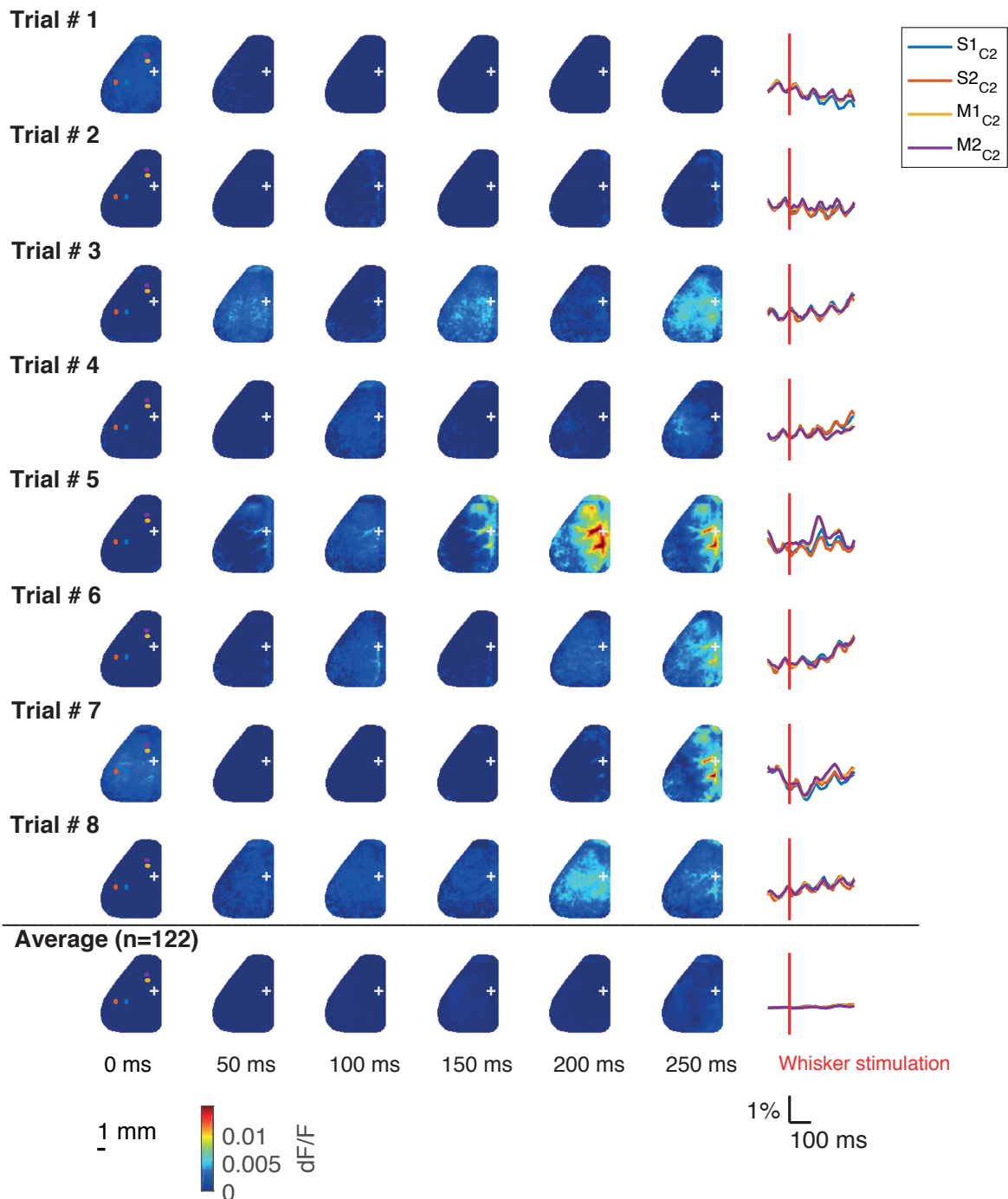
Figure 4.8.b. Example of dF/F maps and signal time course for single trials for one representative GFP mouse.

Wide-field calcium maps averaged over all stimulation trials

We computed an average over all stimulation trials and all sessions of 2-whisker discrimination task. We did not distinguish if the mice were licking or not. These maps gave us the average signal dynamic of calcium waves for stimulation trials. The average of 50 to

100 ms gave a very localised activation in wS1 and S2. Then in the average 100 to 150 ms either wM1 or M2 or sometimes both were activated very locally. During the 150 to 200 ms the different activated spots gain in amplitude. We also noticed an activation in retrosplenial cortex (RSC). In this analysis, during the first 250 ms, the average signal was higher in the sensory areas (S1 and S2) than any other cortical region for both C2 and B2 stimulation. In some example mice, S1 activation was larger in amplitude than S2 and in other mice the opposite effect was observed.
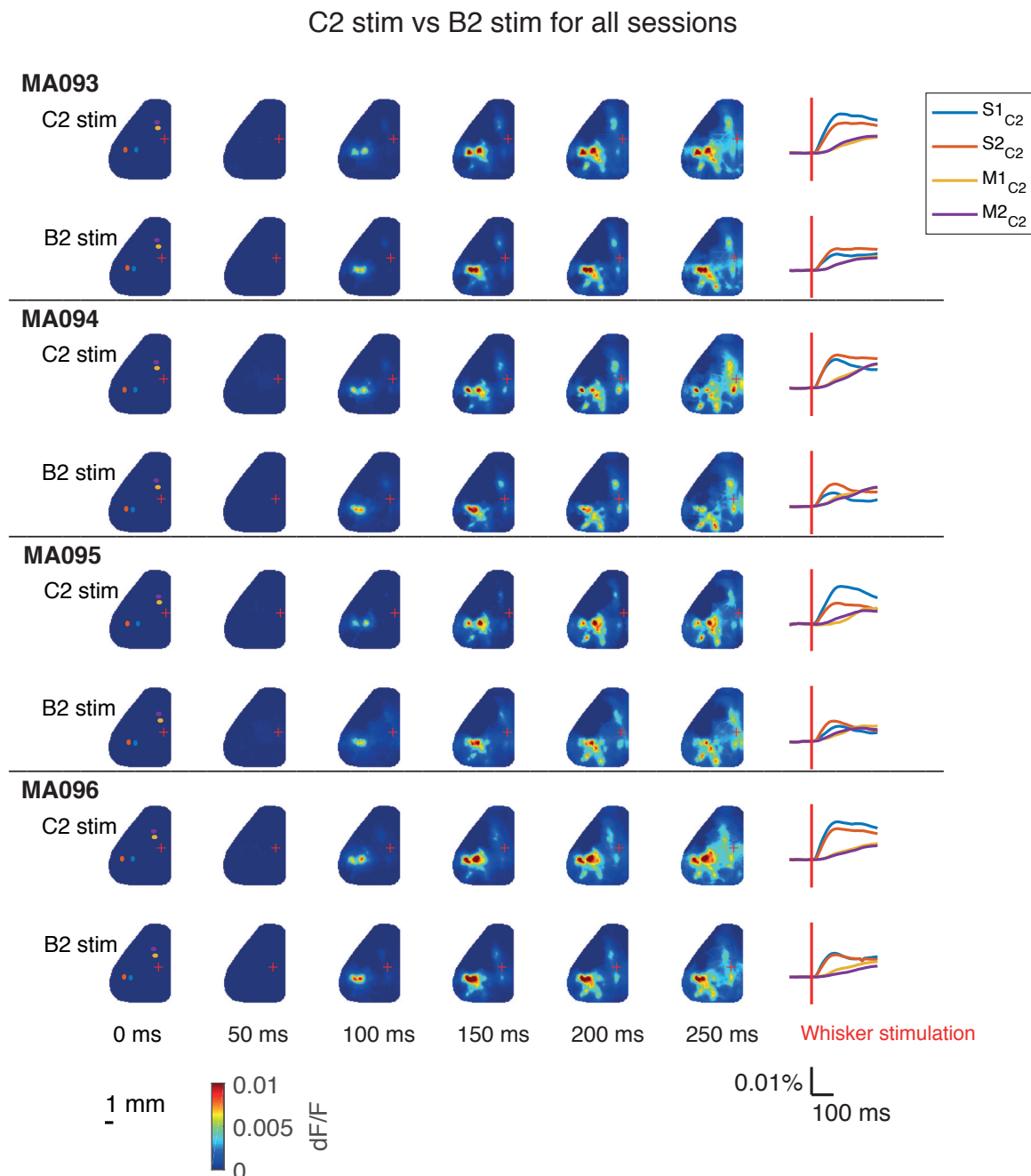
Figure 4.9.a. Wide-field calcium maps during either B2 or C2 stimulation trials, regardless whether the animal licked or not, for four GCaMP6f mice.
Maps over either all B2 or all C2 stimulations for all sessions were averaged for each mouse. The maps on the first column are an average of 5 frames from -50 to 0 ms, on the second

column an average from 0 to 50 ms, on the third column an average from 50 to 100 ms, on the fourth column an average from 100 to 150 ms, on the fifth column an average from 150 to 200 ms and on the last column an average from 200 to 250 ms. All the maps are represented on the same color scale.

The traces on the right side of the panel are the extracted from the ROIs drawn on the maps of the first column located in wS1, S2, wM1 and M2 centered on either B2 or C2 cortical area. The red vertical bar represents the time of the stimulus onset. The stimulus was an oscillation at 25 Hz for 200 ms.

Bregma position was represented by a white cross.

GFP control

We compared the fluorescence change between GCaMP6f and GAD67-GFP mice for either B2 or C2 stimulation trials. We observed that the first 200 ms, GAD67-GFP mice had no response. Later some signals are emerging from the superior sagittal sinus due to intrinsic signal especially for C2 stimulation trials.
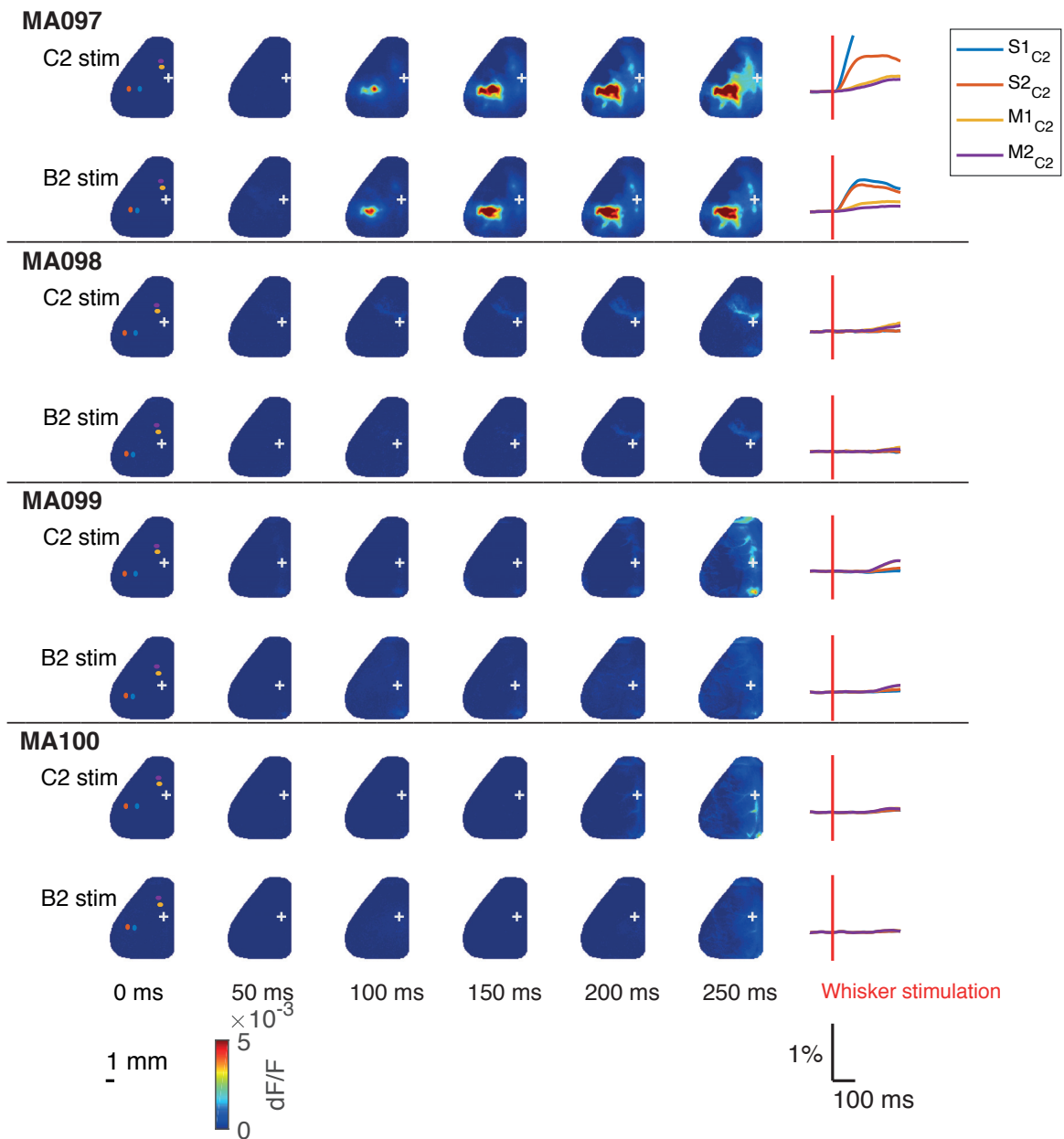
Figure 4.9.b. Wide-field maps during either B2 or C2 stimulation trials, regardless whether the animal was licking or not, for one GCaMP6f mouse (MA097) and three GAD67-GFP mice (MA098, MA099 and MA100).

Wide-field calcium averaged maps of each behavioral condition for one session

We computed the averaged response maps for each behavioral condition: hit (C2 stimulation lick), miss (C2 stimulation nolick), false alarm stim (B2 stimulation lick), correct rejection stim (B2 stimulation nolick), false alarm catch (no stimulation lick), and correct rejection catch (no stimulation nolick). As described in the figure 4.9.a, we observed a response in sensory

areas in all the conditions when the whiskers were stimulated, and as expected, those sensory areas were not recruited in the no stimulation trials. In the lick trials, there was a large increase of activity in motor areas, appearing after 150 ms. These M1/M2 areas were also activated in the no lick trials but in lower amplitude. Then a large activation of tjS1 was observed in the lick conditions after 250 ms, corresponding to the relatively early reaction times for licking.
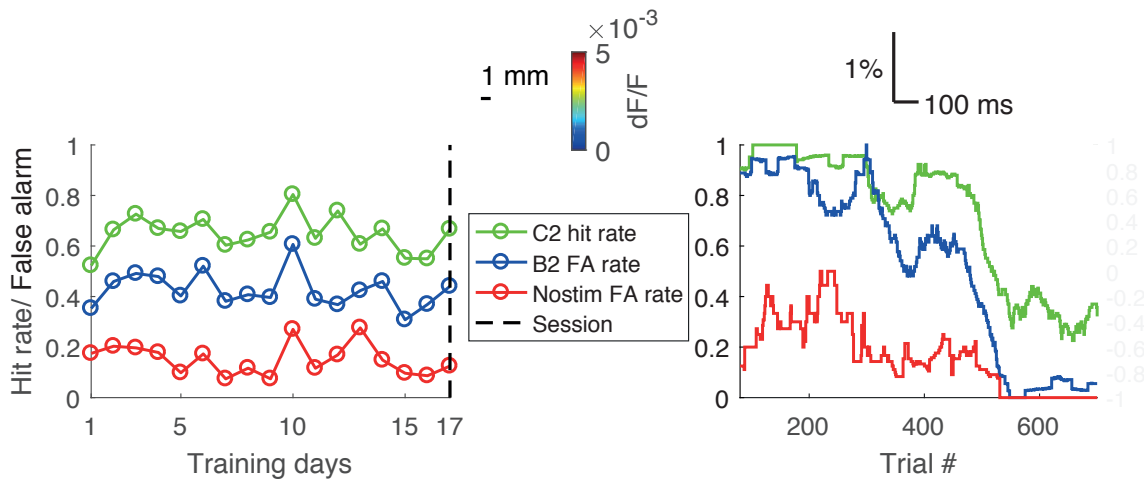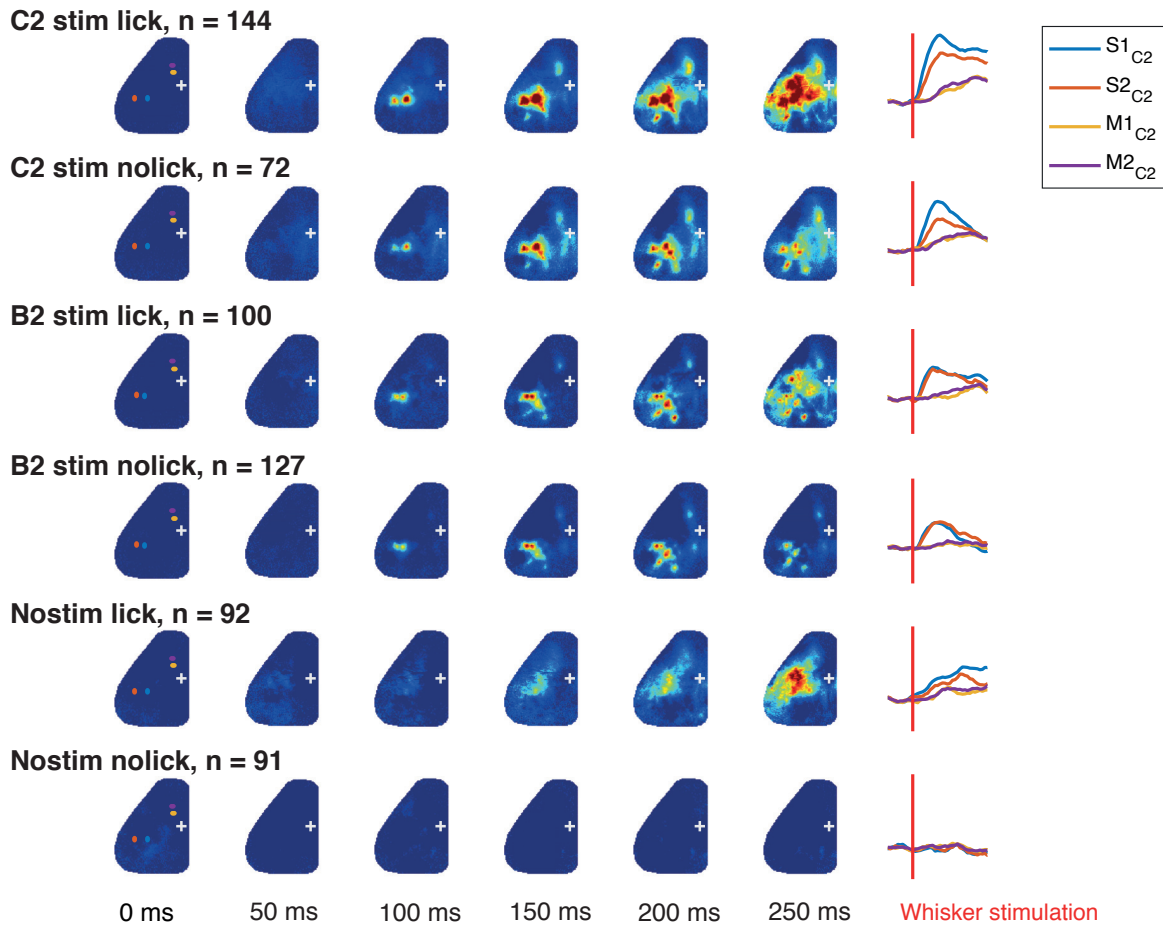

Average behavioral responses for MA093

Figure 4.10. Wide-field calcium maps of the six behavioral conditions during the last session of training for one mouse.

In the top panel, calcium maps were represented for hit (C2 stimulation lick), miss (C2 stimulation nolick), false alarm stim (B2 stimulation lick), correct rejection stim (B2 stimulation nolick), false alarm catch (no stimulation lick), and correct rejection catch (no stimulation nolick). The maps on the first column are an average of 5 frames from -50 to 0 ms, on the second column an average from 0 to 50 ms, on the third column an average from 50 to 100 ms, on the fourth column an average from 100 to 150 ms, on the fifth column an average from 150 to 200 ms and on the last column an average from 200 to 250 ms. All the maps are represented on the same color scale.

The traces on the right side of the panel are the extracted from the ROIs drawn on the maps of the first column located in wS1, S2, wM1 and M2 centered on either B2 or C2 cortical area. The red vertical bar represents the time of the stimulus onset. The stimulus was an oscillation at 25 Hz for 200 ms.

Bregma position was represented by a white cross.

In the bottom panel left, there is the overall performance during 17 days of training of the mouse, represented as in figure 4.6.

In the bottom panel right, there is the performance of the imaged session 17 for the mouse, represented as in figure 4.6.

Statistical comparison maps between hit and correct rejection catch trials

In order to test if the calcium signals detected by GCaMP6f functional imaging during the stimulation trials were significantly different from resting state activity or from the noise, we performed some statistical comparisons (figure 4.11). To be able to compare the signal from one trial to another, we first had to perform to normalise the signal. Two methods of normalisation were used: the dF/F and the z-score.

$$\Delta F/F(i,j,t) \ = \ \frac{F(i,j,t) - F_0(i,j)}{F_0(i,j)}$$

$$zscore(i,j,t) \ = \ \frac{F(i,j,t) - mean(F_0(i,j))}{std(F_0(i,j))}$$

With the z-score, we were able to perform a z-test that assessed if the evoked response was significantly different to the variance of the baseline. A significant singal increase from the baseline was detected in the hit (C2 stim lick) trials after 100 ms in S1/S2 whereas no difference was detected in correct rejection (CR) catch (no stim no lick) trials. The measured signal was reliably reflecting an evoked response in the cortex. The trials where the mouse licked before 200 ms were excluded from all the analysis.

We also wanted to test if hit trials were different to CR catch trials by performing a t-test on these two conditions. For the tested mouse, during the last session, there was a significant difference in wS1 and S2 after 100 ms. Then the divergence from these two conditions was detected also frontally in M1 and M2 from 150 ms and kept increasing.

These tests told us that first there might be a significant evoked response, and second there should be a significant difference between hit and CR catch trials. We wanted to confirm this result to see if it could be generalized to all the mice.
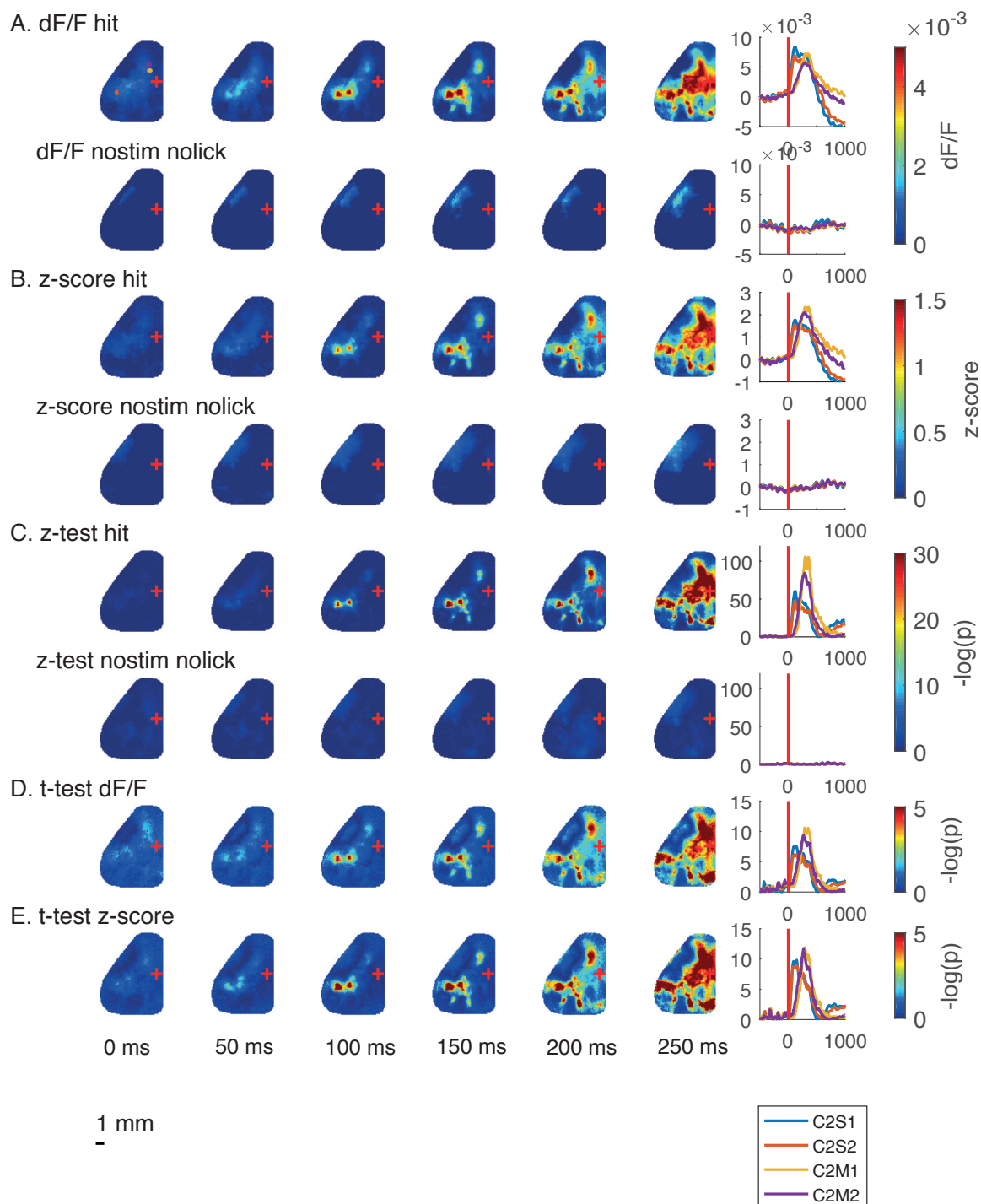
Figure 4.11.a. Statistical significance for hit (C2 stim lick) and correct rejection catch (nostim nolick) trials as well as their difference for one mouse during one session.
A. Maps of dF/F were displayed for both hit and CR catch trials over time.
B. Maps of z-score were displayed for both hit and CR catch trials over time.
C. Maps of -log of the p-values resulting of z-test were displayed for both hit and CR catch trials over time. The z-test is a statistical test that assesses if the evoked response deviates significantly from the normal distribution based on the pre-stimulus baseline.

81

D. Maps of -log of the p-values resulting of t-test difference between dF/F of hit and CR catch trials were displayed over time.

E. Maps of -log of the p-values resulting of t-test difference between z-score of hit and CR catch trials are displayed over time.

On the right, the time courses of S1, S2, M1 and M2 are plotted. The red line corresponds to the stimulus onset.

The trials when the mouse was licking before 200 ms were excluded from this analysis.

Bregma position is indicated by a red cross.

We computed the same tests of significance for the two conditions FA stim and CR catch during the same session.
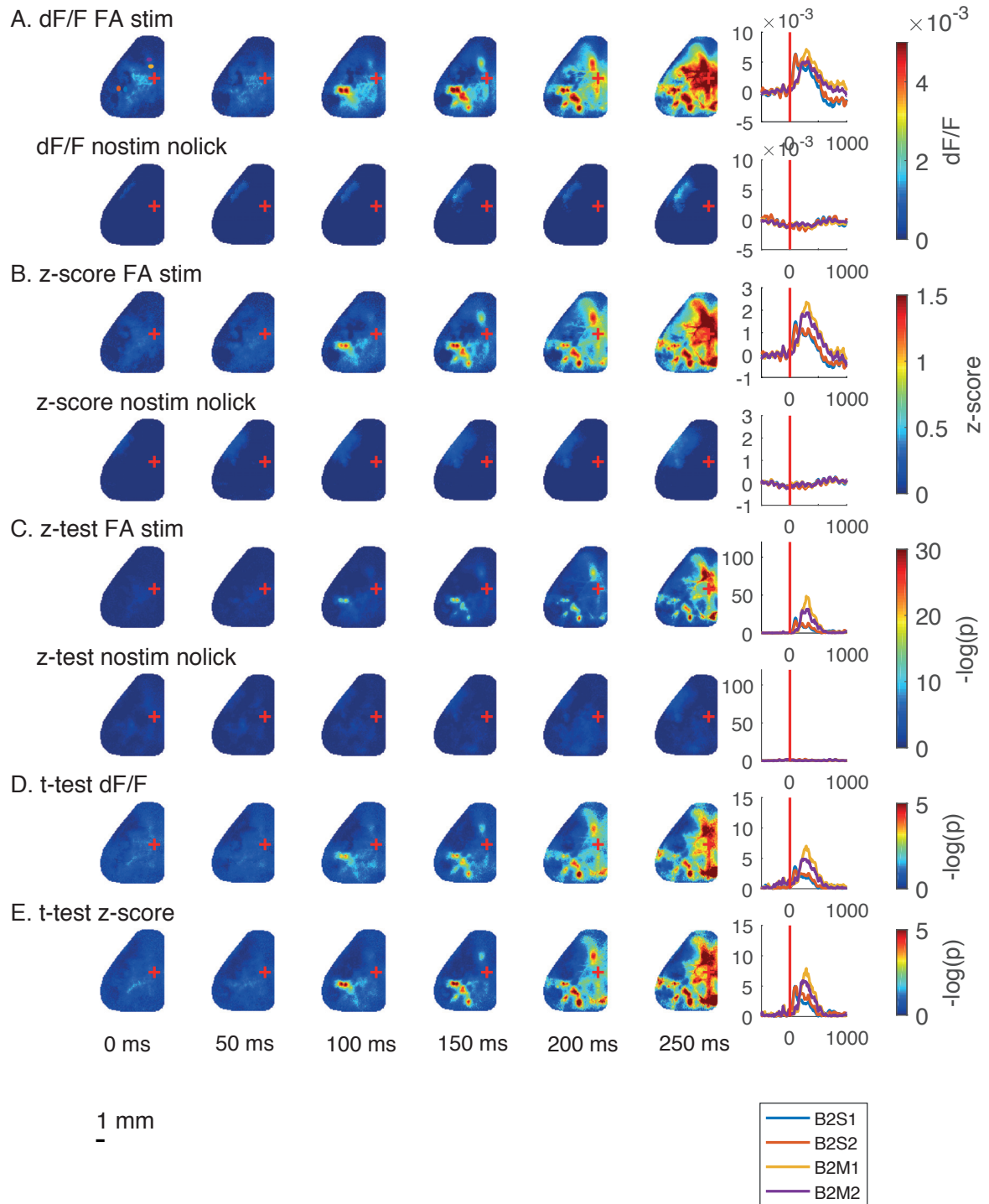
Figure 4.11.b. Statistical significance for false alarm stim (B2 stim lick) and correct rejection catch (nostim nolick) trials as well as their difference for one mouse during one session.
A. Maps of dF/F were displayed for both FA stim and CR catch trials over time.
B. Maps of z-score were displayed for both FA stim and CR catch trials over time.

C. Maps of -log of the p-values resulting of z-test were displayed for both FA stim and CR catch trials over time. The z-test is a statistical test that assesses if the evoked response deviates significantly from the normal distribution based on the pre-stimulus baseline.
D. Maps of -log of the p-values resulting of t-test difference between dF/F of FA stim and CR catch trials were displayed over time.
E. Maps of -log of the p-values resulting of t-test difference between z-score of FA stim and CR catch trials are displayed over time.
On the right, the time courses of S1, S2, M1 and M2 are plotted. The red line corresponds to the stimulus onset.
The trials when the mouse was licking before 200 ms were excluded from this analysis.
Bregma position is indicated by a red cross.

We computed the same tests of significance for the two conditions hit and CR catch in the GFP control mice. Thanks to the z-test, we confirmed that there was no significant evoked response deviating from the baseline in both hit and CR catch trials for the first 250 ms. Also, the t-test confirmed that there was no significant difference between hit and CR catch trials in GFP control mice within the first 250 ms.
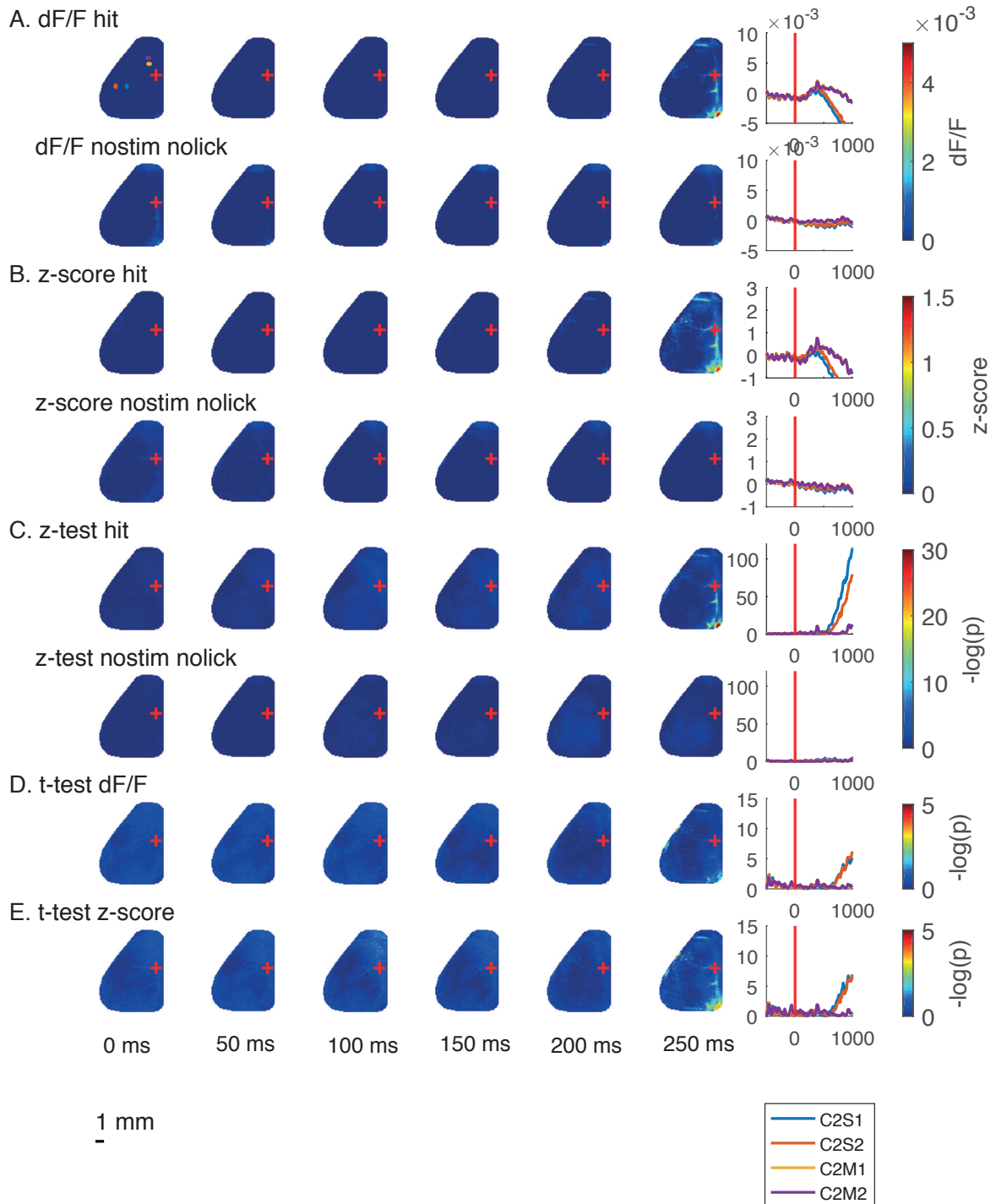
Figure 4.11.c. Statistical significance for hit (C2 stim lick) and correct rejection catch (nostim nolick) trials as well as their difference for one GFP control mouse during one session.

To compare from one mouse to another, we selected an early time period and investigated where we detected a significant difference between hit and CR catch trials (figure 4.12). At 100 ms, in all mice all the tested sessions gave a significant difference. Then for each

mouse, we constructed a mask for each session where the value was equal to 1 where the p-value was below 0.001 (-log(p-value) > 3) and was equal to 0 anywhere else. We averaged the significant mask between 4 sessions. We obtained 11 masks between 0 and 1 that we aligned on C2 center and we summed to have the grand mask of significance. A difference between hit trials and CR catch trials was reliably detected in wS1 and S2 after 100 ms, but it turned out that the difference was not significant on average for all mice, or at least, the differences were not located exactly all at the same locations. This might be due to the somatosensory representation distribution that we saw on figure 4.5.
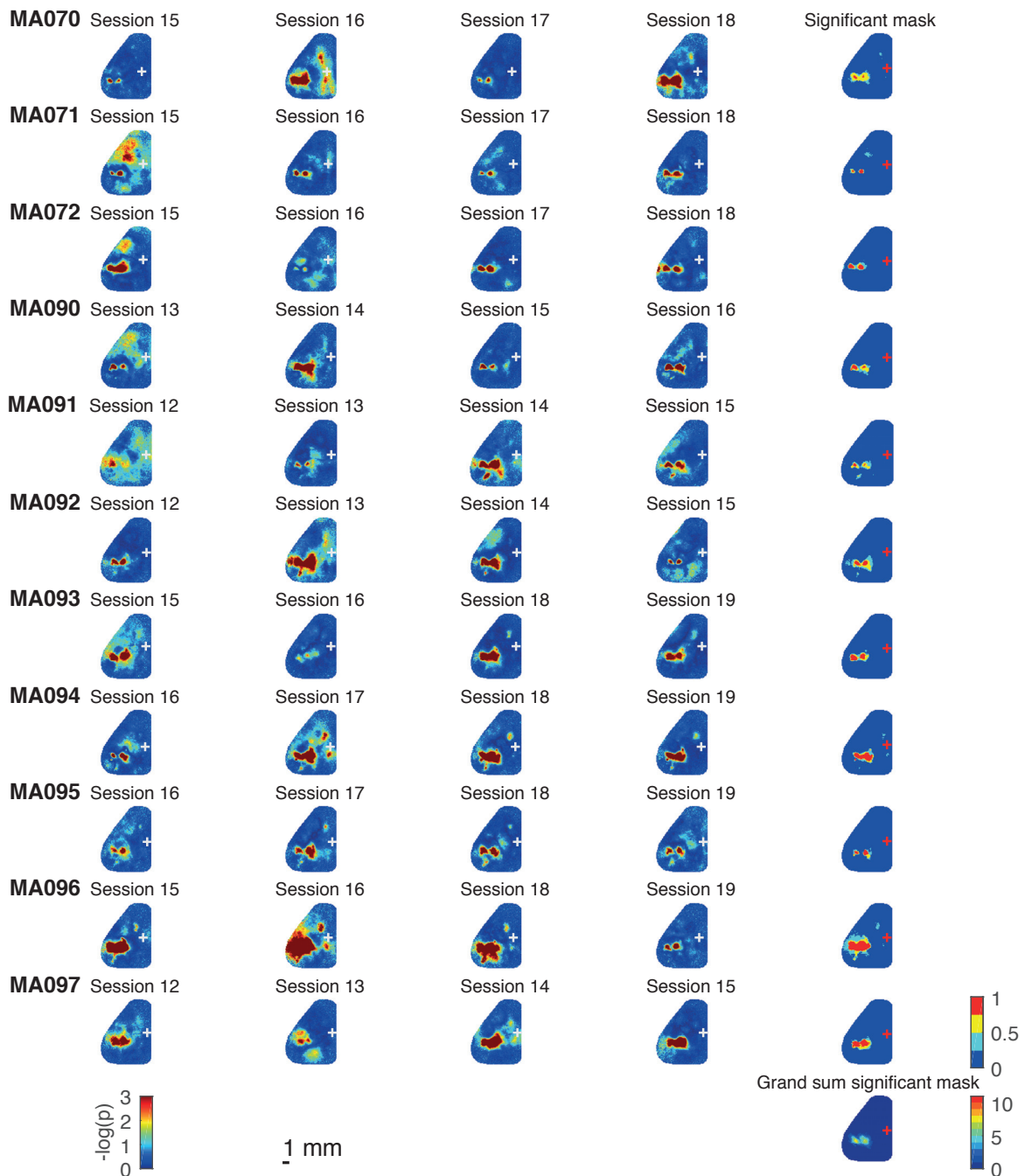

Hit/CR t-test at 100 ms

Figure 4.12. Statistical t-test difference between hit (C2 stim lick) and correct rejection catch (nostim nolick) z-score for all mice averaged from 50 to 100 ms after stimulus onset.

Maps of -log of the p-values resulting of t-test difference between z-score of hit and CR trials for the 4 last sessions. -log(3) corresponds to a p-value below 0.001.

On the right side, there are masks based on the significance of the response, for p-values below 0.001.

The grand sum mask of the significance is the sum of the significant masks above for each mouse aligned on C2 center.

The trials when the mice were licking before 200 ms were excluded from this analysis.

Bregma position is indicated by a white cross on the t-test maps and by a red cross on the masks.

Finally, the latency for detecting a significant difference between hit trails and CR catch trials was computed for all the mice (figure 4.13). Interestingly, various regions of cortex crossed the threshold of a p-value below 0.001 within 250 ms. There was a large variability from one mouse to another and also within the mice from one session to another. The large diversity of cortical activity might be influenced by various parameters that change from day to day, like the motivation, the thirst, and the reaction time. Mainly, the earliest differences between hit trails and CR catch trials occured in wS1 and S2. Also, we could have thought that wM1 and M2 would deviate in hit trials from CR catch trials within 250 ms as the mouse would trigger licking but it was not the case on the grand average latency map.
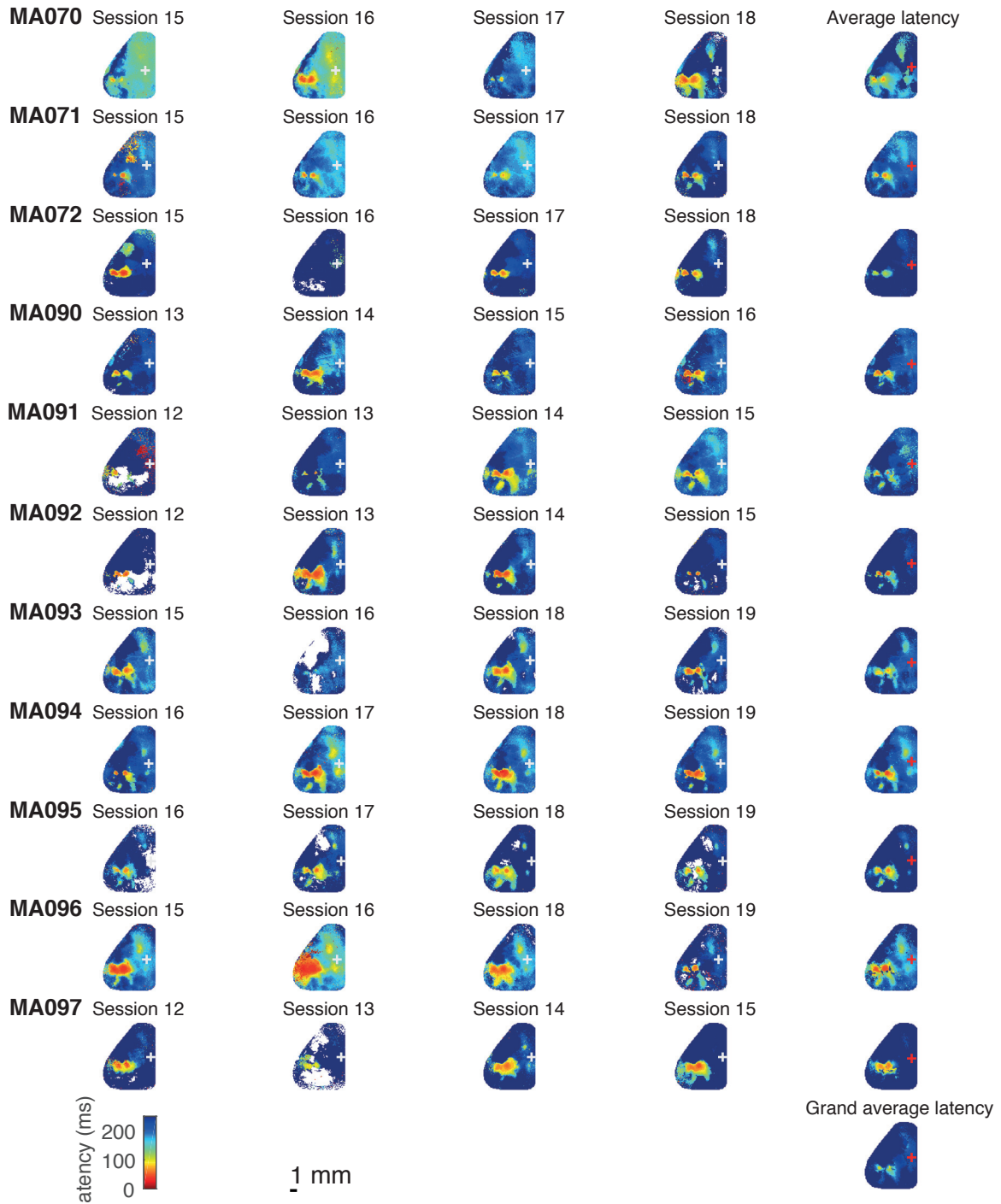
Figure 4.13. Latency of the hit (C2 stim lick) trials deviating significantly from the correct rejection catch (nostim nolick) for all mice.

Maps of the latencies for the last 4 sessions. For the pixels that did not cross the significant threshold of p-values below 0.001, we put them as NaN and are shown as transparent.

On the right, there are the averages of the 4 latency-maps.

The grand average latency was computed by averaging all the averaged latency of each mouse above aligned on C2 center.

The trials when the mice were licking before 200 ms were excluded from this analysis.

Bregma position is indicated by a white cross on the t-test maps and by a red cross on the masks.

The earliest difference observed between hit and CR catch trials was in S1/S2 (at ~100 ms) and then a difference emerged in motor cortex M2 after 200 ms (figure 4.14). The signal was spreading both in wM1 and also more frontally in a region close to ALM after 250 ms. Only the hit trials when mouse licked after 200 ms were kept in this analysis.
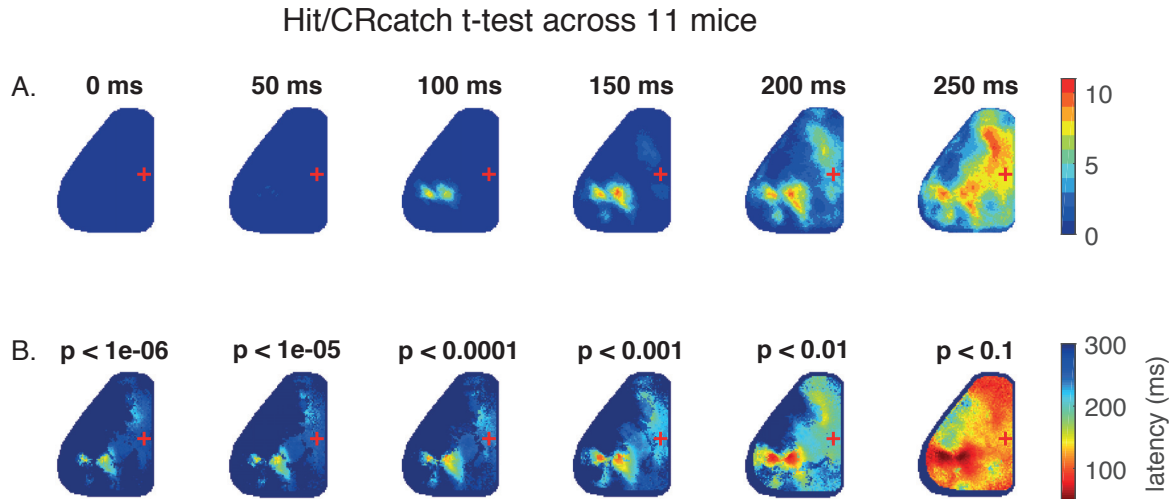

Figure 4.14. Summary t-test maps of the difference between hit (C2 stim lick) and CR catch (no stim no lick) trials for all mice (n=11).
A. Sum of the 11 masks of significance for p-value below 0.001 for 6 time points.
B. Maps of the latencies for threshold of increasing p-values.
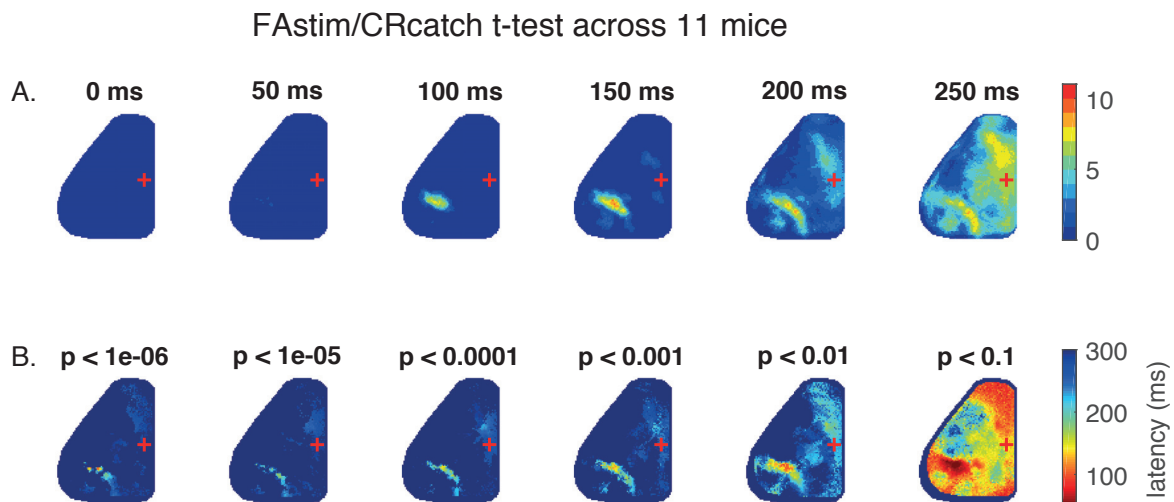*Bregma position is indicated by a red cross.*

Figure 4.15. Summary t-test maps of the difference between FA stim (B2 stim lick) and CR catch (no stim no lick) trials for all mice (n=11).
A. Sum of the 11 masks of significance for p-value below 0.001 for 6 time points.
B. Maps of the latencies for threshold of increasing p-values.
Bregma position is indicated by a red cross.

Statistical comparison maps between hit and miss trials

After making sure that we detected a signal difference in hit trials compare to the CR catch, we wondered if there was a difference between hit and miss trials in layer 2/3 GCaMP6f mice (figure 4.16). To be able to compare the different signals, we computed the two normalisations: dF/F and z-score, using the same formulas as described before.

To assess if the evoked response was significantly different from the variation in the baseline, we computed a z-test. The signal was reliably diverging from baseline in wS1 and S2 after 150 ms from stimulus onset in both lick and no lick conditions. Nonetheless, the signal was more localised in miss trials and larger in hit trials. This might imply a sensory modulation already in wS1 and S2 in layer 2/3.

To test this hypothesis, we did a t-test between hit trials and miss trials. It turned out that for this session in particular there was no early sensory modulation in wS1 and S2. The first significant differences were occuring at 250 ms in wide regions of the cortex. We then wanted to test this hypothesis on all the mice and see if anything would emerged from this analysis, especially in those four regions S1/S2 and M1/M2.
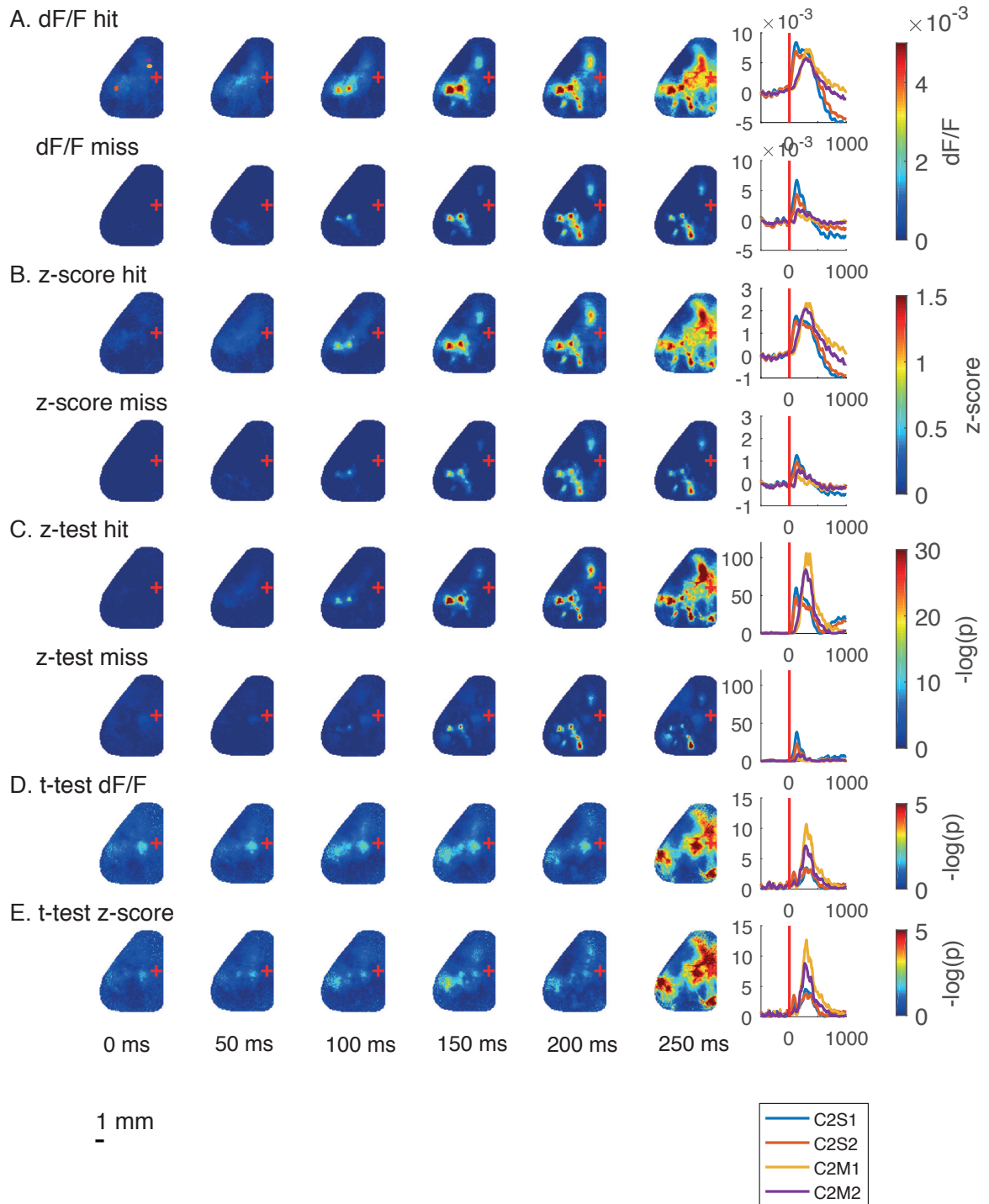
Figure 4.16.a. Statistical significance for hit (C2 stim lick) and miss (C2 stim nolick) trials as well as their difference for one mouse during one session.

A. Maps of dF/F were displayed for both hit and miss trials over time.

B. Maps of z-score were displayed for both hit and miss trials over time.

C. Maps of -log of the p-values resulting of z-test were displayed for both hit and miss trials over time. The z-test is a statistical test that assesses if the evoked response deviates significantly from the normal distribution based on the pre-stimulus baseline.

D. Maps of -log of the p-values resulting of t-test difference between dF/F of hit and miss trials were displayed over time.

E. Maps of -log of the p-values resulting of t-test difference between z-score of hit and miss trials are displayed over time.

On the right, the time courses of S1, S2, M1 and M2 are plotted. The red line corresponds to the stimulus onset.

The trials when the mouse was licking before 200 ms were excluded from this analysis.

Bregma position is indicated by a red cross.

We computed the same tests of significance for the two conditions FA stim and CR catch during the same session.

Figure 4.16.b. Statistical significance for FA stim (B2 stim lick) and CR stim (B2 stim nolick) trials as well as their difference for one mouse during one session.
A. Maps of dF/F were displayed for both FA stim and CR stim trials over time.
B. Maps of z-score were displayed for both FA stim and CR stim trials over time.
C. Maps of -log of the p-values resulting of z-test were displayed for both FA stim and CR stim trials over time. The z-test is a statistical test that assesses if the evoked response deviates significantly from the normal distribution based on the pre-stimulus baseline.

D. Maps of -log of the p-values resulting of t-test difference between dF/F of FA stim and CR stim trials were displayed over time.

E. Maps of -log of the p-values resulting of t-test difference between z-score of FA stim and CR stim trials are displayed over time.

On the right, the time courses of S1, S2, M1 and M2 are plotted. The red line corresponds to the stimulus onset.

The trials when the mouse was licking before 200 ms were excluded from this analysis.

Bregma position is indicated by a red cross.

We computed the same tests of significance for the two conditions hit and miss in the GFP control mice. Thanks to the z-test, we confirmed that there was no significant evoked response deviating from the baseline in both hit and miss trials for the first 250 ms. Also, the t-test confirmed that there was no significant difference between hit and miss trials in GFP control mice within the first 250 ms.
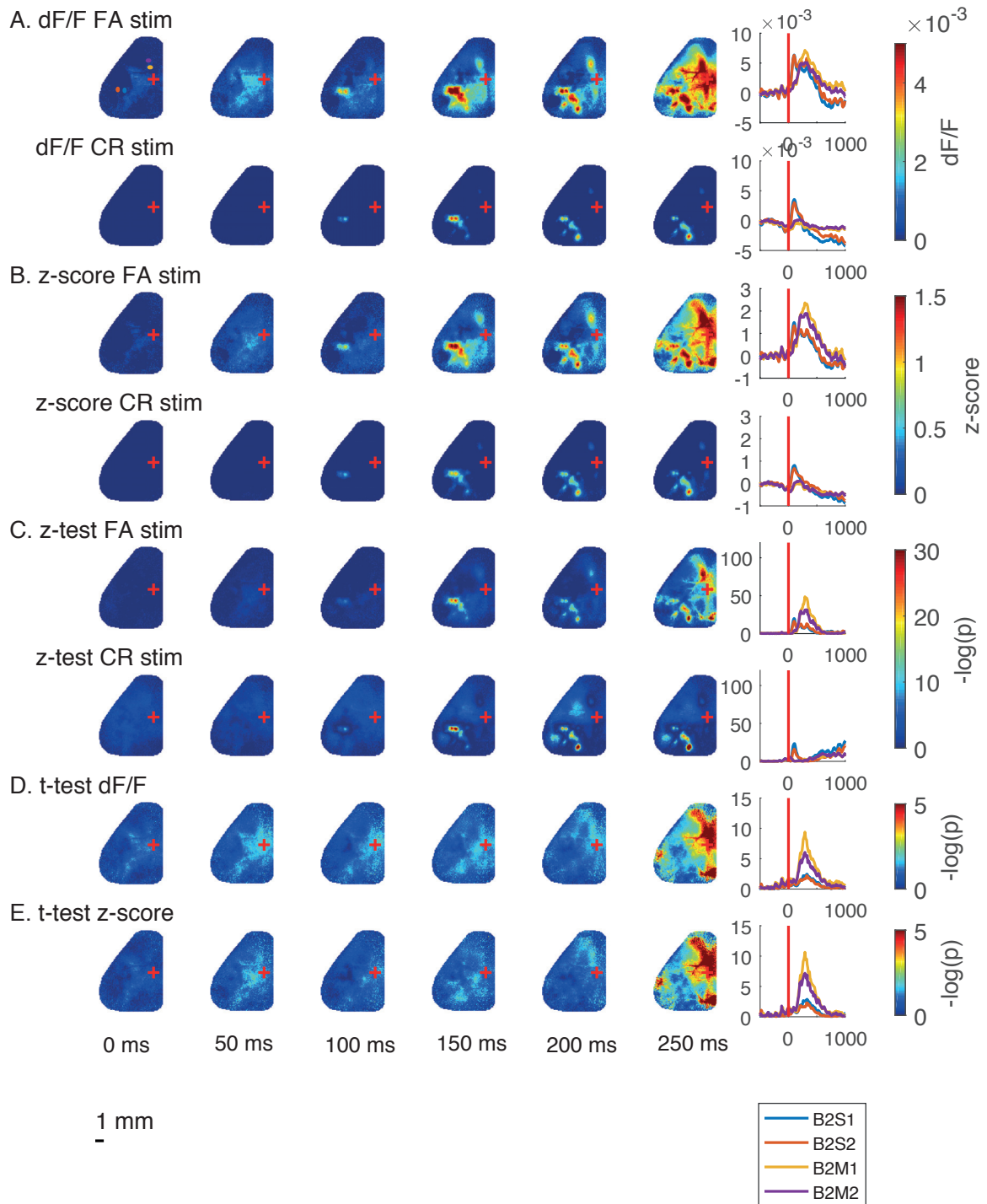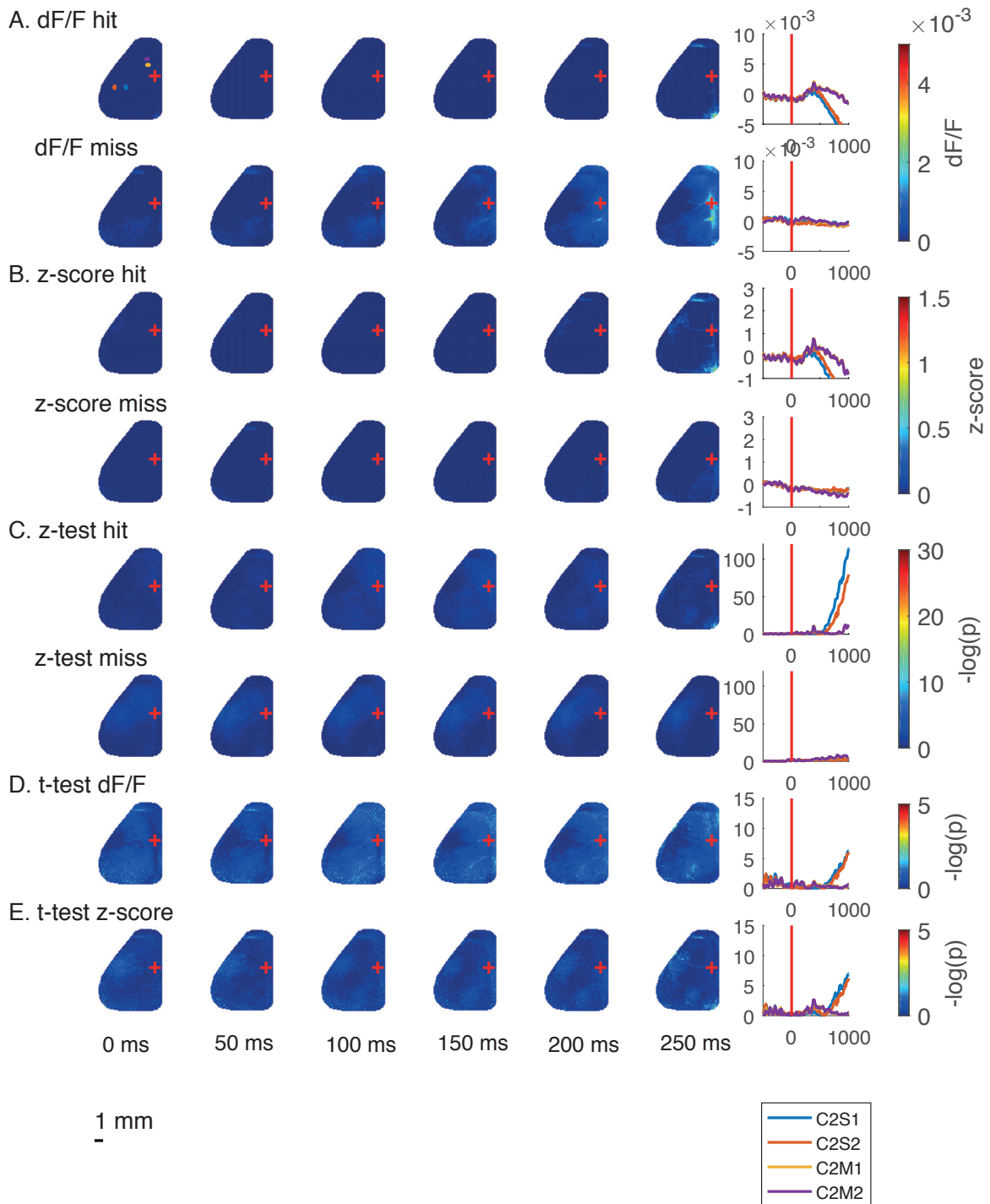
Figure 4.16.c. Statistical significance for hit (C2 stim lick) and miss (C2 stim nolick) trials as well as their difference for one GFP control mouse during one session.

To compare the differences between hit and miss trials in all the mice, we isolated when the earliest statistical difference might be occurring, which was 150 ms (figure 4.17). For each session tested, a mask was computed by giving a value 1 where the difference had a p-value below 0.001 and 0 anywhere else. There was a very large variability from one mouse

to another and from one session to another. In 9 mice out of 11 we had some differences in S1/S2 but it was not detected for all the sessions. In 2 mice, there was also a small difference in M1/M2. In 2 mice, we had no differences detected between hit trials and miss trials at 150 ms. The grand sum mask was almost completely flat, meaning that there was almost no significant difference occurring between hit and miss trials within 150 ms.
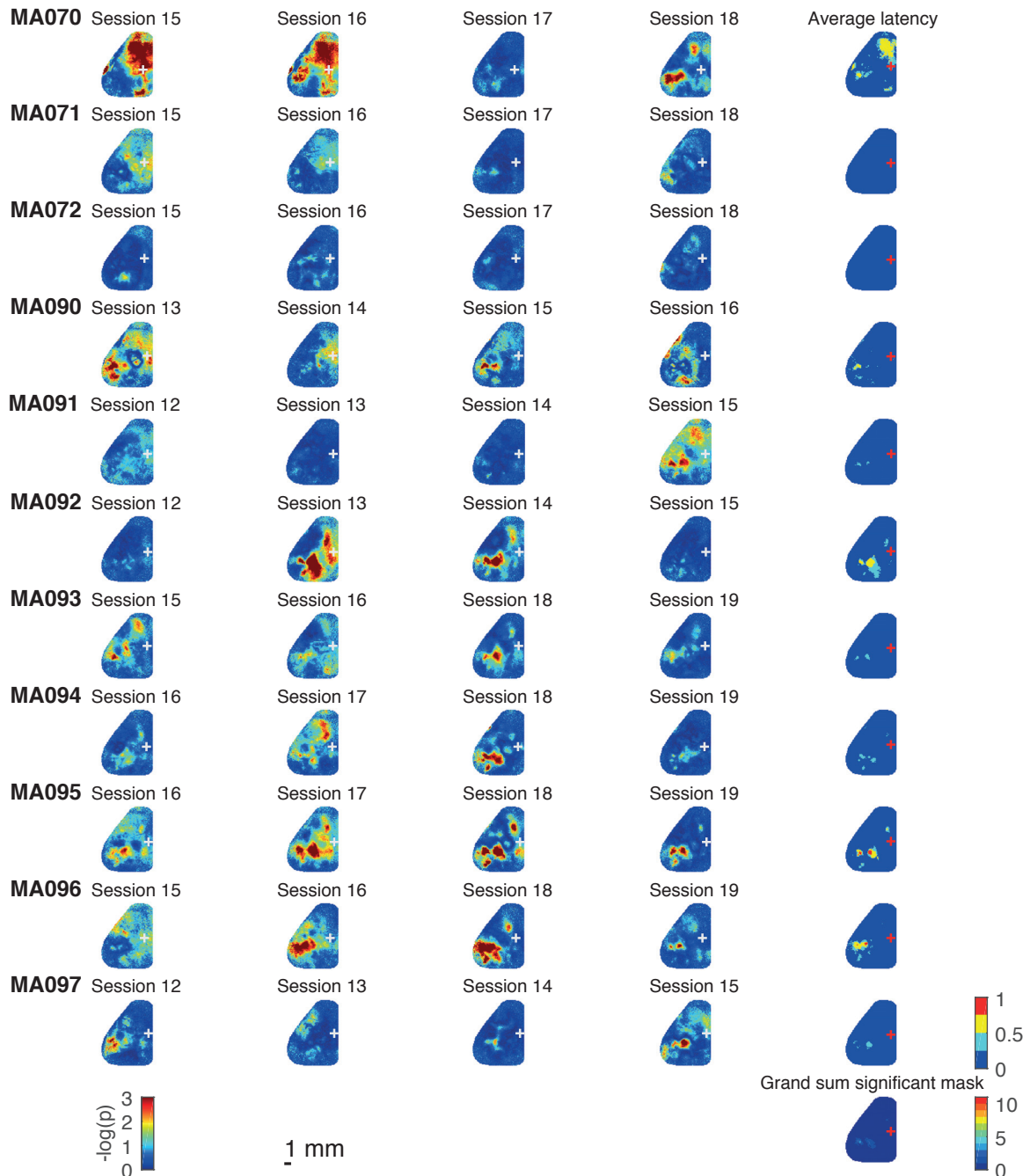

Figure 4.17. Statistical t-test difference between hit (C2 stim lick) and miss (C2 stim nolick) z-score for all mice averaged from 100 to 150 ms after stimulus onset.
Maps of -log of the p-values resulting of t-test difference between z-score of hit and miss trials for the 4 last sessions. -log(3) corresponds to a p-value below 0.001.

96

On the right side, there are masks based on the significance of the response, for p-values below 0.001.
The grand sum mask of the significance is the sum of the significant masks above for each mouse aligned on C2 center.
The trials when the mice were licking before 200 ms were excluded from this analysis.
Bregma position is indicated by a white cross on the t-test maps and by a red cross on the masks.

The latency maps for differences with a p-value below 0.001 were computed for 4 sessions for all mice (figure 4.18). On average, no significant diversions were detected between hit and miss trials for the first 250 ms. In some examples, S1/S2 and even M2 were different between hit and miss before 200 ms. There were very little modulations of the responses between hit and miss trials occurring in layer 2/3.

Hit/Miss t-test latency for p-value < 0.001
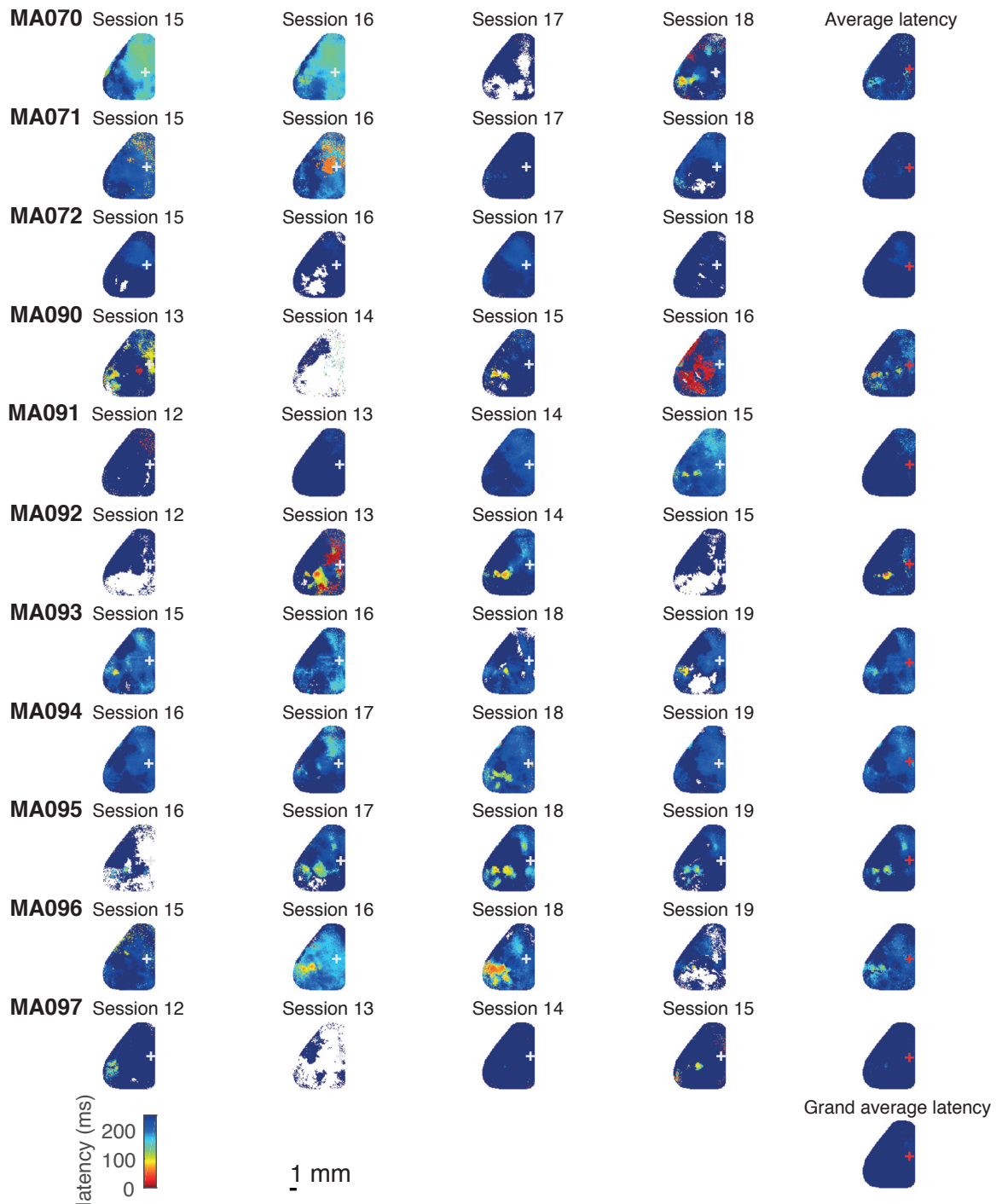
Figure 4.18. Latency of the hit (C2 stim lick) trials deviating significantly from the miss (C2 stim nolick) for all mice.

Maps of the latencies for the last 4 sessions. For the pixels that did not cross the significant threshold of p-values below 0.001, we put them as NaN and are shown as transparent.

On the right, there are the averages of the 4 latency-maps.

The grand average latency was computed by averaging all the averaged latency of each mouse above aligned on C2 center.

The trials when the mice were licking before 200 ms were excluded from this analysis.

Bregma position is indicated by a white cross on the t-test maps and by a red cross on the masks.

So there some significant differences were detected between hit and miss trials. The first detected differences were in S1/S2 in a few mice after 150 ms. Then the largest differences were emerging from M2 at 200 ms and propagating toward ALM. The very frontal part of the cortex might be the structure reflecting the largest difference between lick and no lick decision.

Hit/Miss t-test across 11 mice

Figure 4.19. Summary t-test maps of the difference between hit (C2 stim lick) and miss (C2 stim no lick) trials for all mice (n=11).
A. Sum of the 11 masks of significance for p-value below 0.001 for 6 time points.
B. Maps of the latencies for threshold of increasing p-values.
Bregma position is indicated by a red cross.
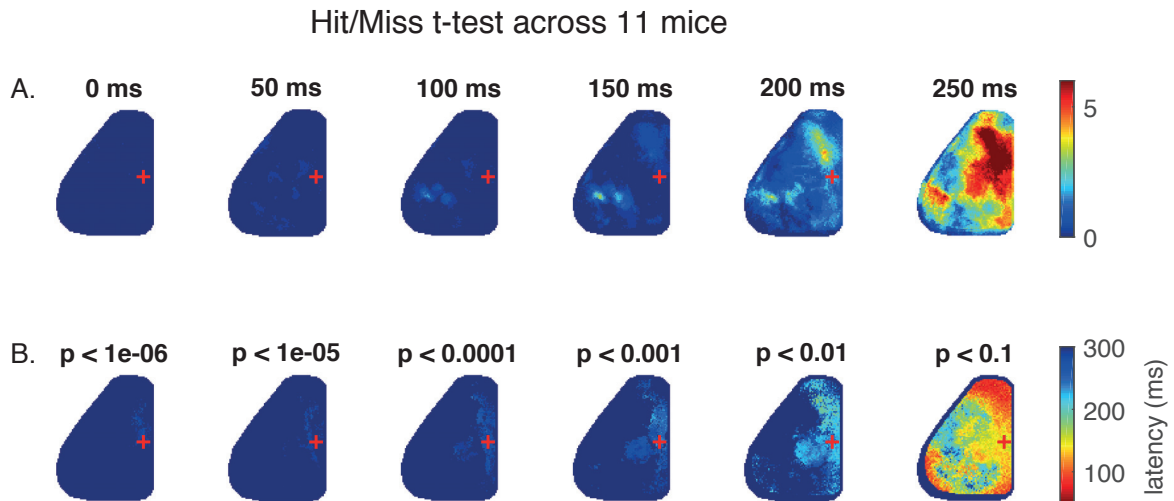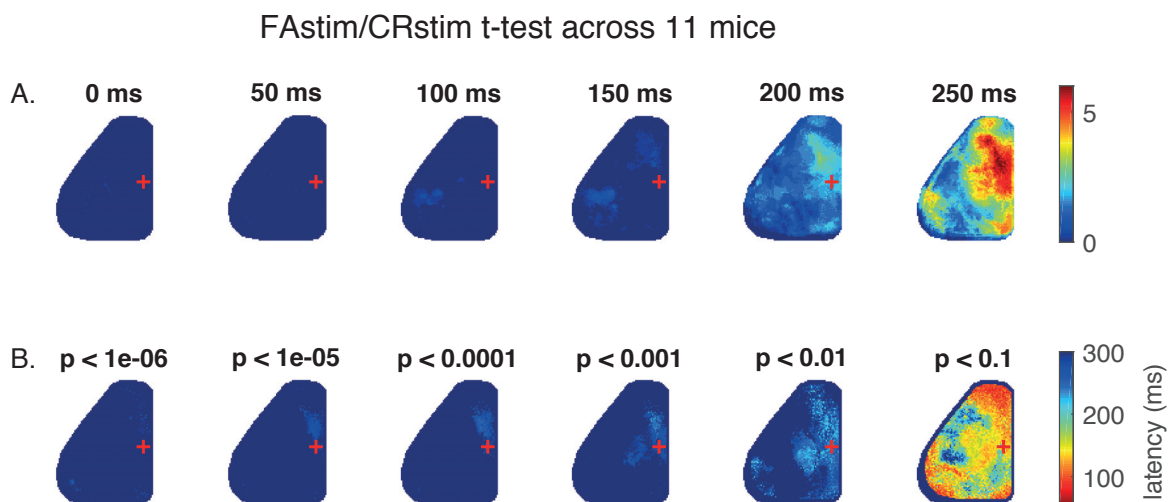
FAstim/CRstim t-test across 11 mice

Figure 4.20. Summary t-test maps of the difference between FA stim (B2 stim lick) and CR stim (B2 stim no lick) trials for all mice (n=11).
A. Sum of the 11 masks of significance for p-value below 0.001 for 6 time points.
B. Maps of the latencies for threshold of increasing p-values.

Bregma position is indicated by a red cross.

Evolution of the signal during learning of the 2-whisker discrimination task

One of the strengths of wide-field calcium imaging using transgenic mouse lines is the possibility to record with a relatively stable signal and a stable preparation for a long time period. The training of the mice can take several days and sometimes several weeks. This gives the opportunity to study the evolution of the signal of the brain during the learning of the task and see the potential changes occurring in the cortex.

We looked at the change in amplitude of the signal for wS1, S2, M1 and M2 at given time points to see if some areas were reflecting the change in behavioral performances (figure 4.21). We computed the average traces for each session and reported the amplitude of the signal for each training day. First for C2 stimulation trials, for all the four tested areas, hit trials were higher than miss trials. Also, it seemed that for both wS1 and S2, signal amplitudes were decreasing over the training days for hit and miss trials. On the other hand, the signal amplitudes in wM1 and M2 were increasing and decreasing back to same level as the first days for hit trails and signals were staying stable over the learning of the task in miss trials. For the analysis, all the trials where the reaction time was below 300 ms were excluded to avoid contamination of the motor command in the early signal responses.

Figure 4.21. Evolution of the signal amplitude for hit (C2 stim lick) and miss (C2 stim no lick) trials at 100 ms in wS1 and S2, and at 250 ms in wM1 and M2 in one mouse over the learning of the 2-whisker discrimination task.

The average of the signal over each session for both hit and miss trials was color coded from cyan to magenta from the earliest training day to the last. The grand average signal is represented with a thick black line.

Each point of the graphs on the right is the amplitude of the corresponding curve of the day of training at the given time point (either at 100 ms for S1 and S2 or at 250 ms for M1 and

We did the same analysis for the B2 stimulation trials, and we observed similar trends (figure 4.22). First, lick trials are always higher in amplitude than no lick trails even long before the first lick occurred. Also, there was a decrease of the response in both wS1 and S2 in false alarm stim and correct rejection stim trials over the training days. Whereas, the signal amplitudes were increasing first and decreasing in a second time for M1 and M2 regions in FA stim trials and signals were staying more stable in CR stim trials along days.
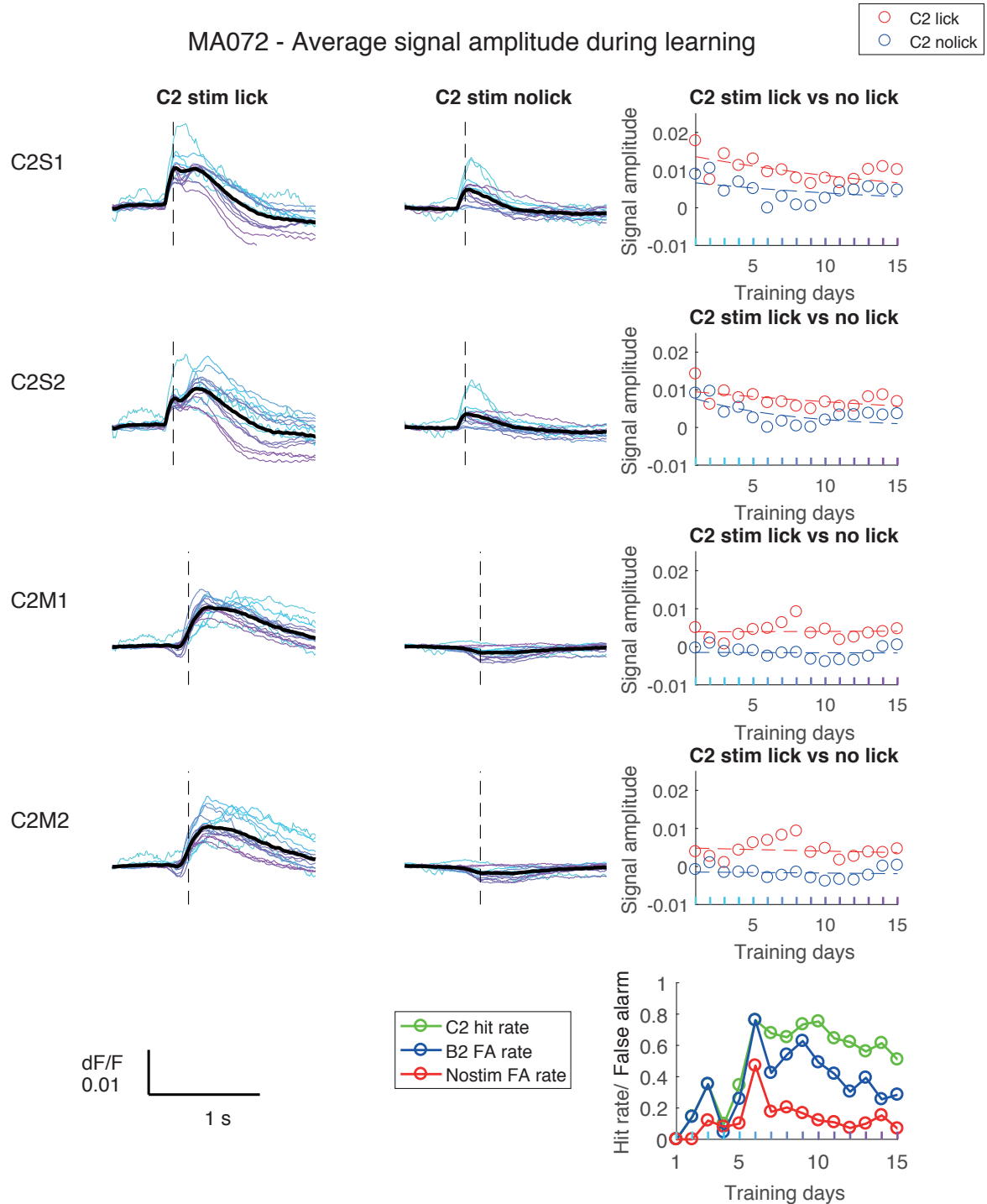
Figure 4.22. Evolution of the signal amplitude for FA stim (B2 stim lick) and CR stim (B2 stim no lick) trials at 100 ms in wS1 and S2, and at 250 ms in wM1 and M2 in one mouse over the learning of the 2-whisker discrimination task.

The average of the signal over each session for both hit and miss trials was color coded from cyan to magenta from the earliest training day to the last. The grand average signal is represented with a thick black line.

Each point of the graphs of the left is the amplitude of the corresponding curve of the day of training at the given time point (either at 100 ms for S1 and S2 or at 250 ms for M1 and M2) indicated by a dashed black line. A single exponential fit was computed on the data points.

The general performance of the mouse is represented on the panel at the bottom right.

To test these trends across the population, we ran the same analysis on all the mice for each region of interest and then averaged across mice. On average, there was a rapid decrease over the first three days of the signal in no lick trials and a constant and slow decrease on the following days (figure 4.23). For hit trials there was a constant gradual decrease of the amplitude in wS1.

Figure 4.23. Evolution of the signal amplitude for hit (C2 stim lick) and miss (C2 stim no lick) trials at 100 ms in wS1 in all the mice over the learning of the 2-whisker discrimination task.

On the panel at the bottom right is represented the grand average of all the mice for both hit and miss conditions with their standard deviation error bars.

For B2 stimulation catch trials, we observed a convergence of the signal amplitudes over the days of training (figure 4.24) between the lick and the no lick trials, with a rapid decrease of the no lick in the first three-four days and a constant decrease in the lick trials.
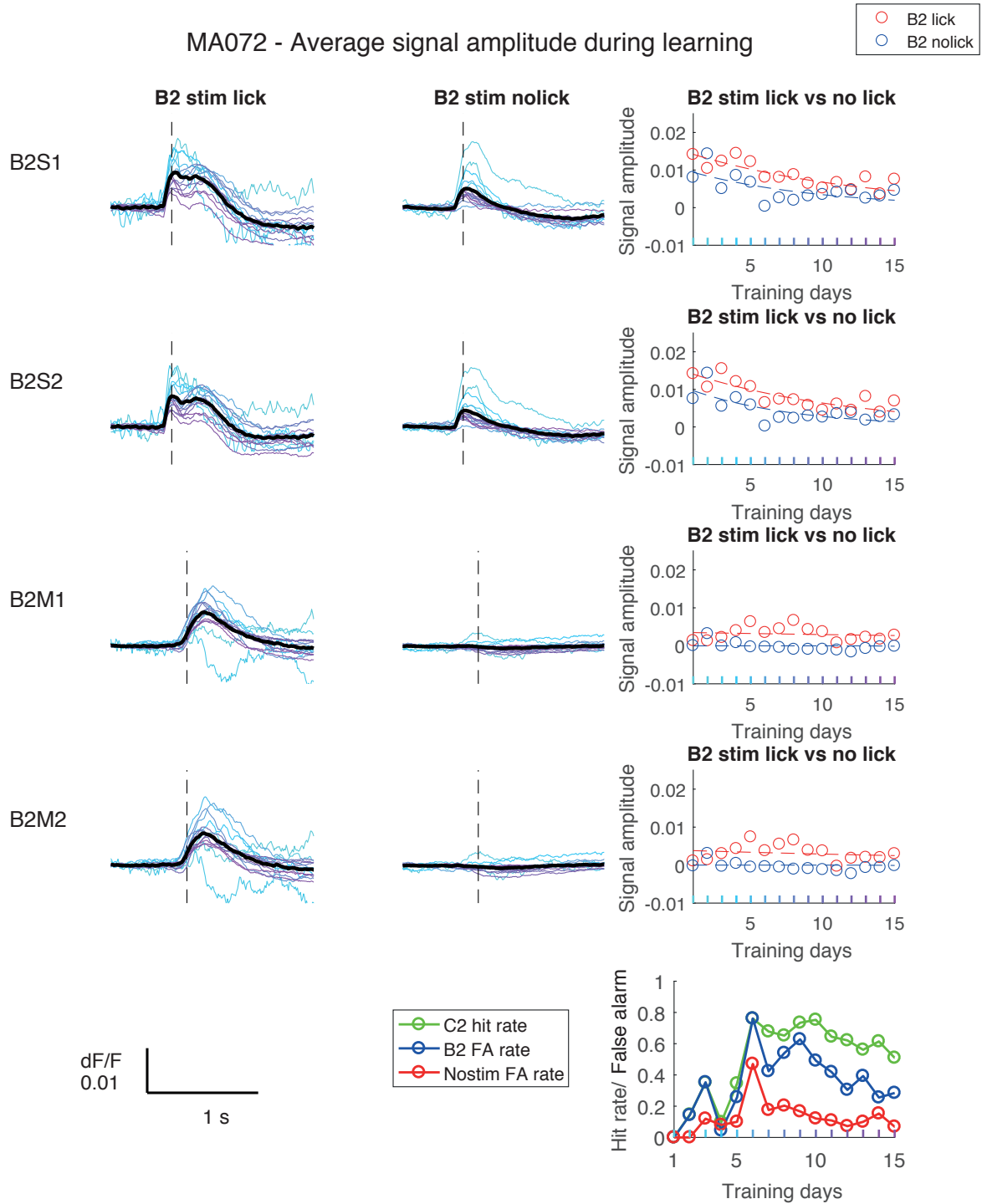

Figure 4.24. Evolution of the signal amplitude for FA stim (B2 stim lick) and CR stim (B2 stim no lick) trials at 100 ms in wS1 in all the mice over the learning of the 2-whisker discrimination task.

In S2, as for wS1, during C2 stimulation trials, there was a decrease in signal amplitude of lick and no lick trials over the days of training (figure 4.25). Lick trials were always significantly higher than no lick trials even before the first lick happened.

Signal amplitude at 100 ms during learning in C2S2

Figure 4.25. Evolution of the signal amplitude for hit (C2 stim lick) and miss (C2 stim no lick) trials at 100 ms in wS2 in all the mice over the learning of the 2-whisker discrimination task.
On the panel at the bottom right is represented the grand average of all the mice for both hit and miss conditions with their standard deviation error bars.

A similar trend was observed during B2 stimulation trials (figure 4.26). Amplitude of the signals was decreasing in S2 over the days. Amplitude of the lick trials were higher than the no lick trials.
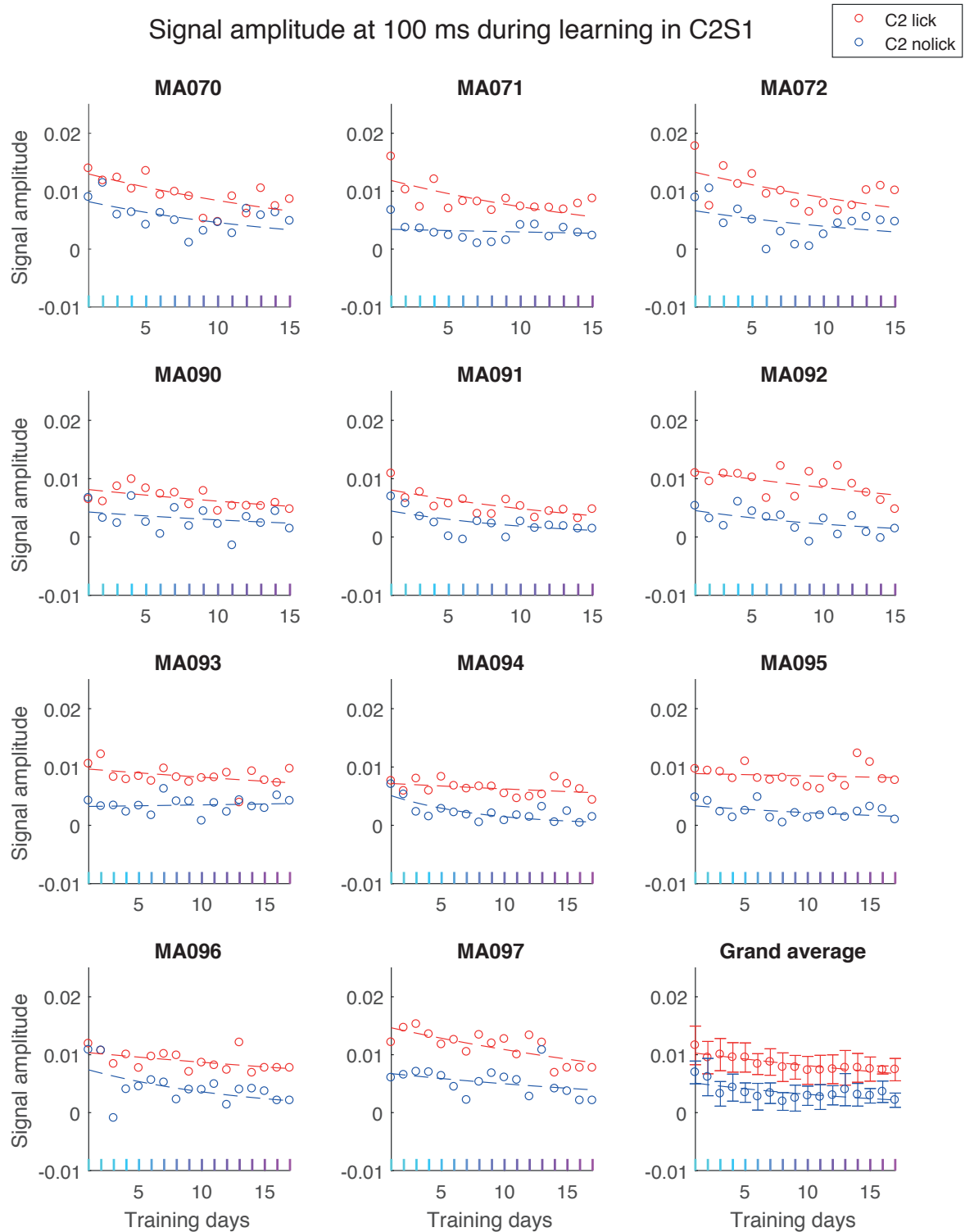
Figure 4.26. Evolution of the signal amplitude for FA stim (B2 stim lick) and CR stim (B2 stim no lick) trials at 100 ms in wS2 in all the mice over the learning of the 2-whisker discrimination task.

On the panel at the bottom right is represented the grand average of all the mice for both hit and miss conditions with their standard deviation error bars.

The signal amplitude into wM1 during C2 stimulation was stable over the days in the no lick trials, whereas the amplitude was lightly increasing over the training days in the lick condition trials (figure 4.27). It seemed that the difference between lick and no lick trials was increasing with the performance over the days, compared to the converging tendency of the signal amplitudes in the sensory areas S1/S2.

Signal amplitude at 250 ms during learning in C2M1

Figure 4.27. Evolution of the signal amplitude for hit (C2 stim lick) and miss (C2 stim no lick) trials at 250 ms in wM1 in all the mice over the learning of the 2-whisker discrimination task.
On the panel at the bottom right is represented the grand average of all the mice for both hit and miss conditions with their standard deviation error bars.

Similar effect for B2 stimulation condition, where the signal amplitude was more increasing over the days in lick trials and slightly decreasing in the no lick trials over the training days (figure 4.28).
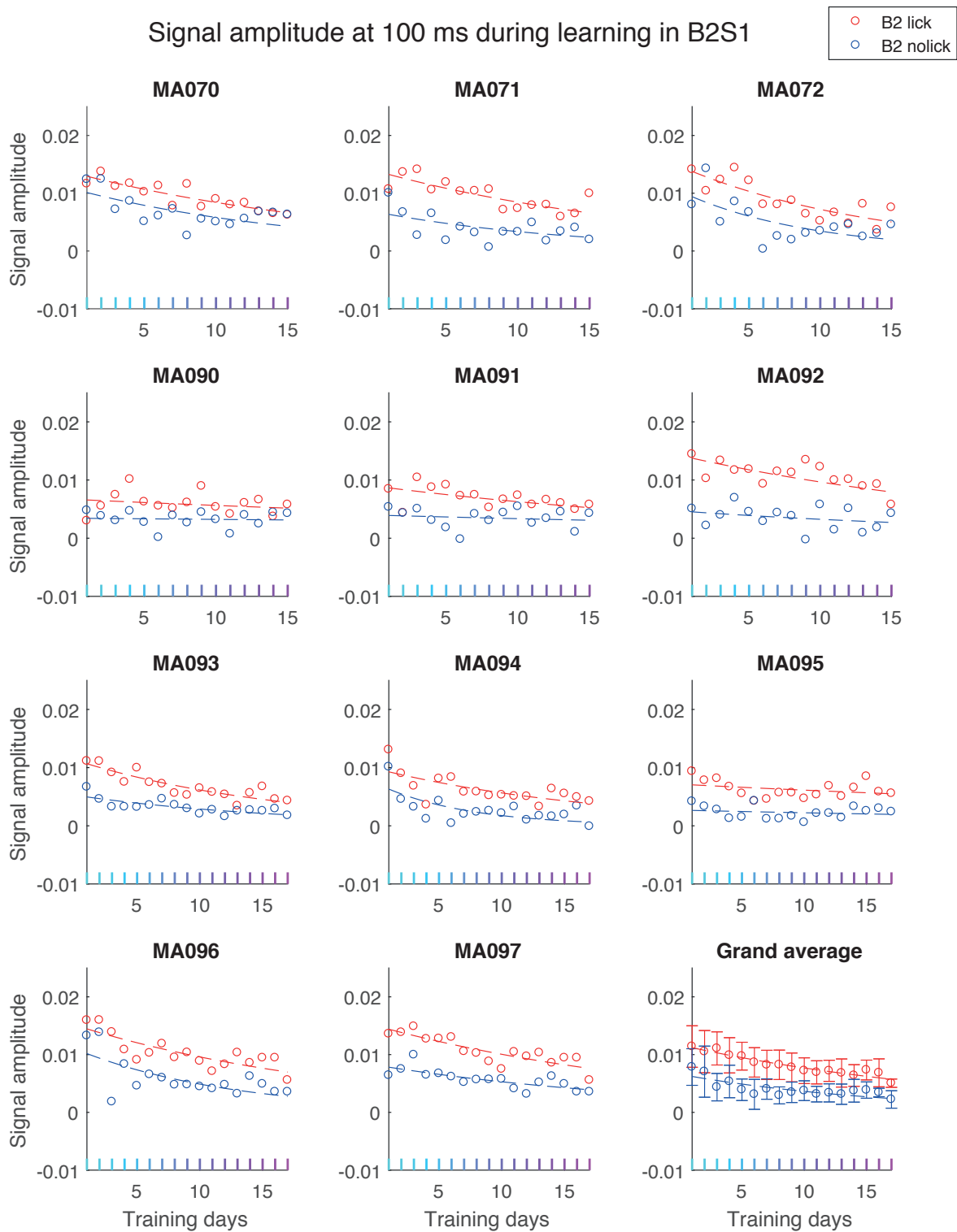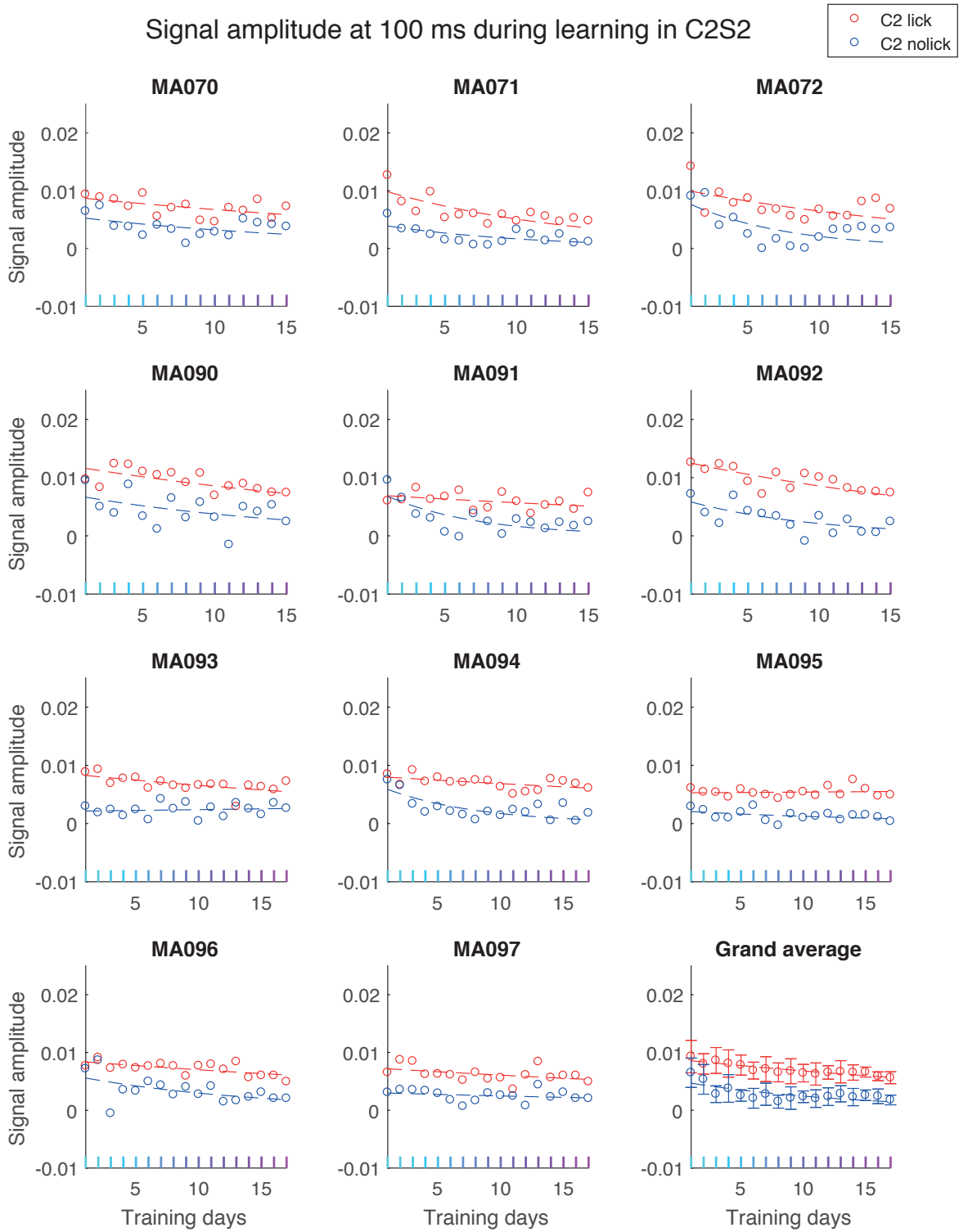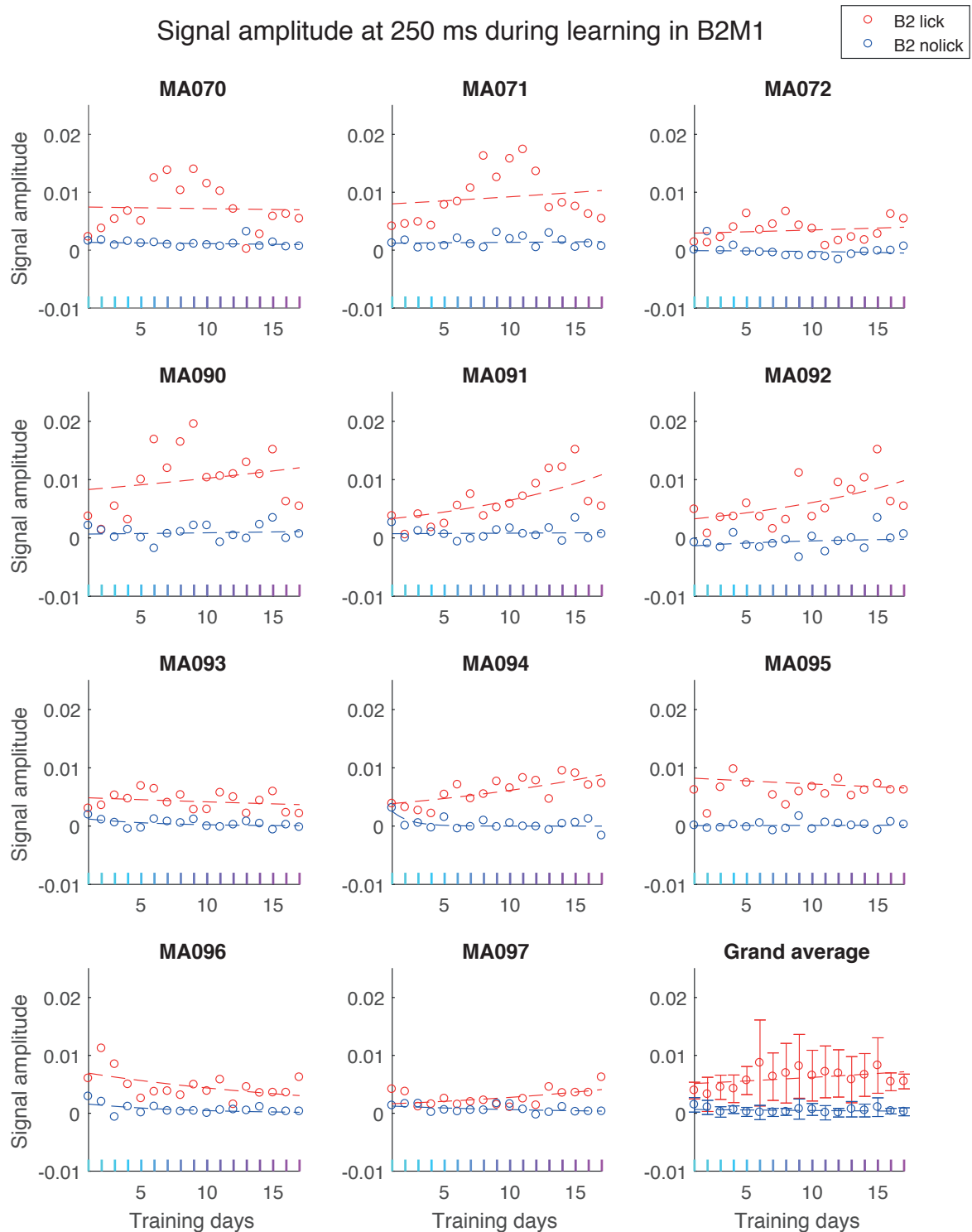
Figure 4.28. Evolution of the signal amplitude for FA stim (B2 stim lick) and CR stim (B2 stim no lick) trials at 250 ms in wM1 in all the mice over the learning of the 2-whisker discrimination task.

On the panel at the bottom right is represented the grand average of all the mice for both hit and miss conditions with their standard deviation error bars.

The trend seen in wM1 appeared to be more prominent in M2, where in C2 stimulation trials, the signal amplitude was growing with the performance of the mice in the lick trials (figure 4.29). As for this analysis, all the trials where reaction time below 300 ms were excluded, there was less of a chance that this effect might be simply explained by simple shortening of the reaction time with the facilitation to detect go stimuli.
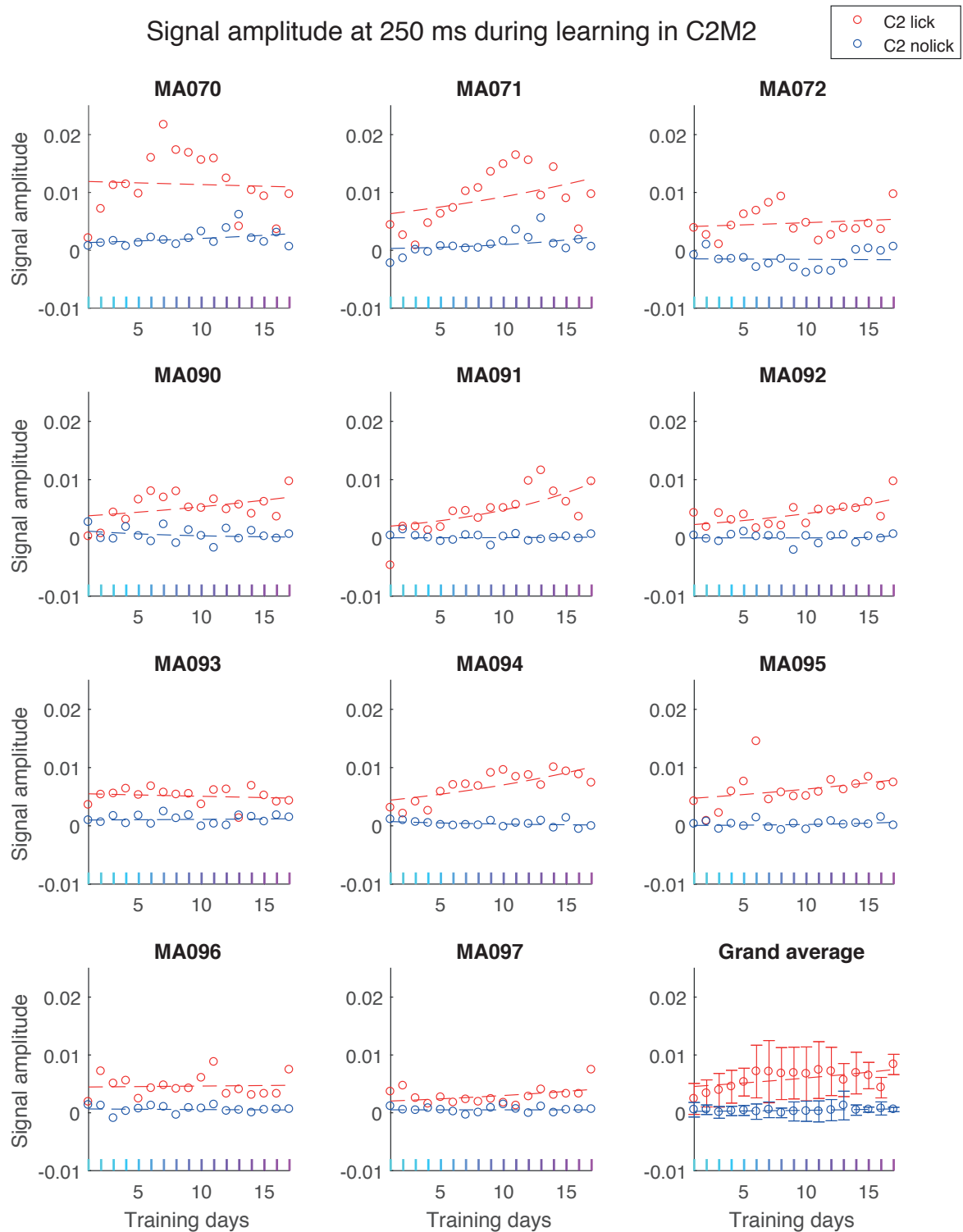
Figure 4.29. Evolution of the signal amplitude for hit (C2 stim lick) and miss (C2 stim no lick) trials at 250 ms in M2 in all the mice over the learning of the 2-whisker discrimination task.

On the panel at the bottom right is represented the grand average of all the mice for both hit and miss conditions with their standard deviation error bars.

The same effect of increasing response over days in M2 motor cortex during B2 stimulation for lick trials was observed (figure 4.30). No lick trials staid more constant over days.
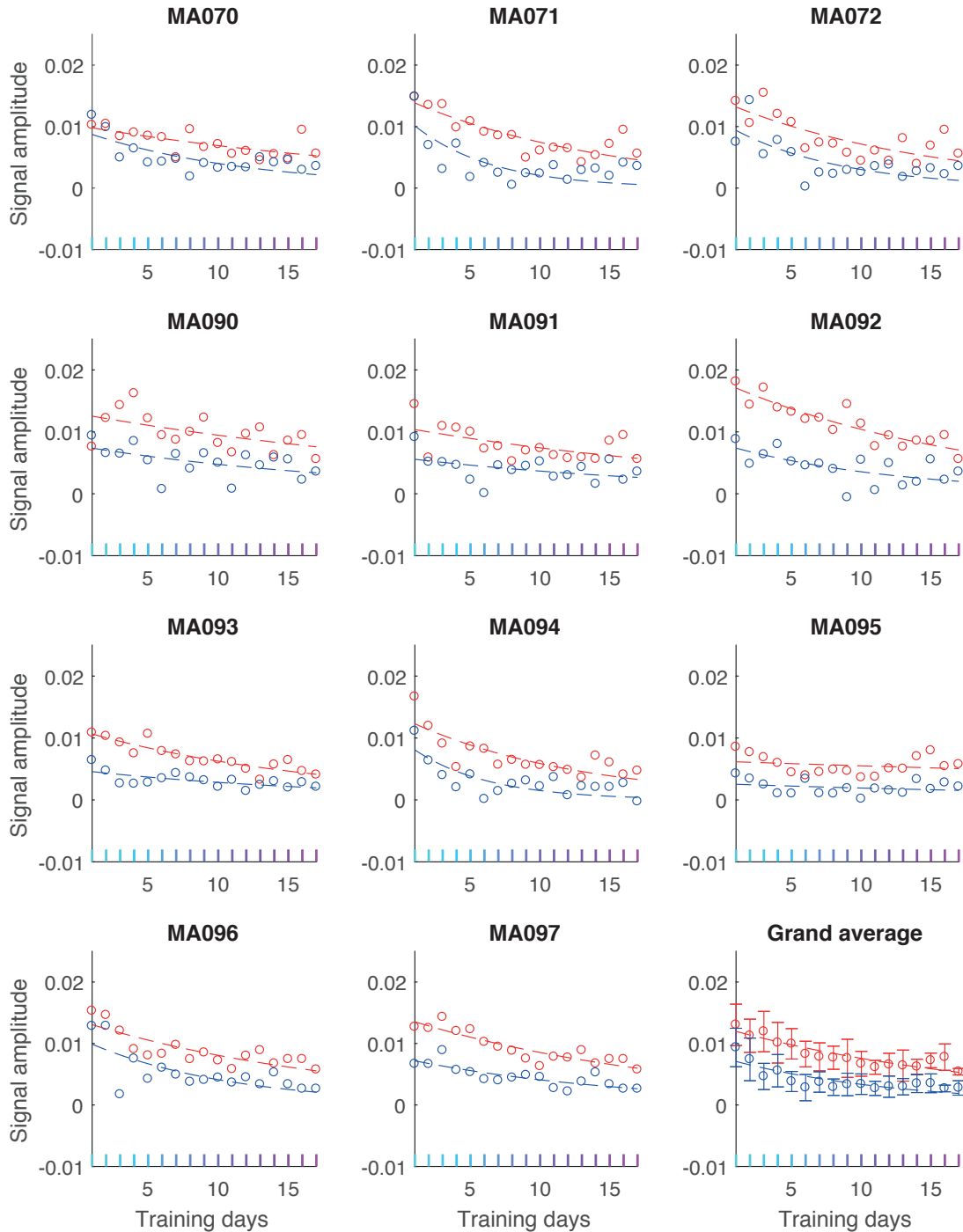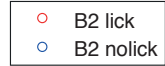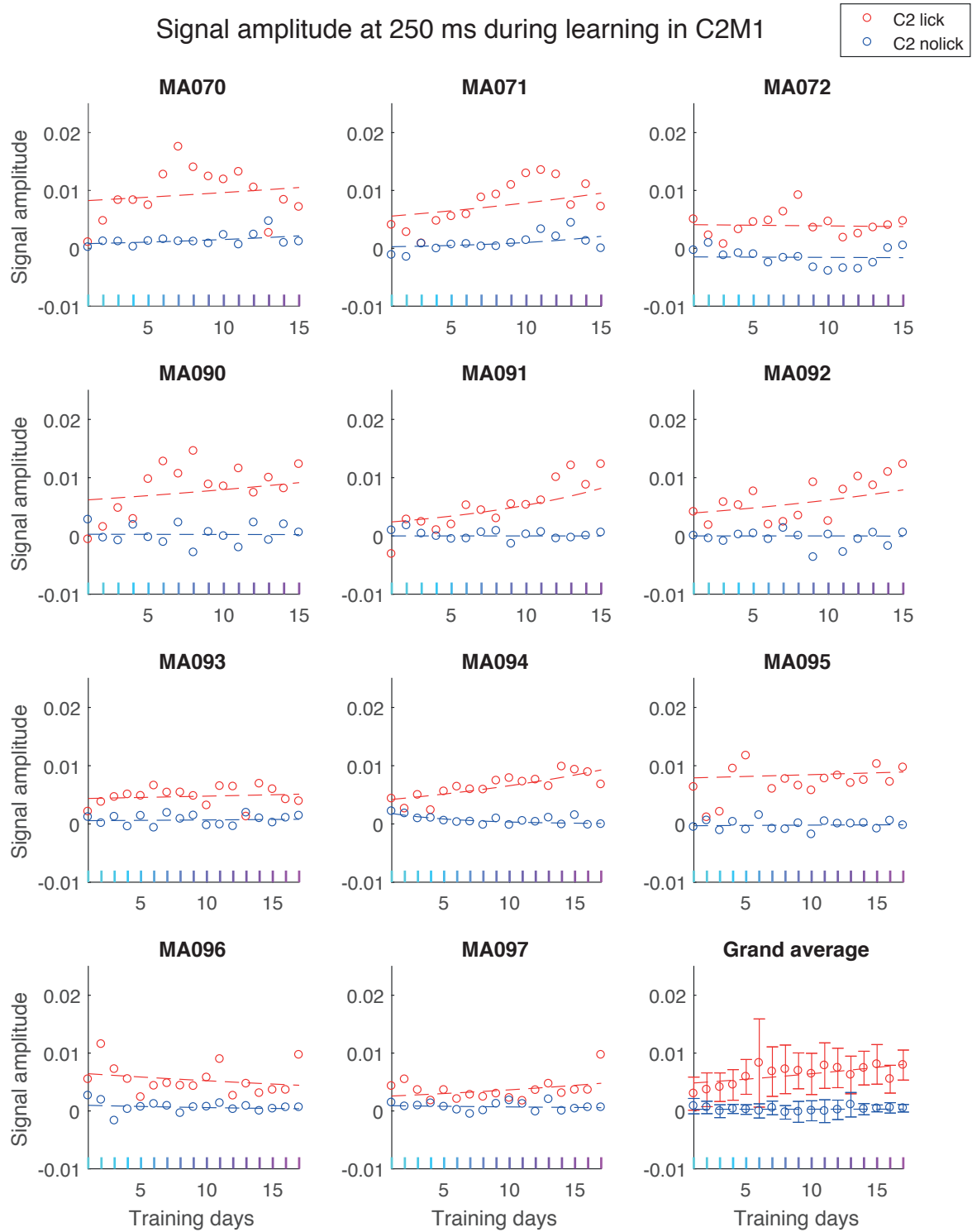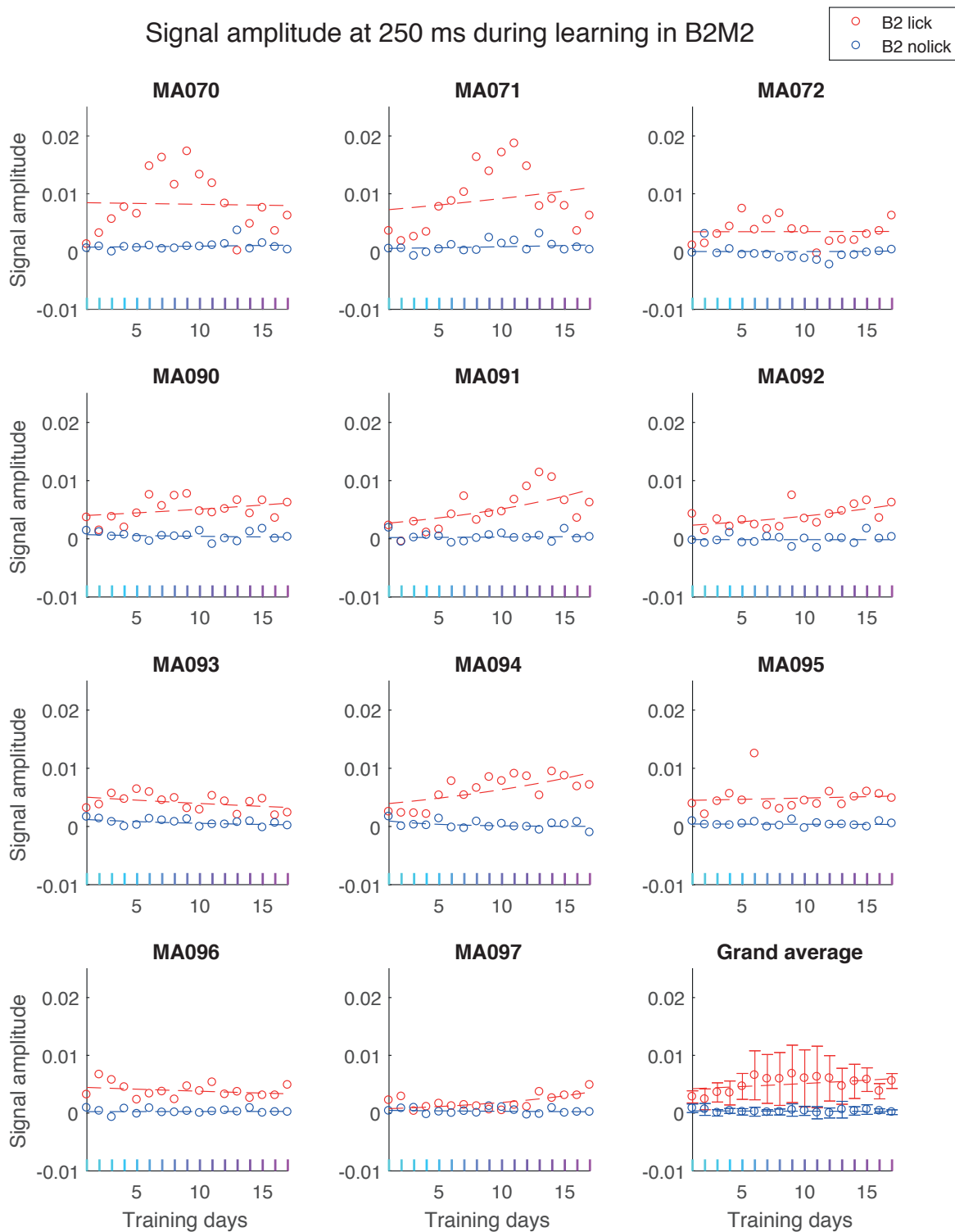

Figure 4.30. Evolution of the signal amplitude for FA stim (C2 stim lick) and CR stim (C2 stim no lick) trials at 250 ms in M2 in all the mice over the learning of the 2-whisker discrimination task.

On the panel at the bottom right is represented the grand average of all the mice for both hit and miss conditions with their standard deviation error bars.

The reported effects were pooled together and quantified with t-test analysis in figure 4.31 and 4.32. In all of the four conditions (hit, miss, FA stim and CR stim) lick trials were significantly higher than no lick trials.
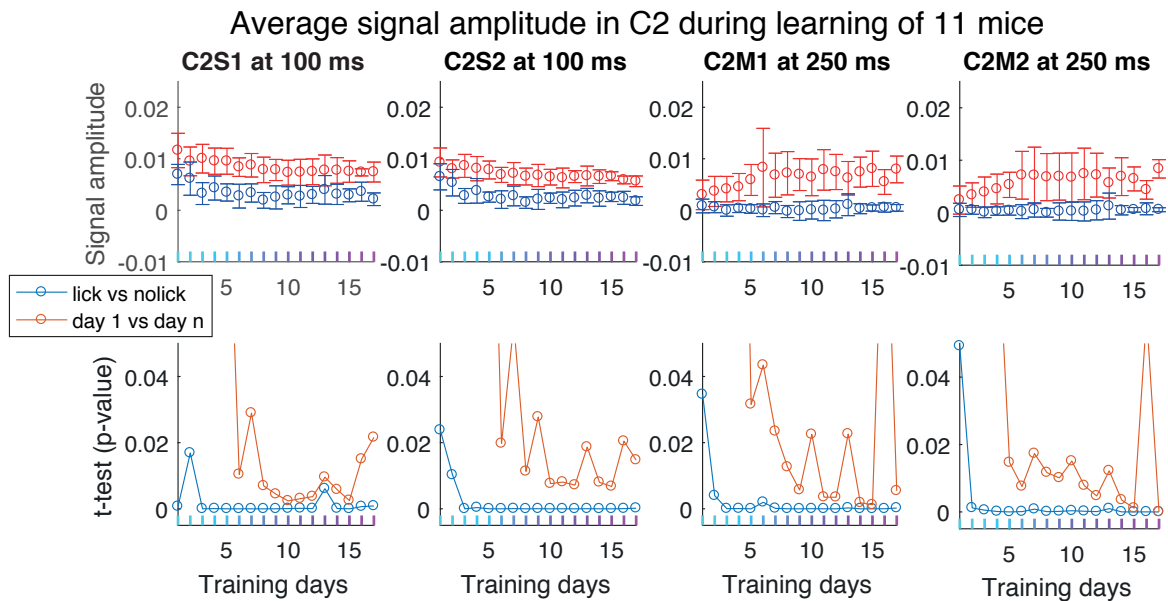
Figure 4.29. Grand average signal amplitude for hit (C2 stim lick) and miss (C2 stim no lick) conditions and p-values of the t-test difference between lick and no lick conditions (in blue) and between the first day and the following days for lick condition (in orange).
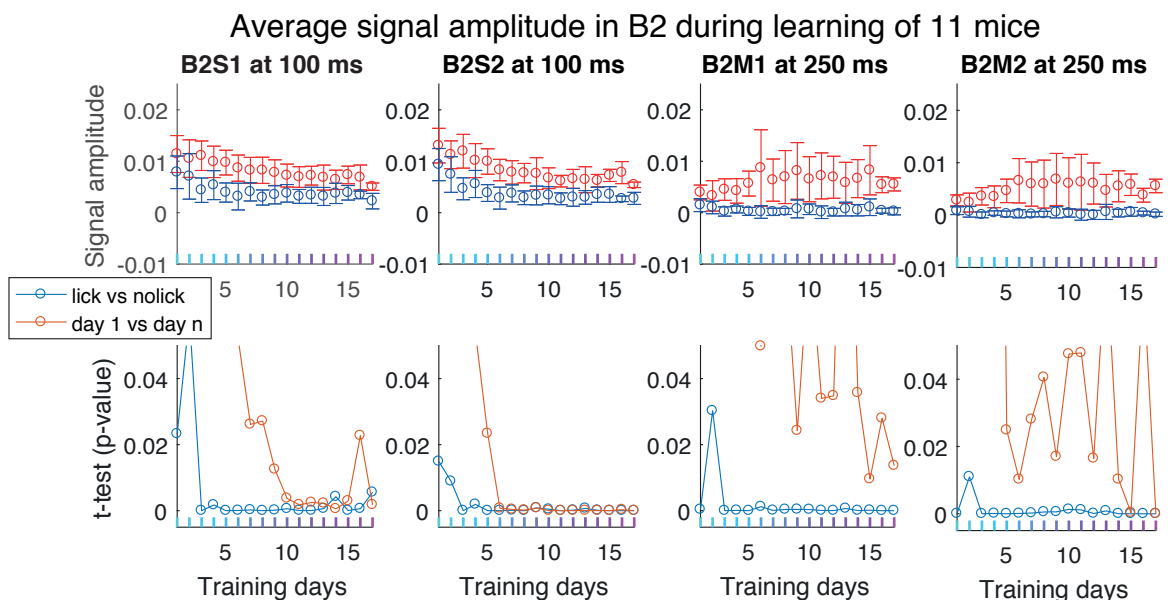
Figure 4.31. Grand average signal amplitude for FA stim (B2 stim lick) and CR stim (C2 stim no lick) conditions and p-values of the t-test difference between lick and no lick conditions (in blue) and between the first day and the following days for lick condition (in orange).

4.4. Discussion

We studied a perceptual discrimination task in mice using wide-field calcium functional imaging along several days of training. This technique provides an unbiased, macroscopic view of the activity dynamics across the mouse dorsal cortex. We found that the earliest evoked response detected in behaving mice was starting in wS1 and S2 during stimulation trials ~100 ms after stimulus onset. Then in the lick trials, the signal was emerging in frontal parts of the cortex first in M2 after 200 ms and in ALM the lick trials after 250 ms. On average, signals in lick trials were always higher in amplitude than no lick trials for S1, S2, M1 and M2. But the statistical test difference between those two conditions, lick and no lick, was not significant within the first 250 ms, except in S1 and S2. Cortical signals were emerging from very distinct location in the somatosensory cortex, with a well define somatotopy and were propagating frontally and converging in more unique location in motor cortex M2. Indeed, M2 was the point of convergence and might play an important role in the decision taking behavior to generate the motor command of licking.

From figure 4.11 to 4.20 all the statistical t-test were ran on trial conditions over each session. From figure 4.21 to 4.31 all the statistical t-test were performed on the averaged conditions over session. It would be interesting to do the same image analysis done on averaged session images. It would be equally interesting to run the ROI analysis on trial basis to see if all the reported effects are robust.

Premotor cortex M2 acts like a conductor that orchestrates the network activity of the rest of the cortex (Makino et al. 2017). In this study, the secondary motor cortex was one of the last areas to activate during early learning of the task and once the animal becomes expert it is one of the first area to activate. Inactivation experiment in M2 increases the number of miss trials and it takes more time for the mouse to initiate movement. This area might be important in the coordination between learnt behavioral movements and motor initiation. M2 can predict the activity in other cortical areas involved in the task once the animal has learnt the task.

It is also important to note that it is unlikely that M2 is the only area driving decision making and motor planning. Anterior lateral motor cortex (ALM) is also involved in delay response and might play a role in movement preparation (Makino et al. 2017; Guo, Li, et al. 2014). ALM might overlap with M2 region also involved in motor preparation. The sensory cortex wS1 and S2 is the input for tactile information from the subcortical to the cortex and wM1 and M2 drives the motor output. ALM is involved in directional licking and in more precise targeted movements. ALM activity increases with the performance of the mouse over the learning of a multi-motor task where the motor action indicates the decision choice in the behavior.

In our study we are limited in layer 2/3 signals corresponding to cortical-cortical processing. We know that the tactile information mostly arrives in the cortex in layer 4 and then this information goes to layer 2/3 and where it travels to other cortical places in these layers. The motor command is then sent through the output layer 5. It would be interesting to understand the evolution of the signal over learning of the 2-whisker discrimination task in a layer 5 mouse to really observe where and when the decision is taken. Then, once we have identified the input regions from the periphery (layer 4), where and when the information is

processed to take the decision (layer 2/3) and then where the output motor action is sent back to the periphery (layer 5), it would be important to optogenetically inactivate those regions at a precise timing during the learning of the task and observe if the animal can still perceive the stimulus or generate a motor command. This would tackle the question of causality and what parts of the cortical network are necessary and sufficient to perform this perceptual decision-making task.

We are concerned about the intrinsic evoked response observed in GFP mice. It would be interesting to evaluate if it would be possible to remove those artifacts. With the current dataset that we have, we might be able to find a mathematical way to filter those effect on a trial basis or to remove the trials that are contaminated by a large intrinsic response. For further experiments, we could use two different colors to excite the cortical surface: a blue LED illumination to excite GCaMP6f to measure the neuronal activity and another color blind to GFP excitation to measure the intrinsic response only. This method was developed by Allen in Prof. Karl Deisseroth's laboratory (Allen et al. 2017). By rapidly switching back and forth between these two excitation lights for each frame acquired, they are able to subtract the intrinsic signal measured with the non-exciting GFP light to the signal measured from GCaMP6f. This is a great method to clean the data.

This study shows the brain as a multi-nodes network that integrates the sensory information from the environnement, processes it and send a motor command to interact properly with the environment. Even simple behavior task recruits multiple brain regions that need to interact in a define events succession order at precise time points. We need to have a global understanding of the dynamic of the signals in the brain network to dig into the kinetics and the connectivity of the microcircuitry between neurons. With this knowledge we will be able to understand the mechanisms that have been implemented by the evolution of the brain organ. The sensorimotor integration that motivates our decision making must be in agreement with our close environment to behave properly for the sustainability of our species in terms of pure evolutionary point of view.

5. Optogenetic stimulation of cortex to map evoked whisker movements in awake head-restrained mice

Author contributions

M.A. and C.C.H.P. designed the project and wrote the manuscript. M.F.A.P. and C.C.H.P. constructed the experimental setup and carried out pilot experiments. M. A., V.L.R., G.M.C.R. and N.H. carried out all experiments and analyzed data. All authors commented on the manuscript.

Abstract

Whisker movements are used by rodents to touch objects in order to extract spatial and textural tactile information about their immediate surroundings. To understand the mechanisms of such active sensorimotor processing it is important to investigate whisker motor control. The activity of neurons in the neocortex affects whisker movements, but many aspects of the organization of cortical whisker motor control remain unknown. Here, we filmed whisker movements evoked by sequential optogenetic stimulation of different locations across the left dorsal sensorimotor cortex of awake head-restrained mice. Whisker movements were evoked by optogenetic stimulation of many regions in the dorsal sensorimotor cortex. Optogenetic stimulation of whisker sensory barrel cortex evoked retraction of the contralateral whisker after a short latency, and a delayed rhythmic protraction of the ipsilateral whisker. Optogenetic stimulation of frontal cortex evoked rhythmic bilateral whisker protraction with a longer latency compared to stimulation of sensory cortex. Compared to frontal cortex stimulation, larger amplitude bilateral rhythmic whisking in a less protracted position was evoked at a similar latency by stimulating a cortical region posterior to Bregma and close to the midline. These data suggest that whisker motor control might be broadly distributed across the dorsal mouse sensorimotor cortex. Future experiments must investigate the complex neuronal circuits connecting specific cell-types in various cortical regions with the whisker motor neurons located in the facial nucleus.

5.1. Introduction

Rodents use their array of mystacial whiskers to obtain tactile information about their immediate facial surroundings (Brecht 2007; Petersen 2007; Mathew E. Diamond et al. 2008; Bosman et al. 2011; Feldmeyer et al. 2013). During active exploration rodents typically move their whiskers back and forth at high frequencies (~10Hz) to sample the space around their snouts (W. I. Welker 1964). As a whisker contacts an object, it bends and the resulting force is transduced into action potential firing in the primary sensory neurons of the trigeminal ganglion, which innervate the whisker follicles. Sensory information can therefore be actively acquired by rodents through self-generated movements causing whisker– object contact. Whisker sensory information flowing into the rodent brain is thus in part determined by whisker motor control. In order to understand whisker sensory perception, we therefore also need to investigate the mechanisms underlying the control of whisker movements.

Movements are controlled by complex neuronal circuits, including an important influence by the neocortex. Pioneering experiments in dogs (Fritsch and Hitzig 2009), monkeys (Ferrier 1874; Sherrington 1906), and man (Penfield and Boldrey 1937) revealed important organizing principles of mammalian cortical motor control. Electrical stimulation of different cortical regions evoked different movements, with the most important region, the primary motor cortex (M1), being located in the frontal cortex, anterior to the central sulcus. Stimulation of different sites in M1 evoked movements, which appear to mirror the somatotopic organization of sensory cortex.

Early experiments in rodents suggested that movements could be evoked by stimulating many different regions of the neocortex (Hall and Lindholm 1974; Donoghue and Wise 1982; Gioanni and Lamarche 1985). Motor maps revealed forelimb and hindlimb motor representations bordering with their sensory representations, whereas head, whisker, and eye movements were found to be preferentially evoked by stimulation of more anterior and medial locations (Hall and Lindholm 1974; Donoghue and Wise 1982; Neafsey et al. 1986; Miyashita, Keller, and Asanuma 1994; Brecht, Krauss, et al. 2004).

A number of studies have specifically investigated the effects of cortical stimulation upon whisker movements finding diverse results. In awake head-restrained mice, stimulation of the primary somatosensory whisker barrel cortex (wS1) has been proposed to evoke retraction of the contralateral whisker, whereas the direct effect of stimulation of a frontal region wM1, which is strongly innervated by wS1, is proposed to drive rhythmic whisker protraction (Matyas et al. 2010; Petersen 2014; Sreenivasan et al. 2015, 2016). In contrast, recent work in freely moving rats suggested that neuronal activity in an apparently analogous region to wM1, may suppress contralateral whisking (Ebbesen et al. 2017). A further study in lightly anesthetized rats, proposed that a rhythmic whisking region be located in a more posterior and medial cortical region (Haiss and Schwarz 2005). The diverse results in terms of whisker movements evoked by stimulating different regions of the rodent cortex may result from differences in species, stimulation methods, or behavioral context. Further experiments are therefore necessary in order to understand the organization of cortical whisker motor control. Here, we use optogenetic stimulation of cortex in transgenic mice expressing channelrhodopsin-2 (ChR2) (Nagel et al. 2003; Boyden et al. 2005; Arenkiel et al. 2007; Ayling et al. 2009; Hira et al. 2009; Matyas et al. 2010; Harrison, Ayling, and Murphy 2012) to begin to map the whisker movements evoked by the same light stimulus

applied to many different regions of the dorsal cortex. Our results indicate that whisker movements can be evoked by stimulating many cortical regions, with short latency retraction of contralateral whiskers being evoked from wS1, and rhythmic bilateral whisker protraction being evoked by stimulation of other cortical areas including a frontal and a more posterior midline cortical region.

5.2. Experimental procedures

Animal preparation and surgery

All experiments were carried out in accordance with protocols approved by the Swiss Federal Veterinary Office. In this study we used four transgenic mice (two male and two female, age ~3 months) expressing ChR2 under the Thy1 promoter: mouse strain name B6.Cg-Tg(Thy1-COP4/EYFP)18Gfng/J, JAX mouse number 07612, RRID: IMSR_JAX:007612 (Arenkiel et al. 2007). Mice were anesthetized under deep isoflurane and a metal head-holder implanted. A relatively transparent view of the left dorsal cortex was prepared following previously published methods (Guo, Hires, et al. 2014). In brief, the skull was covered with a thin layer of cyanoacrylic glue, and then a thick layer of transparent dental acrylic cement (Jet Repair Acrylic) was applied. Three days after the implantation the cement was polished using a polishing kit. In a final step, the polished cement was covered with nail polish, to make the surface of the skull even and transparent. All whiskers were trimmed except the C2 whiskers on either side.

Optogenetic mapping of evoked whisker movements

Mice were adapted to head-restraint through daily training sessions (Crochet and Petersen 2006). The first head- fixation session was brief (~15 min), and over the next days the duration of head-restraint was gradually extended to one hour. After adaptation to head-restraint, optogenetic stimuli were applied to different regions of the left cortex, while left and right C2 whiskers were filmed at 500 Hz illuminated with blue light below the mouse to show silhouette and whiskers (Figure 5.1). Each trial lasted 1 s with 500 ms of a prestimulus baseline period followed by 500 ms of optogenetic stimulation. The minimal inter- trial interval was 5 s. Auditory white noise was constantly played through earphones near to the ears of the mice to mask the noise of the galvanometer mirrors and any ambient noise. The optogenetic stimulus consisted of a blue light spot of ~500-mm diameter, which varied in intensity with a 50-Hz sine wave modulation, with a peak power of 3.49 mW and mean power of 1.75 mW (Figures. 5.1–5.9). In some experiments we used a lower light power with a peak power of 0.72 mW and mean power of 0.36 mW (Figure 5.7). The blue light was generated by a 473-nm fiber-coupled laser (Thorlabs, Newton, New Jersey, USA), focused onto the mouse cortex through a 50-mm focal length camera lens (Nikon, Tokyo, Japan), and directed to specific locations on the mouse cortex using 2D scanning galvanometer mirrors (Thorlabs, Newton, New Jersey, USA) controlled by a computer via a digital-to-analog converter (National Instruments, Austin, Texas, USA) (Guo, Li, et al. 2014). A photostimulation grid of 6 × 8 pixels covering an area of 3.9 × 5.0 mm over the left

hemisphere was aligned to Bregma, and each point was stimulated in a random order. The whole grid was covered before repeating the stimulus protocol, with each mapping sequence lasting ~10 min. Altogether, each coordinate was stimulated 12 times at the high laser power and 6 times at the low laser power. For each mouse, motor mapping was conducted across 2 or 3 days in three sessions, each with six repetitions covering the entire stimulus grid.
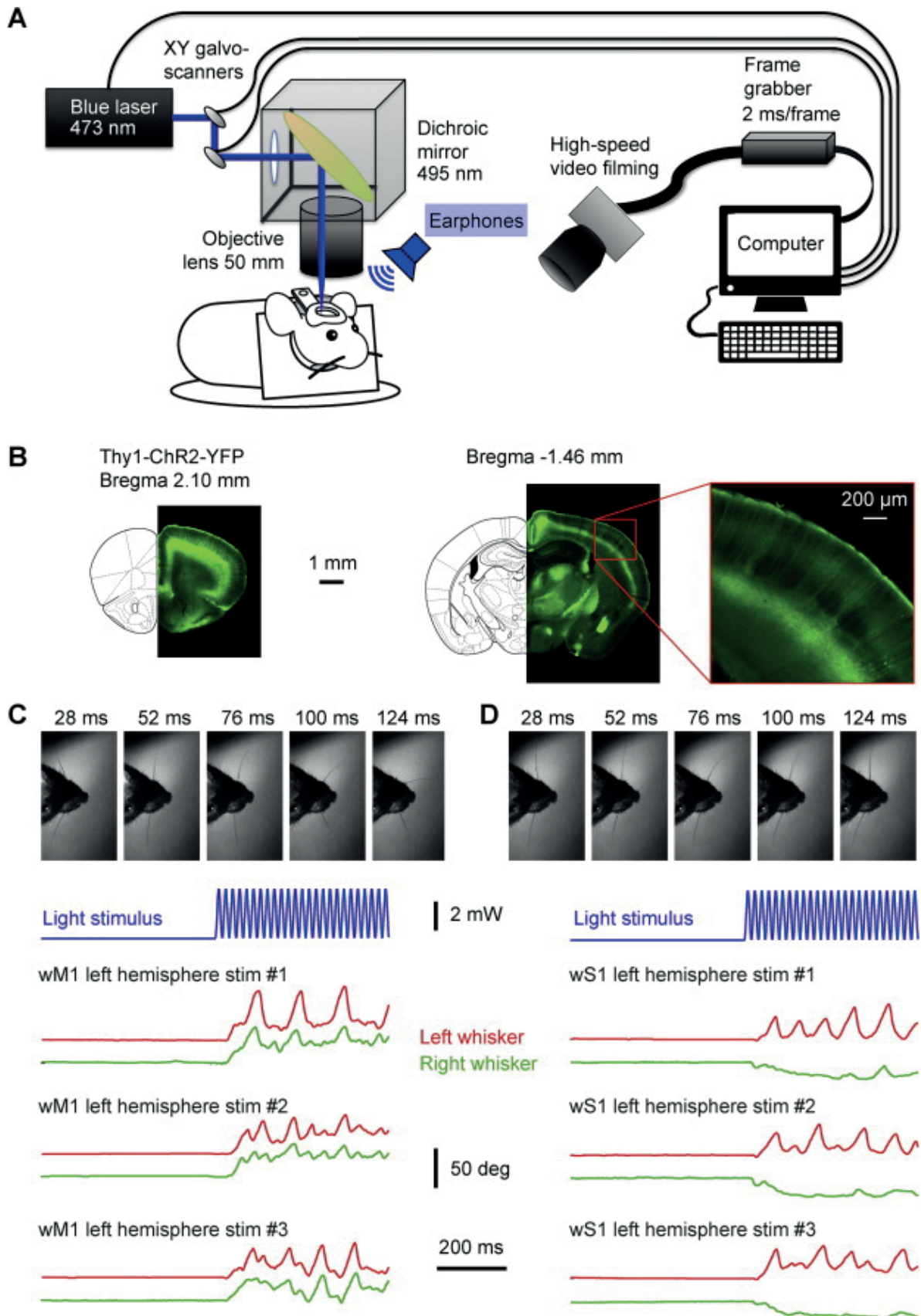
Figure 5.1. Experimental setup for optogenetic whisker motor mapping.
A. The left hemisphere of Thy1-ChR2-YFP mice was stimulated by 473 nm blue laser light with a 50-Hz sine wave modulation. The beam was directed by two scanning galvanometer

mirrors onto a dichroic mirror that reflected the blue light to the surface of the skull through a 50-mm focal length camera lens to focus the beam on specific locations of the mouse cortex. A high-speed video camera filmed the C2 whiskers of both left and right sides at 500 Hz. Blue ambient light indirectly illuminated the background and masked the laser light. White noise was played to cover noise from galvanometer mirrors and any ambient noise. Laser stimulation, galvanometer mirrors and high-speed video filming were controlled by a computer.

B. YFP fluorescence in fixed coronal slices of a Thy1-ChR2- YFP mouse imaged at 4× magnification at two different anterior–posterior locations, ~2.10 mm frontal to Bregma (close to wM2, left image) and ~1.48 mm posterior to Bregma (center image) where we observed the barrel cortex structure of wS1. Schematic drawings were adapted from Paxinos and Franklin (2001). A zoomed-in version of the barrel cortex was acquired with a 10× magnification lens (right image). Layer 5 pyramidal neurons and their dendritic arborizations extending to superficial layers were observed.

C and D. Example of raw movie images of the mouse MA034 at five different times (28, 52, 76, 100 and 124 ms after stimulus onset), during wM1 (left) and wS1 (right) stimulation trial #1 of left hemisphere. The temporal pattern of the laser light stimulus delivered to the mouse cortex at wM1 and wS1 localization is shown in blue. Below are three example trials of left and right whisker angles tracked from the high-speed movies for both wM1 (left) and wS1 (right) stimulation. wM1 stimulation drove protraction of both whiskers, whereas wS1 stimulation drove protraction of the ipsilateral whisker and retraction of the contralateral whisker.

A

Light stimulus

100 ms

• wS1

Left whisker

Mean angle

B

	Left whisker	Right whisker
MA029		
MA030		
MA032		
MA034		

Mean angle (deg)

40

20

0

1 mm

Anterior

Lateral

C

	Left whisker	Right whisker
Average		

Mean angle (deg)

30

20

10

0

-10
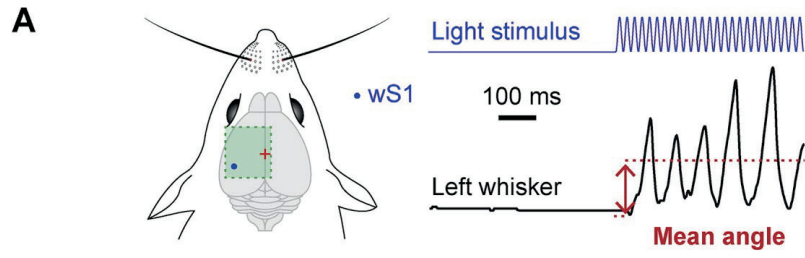
Figure 5.2. Mapping of the average change in whisker angle evoked by optogenetic stimulation.

A. Schematic drawing of wS1 stimulation (left) and an example of the left whisker angle (right) showing how the mean angle was computed: the difference in mean whisker angle during the 500 ms of optogenetic stimulation compared to the mean whisker angle during the two frames (4 ms) before the stimulus onset.

B. The mean change in angle for the left C2 whisker and right C2 whisker of each mouse represented on a 2D color-coded map corresponding to each stimulation coordinate on the left hemisphere. The amplitude of the mean change in angle corresponds to the median of all the trials where the mouse did not whisk 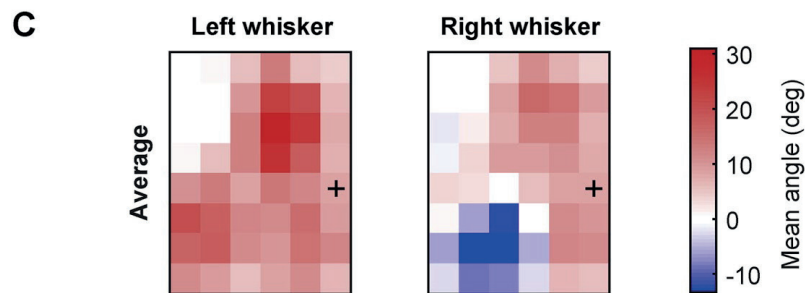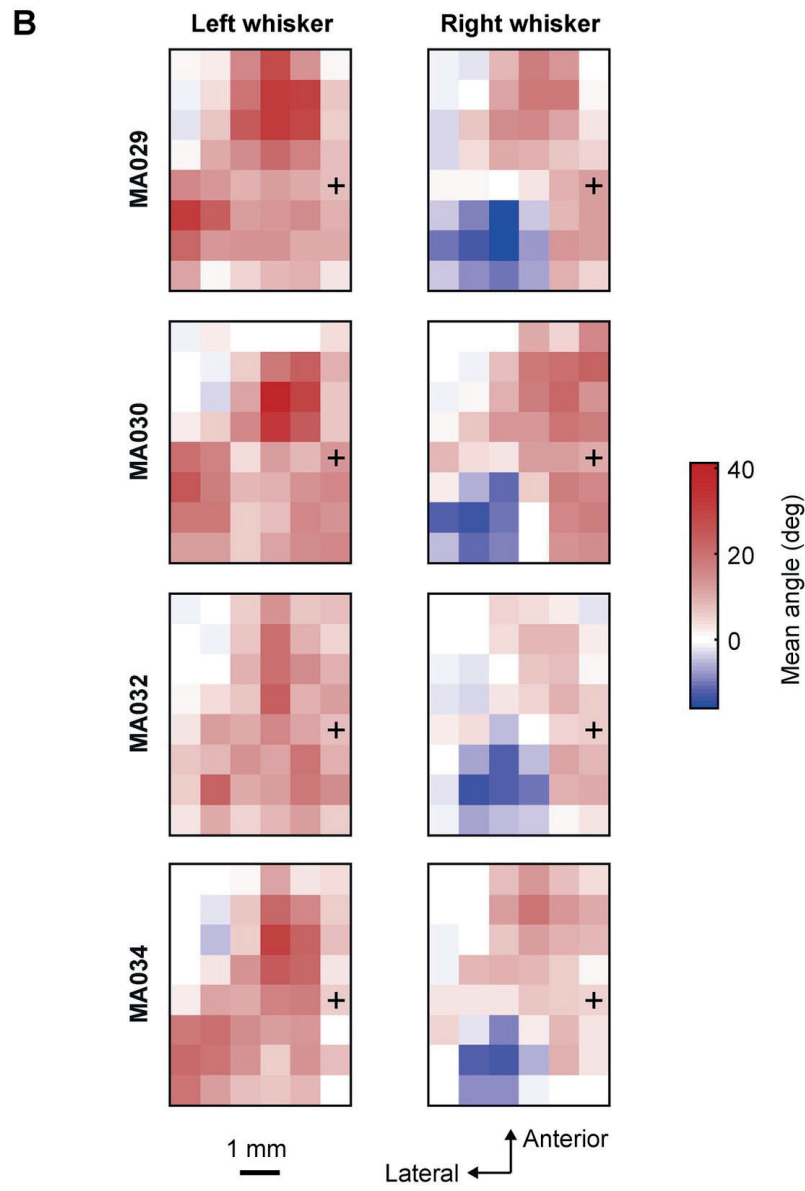before the stimulus (whisker angle standard deviation less than 1 for 200 ms before the stimulation). Positive values reflect a protraction of the whisker and negative values indicate retraction. Bregma position is represented by a black cross.

C. Average over the four mice of the mean angle positions for left and right C2 whiskers relative to the stimulation coordinates on the left hemisphere. There was a large protraction of both whiskers when wM1/wM2 was stimulated. Protraction of the ipsilateral whisker and a retraction of the contralateral whisker was evoked when wS1 was stimulated.

Intrinsic optical imaging to map sensory-evoked activity

After allowing the whiskers to regrow for several weeks, we carried out intrinsic optical imaging experiments to map sensory representations. Mice were lightly anesthetized with ~0.5% isoflurane. The body temperature of the mouse was maintained at 37 °C by a heating pad. A first image of the cortical surface was acquired with 530 nm green LED light in order to locate Bregma and blood vessels. For functional imaging, the illumination was changed to 625-nm red LED light. Different body parts were sequentially mechanically stimulated by a glass capillary attached to a piezo-bender. Three different right whiskers were stimulated (A1, C2 and D1) to assess the whisker somatotopic organization for each individual mouse. The whisker was inserted into the glass tube and was stimulated at 10 Hz for 4 s. The right forepaw, the right hindpaw, the tail, the lip and the tongue were similarly stimulated by tapping the body part with the same piezo system at 10 Hz for 4 s. Auditory stimuli were delivered by click sound pulses at 10 Hz for 4 s. Visual stimuli to the right eye were delivered by flashing a blue LED at 10 Hz for 4 s. Each trial consisted of a 4-s baseline period, followed by 4 s of stimulation, and then 2 s poststimulus. The total trial duration was 10s and the intertrial interval was 4s. Images were acquired at 10 Hz with 8.7×8.7-mm field of view and a detector of 1024×1024 pixels (Photon Focus, Lachen, Switzerland, MV-D1024E-40). Stimulus delivery and image processing were carried out using custom written routines in Matlab (Mathworks, Natick, Massachusetts, USA). For each stimulus, the fractional change in reflected light was computed across an average of 20 trials, and aligned to the location of Bregma.

Data analysis

Whisker angle was quantified using semi-automated custom-written routines in IgorPro (Wavemetrics, Lake Oswego, Oregon, USA). In a small fraction (3.6%) of trials we were not able to track the whisker angle. Further data analysis was conducted in Matlab. Only trials in which the mouse was not moving its whiskers (<1 standard deviation in whisker angle during the 100 frames, i.e. 200ms, before the stimulation) were included in our analyses. Using this analysis criterion, 32.1% of the remaining trials were rejected because of prestimulus whisker movement. All numbers in the text are presented as mean ± standard deviation for n = 4 mice.

Mean evoked change in whisker angle (Figure 5.2) for both right and left C2 whiskers was computed for each trial as the difference in the mean whisker angle during the 500ms of optogenetic stimulation compared to the mean whisker angle during the 4 ms immediately before optogenetic stimulation. Positive values indicate whisker protraction and negative values whisker retraction. The median value was color-coded in the maps across trials for each mouse (Figure 5.2B), and then averaged across the four mice (Figure 5.2C).

Time-dependent mean evoked change in whisker angle (Figure 5.3) for both right and left C2 whiskers was computed for each trial as the difference in the mean whisker angle compared to the mean whisker angle during 4 ms immediately before optogenetic stimulation subdivided in 20-ms time-bins over the first 120 ms of stimulation, leading to 6 time-dependent whisker motor maps. The median value was color-coded in the maps across each mouse (Figure 5.3B), and as the average of these maps across the four mice (Figure 5.3C).

A

Light stimulus

Left whisker

120 ms

Time-dependent mean angle

• wS1

B

| | 20 ms | 40 ms | 60 ms | 80 ms | 100 ms | 120 ms |

Right whisker: MA029, MA030, MA032, MA034

Left whisker: MA029, MA030, MA032, MA034

deg
40
20
0

2 mm

Anterior

Lateral

C

| | 20 ms | 40 ms | 60 ms | 80 ms | 100 ms | 120 ms |

Right Average

Left Average

deg
40
20
0

Figure 5.3. Mapping of the time-dependent change in whisker angle evoked by optogenetic   stimulation.

A. Schematic drawing of wS1 stimulation (left) and an example of the left whisker angle (right) showing how the time-dependent whisker angle was computed: the mean change in whisker angle during six consecutive time bins (0–20, 20–40, 40–60, 60–80, 80–100, and 100–120 ms relative to stimulation onset) from the mean whisker position during the 4 ms before the stimulus onset.

B. Mean whisker angle during the six 20-ms time bins for the left C2 whisker and right C2 whisker of each mouse represented on a 2D color-coded map corresponding to each stimulation coordinate of the left hemisphere. The amplitude of the mean angles reported corresponds to the median of all the trials where the mouse did not whisk before the stimulus (whisker angle standard deviation less than 1 for 200ms before the stimulation). Positive values reflect a protraction of the whisker and negative values indicate retraction. Bregma position is represented by a black cross.

C. Average over the four mice of the time-dependent mean angle positions for left and right C2 whiskers relative to the stimulation coordinates of the left hemisphere. The first movement evoked was in the 20–40-ms time- window, and was a retraction of the contralateral whisker when wS1 cortex was stimulated. In the 40–60-ms time-window, a protraction of both whiskers was evoked when wM1/wM2 and PtA were stimulated.

The latency for evoking whisker movements (Figure 5.4) for both right and left C2 whiskers was computed for each trial as the time corresponding to when the whisker angle changed more than ±4° compared to the whisker angle during the 4 ms immediately before optogenetic stimulation. If the whisker did not change angle by more than 4° during the optogenetic stimulation then the trial was not included in the latency analysis (7.9% of trials did not pass threshold). The median value of the latency was color-coded in the maps across each mouse (Figure 5.4B), and then averaged across the four mice (Figure 5.4C).

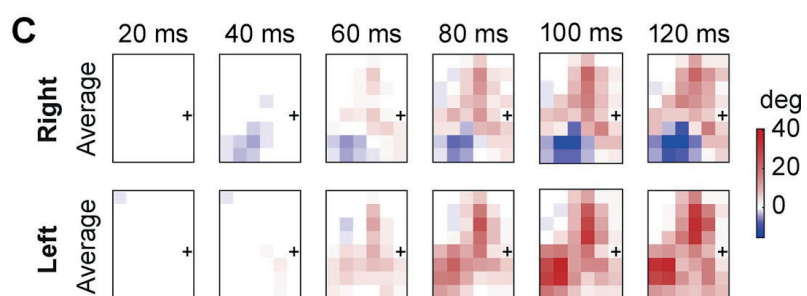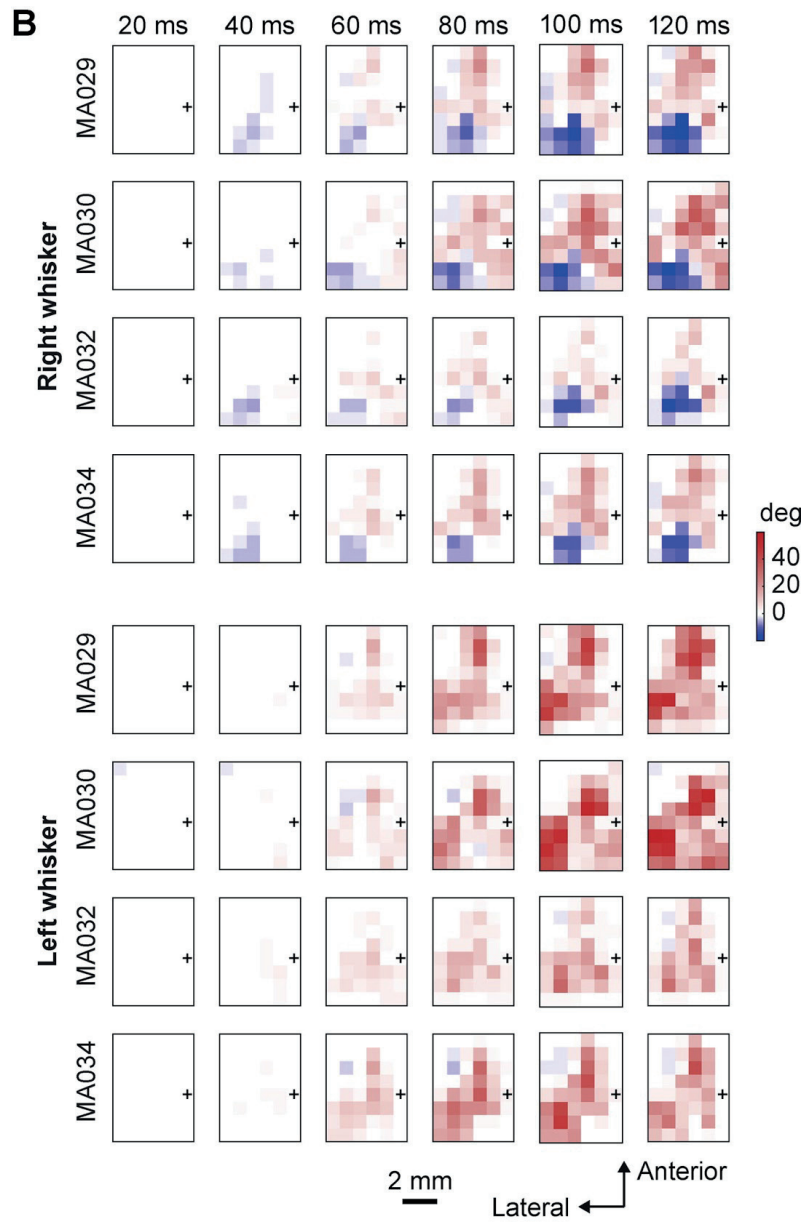**A**

Light stimulus

·wS1

4° threshold

Left whisker

Latency

B

Left whisker   Right whisker

MA029

MA030

MA032

MA034

1 mm

Anterior

Lateral

Latency (ms)

C

Left whisker   Right whisker

Average

Latency (ms)

Figure 5.4. Latency maps of whisker movements evoked by optogenetic stimulation.
A. Schematic drawing of wS1 stimulation (left) and an example of the left whisker angle (right) showing how the latency was computed: time relative to stimulation onset when the whisker moved more than 4° compared to its initial position.
B. Latencies for the left C2 whisker and right C2 whisker of each mouse represented on a 2D color-coded map corresponding to each stimulation coordinate of the left hemisphere. Trials in which the mouse did not move its whisker by more than 4° were not included in the latency analysis. The value of latencies reported corresponds to the median of all the trials where the mouse did not whisk before the stimulus (whisker angle standard deviation below 1° for 200ms before the stimulation). Bregma position is represented by a red cross.
C. Average over the four mice of the latencies for left and right C2 whiskers relative to the stimulation coordinates on the left hemisphere. The shortest latencies were for contralateral whisker retraction when wS1 was stimulated.

The peak amplitude of early changes in whisker angle within the first 100 ms of optogenetic stimulation (Figure 5.5) for both right and left C2 whiskers was computed for each trial as the maximum change in whisker angle (considering both positive values for protraction and negative values for retraction) compared to the whisker angle during 4 ms immediately before optogenetic stimulation. The median value of the early phase peak amplitude was color-coded in the maps across each mouse (Figure 5.5B), and then averaged across the four mice (Figure 5.5C).

A

Light stimulus
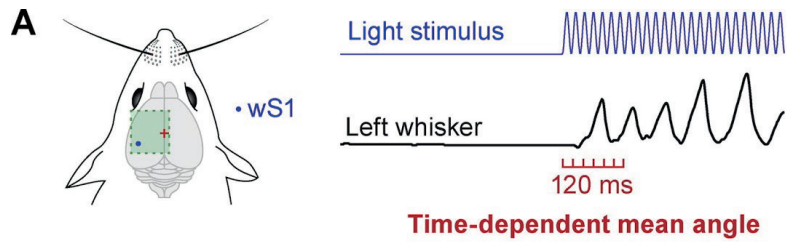
100 ms

Left whisker

Early peak < 100 ms

•wS1

B

Left whisker   Right whisker

MA029

MA030

MA032

MA034

Early peak (deg)

40

20

0

1 mm

Anterior

Lateral

C

Left whisker   Right whisker

Average

Early peak (deg)

40

20

0

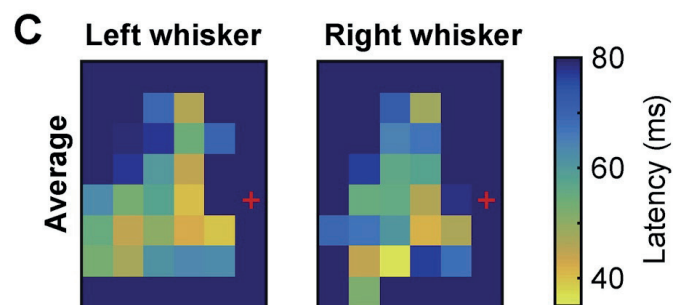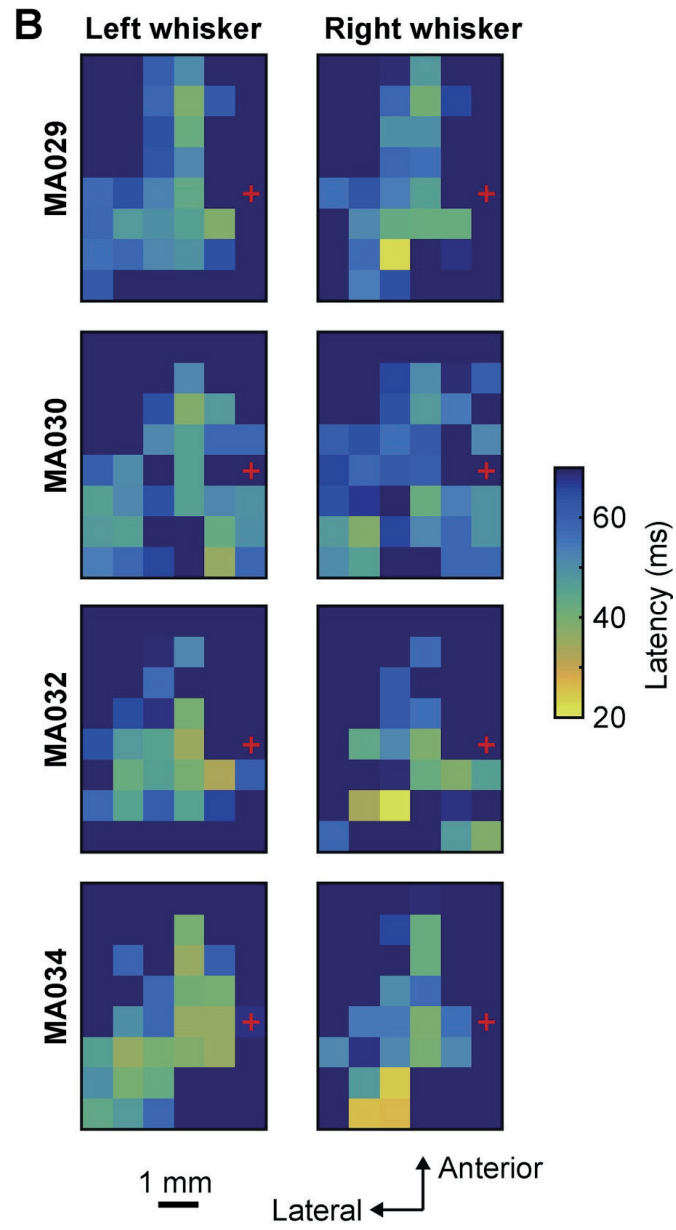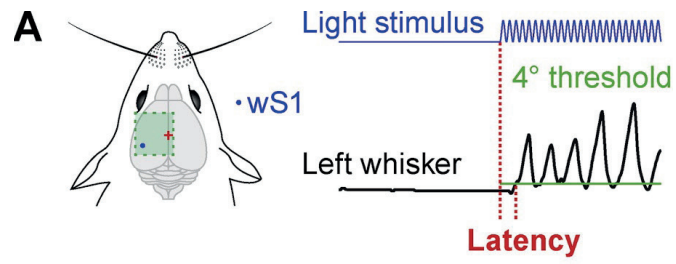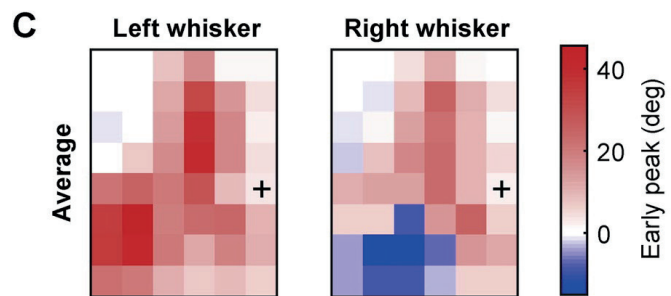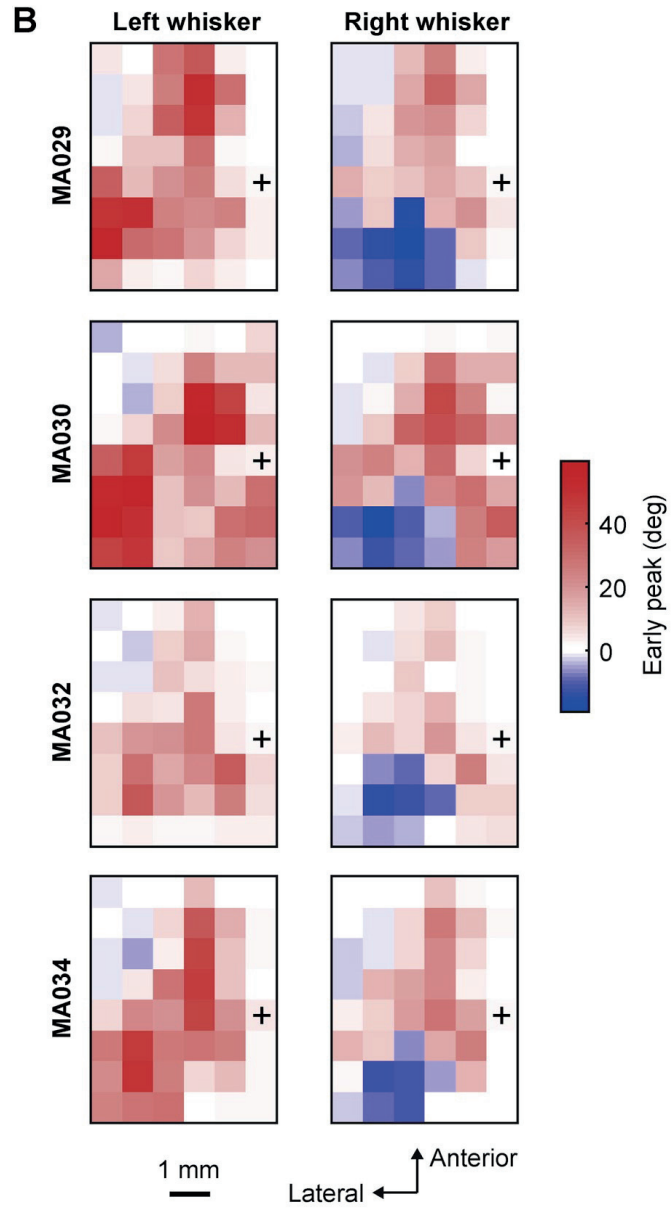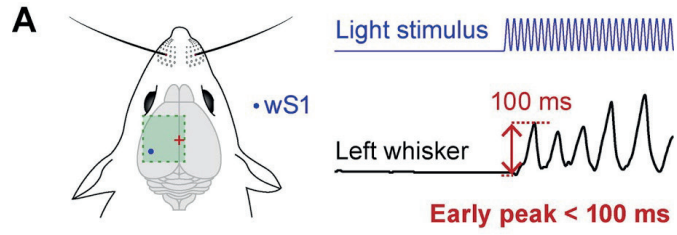***Figure 5.5. Maps of the early peak whisker movement evoked by optogenetic stimulation.***

A. Schematic drawing of wS1 stimulation (left) and an example of the left whisker angle (right) showing how the early peak parameter was computed: the maximum (for protraction) or minimum (for retraction) change in whisker angle during the first 100 ms after the stimulus onset.

B. Early peak whisker movement for the left C2 whisker and right C2 whisker of each mouse represented on a 2D color-coded map corresponding to each stimulation coordinate on the left hemisphere. The value of the early peak movement reported corresponds to the median of all the trials where the mouse did not whisk before the stimulus (whisker angle standard deviation below 1° for 200 ms before the stimulation). Positive values reflect a protraction of the whisker and negative values indicate retraction. Bregma position is represented by a black cross.

C. Average over the four mice of the early peak change in whisker angle for left and right C2 whiskers relative to the stimulation coordinates on the left hemisphere. The largest early whisker protraction was evoked by stimulating wM1/wM2. Stimulating wS1 evoked a large early protraction of the ipsilateral whisker and a large early retraction of the contralateral whisker.

The amplitude of whisker movements occurring within the frequency range of 5–15 Hz (Figure 5.6) for both right and left C2 whiskers was computed for each trial as the integral between 5Hz and 15Hz of the fast Fourier transform (FFT) of whisker angle (with the mean value subtracted) during the last 400 ms of the optogenetic stimulation (from 100 ms to 500 ms after the stimulus onset). The median value of the 5–15-Hz FFT integral across trials was color-coded in the maps for each mouse (Figure 5.6B), and then averaged across the four mice (Figure 5.6C).

A

Light stimulus

· wS1

400 ms

Left whisker

FFT integral 5 - 15 Hz

B

Left whisker   Right whisker

MA029

MA030

MA032

MA034

FFT (deg)

30

20

10

1 mm

Anterior

Lateral

C

Left whisker   Right whisker

Average

FFT (deg)

30

20

10
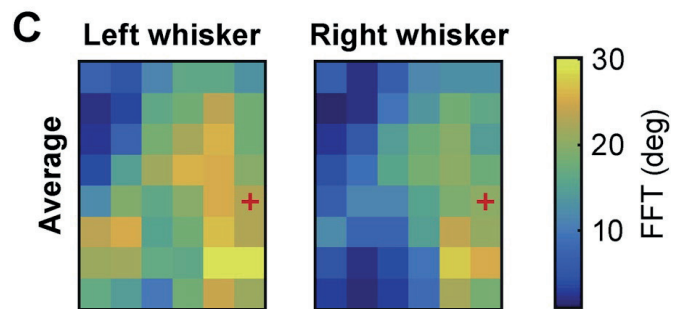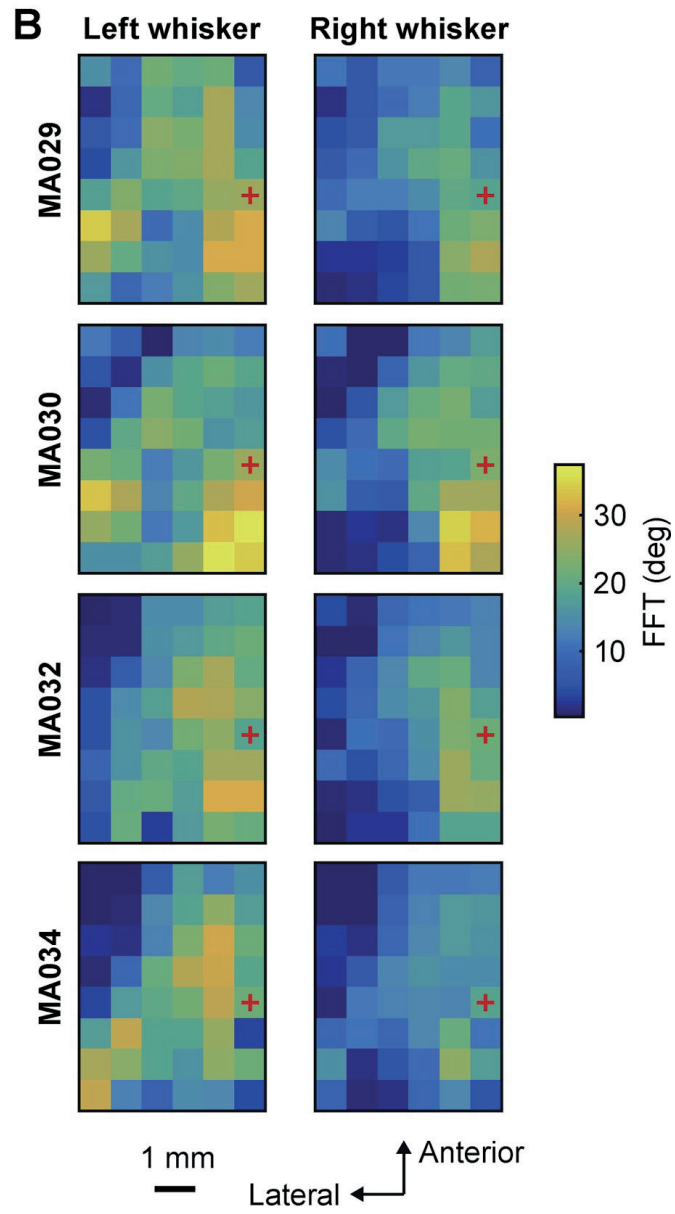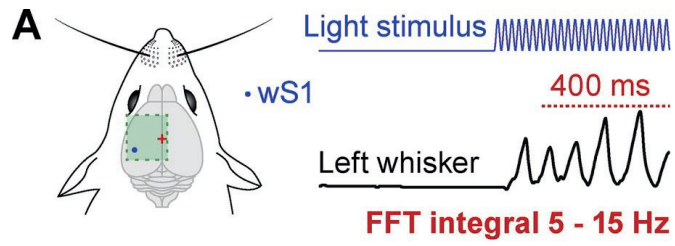
Figure 5.6. Maps of the amplitude of whisker movements in the 5–15-Hz frequency range evoked by optogenetic stimulation.

A. Schematic drawing of wS1 stimulation (left) and an example of the left whisker angle (right) showing how the fast Fourier transform (FFT) was computed: the integral from 5 Hz to 15 Hz of the FFT during the last 400 ms of the laser light stimulation.

B. FFT values for the left C2 whisker and right C2 whisker of each mouse represented on a 2D color-coded map corresponding to each stimulation coordinate on the left hemisphere. The value of FFT reported corresponds to the median of all the trials where the mouse did not whisk before the stimulus (whisker angle standard deviation less than 1° for 200 ms before the stimulation). Bregma position is represented by a red cross.

C. Average over the four mice of the FFT for left and right C2 whiskers relative to the stimulation coordinates on the left hemisphere. The largest 5–15-Hz whisker movements were evoked by stimulating the PtA region (posterior to Bregma close to the midline).

In order to assess the influence of the laser power on the evoked whisker movements of both right and left C2 whiskers, we repeated the same analysis procedures described above to compute the mean angle, the latency, the early peak and the FFT for the lower laser light power. The average value across mice of the mean angle (Figure 5.7B), the latency (Figure 5.7C), the early peak (Figure 5.7D) and the 5–15-Hz FFT (Figure 5.7E) was color- coded in the maps for high and low laser light power.

A

High light power

Left whisker

Low light power

Left whisker

B Average whisker angle

Left whisker   Right whisker

High power

Low power

deg

30
20
10
0
-10

1 mm

C Latency

Left whisker   Right whisker

High power

Low power

ms

120
100
80
60
40

Anterior

Lateral

D Early peak

Left whisker   Right whisker

High power

Low power

deg

40
30
20
10
0
-10

E FFT 5 - 15 Hz

Left whisker   Right whisker

High power

Low power

deg

30
25
20
15
10
5

· wS1

Figure 5.7. Motor maps evoked by different blue light intensities.

A. Schematic drawing of wS1 stimulation (left) and examples of the left whisker angle (right) for two wS1 stimulation trials with either high laser light power (mean power 1.75 mW) or low laser light power (mean power 0.36 mW).

B. Comparison of the averaged left and right whisker mean angle positions for the high and low power trials. The whiskers protracted/retracted less for low power stimulation compared to the high power, but the motor map pattern stayed relatively comparable. The high power map is the same as shown in Figure 5.2C.

C. Comparison of the averaged left and right whisker movement latencies for the high and low light power trials. The latencies of the whisker movements increased in low power stimulation compared to high power, but the smallest latencies observed were still located around wS1. The high power map is the same data as shown in Figure 5.4C.

D. Comparison of the averaged left and right early peak whisker movement amplitudes for the high and low light power trials during the first 100 ms after stimulus onset. The amplitudes of the early movements were reduced with low power but the largest protractions observed for both conditions were located in wM1/wM2 for the two whiskers and wS1 for the ipsilateral whisker, and the largest retraction was still observed around wS1 for the contralateral whisker. The high power map is the same as shown in Figure 5.5C.

E. Comparison of the averaged left and right whisker 5–15 Hz FFT for the high and low light power trials during the last 400 ms of the stimulation. The whisking amplitudes were reduced for low power stimulation compared to high power stimulation, but the largest 5–15-Hz FFT values for both conditions were localized in the PtA region posterior to Bregma close the midline. The high power map is the same as shown in Figure 5.6C.

The difference of mean change in angle between left and right C2 whiskers was computed for each trial as the difference in the mean angle of the left whisker minus the mean angle of the right whisker during the 500ms of optogenetic stimulation. The median value was color-coded in the maps across trials for each mouse, and then averaged across all mice (Figure 5.8B). The cross-correlation between right and left C2 whiskers was computed by taking the amplitude of the cross- correlation between the normalized right whisker trace during the 500ms of optogenetic stimulation (the whisker trace with the mean value subtracted is divided by its standard deviation) and the normalized left whisker trace at zero time lag. The median value was color-coded in the maps across trials for each mouse, and then averaged across all mice (Figure 4:8C).
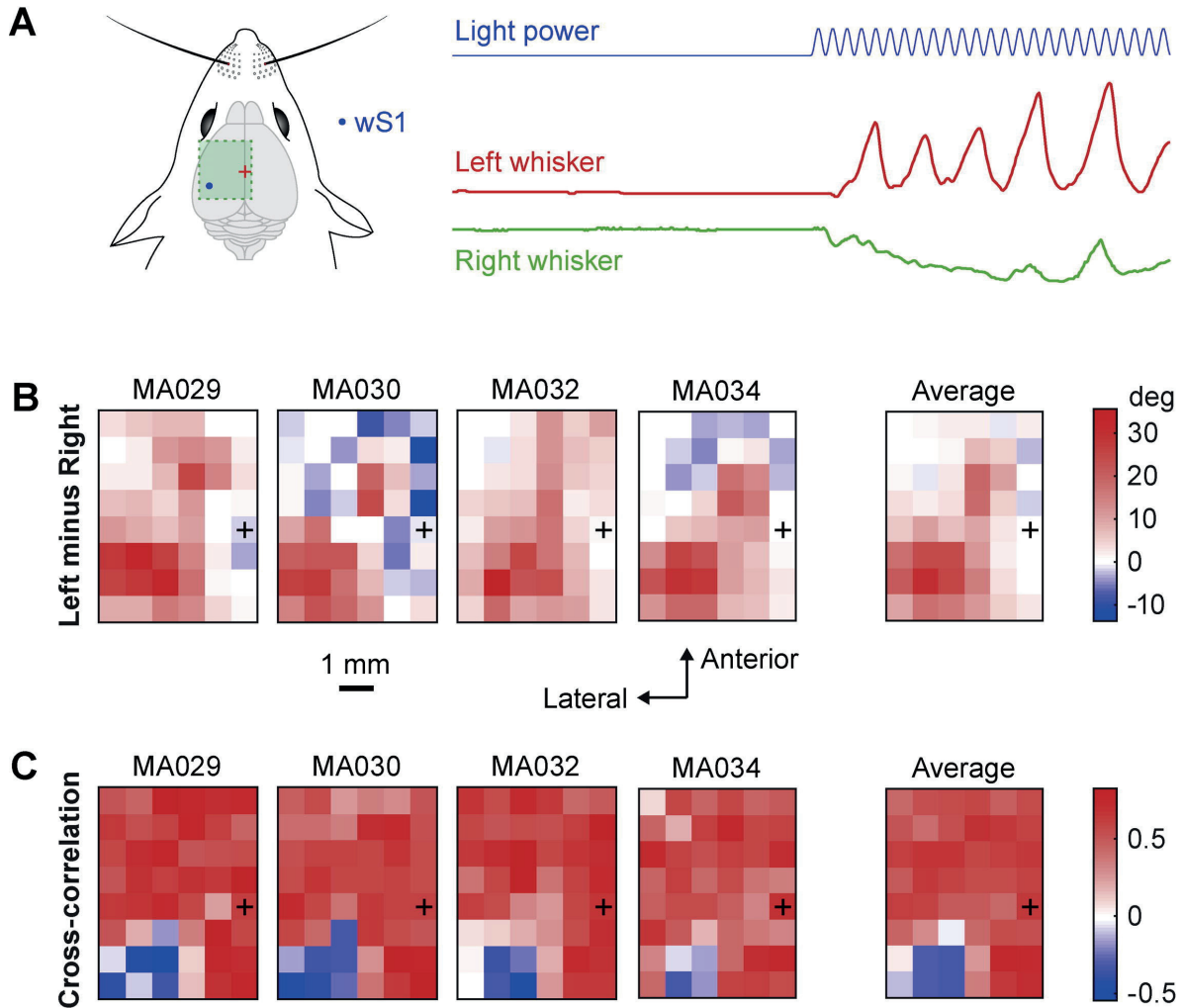
Figure 5.8. Correlations and differences in the ipsilateral and contralateral whisker movements evoked by optogenetic stimulation.

A. Schematic drawing of wS1 stimulation (left) and an example of the corresponding left and right whisker angles (right).

B. Difference between the left whisker angle and right whisker angle (left minus right) reported on a 2D color-coded map for each mouse (left images) and averaged across the four mice (right image). The left whisker usually protracted more than the right whisker when the left hemisphere was stimulated.

C. Cross-correlations of the left and right whiskers positions during the stimulation were high in almost all cortical areas except for stimulation of wS1, where there was an anti- correlation of the two whiskers.

The sensory maps for each mouse were computed by taking the contours at near minimal values of the smoothed intrinsic signal image for each body part. The primary sensory cortex region of each stimulated body part was color-coded, aligned to Bregma, and superimposed (Figure 5.9A). The sensory maps aligned to Bregma were overlaid with the averaged mean angle of the right C2 whisker motor map across all mice, as shown in Figures. 5.2C, 5.9B).
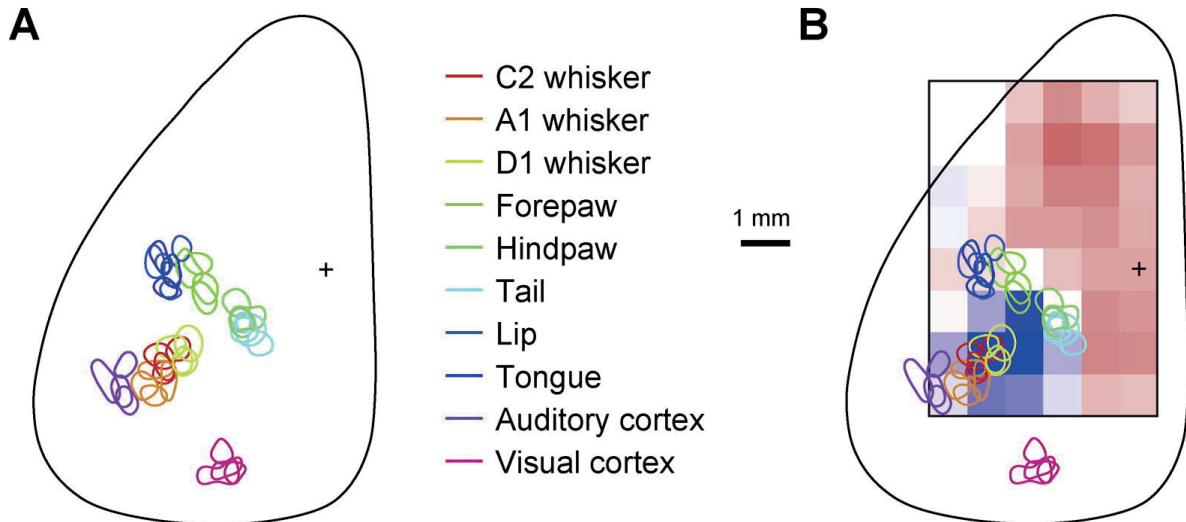
Figure 5.9. Whisker motor maps in the context of sensory maps.

A. Sensory map obtained with intrinsic optical imaging. Right C2, A1 and D1 whiskers, right forepaw, right hindpaw, tail, lip and tongue were deflected at a frequency of 10 Hz using a mechanical stimulator. A train of click sounds was used to deliver auditory stimuli. Light flashes pointed toward the right eye were used to deliver visual stimuli. The color-coded contours indicate the region of maximal evoked activity in each mouse.

B. Overlay of the sensory map obtained in panel A with the motor map of the right whisker mean angle positions (as shown in Figure 5.2C). There was a good overlap between the primary sensory whisker cortex (wS1) and the region where stimulation evoked a large retraction of the contralateral whisker.

All whisker angle data in Matlab, Python and Excel formats together with the location and timing of optogenetic stimulation are available in the Petersen- lab-data community hosted at https://zenodo.org together with the Matlab analysis code used to generate the results (http://dx.doi.org/10.5281/zenodo.437933).

5.3. Results

Optogenetic stimulation of whisker movement

A computer-controlled 2D scanning galvanometer mirror directed a blue laser light spot (~500-mm diameter) onto different regions of the left dorsal sensorimotor cortex of awake head-restrained mice while we filmed left and right C2 whisker movements at 500 Hz (Figure 5.1A). We used Thy1-ChR2-YFP line 18 mice (Arenkiel et al. 2007), which express ChR2 at high levels in many brain regions including prominent expression in layer 5 pyramidal neurons of the neocortex (Figure 5.1B). Each trial consisted of an initial 500 ms prestimulus period, followed by 500 ms of optogenetic stimulation during which the blue light was pulsed at 50 Hz with a mean power of 1.75 mW. The minimal intertrial interval was 5 s. Whisker movements of different latencies, amplitudes, directions and rhythmicity were evoked from

different cortical regions. Stimulation of some cortical regions reliably evoked bilateral rhythmic whisking (Figure 5.1C), whereas stimulation of other cortical regions reliably evoked contralateral whisker retraction together with ipsilateral rhythmic whisking (Figure 5.1D). Only trials in which the mouse was not moving its whiskers during the baseline period were included in our analyses (less than 1° of whisker angle standard deviation in the 200 ms preceding the optogenetic stimulus).

Mapping the average change in whisker angle

We first computed the average change in whisker angle for left and right whiskers evoked by stimulating different cortical regions, by subtracting the mean whisker angle during the 500 ms of optogenetic stimulation from the prestimulus angle (Figure 5.2A). For each stimulated cortical region in each of the mice, we computed the median change in whisker angle across individual trials and color- coded the result with red colors indicating protraction, blue colors indicating retraction, and white if the mean whisker angle remained unchanged during the stimulation period (Figure 5.2B). Whisker movements were evoked by the stimulation of many different cortical locations. In general, the stimulation of nearby cortical locations evoked similar movements. Visual inspection of the whisker motor maps suggested three regions containing separate hot-spots for evoking whisker movement.

In each mouse, we found that stimulation of a posteriolateral region evoked retraction of the contralateral whisker and protraction of the ipsilateral whisker. The stimulus site evoking the largest retraction of the contralateral whisker was located at 2.7 ± 0.5 mm lateral to Bregma and 1.2 ± 0.4 mm posterior to Bregma (mean ± SD, n = 4 mice). According to mouse brain atlases, this region is within the whisker primary somatosensory barrel cortex, and we shall henceforth refer to this region as wS1. Computed for this location evoking the largest contralateral retraction in each mouse, the mean change in whisker angle over the 500-ms stimulation period was −14.3 ± 1.2° for the right whisker (i.e. retraction of the contralateral whisker) and 17.0 ± 4.8° for the left whisker (i.e. protraction of the ipsilateral whisker).

Optogenetic stimulation of regions anterior to Bregma evoked protraction of both contralateral and ipsilateral whiskers in each mouse. The stimulus site evoking the largest protraction of the contralateral whisker was located at 0.8±0.7mm lateral to Bregma and 1.8 ± 0.7 mm anterior to Bregma. This region is typically considered to be part of the primary or secondary motor cortex, and we shall henceforth refer to this region as wM1/wM2. Computed for this anterior location evoking the largest contralateral protraction for each mouse, the mean change in whisker angle over the 500-ms stimulation period was 17.3 ± 5.4° for the right whisker and 17.9 ± 10.4° for the left whisker.

In addition, stimulation of a region posterior to Bregma also evoked protraction of both contralateral and ipsilateral whiskers in each mouse. The stimulus site posterior to Bregma evoking the largest protraction of the contralateral whisker was located at 0.6 ± 0.4 mm lateral to Bregma and 1.2 ± 0.4 mm posterior to Bregma. This region is close to parietal association cortex (PtA), cingulate cortex and retrosplenial cortex, and we shall henceforth refer to this relatively poorly defined region as PtA. Computed for this posterior location evoking the largest contralateral protraction for each mouse, the mean change in whisker

angle over the 500- ms stimulation period was 12.7 ± 3.8° for the right whisker and 14.2 ± 3.6° for the left whisker.

We next averaged the whisker motor maps from the four mice to generate a grand-average map of the mean change in whisker angle during the optogenetic stimulus (Figure 4:2C). This revealed the same overall pattern of evoked movements observed in individual mice, indicating the robustness of the method across different mice. In this average map, the peak of the wS1 retraction region was located at 3.1mm lateral to Bregma and 1.4 mm posterior to Bregma, with a 13.3 ± 0.8° retraction of the right whisker and 18.3 ± 4.3° protraction of the left whisker. The peak of the wM1/ wM2 protraction region in the average map was located at 1.6mm lateral to Bregma and 2.1mm anterior to Bregma, with a 16.1 ± 5.1° protraction of the right whisker and 23.0 ± 6.1° protraction of the left whisker. In the average map, the peak of the PtA protraction region was located at 0.8mm lateral to Bregma and 1.4 mm posterior to Bregma, with a 11.9 ± 3.3° protraction of the right whisker and 14.5 ± 3.4° protraction of the left whisker.

Mapping the time-dependent change in whisker angle

Whisker movements are highly dynamic and the time- averaged mean change in whisker angle during the optogenetic stimulation could average out important aspects of whisker motor control. The earliest evoked movements are likely to be particularly important to study, since these are likely to reflect the most direct effects of the optogenetic stimulation. We therefore investigated the change in whisker angle in 20-ms bins after the onset of the optogenetic stimulation (Figure 5.3A). In each mouse, we found that the earliest movements were evoked in the time period 20–40 ms after stimulus onset (Figure 5.3B). The earliest movements were retraction of the contralateral whisker evoked by stimulation of wS1 (Figure 5.3B). In the time period 40–60 ms, protraction of both contralateral and ipsilateral whiskers was evident upon stimulation of wM1/wM2. Early bilateral whisker protraction also appeared to be evoked by stimulation of an additional more posterior region, which we labeled PtA. These evoked whisker movements became increasingly large over the first 100 ms of optogenetic stimulation, without an obvious change in the spatial mapping of protraction and retraction movements. Averaging these time-dependent maps across the four mice revealed a robust spatiotemporal organization of the evoked whisker movements (Figure 5.3C).

Latency maps for evoked whisker movements

In order to examine when the first evoked whisker movements took place, we measured the time from the onset of optogenetic stimulation until the first time that the whisker angle changed more than ±4° relative to the prestimulus baseline whisker angle for each trial in each mouse (Figure 5.4A). If the whisker did not change angle by more than 4° then the trial was not included in the analysis. The spatial latency maps of individual mice showed some variability, but in general the shortest latency for evoking movement in each mouse was for the wS1-evoked retraction of the contralateral whisker (Figure 5.4B), which was also found in the average latency map across mice (Figure 5.4C). Stimulation of wS1 evoked retraction of the contralateral whisker with a latency of 33.8 ± 21.5 ms and protraction of the ipsilateral whisker with a latency of 61.5 ± 20.4 ms. Stimulation of wM1/ wM2 evoked protraction of the

contralateral whisker with a latency of 47.8 ± 7.6 ms and protraction of the ipsilateral whisker with a latency of 45.8 ± 7.2 ms. Stimulation of PtA evoked protraction of the contralateral whisker with a latency of 46.5 ± 7.7 ms and protraction of the ipsilateral whisker with a latency of 39.8 ± 8.4 ms.

Maps of early peak change in whisker angle

In order to further characterize the early-evoked whisker movements, we measured the maximal change in whisker angle during the first 100 ms of stimulation in each trial for each mouse (Figure 5.5A). In each mouse (Figure 5.5B) and average across mice (Figure 5.5C), we observed contralateral whisker retraction (−15.1 ± 2.9°) and ipsilateral whisker protraction (41.9 ± 9.6°) evoked by stimulation of wS1. Stimulation of the wM1/wM2 region evoked bilateral protraction (25.4 ± 9.1for the right whisker and 32.0 ± 15.5° for the left whisker). The PtA region also evoked bilateral protraction (25.2 ± 4.0° for the right whisker and 25.5 ± 9.3° for the left whisker). In the early peak maps of some individual mice, the anterior wM1/wM2 region appeared relatively localized and separated from the more posteriomedial PtA region (Figure 5.5B), however, in the average peak maps across mice, the posteriomedial PtA protraction region appeared to be more-or-less continuous with the more anterior wM1/wM2 region (Figure 5.5C).

Movement maps for the 5–15 Hz frequency band

Stimulation of some locations evoked rhythmic back-and- forward movements of the whisker (Figure 5.1C), similar to exploratory whisking, which typically occurs in the 5– 15 Hz range. We therefore quantified the amplitude of oscillatory whisker movements by integrating the FFT of the whisker angle across the 5–15 Hz range during the last 400ms of each optogenetic stimulation trial (Figure 5.6A). Averaged across trials for each individual mouse (Figure 5.6B) and in the grand average across mice (Figure 5.6C), we found that the largest amplitude 5–15-Hz movements of both left (27.5 ± 5.0°) and right whiskers (30.1 ± 3.5°) were evoked by stimulation of PtA. The lowest amplitude 5–15-Hz movements for the contralateral whisker (2.2 ± 0.2°) were evoked by stimulation of wS1. Stimulation of this region however evoked large amplitude 5–15-Hz movements for the ipsilateral whisker (21.8 ± 1.9°). Stimulation of wM1/ wM2 also evoked large amplitude 5–15-Hz movements for both left (20.4 ± 3.9°) and right (25.4 ± 6.7°) whiskers.

Whisker movement maps evoked at lower stimulation intensity

It is likely that lower light powers would stimulate fewer neurons, which might also be more spatially localized. In a subset of sessions, we used a lower mean light power of 0.36mW (rather than 1.75mW) to optogenetically evoke movements (Figure 5.7A). In general, the evoked whisker movements at this lower light intensity were less reliable, delayed and smaller in amplitude. Qualitatively, however, most features of the maps remained unchanged. We compared the grand average maps across mice for the mean change in whisker angle during the optogenetic stimulation (Figure 5.7B), the latency of evoked whisker movements (Figure 5.7C), the early peak change in whisker angle over the first 100

ms of stimulation (Figure 5.7D) and the 5–15-Hz FFT of whisker angle during the last 400ms of stimulation (Figure 5.7E). A contralateral whisker retraction region (wS1) was found at both high and low optogenetic stimulus intensities with a similar broad spatial location. The frontal rhythmic protraction region (wM1/wM2) appeared more localized at low stimulus intensities but similarly centered at ~2 mm anterior and ~1.5 mm lateral to Bregma. A rhythmic bilateral protraction region located close to the midline and posterior to Bregma (PtA) was also present at low stimulus intensities.

For the mean change in whisker angle during the optogenetic stimulation at low light power (Figure 5.7B), the wS1-evoked retraction of the contralateral whisker was reduced by 53.6% of the high light power, and the ipsilateral protraction was reduced by 54.8%. The wM1/wM2-evoked protraction of the contralateral whisker was reduced by 64.1% of the high light power, and the ipsilateral protraction was reduced by 78.9%. The PtA-evoked protraction of the contralateral whisker was reduced by 79.9% of the high light power, and the ipsilateral protraction was reduced by 42.4%.

For the latency (Figure 5.7C), the wS1-evoked retraction of the contralateral whisker was increased by 160.8% of the high light power, and the ipsilateral protraction was increased by 142.8%. The latency of wM1-evoked protraction of the contralateral whisker was increased by 223.8% of the high light power, and the ipsilateral protraction was increased by 266.2%. The latency of PtA-evoked protraction of the contralateral whisker was increased by 101.0% of the high light power, and the ipsilateral protraction was increased by 129.7%.

Comparison of evoked ipsilateral and contralateral whisker movements

Depending upon the location stimulated, the left and right whiskers could move in either a similar (Figure 5.1C) or different (Figure 5.1D) manner (Figure 5.8A). We first quantified the difference in the evoked change in whisker position by subtracting the angle of the two whiskers (left minus right) (Figure 5.8B). On average the left whisker protracted more than the right whisker. In many locations there was little difference in whisker angle, suggesting bilaterally symmetric movements. However, stimulation of wS1 and wM1/wM2 evoked an asymmetric whisker movement, with larger protraction of the ipsilateral whisker.

We next correlated the time-dependent angle of the left and right whisker for each trial (Figure 5.8C). This revealed that whisker movements were in general highly correlated for most locations stimulated, including frontal wM1/wM2 regions and the posteriomedial PtA region. Strongly anticorrelated movement of the left and right whiskers was found only for stimulation of wS1.

Comparison of sensory and whisker motor maps in mouse dorsal cortex

In order to compare our whisker motor maps with sensory maps of the dorsal mouse cortex we carried out intrinsic optical imaging under anesthesia while delivering deflections of different right whiskers, mechanical tactile tappings of the right forepaw, right hindpaw, tail, lip and tongue, auditory click stimuli and visual stimuli to the right eye (Figure 5.9). There was a good match of the locations of the different evoked sensory responses across the four

mice (Figure 5.9A). We next directly compared the contralateral whisker motor map (Figure 5.2C) with this sensory map (Figure 5.9B). As expected from mouse brain atlases, there was a clear overlap of the whisker primary somatosensory cortex identified with intrinsic signal optical imaging with the region that drove retraction of the contralateral whisker, which we have consistently labeled wS1. The stripe between wS1 and wM1/wM2 where we observed less optogenetically evoked whisker movements appeared to correspond to the forelimb, hindlimb, tongue and lip somatosensory cortex.

5.4. Discussion

In this study, we delivered blue light stimuli in an unbiased manner to the left dorsal sensorimotor cortex of Thy1-ChR2 mice, and quantified the evoked whisker movements. Whisker movements were evoked by stimulation of many different locations in the dorsal cortex, and whisker motor control may therefore be spatially highly distributed in the mouse neocortex. Stimulation of a region near to wS1 evoked the shortest latency whisker movement, which consisted of a sustained retraction of the contralateral whisker followed by initiation of rhythmic protraction of the ipsilateral whisker. Stimulation of most other regions of the dorsal cortex evoked rhythmic bilateral whisker protraction with slightly longer latencies compared to wS1 and varying amplitudes and degrees of rhythmicity. The regions driving rhythmic whisker protraction might be divided into at least two subdivisions, a frontal region located in the neighborhood of wM1/wM2 and a midline region located near and posterior to Bregma, which we labeled PtA. Below we consider each of these regions separately.

wS1 evoked retraction of the contralateral whisker

Stimulation of a region ~3mm lateral and ~1.5mm posterior to Bregma caused retraction of the contralateral whisker (Figure 5.2) with short latency (Figure 5.3 and Figure 5.4). This region overlaps with the whisker primary somatosensory barrel cortex wS1 (Figure 5.9). Our data are therefore consistent with previous studies suggesting a relatively direct role for whisker sensory cortex in whisker motor control (Matyas et al. 2010; Sreenivasan et al. 2015). Whisker retraction driven by sensory cortex might serve as a negative feedback signal, perhaps serving to attenuate strong sensory input (Matyas et al. 2010).

Layer 5 pyramidal-tract neurons in the barrel cortex project to the spinal trigeminal interpolaris nucleus, which contains many premotor neurons for motor neurons innervating extrinsic muscles (Matyas et al. 2010; Sreenivasan et al. 2015). Extrinsic muscles (i.e. the muscles anchored outside the mystacial pad) pull the whiskers and the mystacial pad in different directions, with prominent retraction caused by contraction of muscles nasolabialis and maxillolabialis (Dörfl 1982; Haidarliu et al. 2012; Moore et al. 2013). It is therefore possible that the short latency retraction of the contralateral whisker evoked by stimulation of wS1 is evoked by monosynaptic excitation of premotor neurons in spinal trigeminal nuclei, which in turn innervate motor neurons of the extrinsic muscles. Future experiments must directly test this hypothesized circuit mechanism. It would be of great interest to explore the

effects of optogenetically manipulating the relevant neuronal cell-types in different brainstem nuclei connected with the different facial nucleus whisker motor neuron pools. wS1 neurons innervate many other brain regions, and it is likely that they also contribute to the evoked whisker movements.

Interestingly, shortly after the start of contralateral whisker retraction, the ipsilateral whisker begins to protract. The underlying neuronal circuit is unknown, but bilateral connectivity is prominent in cortex, as well as in brainstem and many other motor structures. In head-centered coordinates, the net effect of stimulating the left somatosensory cortex is clockwise rotation of the whiskers, which could be interpreted as a rotation of a 'foveal' whisking region to the right. This could represent the beginning of an orienting body movement toward a region of interest from which sensory information is arriving. Here, we only investigated evoked movements in head-restrained mice, and, in future studies, it will be of great interest to carry out the same experiments in freely moving mice, to see if a rightward (clockwise) rotation of the head accompanies the clockwise rotation of the whiskers. It will also be important to study movements evoked by wS1 stimulation in diverse behavioral contexts, such as during the execution of learned tasks, and to examine if stimulation of different specific neuronal cell-types in wS1 evoke different movements.

Whisker movements evoked by stimulation of frontal cortex

Stimulation of neuronal activity in frontal cortex also evoked whisker movements. Most cortical areas anterior to Bregma evoked bilateral protraction of the C2 whiskers, with latencies slightly longer than the whisker retraction evoked by stimulation of primary sensory cortex. These data are consistent with previous investigations suggesting that stimulation of a frontal region innervated by wS1, located ~1 mm lateral and ~1 mm anterior to Bregma (often labeled wM1), evokes prominent contralateral rhythmic whisker protraction (Matyas et al. 2010; Sreenivasan et al. 2015, 2016). Pyramidal neurons in wM1 send direct projections to brainstem reticular formation, which contains many pre- motor neurons for motor neurons innervating intrinsic muscle (Matyas et al. 2010; Sreenivasan et al. 2015), as well as a central pattern generator for whisking (Moore et al. 2013; Deschênes et al. 2016). Intrinsic muscles (i.e. the muscles contained within the mystacial pad) attach to the base of individual whisker follicles, and their contraction causes the protraction of that whisker, pivoting the whisker forward around the insertion point in the pad (Dörfl 1982; Haidarliu et al. 2012; Moore et al. 2013). It is therefore possible that wM1 evokes contralateral whisker protraction by exciting pre- motor neurons in the brainstem reticular formation, which subsequently excite motor neurons innervating intrinsic muscles driving whisker protraction. Future experiments must carefully test this hypothesis, by optogenetically stimulating and inactivating specific groups of neurons in the brainstem. wM1 also innervates many other brain regions, and it is likely that they will also contribute to controlling whisker movement.

Although stimulating wM1 evoked reliable movements, in our unbiased optogenetic mapping experiments the largest protraction appeared to be evoked by stimulating a region ~1 mm anterior to wM1. This region may correspond to a premotor-like region of cortex, which could be labeled wM2. M2 regions strongly innervate M1 (Hira et al. 2013; Hooks et al. 2013), and thus stimulation of wM2 could evoke whisker movements by exciting wM1. However, the shortest latency for protraction of the contralateral whisker evoked by stimulation of frontal

cortex was typically also located anterior to wM1. It is therefore possible that wM2 has a more direct role in controlling whisker protraction, and future studies must investigate the underlying neuronal circuits linking wM2 to motor neurons innervating the intrinsic muscles driving whisker protraction.

Our results in head-restrained mice differ from a recent study, which concluded that rat "vibrissa motor cortex activity suppresses contralateral whisking" (Ebbesen et al. 2017). There are a number of important differences including species, methods and behavioral context. Further research is necessary to understand the key determinants giving rise to different results.

Whisker movements evoked by stimulation of posterior midline cortex

Optogenetic stimulation of a midline region close and posterior to Bregma, which we labeled PtA, also evoked strong bilateral whisker protraction. The amplitude of whisker movements in the 5–15-Hz range computed by the FFT of whisker position was larger in this region than for any other cortical region (Figure 5.6). Latencies for evoking whisker movements from this posteriomedial region were similar to frontal cortex and slightly slower than wS1-evoked whisker movements (Figure 5.4). How activity in this brain region contributes to the control of whisker movements is unknown. This parietal region is an associative area, receiving input from different sensory regions and thus likely integrating multisensory signals. Future studies must investigate how neuronal activity in this region contributes to controlling whisker movements under diverse behavioral conditions.

Future perspectives

Whisker motor control is complex, with premotor neurons for whisker motor control being widely distributed across brainstem, midbrain and cortex (Hattox, Priest, and Keller 2002; Grinevich, Brecht, and Osten 2005; Takatoh et al. 2013; Sreenivasan et al. 2015). Whisker motor control is therefore likely to be regulated by many different synaptic circuits in the rodent brain. There are a large number of limitations to the current study, which need to be overcome by further experimental investigation. It would be of interest to repeat the current experiments at higher spatial resolution, testing different stimulation paradigms, and in mice expressing optogenetic actuators in different cell-types. Optogenetic inactivation maps will also be of obvious importance investigating both the hypothesis that inhibition of some cortical regions might promote whisker movement (Ebbesen et al. 2017), and also the hypothesis that inhibition of some cortical regions, including wS1 and wM1, might reduce the probability for initiation of spontaneous whisking (Sreenivasan et al. 2016). Because optogenetic stimulation and inhibition can evoke changes in activity not just in the photo-stimulated region, but also in axons of passage and downstream synaptically connected brain regions (Otchy et al. 2015; Sreenivasan et al. 2016), it will also be of great importance in future experiments to simultaneously measure the spatiotemporal dynamics of optogenetically evoked brain-wide neural activity. This is now becoming technically possible through combining optogenetic motor mapping with wide-field imaging of cortical activity using fluorescent voltage-sensitive dyes (Amiram Grinvald and Hildesheim 2004; Ferezou et al. 2007; Mohajerani et al. 2013) or genetically encoded activity indicators (Akemann et al.

2010; Minderer et al. 2012; Vanni and Murphy 2014; Hochbaum et al. 2014; Madisen et al. 2015; Xie et al. 2016; Zhuang et al. 2017).

Our results suggest that a large part of the dorsal cortex of mice can contribute to controlling whisker movement. It is possible that these whisker motor maps can be modulated by behavioral context and learning. It will therefore be important to investigate whisker motor control in different behavioral contexts, measured across learning of simple goal-directed sensorimotor behaviors. Here, we correlated stimulus location with C2 whisker movements, but it is likely that many other movements, such as limb and body movements, would also have been evoked during our experiments, which we did not monitor. Investigating the coordination of diverse types of movements evoked by stimulating a given cortical region may help investigate other potential organizing principles of motor cortex, such as the suggestion of action zones for different types of behavior in primate motor cortex (Graziano, Taylor, and Moore 2002).

6. General discussion and future perspectives

Wide-field intrinsic optical imaging for sensory mapping

In this thesis I have described different methods to investigate the mouse cortex with various approaches and strategies. I started with a very well-established and routinely used technique: wide-field intrinsic optical imaging (A. Grinvald et al. 1986; Pouratian and Toga 2002). This tool has been extensively used in neuroscience to investigate sensory mapping in various animal models like monkeys, cats, rats or mice applied to various systems like visual cortex (Bonhoeffer and Grinvald 1991; Antonini, Fagiolini, and Stryker 1999; Schuett, Bonhoeffer, and Hübener 2002), auditory cortex (Bakin et al. 1996; Tsytsarev and Tanaka 2002; Kalatsky et al. 2005), barrel cortex (Masino et al. 1993; L. M. Chen, Friedman, and Roe 2003), olfactory bulb (Rubin and Katz 1999; Belluscio and Katz 2001; Vincis et al. 2015) among others.

In the laboratory, I developed a transparent preparation surgery to image wide-field signal through the skull of head restrained mice. Moreover, I developed a MATLAB program that controls a highly sensitive camera needed to get reliable optical intrinsic signals of the barrel cortex. Also, I was able to get sensory evoked response from the right forepaw and hindpaw, from the tail, the lip, the tongue and from the auditory cortex and the visual cortex. This provided a detailed sensory map of the highly organised primary sensory cortices.

In another set of experiments I combined optogenetic stimulation with optical intrinsic signal imaging. Because of the very strong activation of the barrel cortex generated by the blue light pulse, I could observe the projection of the activity in the connected areas. This is a promising technique to investigate the connectome within the whole mouse cortex in both hemispheres.

Tongue-jaw sensory and motor cortex mapping

I used the transparent skull preparation protocol that I developed to record cortical activity using the emerging technique of wide-field calcium imaging, making use of genetically-encoded calcium indicator mouse lines. In particular I used the Thy1-GCaMP6f mouse (Dana et al. 2014) to map tongue-jaw sensory and motor cortex in anesthetized mice. In these experiments I assumed that the frontal secondary area that emerged upon tongue or jaw mechanical stimulation corresponded to tjM1, located anterior to tjS1. This interpretation was based on previous work showing that whisker primary motor cortex (wM1) is activated by the direct projection from wS1 to wM1 (Ferezou et al. 2007; Petersen 2007). I discovered that tjS1 is located 3.76 ± 0.16 mm lateral to Bregma and -0.01 ± 0.35 mm at Brema level on the anteroposterior axis, and tjM1 is located 2.44 ± 0.45 mm lateral to Bregma and 1.79 ± 0.09 mm anterior to Bregma.

To test whether the tongue-jaw sensorimotor system has a similar organisation to the whisker system, it would be interesting to inject an anterograde virus in tjS1 and see if it projects to tjM1. This would give anatomical evidence of connectivity between tjS1 and tjM1.

A further important experiment would be to perform functional motor mapping using optogenetics to see if we could generate evoked movement of the jaw in awake mice. Also,

it would be interesting to inactivate tjM1 using either pharmacology or optogenetic inactivation while the mouse is performing a behavioral task to see if it changes the licking probability. As the tongue and jaw are midline organs, it might be important to do cortical activation or inactivation experiments in both hemispheres. If stimulation of tjM1 can trigger licking or at least jaw movements upon optogenetic stimulation or if licking can be blocked by inactivating tjM1 this would provide causal evidence of this area contributing licking motor commands to the tongue and jaw.

Wide-field calcium imaging in cortical layer 2/3 mice during 2-whisker task

I next used the TIGRE2.0-GCaMP6f mice crossed with the Rasgrf2-2A-dCre mice to get a high and specific expression in layer 2/3 of the cortex. The mice performed a 2-whisker discrimination task where they had to lick after C2 whisker stimulation to get a water reward and to withhold licking after B2 whisker stimulation, otherwise they would get a 10 s time out punishment. The mice were able to reach a good level of discrimination after a few days of training, usually three to four days on average. I observed that, on average, there was a significant difference between hit and miss trials in wS1, S2, wM1 and M2. On average, the amplitude of the responses in wS1 and S2 was decreasing over training days in both hit and miss conditions, whereas it had the tendency to increase in wM1 and M2 along the learning of the task. There was an important trial-to-trial variability that made the effect of the signal propagation difficult to study with a large noise in one pixel data. By looking at the response at given times we could still identify early significant differences between hit versus miss trials in wS1 and S2 starting at 100 ms. Then the signals converged toward M2 were both parallel sensorimotor pathways S1-M1 and S2-M2 meet and amplify the response. This amplification occurs when the mouse decides to lick and C2 sensory input is transformed into a lick motor command output.

The mice go under three major phases during one training session. Usually, they start with a compulsive phase where they lick all the time, leading to a ~100% lick rate for C2 Go trials as well as ~100% lick rate for B2 NoGo trials and a high false alarm catch lick rate. Perhaps, at the beginning of the session, the mouse is very thirsty and motivated and does not pay attention on the nature of the stimulus and just licks. It seems that once the mouse stays longer on the setup and gets a little bit of water, it starts calming down and focusing more its attention on the stimulus. During this second phase of the behavior, the mouse is still highly motivated but less stressed by thirst and it starts discriminating between C2 and B2 stimulation. C2 lick rate usually stays high and B2 lick rate decreases gradually to reach the peak performance of the session. The false alarm catch lick rate decreases also. After the peak performance is reached, the mouse starts disengaging from the task and its lick rate for C2 decreases. This third phase of the behavior occurs when the mouse stayed a long time on the setup and it had enough water. False alarm catch lick rate is usually at 0% and if we keep sufficient time the mouse on the setup first B2 lick rate will be 0% and then C2 lick rate will reach 0% too. I did not study the cortical signal dynamics difference between those three different phases. It is unlikely that the signal would have the same amplitude and latency, first because the reaction times are usually different. Also, there might be a top down modulation occurring during those phases that would be interesting to investigate. In future analyses, one should define an objective criteria to efficiently separate those phases. By averaging signal over the entire session, one might wash out some important effects

emerging from the cortical processing of the sensorimotor information. It might be interesting to make this analysis, and maybe averaging those phases across sessions to get sufficient statistical power.

Moreover, to more specifically examine the circuit between M2 and S2 and maybe also S1 through M1, it would be interesting to inject a retrograde virus in M2 to express Cre-recombinase in neurons sending axons to these frontal regions in TIGRE2.0-GcaMP6f mice. In such an experiment one might detect at a macroscale the activity of neurons specifically projecting to M2 and processing the information while the mouse is performing the task.

Finally, inactivating M2 using either pharmacology or optogenetics while the mouse is performing the task to see how it influences the performance would be an interesting approach to describe the functional connectivity of this neural circuit that seems to play a very important role in sensorimotor integration and decision making (Makino et al. 2017). We would observe if the mouse can still perform when we interfere with this M2 circuit by cutting signals in M2.

Optogenetic stimulation of cortex to map evoked whisker movements in awake head-restrained mice

I obtained a motor map of the whisker cortex by filming both C2 whiskers (on each side of the snout) and quantifying movements evoked by unbiased optogenetic stimulation across the entire left sensorimotor cortex of Thy1-ChR2 mice. I triggered large oscillating protraction movements by stimulating wM1 and I generated a large oscillating protraction of the ipsilateral and a prolonged retraction of the contralateral whisker while stimulating wS1 (Matyas et al. 2010; Sreenivasan et al. 2015). Interestingly, whisker movements were evoked by stimulation of various locations of the dorsal cortex suggesting that whisker motor control may therefore be spatially highly distributed in the mouse neocortex. Stimulation in wS1 evoked movements with the shortest latency. Other places of the cortex evoked whisker rhythmic protractions with longer latencies and different frequency oscillations. The largest whisking oscillations were generated when PtA area was stimulated.

Interesting further experiments would be to reproduce this map with a finer stimulation grid to increase the spatial resolution. One could also try different stimulation paradigms to see if some different behavioral responses emerge. Furthermore, one could repeat these motor-mapping experiments expressing ChR2 in different cell-types and layer specific mouse lines.

Finally, one could try optogenetic inactivation mapping experiments. It has been suggested that inactivating wM1 could reduce the probability for the mouse to start spontaneous whisking (Sreenivasan et al. 2016). On the other hand, by inhibiting some specific cortical regions (e.g. wM1) it could promote whisker movement by disinhibiting contralateral whisker movements and leading to contralateral whisker protraction (Ebbesen et al. 2017).

Future perspectives

Mice go through different phases both during the learning of the discrimination task, that within a session. During learning, the mice first learn to lick, then to detect any whisker stimulus and finally to discriminate between the two whisker stimuli. It would be interesting to study the evolution of the signal by analyzing the potential differences of the cortical responses when the mice are naive compared to when the mice are expert. It would be interesting to see if there is some plasticity that takes place in the cortex to learn this task and where are the most significant areas. In addition, during a session mice go through three phases: at first they are highly motivated and compulsive and do not pay attention to the nature of the stimulus, in a second time they focus their attention on the stimulus to lick at the right moment until they reach their peak performance, then finally in a third time they are demotivated and almost no longer lick and do a lot of miss trials. It would be necessary to be able to compare the cortical activities during these three phases in order to determine if the motivation has a great influence on the signal or if the attention has a greater importance.

Another experiment would be to perform wide-field calcium imaging experiment in a behaving mouse during pharmacological inactivation of a specific area (e.g. muscimol inactivation) and observe the influence on the cortical activity and the performance of the mouse. This would help to investigate the causality of the pathway used by the mouse to take the decision to lick or not. If the inactivation has a big influence on the performance of the mouse it would be interesting to see if there is change in the cortical activity or not. On the other hand, if the inactivation does not affect the mouse performance, it would be interesting to observe if there is no change in the cortical activity or there is.

Having explored the cortex of the mouse with all these different wide-field techniques, it would be interesting to combine them in behaving mice. It is now becoming technically possible to generate optogenetic stimulation while imaging cortical activity at the same time using fluorescent voltage-sensitive dyes (Mohajerani et al. 2013) or genetically encoded activity indicators (Hochbaum et al. 2014). Optogenetic activation or inhibition can evoke changes in the cortical activity throughout the whole cortex. It would be interesting to activate or inhibit at specific times and locations to see if we could enhance or limit the discrimination performances of the mouse.

7. References

-. 2012. *Brain Facts: A Primer on the Brain and Nervous System*. Society for Neuroscience.

Akemann, Walther, Hiroki Mutoh, Amélie Perron, Yun Kyung Park, Yuka Iwamoto, and Thomas Knöpfel. 2012. "Imaging Neural Circuit Dynamics with a Voltage-Sensitive Fluorescent Protein." *Journal of Neurophysiology* 108 (8): 2323–37.

Akemann, Walther, Hiroki Mutoh, Amélie Perron, Jean Rossier, and Thomas Knöpfel. 2010. "Imaging Brain Electric Signals with Genetically Targeted Voltage-Sensitive Fluorescent Proteins." *Nature Methods* 7 (8): 643–49.

Allen, William E., Isaac V. Kauvar, Michael Z. Chen, Ethan B. Richman, Samuel J. Yang, Ken Chan, Viviana Gradinaru, Benjamin E. Deverman, Liqun Luo, and Karl Deisseroth. 2017. "Global Representations of Goal-Directed Behavior in Distinct Cell Types of Mouse Neocortex." *Neuron* 94 (4): 891–907.e6.

Amato, Stephen P., Feng Pan, Joel Schwartz, and Timothy M. Ragan. 2016. "Whole Brain Imaging with Serial Two-Photon Tomography." *Frontiers in Neuroanatomy* 10 (March): 31.

Antonini, A., M. Fagiolini, and M. P. Stryker. 1999. "Anatomical Correlates of Functional Plasticity in Mouse Visual Cortex." *The Journal of Neuroscience: The Official Journal of the Society for Neuroscience* 19 (11): 4388–4406.

Aoki, Ryo, Tadashi Tsubota, Yuki Goya, and Andrea Benucci. 2017. "An Automated Platform for High-Throughput Mouse Behavior and Physiology with Voluntary Head-Fixation." *Nature Communications* 8 (1): 1196.

Arabzadeh, Ehsan, Erik Zorzin, and Mathew E. Diamond. 2005. "Neuronal Encoding of Texture in the Whisker Sensory Pathway." *PLoS Biology* 3 (1): e17.

Arenkiel, Benjamin R., Joao Peca, Ian G. Davison, Catia Feliciano, Karl Deisseroth, George J. Augustine, Michael D. Ehlers, and Guoping Feng. 2007. "In Vivo Light-Induced Activation of Neural Circuitry in Transgenic Mice Expressing Channelrhodopsin-2." *Neuron* 54 (2): 205–18.

Aronoff, Rachel, Ferenc Matyas, Celine Mateo, Carine Ciron, Bernard Schneider, and Carl C. H. Petersen. 2010. "Long-Range Connectivity of Mouse Primary Somatosensory Barrel Cortex." *The European Journal of Neuroscience* 31 (12): 2221–33.

Asaba, Akari, Tatsuya Hattori, Kazutaka Mogi, and Takefumi Kikusui. 2014. "Sexual Attractiveness of Male Chemicals and Vocalizations in Mice." *Frontiers in Neuroscience* 8 (August): 231.

Auffret, Matthieu, Veronica L. Ravano, Giulia M. C. Rossi, Nicolas Hankov, Merissa F. A. Petersen, and Carl C. H. Petersen. 2018. "Optogenetic Stimulation of Cortex to Map Evoked Whisker Movements in Awake Head-Restrained Mice." *Neuroscience* 368 (January): 199–213.

Avivi-Arber, Limor, Jye-Chang Lee, and Barry J. Sessle. 2010. "Effects of Incisor Extraction on Jaw and Tongue Motor Representations within Face Sensorimotor Cortex of Adult Rats." *The Journal of Comparative Neurology* 518 (7): 1030–45.

Ayling, Oliver G. S., Thomas C. Harrison, Jamie D. Boyd, Alexander Goroshkov, and Timothy H. Murphy. 2009. "Automated Light-Based Mapping of Motor Cortex by Photoactivation of Channelrhodopsin-2 Transgenic Mice." *Nature Methods* 6 (3): 219–24.

Bakin, J. S., M. C. Kwon, S. A. Masino, N. M. Weinberger, and R. D. Frostig. 1996. "Suprathreshold Auditory Cortex Activation Visualized by Intrinsic Signal Optical Imaging." *Cerebral Cortex* 6 (2): 120–30.

Belluscio, L., and L. C. Katz. 2001. "Symmetry, Stereotypy, and Topography of Odorant Representations in Mouse Olfactory Bulbs." *The Journal of Neuroscience: The Official Journal of the Society for Neuroscience* 21 (6): 2113–22.

Berg, Rune W., and David Kleinfeld. 2003a. "Rhythmic Whisking by Rat: Retraction as Well

as Protraction of the Vibrissae Is Under Active Muscular Control." *Journal of Neurophysiology* 89 (1): 104–17.

———. 2003b. "Vibrissa Movement Elicited by Rhythmic Electrical Microstimulation to Motor Cortex in the Aroused Rat Mimics Exploratory Whisking." *Journal of Neurophysiology* 90 (5): 2950–63.

Bonhoeffer, T., and A. Grinvald. 1991. "Iso-Orientation Domains in Cat Visual Cortex Are Arranged in Pinwheel-like Patterns." *Nature* 353 (6343): 429–31.

Bosman, Laurens W. J., Arthur R. Houweling, Cullen B. Owens, Nouk Tanke, Olesya T. Shevchouk, Negah Rahmati, Wouter H. T. Teunissen, et al. 2011. "Anatomical Pathways Involved in Generating and Sensing Rhythmic Whisker Movements." *Frontiers in Integrative Neuroscience* 5 (October): 53.

Boyden, Edward S., Feng Zhang, Ernst Bamberg, Georg Nagel, and Karl Deisseroth. 2005. "Millisecond-Timescale, Genetically Targeted Optical Control of Neural Activity." *Nature Neuroscience* 8 (9): 1263–68.

Brecht, Michael. 2007. "Barrel Cortex and Whisker-Mediated Behaviors." *Current Opinion in Neurobiology* 17 (4): 408–16.

Brecht, Michael, Andreas Krauss, Sajjad Muhammad, Laleh Sinai-Esfahani, Sebastiano Bellanca, and Troy W. Margrie. 2004. "Organization of Rat Vibrissa Motor Cortex and Adjacent Areas according to Cytoarchitectonics, Microstimulation, and Intracellular Stimulation of Identified Cells." *The Journal of Comparative Neurology* 479 (4): 360–73.

Brecht, Michael, Miriam Schneider, Bert Sakmann, and Troy W. Margrie. 2004. "Whisker Movements Evoked by Stimulation of Single Pyramidal Cells in Rat Motor Cortex." *Nature* 427 (6976): 704–10.

Bukhari, Qasim, Aileen Schroeter, David M. Cole, and Markus Rudin. 2017. "Resting State fMRI in Mice Reveals Anesthesia Specific Signatures of Brain Functional Networks and Their Interactions." *Frontiers in Neural Circuits* 11 (February): 5.

Busse, Laura, Asli Ayaz, Neel T. Dhruv, Steffen Katzner, Aman B. Saleem, Marieke L. Schölvinck, Andrew D. Zaharia, and Matteo Carandini. 2011. "The Detection of Visual Contrast in the Behaving Mouse." *The Journal of Neuroscience: The Official Journal of the Society for Neuroscience* 31 (31): 11351–61.

Cannestra, A. F., A. J. Blood, K. L. Black, and A. W. Toga. 1996. "The Evolution of Optical Signals in Human and Rodent Cortex." *NeuroImage* 3 (3 Pt 1): 202–8.

Carvell, G. E., and D. J. Simons. 1990. "Biometric Analyses of Vibrissal Tactile Discrimination in the Rat." *The Journal of Neuroscience: The Official Journal of the Society for Neuroscience* 10 (8): 2638–48.

Chakrabarti, Shubhodeep, and Kevin D. Alloway. 2006. "Differential Origin of Projections from SI Barrel Cortex to the Whisker Representations in SII and MI." *The Journal of Comparative Neurology* 498 (5): 624–36.

Chang, Pei-Ching, Daniel Procissi, Qiyuan Bao, Maria Virginia Centeno, Alex Baria, and A. Vania Apkarian. 2016. "Novel Method for Functional Brain Imaging in Awake Minimally Restrained Rats." *Journal of Neurophysiology* 116 (1): 61–80.

Charitidi, K., and B. Canlon. 2010. "Estrogen Receptors in the Central Auditory System of Male and Female Mice." *Neuroscience* 165 (3): 923–33.

Chen-Bee, C. H., D. B. Polley, B. Brett-Green, N. Prakash, M. C. Kwon, and R. D. Frostig. 2000. "Visualizing and Quantifying Evoked Cortical Activity Assessed with Intrinsic Signal Imaging." *Journal of Neuroscience Methods* 97 (2): 157–73.

Chen-Bee, Cynthia H., Teodora Agoncillo, Christopher C. Lay, and Ron D. Frostig. 2010. "Intrinsic Signal Optical Imaging of Brain Function Using Short Stimulus Delivery Intervals." *Journal of Neuroscience Methods* 187 (2): 171–82.

Chen-Bee, Cynthia H., Teodora Agoncillo, Ying Xiong, and Ron D. Frostig. 2007. "The Triphasic Intrinsic Signal: Implications for Functional Imaging." *The Journal of Neuroscience: The Official Journal of the Society for Neuroscience* 27 (17): 4572–86.

Chen, Li M., Robert M. Friedman, and Anna W. Roe. 2003. "Optical Imaging of a Tactile Illusion in Area 3b of the Primary Somatosensory Cortex." *Science* 302 (5646): 881–85.

Chen, Tsai-Wen, Nuo Li, Kayvon Daie, and Karel Svoboda. 2017. "A Map of Anticipatory

Activity in Mouse Motor Cortex." *Neuron* 94 (4): 866–79.e4.

Chen, Tsai-Wen, Trevor J. Wardill, Yi Sun, Stefan R. Pulver, Sabine L. Renninger, Amy Baohan, Eric R. Schreiter, et al. 2013. "Ultrasensitive Fluorescent Proteins for Imaging Neuronal Activity." *Nature* 499 (7458): 295–300.

Chery, Romain, Barbara L'Heureux, Mounir Bendahmane, Rémi Renaud, Claire Martin, Frédéric Pain, and Hirac Gurden. 2011. "Imaging Odor-Evoked Activities in the Mouse Olfactory Bulb Using Optical Reflectance and Autofluorescence Signals." *Journal of Visualized Experiments: JoVE*, no. 56 (October): e3336.

Choi, Jee Hyun, Klaus Peter Koch, Wigand Poppendieck, Mina Lee, Thomas Doerge, and Hee Sup Shin. 2009. "A Flexible Microelectrode for Mouse EEG." *Conference Proceedings: ... Annual International Conference of the IEEE Engineering in Medicine and Biology Society. IEEE Engineering in Medicine and Biology Society. Conference* 2009: 1600–1603.

Cicirata, F., P. Angaut, M. Cioni, M. F. Serapide, and A. Papale. 1986. "Functional Organization of Thalamic Projections to the Motor Cortex. An Anatomical and Electrophysiological Study in the Rat." *Neuroscience* 19 (1): 81–99.

Colechio, Elizabeth M., and Kevin D. Alloway. 2009. "Differential Topography of the Bilateral Cortical Projections to the Whisker and Forepaw Regions in Rat Motor Cortex." *Brain Structure & Function* 213 (4-5): 423–39.

Crick, F. 1999. "The Impact of Molecular Biology on Neuroscience." *Philosophical Transactions of the Royal Society of London. Series B, Biological Sciences* 354 (1392): 2021–25.

Crochet, Sylvain, and Carl C. H. Petersen. 2006. "Correlating Whisker Behavior with Membrane Potential in Barrel Cortex of Awake Mice." *Nature Neuroscience* 9 (5): 608–10.

Daigle, Tanya L., Linda Madisen, Travis A. Hage, Matthew T. Valley, Ulf Knoblich, Rylan S. Larsen, Marc M. Takeno, et al. 2018. "A Suite of Transgenic Driver and Reporter Mouse Lines with Enhanced Brain-Cell-Type Targeting and Functionality." *Cell* 174 (2): 465–80.e22.

Dana, Hod, Tsai-Wen Chen, Amy Hu, Brenda C. Shields, Caiying Guo, Loren L. Looger, Douglas S. Kim, and Karel Svoboda. 2014. "Thy1-GCaMP6 Transgenic Mice for Neuronal Population Imaging in Vivo." *PloS One* 9 (9): e108697.

Deschênes, Martin, Jun Takatoh, Anastasia Kurnikova, Jeffrey D. Moore, Maxime Demers, Michael Elbaz, Takahiro Furuta, Fan Wang, and David Kleinfeld. 2016. "Inhibition, Not Excitation, Drives Rhythmic Whisking." *Neuron* 90 (2): 374–87.

Diamond, Mathew E., and Ehsan Arabzadeh. 2013. "Whisker Sensory System - from Receptor to Decision." *Progress in Neurobiology* 103 (April): 28–40.

Diamond, Mathew E., Moritz von Heimendahl, Per Magne Knutsen, David Kleinfeld, and Ehud Ahissar. 2008. "'Where' and 'What' in the Whisker Sensorimotor System." *Nature Reviews. Neuroscience* 9 (8): 601–12.

Diamond, M. E., M. Armstrong-James, M. J. Budway, and F. F. Ebner. 1992. "Somatic Sensory Responses in the Rostral Sector of the Posterior Group (POm) and in the Ventral Posterior Medial Nucleus (VPM) of the Rat Thalamus: Dependence on the Barrel Field Cortex." *The Journal of Comparative Neurology* 319 (1): 66–84.

Donoghue, J. P., and S. P. Wise. 1982. "The Motor Cortex of the Rat: Cytoarchitecture and Microstimulation Mapping." *The Journal of Comparative Neurology* 212 (1): 76–88.

Dörfl, J. 1982. "The Musculature of the Mystacial Vibrissae of the White Mouse." *Journal of Anatomy* 135 (Pt 1): 147–54.

Dubova, G. S., A. Ya. Khairullina, and S. F. Shumilina. 1982. "The Recovery of the Absorption Spectra of Oxy- and Deoxyhemoglobin from the Coefficients of Diffuse Transmission and Reflection of Whole Blood." *Journal of Applied Spectroscopy* 36 (1): 66–71.

Eaton, William A., Louise Karle Hanson, P. J. Stephens, J. C. Sutherland, and J. B. R. Dunn. 1978. "Optical Spectra of Oxy- and Deoxyhemoglobin." *Journal of the American Chemical Society* 100 (16): 4991–5003.

Ebbesen, Christian Laut, Guy Doron, Constanze Lenschow, and Michael Brecht. 2017. "Vibrissa Motor Cortex Activity Suppresses Contralateral Whisking Behavior." *Nature Neuroscience* 20 (1): 82–89.

Empson, Ruth M., Chelsea Goulton, David Scholtz, Yasir Gallero-Salas, Hongkui Zeng, and Thomas Knöpfel. 2015. "Validation of Optical Voltage Reporting by the Genetically Encoded Voltage Indicator VSFP-Butterfly from Cortical Layer 2/3 Pyramidal Neurons in Mouse Brain Slices." *Physiological Reports* 3 (7). https://doi.org/10.14814/phy2.12468.

Feldmeyer, Dirk. 2012. "Excitatory Neuronal Connectivity in the Barrel Cortex." *Frontiers in Neuroanatomy* 6 (July): 24.

Feldmeyer, Dirk, Michael Brecht, Fritjof Helmchen, Carl C. H. Petersen, James F. A. Poulet, Jochen F. Staiger, Heiko J. Luhmann, and Cornelius Schwarz. 2013. "Barrel Cortex Function." *Progress in Neurobiology* 103 (April): 3–27.

Ferezou, Isabelle, Florent Haiss, Luc J. Gentet, Rachel Aronoff, Bruno Weber, and Carl C. H. Petersen. 2007. "Spatiotemporal Dynamics of Cortical Sensorimotor Integration in Behaving Mice." *Neuron* 56 (5): 907–23.

Ferrier, D. 1874. "Experiments on the Brain of Monkeys.--No. I." *Proceedings of the Royal Society of London* 23 (156-163): 409–30.

Fritsch, G., and E. Hitzig. 2009. "Electric Excitability of the Cerebrum (Über Die Elektrische Erregbarkeit Des Grosshirns)." *Epilepsy & Behavior: E&B* 15 (2): 123–30.

Frostig, R. D., E. E. Lieke, D. Y. Ts'o, and A. Grinvald. 1990. "Cortical Functional Architecture and Local Coupling between Neuronal Activity and the Microcirculation Revealed by in Vivo High-Resolution Optical Imaging of Intrinsic Signals." *Proceedings of the National Academy of Sciences of the United States of America* 87 (16): 6082–86.

Frostig, Ron, Cynthia Chen-Bee, and Daniel Polley. 2002. "Visualizing Adult Cortical Plasticity Using Intrinsic Signal Optical Imaging." In *Frontiers in Neuroscience*.

Frostig, Ron D. 2009. *In Vivo Optical Imaging of Brain Function, Second Edition*. CRC Press.

Frostig, Ron D., and Cynthia H. Chen-Bee. n.d. "Intrinsic Signal Optical Imaging." In *Handbook of Neural Activity Measurement*, 287–326.

Gao, P., R. Bermejo, and H. P. Zeigler. 2001. "Whisker Deafferentation and Rodent Whisking Patterns: Behavioral Evidence for a Central Pattern Generator." *The Journal of Neuroscience: The Official Journal of the Society for Neuroscience* 21 (14): 5374–80.

Gao, Puhong, Alexis M. Hattox, Lauren M. Jones, Asaf Keller, and H. Philip Zeigler. 2003. "Whisker Motor Cortex Ablation and Whisker Movement Patterns." *Somatosensory & Motor Research* 20 (3-4): 191–98.

Gilad, Ariel, Yasir Gallero-Salas, Dominik Groos, and Fritjof Helmchen. 2018. "Behavioral Strategy Determines Frontal or Posterior Location of Short-Term Memory in Neocortex." *Neuron* 99 (4): 814–28.e7.

Gioanni, Y., and M. Lamarche. 1985. "A Reappraisal of Rat Motor Cortex Organization by Intracortical Microstimulation." *Brain Research* 344 (1): 49–61.

Graziano, Michael S. A., Charlotte S. R. Taylor, and Tirin Moore. 2002. "Complex Movements Evoked by Microstimulation of Precentral Cortex." *Neuron* 34 (5): 841–51.

Grinevich, Valery, Michael Brecht, and Pavel Osten. 2005. "Monosynaptic Pathway from Rat Vibrissa Motor Cortex to Facial Motor Neurons Revealed by Lentivirus-Based Axonal Tracing." *The Journal of Neuroscience: The Official Journal of the Society for Neuroscience* 25 (36): 8250–58.

Grinvald, A., E. Lieke, R. D. Frostig, C. D. Gilbert, and T. N. Wiesel. 1986. "Functional Architecture of Cortex Revealed by Optical Imaging of Intrinsic Signals." *Nature* 324 (6095): 361–64.

Grinvald, Amiram, and Rina Hildesheim. 2004. "VSDI: A New Era in Functional Imaging of Cortical Dynamics." *Nature Reviews. Neuroscience* 5 (11): 874–85.

Grinvald, Amiram, David Omer, Shmuel Naaman, and Dahlia Sharon. 2015. "Imaging the Dynamics of Mammalian Neocortical Population Activity In-Vivo." *Advances in Experimental Medicine and Biology* 859: 243–71.

Grubb, Matthew S., and Ian D. Thompson. 2003. "Quantitative Characterization of Visual Response Properties in the Mouse Dorsal Lateral Geniculate Nucleus." *Journal of*

Neurophysiology 90 (6): 3594–3607.

Guilfoyle, David N., Scott V. Gerum, Jamie L. Sanchez, Andrea Balla, Henry Sershen, Daniel C. Javitt, and Matthew J. Hoptman. 2013. "Functional Connectivity fMRI in Mouse Brain at 7T Using Isoflurane." *Journal of Neuroscience Methods* 214 (2): 144–48.

Guo, Zengcai V., S. Andrew Hires, Nuo Li, Daniel H. O'Connor, Takaki Komiyama, Eran Ophir, Daniel Huber, et al. 2014. "Procedures for Behavioral Experiments in Head-Fixed Mice." *PloS One* 9 (2): e88678.

Guo, Zengcai V., Nuo Li, Daniel Huber, Eran Ophir, Diego Gutnisky, Jonathan T. Ting, Guoping Feng, and Karel Svoboda. 2014. "Flow of Cortical Activity Underlying a Tactile Decision in Mice." *Neuron* 81 (1): 179–94.

Haidarliu, Sebastian, David Golomb, David Kleinfeld, and Ehud Ahissar. 2012. "Dorsorostral Snout Muscles in the Rat Subserve Coordinated Movement for Whisking and Sniffing." *Anatomical Record* 295 (7): 1181–91.

Haidarliu, Sebastian, Erez Simony, David Golomb, and Ehud Ahissar. 2010. "Muscle Architecture in the Mystacial Pad of the Rat." *Anatomical Record* 293 (7): 1192–1206.

Haiss, Florent, and Cornelius Schwarz. 2005. "Spatial Segregation of Different Modes of Movement Control in the Whisker Representation of Rat Primary Motor Cortex." *The Journal of Neuroscience: The Official Journal of the Society for Neuroscience* 25 (6): 1579–87.

Hall, Robert D., and Ernest P. Lindholm. 1974. "Organization of Motor and Somatosensory Neocortex in the Albino Rat." *Brain Research* 66 (1): 23–38.

Han, Yunyun, Justus M. Kebschull, Robert A. A. Campbell, Devon Cowan, Fabia Imhof, Anthony M. Zador, and Thomas D. Mrsic-Flogel. 2018. "The Logic of Single-Cell Projections from Visual Cortex." *Nature* 556 (7699): 51–56.

Harris, Anjanette P., Ross J. Lennen, Ian Marshall, Maurits A. Jansen, Cyril R. Pernet, Nichola M. Brydges, Ian C. Duguid, and Megan C. Holmes. 2015. "Imaging Learned Fear Circuitry in Awake Mice Using fMRI." *The European Journal of Neuroscience* 42 (5): 2125–34.

Harris, Julie A., Karla E. Hirokawa, Staci A. Sorensen, Hong Gu, Maya Mills, Lydia L. Ng, Phillip Bohn, et al. 2014. "Anatomical Characterization of Cre Driver Mice for Neural Circuit Mapping and Manipulation." *Frontiers in Neural Circuits* 8 (July): 76.

Harrison, Thomas C., Oliver G. S. Ayling, and Timothy H. Murphy. 2012. "Distinct Cortical Circuit Mechanisms for Complex Forelimb Movement and Motor Map Topography." *Neuron* 74 (2): 397–409.

Hasegawa, Masashi, Kei Majima, Takahide Itokazu, Takakuni Maki, Urban-Raphael Albrecht, Nora Castner, Mariko Izumo, et al. 2017. "Selective Suppression of Local Circuits during Movement Preparation in the Mouse Motor Cortex." *Cell Reports* 18 (11): 2676–86.

Hattox, Alexis M., Catherine A. Priest, and Asaf Keller. 2002. "Functional Circuitry Involved in the Regulation of Whisker Movements." *The Journal of Comparative Neurology* 442 (3): 266–76.

Helmchen, Fritjof, and Winfried Denk. 2005. "Deep Tissue Two-Photon Microscopy." *Nature Methods* 2 (12): 932–40.

Helmchen, Fritjof, Ariel Gilad, and Jerry L. Chen. 2018. "Neocortical Dynamics during Whisker-Based Sensory Discrimination in Head-Restrained Mice." *Neuroscience* 368 (January): 57–69.

Herculano-Houzel, Suzana. 2009. "The Human Brain in Numbers: A Linearly Scaled-up Primate Brain." *Frontiers in Human Neuroscience* 3. https://doi.org/10.3389/neuro.09.031.2009.

Hickok, Gregory, John Houde, and Feng Rong. 2011. "Sensorimotor Integration in Speech Processing: Computational Basis and Neural Organization." *Neuron* 69 (3): 407–22.

Hill, D. N., R. Bermejo, H. P. Zeigler, and D. Kleinfeld. 2008. "Biomechanics of the Vibrissa Motor Plant in Rat: Rhythmic Whisking Consists of Triphasic Neuromuscular Activity." *Journal of Neuroscience* 28 (13): 3438–55.

Hira, Riichiro, Naoki Honkura, Jun Noguchi, Yoshio Maruyama, George J. Augustine, Haruo Kasai, and Masanori Matsuzaki. 2009. "Transcranial Optogenetic Stimulation for Functional Mapping of the Motor Cortex." *Journal of Neuroscience Methods* 179 (2): 258–63.

Hira, Riichiro, Fuki Ohkubo, Yasuhiro R. Tanaka, Yoshito Masamizu, George J. Augustine, Haruo Kasai, and Masanori Matsuzaki. 2013. "In Vivo Optogenetic Tracing of Functional Corticocortical Connections between Motor Forelimb Areas." *Frontiers in Neural Circuits* 7 (April): 55.

Hochbaum, Daniel R., Yongxin Zhao, Samouil L. Farhi, Nathan Klapoetke, Christopher A. Werley, Vikrant Kapoor, Peng Zou, et al. 2014. "All-Optical Electrophysiology in Mammalian Neurons Using Engineered Microbial Rhodopsins." *Nature Methods* 11 (8): 825–33.

Hooks, Bryan M., Tianyi Mao, Diego A. Gutnisky, Naoki Yamawaki, Karel Svoboda, and Gordon M. G. Shepherd. 2013. "Organization of Cortical and Thalamic Input to Pyramidal Neurons in Mouse Motor Cortex." *The Journal of Neuroscience: The Official Journal of the Society for Neuroscience* 33 (2): 748–60.

Hutson, K. A., and R. B. Masterton. 1986. "The Sensory Contribution of a Single Vibrissa's Cortical Barrel." *Journal of Neurophysiology* 56 (4): 1196–1223.

Huttunen, Annamarie W., Geoffrey K. Adams, and Michael L. Platt. 2017. "Can Self-Awareness Be Taught? Monkeys Pass the Mirror Test-Again." *Proceedings of the National Academy of Sciences of the United States of America* 114 (13): 3281–83.

Issa, Naoum, and T. Robert Husson. 2009. "Functional Imaging with Mitochondrial Flavoprotein Autofluorescence." In *Frontiers in Neuroscience*, 221–53.

Jöbsis, F. F. 1977. "Noninvasive, Infrared Monitoring of Cerebral and Myocardial Oxygen Sufficiency and Circulatory Parameters." *Science* 198 (4323): 1264–67.

Jonckers, Elisabeth, Disha Shah, Julie Hamaide, Marleen Verhoye, and Annemie Van der Linden. 2015. "The Power of Using Functional fMRI on Small Rodents to Study Brain Pharmacology and Disease." *Frontiers in Pharmacology* 6 (October): 231.

Juavinett, Ashley L., Ian Nauhaus, Marina E. Garrett, Jun Zhuang, and Edward M. Callaway. 2017. "Automated Identification of Mouse Visual Areas with Intrinsic Signal Imaging." *Nature Protocols* 12 (1): 32–43.

Kaas, J. H. 2015. "Somatosensory Cortex." In *Brain Mapping*, 283–86.

Kalatsky, Valery A., Daniel B. Polley, Michael M. Merzenich, Christoph E. Schreiner, and Michael P. Stryker. 2005. "Fine Functional Organization of Auditory Cortex Revealed by Fourier Optical Imaging." *Proceedings of the National Academy of Sciences of the United States of America* 102 (37): 13325–30.

Kleinfeld, David, Ehud Ahissar, and Mathew E. Diamond. 2006. "Active Sensation: Insights from the Rodent Vibrissa Sensorimotor System." *Current Opinion in Neurobiology* 16 (4): 435–44.

Kleinfeld, David, and Martin Deschênes. 2011. "Neuronal Basis for Object Location in the Vibrissa Scanning Sensorimotor System." *Neuron* 72 (3): 455–68.

Kohn, A., C. Metz, M. Quibrera, M. A. Tommerdahl, and B. L. Whitsel. 2000. "Functional Neocortical Microcircuitry Demonstrated with Intrinsic Signal Optical Imaging in Vitro." *Neuroscience* 95 (1): 51–62.

Komiyama, Takaki, Takashi R. Sato, Daniel H. O'Connor, Ying-Xin Zhang, Daniel Huber, Bryan M. Hooks, Mariano Gabitto, and Karel Svoboda. 2010. "Learning-Related Fine-Scale Specificity Imaged in Motor Cortex Circuits of Behaving Mice." *Nature* 464 (7292): 1182–86.

Kramer, K., S. A. van Acker, H. P. Voss, J. A. Grimbergen, W. J. van der Vijgh, and A. Bast. 1993. "Use of Telemetry to Record Electrocardiogram and Heart Rate in Freely Moving Mice." *Journal of Pharmacological and Toxicological Methods* 30 (4): 209–15.

Krupa, D. J., M. S. Matell, A. J. Brisben, L. M. Oliveira, and M. A. Nicolelis. 2001. "Behavioral Properties of the Trigeminal Somatosensory System in Rats Performing Whisker-Dependent Tactile Discriminations." *The Journal of Neuroscience: The Official Journal of the Society for Neuroscience* 21 (15): 5752–63.

Kyriakatos, Alexandros, Vijay Sadashivaiah, Yifei Zhang, Alessandro Motta, Matthieu Auffret, and Carl C. H. Petersen. 2017. "Voltage-Sensitive Dye Imaging of Mouse Neocortex during a Whisker Detection Task." *Neurophotonics* 4 (3): 031204.

Lee, Mina, Dongwook Kim, Hee-Sup Shin, Ho-Geun Sung, and Jee Hyun Choi. 2011. "High-Density EEG Recordings of the Freely Moving Mice Using Polyimide-Based Microelectrode." *Journal of Visualized Experiments: JoVE*, no. 47 (January). https://doi.org/10.3791/2562.

Lee, Mina, Hee-Sup Shin, and Jee Hyun Choi. 2009. "Simultaneous Recording of Brain Activity and Functional Connectivity in the Mouse Brain." *Conference Proceedings: ... Annual International Conference of the IEEE Engineering in Medicine and Biology Society. IEEE Engineering in Medicine and Biology Society. Conference* 2009: 2934–36.

Lefort, Sandrine, Christian Tomm, J-C Floyd Sarria, and Carl C. H. Petersen. 2009. "The Excitatory Neuronal Network of the C2 Barrel Column in Mouse Primary Somatosensory Cortex." *Neuron* 61 (2): 301–16.

Le Merre, Pierre, Vahid Esmaeili, Eloïse Charrière, Katia Galan, Paul-A Salin, Carl C. H. Petersen, and Sylvain Crochet. 2018. "Reward-Based Learning Drives Rapid Sensory Signals in Medial Prefrontal Cortex and Dorsal Hippocampus Necessary for Goal-Directed Behavior." *Neuron* 97 (1): 83–91.e5.

Lima, Susana Q., and Gero Miesenböck. 2005. "Remote Control of Behavior through Genetically Targeted Photostimulation of Neurons." *Cell* 121 (1): 141–52.

Lim, Diana H., Jeffrey Ledue, Majid H. Mohajerani, Matthieu P. Vanni, and Timothy H. Murphy. 2013. "Optogenetic Approaches for Functional Mouse Brain Mapping." *Frontiers in Neuroscience* 7 (April): 54.

Lin, X. B., D. R. Pierce, K. E. Light, and A. Hayar. 2013. "The Fine Temporal Structure of the Rat Licking Pattern: What Causes the Variabiliy in the Interlick Intervals and How Is It Affected by the Drinking Solution?" *Chemical Senses* 38 (8): 685–704.

Lodato, Simona, and Paola Arlotta. 2015. "Generating Neuronal Diversity in the Mammalian Cerebral Cortex." *Annual Review of Cell and Developmental Biology* 31 (September): 699–720.

Lütcke, Henry, Felipe Gerhard, Friedemann Zenke, Wulfram Gerstner, and Fritjof Helmchen. 2013. "Inference of Neuronal Network Spike Dynamics and Topology from Calcium Imaging Data." *Frontiers in Neural Circuits* 7. https://doi.org/10.3389/fncir.2013.00201.

Madisen, Linda, Aleena R. Garner, Daisuke Shimaoka, Amy S. Chuong, Nathan C. Klapoetke, Lu Li, Alexander van der Bourg, et al. 2015. "Transgenic Mice for Intersectional Targeting of Neural Sensors and Effectors with High Specificity and Performance." *Neuron* 85 (5): 942–58.

Makino, Hiroshi, Chi Ren, Haixin Liu, An Na Kim, Neehar Kondapaneni, Xin Liu, Duygu Kuzum, and Takaki Komiyama. 2017. "Transformation of Cortex-Wide Emergent Properties during Motor Learning." *Neuron* 94 (4): 880–90.e8.

Malonek, D., and A. Grinvald. 1996. "Interactions between Electrical Activity and Cortical Microcirculation Revealed by Imaging Spectroscopy: Implications for Functional Brain Mapping." *Science* 272 (5261): 551–54.

Mao, Tianyi, Deniz Kusefoglu, Bryan M. Hooks, Daniel Huber, Leopoldo Petreanu, and Karel Svoboda. 2011. "Long-Range Neuronal Circuits Underlying the Interaction between Sensory and Motor Cortex." *Neuron* 72 (1): 111–23.

Masino, S. A., M. C. Kwon, Y. Dory, and R. D. Frostig. 1993. "Characterization of Functional Organization within Rat Barrel Cortex Using Intrinsic Signal Optical Imaging through a Thinned Skull." *Proceedings of the National Academy of Sciences of the United States of America* 90 (21): 9998–10002.

Matyas, Ferenc, Varun Sreenivasan, Fred Marbach, Catherine Wacongne, Boglarka Barsy, Celine Mateo, Rachel Aronoff, and Carl C. H. Petersen. 2010. "Motor Control by Sensory Cortex." *Science* 330 (6008): 1240–43.

Ma, Ying, Mohammed A. Shaik, Sharon H. Kim, Mariel G. Kozberg, David N. Thibodeaux, Hanzhi T. Zhao, Hang Yu, and Elizabeth M. C. Hillman. 2016. "Wide-Field Optical

Mapping of Neural Activity and Brain Haemodynamics: Considerations and Novel Approaches." *Philosophical Transactions of the Royal Society of London. Series B, Biological Sciences* 371 (1705). https://doi.org/10.1098/rstb.2015.0360.

Minderer, Matthias, Wenrui Liu, Lazar T. Sumanovski, Sebastian Kügler, Fritjof Helmchen, and David J. Margolis. 2012. "Chronic Imaging of Cortical Sensory Map Dynamics Using a Genetically Encoded Calcium Indicator." *The Journal of Physiology* 590 (1): 99–107.

Miyashita, E., A. Keller, and H. Asanuma. 1994. "Input-Output Organization of the Rat Vibrissal Motor Cortex." *Experimental Brain Research. Experimentelle Hirnforschung. Experimentation Cerebrale* 99 (2): 223–32.

Mohajerani, Majid H., Allen W. Chan, Mostafa Mohsenvand, Jeffrey LeDue, Rui Liu, David A. McVea, Jamie D. Boyd, Yu Tian Wang, Mark Reimers, and Timothy H. Murphy. 2013. "Spontaneous Cortical Activity Alternates between Motifs Defined by Regional Axonal Projections." *Nature Neuroscience* 16 (10): 1426–35.

Moore, Jeffrey D., Martin Deschênes, Takahiro Furuta, Daniel Huber, Matthew C. Smear, Maxime Demers, and David Kleinfeld. 2013. "Hierarchy of Orofacial Rhythms Revealed through Whisking and Breathing." *Nature* 497 (7448): 205–10.

Morone, Katherine A., Joseph S. Neimat, Anna W. Roe, and Robert M. Friedman. 2017. "Review of Functional and Clinical Relevance of Intrinsic Signal Optical Imaging in Human Brain Mapping." *Neurophotonics* 4 (3): 031220.

Nagel, Georg, Tanjef Szellas, Wolfram Huhn, Suneel Kateriya, Nona Adeishvili, Peter Berthold, Doris Ollig, Peter Hegemann, and Ernst Bamberg. 2003. "Channelrhodopsin-2, a Directly Light-Gated Cation-Selective Membrane Channel." *Proceedings of the National Academy of Sciences of the United States of America* 100 (24): 13940–45.

Nakai, J., M. Ohkura, and K. Imoto. 2001. "A High Signal-to-Noise Ca(2+) Probe Composed of a Single Green Fluorescent Protein." *Nature Biotechnology* 19 (2): 137–41.

Neafsey, E. J., E. L. Bold, G. Haas, K. M. Hurley-Gius, G. Quirk, C. F. Sievert, and R. R. Terreberry. 1986. "The Organization of the Rat Motor Cortex: A Microstimulation Mapping Study." *Brain Research* 396 (1): 77–96.

Niranjan, Arun, Isabel N. Christie, Samuel G. Solomon, Jack A. Wells, and Mark F. Lythgoe. 2016. "fMRI Mapping of the Visual System in the Mouse Brain with Interleaved Snapshot GE-EPI." *NeuroImage* 139 (October): 337–45.

Noback, Charles R., Norman L. Strominger, Robert J. Demarest, and David A. Ruggiero. 2005. *The Human Nervous System: Structure and Function*. Springer Science & Business Media.

O'Connor, Daniel H., Nathan G. Clack, Daniel Huber, Takaki Komiyama, Eugene W. Myers, and Karel Svoboda. 2010. "Vibrissa-Based Object Localization in Head-Fixed Mice." *The Journal of Neuroscience: The Official Journal of the Society for Neuroscience* 30 (5): 1947–67.

O'Connor, Daniel H., S. Andrew Hires, Zengcai V. Guo, Nuo Li, Jianing Yu, Qian-Quan Sun, Daniel Huber, and Karel Svoboda. 2013. "Neural Coding during Active Somatosensation Revealed Using Illusory Touch." *Nature Neuroscience* 16 (7): 958–65.

O'Connor, Daniel H., Simon P. Peron, Daniel Huber, and Karel Svoboda. 2010. "Neural Activity in Barrel Cortex Underlying Vibrissa-Based Object Localization in Mice." *Neuron* 67 (6): 1048–61.

Otchy, Timothy M., Steffen B. E. Wolff, Juliana Y. Rhee, Cengiz Pehlevan, Risa Kawai, Alexandre Kempf, Sharon M. H. Gobes, and Bence P. Ölveczky. 2015. "Acute off-Target Effects of Neural Circuit Manipulations." *Nature* 528 (7582): 358–63.

Paxinos, George. 2014. *The Rat Nervous System*. Academic Press.

Paxinos, George, and Keith B. J. Franklin. 2004. *The Mouse Brain in Stereotaxic Coordinates*. Gulf Professional Publishing.

Penfield, Wilder, and Edwin Boldrey. 1937. "SOMATIC MOTOR AND SENSORY REPRESENTATION IN THE CEREBRAL CORTEX OF MAN AS STUDIED BY ELECTRICAL STIMULATION." *Brain: A Journal of Neurology* 60 (4): 389–443.

Petersen, Carl C. H. 2007. "The Functional Organization of the Barrel Cortex." *Neuron* 56 (2): 339–55.

———. 2014. "Cortical Control of Whisker Movement." *Annual Review of Neuroscience* 37 (May): 183–203.

Petersen, Carl C. H., and Sylvain Crochet. 2013. "Synaptic Computation and Sensory Processing in Neocortical Layer 2/3." *Neuron* 78 (1): 28–48.

Petreanu, Leopoldo, Diego A. Gutnisky, Daniel Huber, Ning-Long Xu, Dan H. O'Connor, Lin Tian, Loren Looger, and Karel Svoboda. 2012. "Activity in Motor-Sensory Projections Reveals Distributed Coding in Somatosensation." *Nature* 489 (7415): 299–303.

Polley, D. B., C. H. Chen-Bee, and R. D. Frostig. 1999. "Varying the Degree of Single-Whisker Stimulation Differentially Affects Phases of Intrinsic Signals in Rat Barrel Cortex." *Journal of Neurophysiology* 81 (2): 692–701.

Pouratian, Nader, and Arthur W. Toga. 2002. "Optical Imaging Based on Intrinsic Signals." In *Brain Mapping: The Methods*, 97–140.

Prakash, Neal, Falk Uhlemann, Sameer A. Sheth, Susan Bookheimer, Neil Martin, and Arthur W. Toga. 2009. "Current Trends in Intraoperative Optical Imaging for Functional Brain Mapping and Delineation of Lesions of Language Cortex." *NeuroImage* 47 Suppl 2 (August): T116–26.

Priebe, Nicholas J., and David Ferster. 2008. "Inhibition, Spike Threshold, and Stimulus Selectivity in Primary Visual Cortex." *Neuron* 57 (4): 482–97.

Ragan, Timothy, Lolahon R. Kadiri, Kannan Umadevi Venkataraju, Karsten Bahlmann, Jason Sutin, Julian Taranda, Ignacio Arganda-Carreras, Yongsoo Kim, H. Sebastian Seung, and Pavel Osten. 2012. "Serial Two-Photon Tomography for Automated Ex Vivo Mouse Brain Imaging." *Nature Methods* 9 (3): 255–58.

Rakic, Pasko. 2009. "Evolution of the Neocortex: A Perspective from Developmental Biology." *Nature Reviews. Neuroscience* 10 (10): 724–35.

Ratzlaff, E. H., and A. Grinvald. 1991. "A Tandem-Lens Epifluorescence Macroscope: Hundred-Fold Brightness Advantage for Wide-Field Imaging." *Journal of Neuroscience Methods* 36 (2-3): 127–37.

Roe, Anna W. 2009. *Imaging the Brain with Optical Methods*. Springer Science & Business Media.

Rubin, B. D., and L. C. Katz. 1999. "Optical Imaging of Odorant Representations in the Mammalian Olfactory Bulb." *Neuron* 23 (3): 499–511.

Sachidhanandam, Shankar, Varun Sreenivasan, Alexandros Kyriakatos, Yves Kremer, and Carl C. H. Petersen. 2013. "Membrane Potential Correlates of Sensory Perception in Mouse Barrel Cortex." *Nature Neuroscience* 16 (11): 1671–77.

Sasamoto, K., G. Zhang, and M. Iwasaki. 1990. "Two Types of Rhythmical Jaw Movements Evoked by Stimulation of the Rat Cortex." *Shika Kiso Igakkai Zasshi = Japanese Journal of Oral Biology* 32 (1): 57–68.

Sato, Takashi R., and Karel Svoboda. 2010. "The Functional Properties of Barrel Cortex Neurons Projecting to the Primary Motor Cortex." *The Journal of Neuroscience: The Official Journal of the Society for Neuroscience* 30 (12): 4256–60.

Schuett, Sven, Tobias Bonhoeffer, and Mark Hübener. 2002. "Mapping Retinotopic Structure in Mouse Visual Cortex with Optical Imaging." *The Journal of Neuroscience: The Official Journal of the Society for Neuroscience* 22 (15): 6549–59.

Seidemann, Eyal, Yuzhi Chen, Yoon Bai, Spencer C. Chen, Preeti Mehta, Bridget L. Kajs, Wilson S. Geisler, and Boris V. Zemelman. 2016. "Calcium Imaging with Genetically Encoded Indicators in Behaving Primates." *eLife* 5 (July). https://doi.org/10.7554/eLife.16178.

Sherrington, Charles Scott. 1906. *The Integrative Action of the Nervous Systems*.

Simons, D. J., and G. E. Carvell. 1989. "Thalamocortical Response Transformation in the Rat Vibrissa/barrel System." *Journal of Neurophysiology* 61 (2): 311–30.

Smith, Jared B., and Kevin D. Alloway. 2013. "Rat Whisker Motor Cortex Is Subdivided into Sensory-Input and Motor-Output Areas." *Frontiers in Neural Circuits* 7 (January): 4.

Späni, D., M. Arras, B. König, and T. Rülicke. 2003. "Higher Heart Rate of Laboratory Mice Housed Individually vs in Pairs." *Laboratory Animals* 37 (1): 54–62.

Sprague, James M. 1996. "Chapter 1 Neural Mechanisms of Visual Orienting Responses." In

Progress in Brain Research, 1–15.

Sreenivasan, Varun, Vahid Esmaeili, Taro Kiritani, Katia Galan, Sylvain Crochet, and Carl C. H. Petersen. 2016. "Movement Initiation Signals in Mouse Whisker Motor Cortex." *Neuron* 92 (6): 1368–82.

Sreenivasan, Varun, Kajari Karmakar, Filippo M. Rijli, and Carl C. H. Petersen. 2015. "Parallel Pathways from Motor and Somatosensory Cortex for Controlling Whisker Movements in Mice." *The European Journal of Neuroscience* 41 (3): 354–67.

Stevens, F. C. 1983. "Calmodulin: An Introduction." *Canadian Journal of Biochemistry and Cell Biology = Revue Canadienne de Biochimie et Biologie Cellulaire* 61 (8): 906–10.

Stüttgen, Maik C., and Cornelius Schwarz. 2008. "Psychophysical and Neurometric Detection Performance under Stimulus Uncertainty." *Nature Neuroscience* 11 (9): 1091–99.

Svoboda, Karel, and Nuo Li. 2018. "Neural Mechanisms of Movement Planning: Motor Cortex and beyond." *Current Opinion in Neurobiology* 49 (April): 33–41.

Svoboda, Karel, and Ryohei Yasuda. 2006. "Principles of Two-Photon Excitation Microscopy and Its Applications to Neuroscience." *Neuron* 50 (6): 823–39.

Takahashi, Manami, Takuya Urushihata, Hiroyuki Takuwa, Kazumi Sakata, Yuhei Takado, Eiji Shimizu, Tetsuya Suhara, Makoto Higuchi, and Hiroshi Ito. 2017. "Imaging of Neuronal Activity in Awake Mice by Measurements of Flavoprotein Autofluorescence Corrected for Cerebral Blood Flow." *Frontiers in Neuroscience* 11: 723.

Takahashi, Naoya, Thomas G. Oertner, Peter Hegemann, and Matthew E. Larkum. 2016. "Active Cortical Dendrites Modulate Perception." *Science* 354 (6319): 1587–90.

Takatoh, Jun, Anders Nelson, Xiang Zhou, M. Mclean Bolton, Michael D. Ehlers, Benjamin R. Arenkiel, Richard Mooney, and Fan Wang. 2013. "New Modules Are Added to Vibrissal Premotor Circuitry with the Emergence of Exploratory Whisking." *Neuron* 77 (2): 346–60.

Tamamaki, Nobuaki, Yuchio Yanagawa, Ryohei Tomioka, Jun-Ichi Miyazaki, Kunihiko Obata, and Takeshi Kaneko. 2003. "Green Fluorescent Protein Expression and Colocalization with Calretinin, Parvalbumin, and Somatostatin in the GAD67-GFP Knock-in Mouse." *The Journal of Comparative Neurology* 467 (1): 60–79.

Toda, Koji, and Michael L. Platt. 2015. "Animal Cognition: Monkeys Pass the Mirror Test." *Current Biology: CB* 25 (2): R64–66.

Ts'o, D. Y., R. D. Frostig, E. E. Lieke, and A. Grinvald. 1990. "Functional Organization of Primate Visual Cortex Revealed by High Resolution Optical Imaging." *Science* 249 (4967): 417–20.

Tsytsarev, Vassiliy, and Shigeru Tanaka. 2002. "Intrinsic Optical Signals from Rat Primary Auditory Cortex in Response to Sound Stimuli Presented to Contralateral, Ipsilateral and Bilateral Ears." *Neuroreport* 13 (13): 1661–66.

Urbain, Nadia, and Martin Deschênes. 2007. "Motor Cortex Gates Vibrissal Responses in a Thalamocortical Projection Pathway." *Neuron* 56 (4): 714–25.

Vanni, Matthieu P., and Timothy H. Murphy. 2014. "Mesoscale Transcranial Spontaneous Activity Mapping in GCaMP3 Transgenic Mice Reveals Extensive Reciprocal Connections between Areas of Somatomotor Cortex." *The Journal of Neuroscience: The Official Journal of the Society for Neuroscience* 34 (48): 15931–46.

Veinante, P., and M. Deschênes. 1999. "Single- and Multi-Whisker Channels in the Ascending Projections from the Principal Trigeminal Nucleus in the Rat." *The Journal of Neuroscience: The Official Journal of the Society for Neuroscience* 19 (12): 5085–95.

Vincis, Roberto, Samuel Lagier, Dimitri Van De Ville, Ivan Rodriguez, and Alan Carleton. 2015. "Sensory-Evoked Intrinsic Imaging Signals in the Olfactory Bulb Are Independent of Neurovascular Coupling." *Cell Reports* 12 (2): 313–25.

Wang, Quanxin, and Andreas Burkhalter. 2007. "Area Map of Mouse Visual Cortex." *The Journal of Comparative Neurology* 502 (3): 339–57.

Weber, Bruno, and L. Felipe Barros. 2015. "The Astrocyte: Powerhouse and Recycling Center." *Cold Spring Harbor Perspectives in Biology* 7 (12). https://doi.org/10.1101/cshperspect.a020396.

Welker, C. 1971. "Microelectrode Delineation of Fine Grain Somatotopic Organization of (SmI) Cerebral Neocortex in Albino Rat." *Brain Research* 26 (2): 259–75.

Welker, W. I. 1964. "Analysis of Sniffing of the Albino Rat 1)." *Behaviour* 22 (3): 223–44.

Woolsey, T. A., and H. Van der Loos. 1970. "The Structural Organization of Layer IV in the Somatosensory Region (SI) of Mouse Cerebral Cortex. The Description of a Cortical Field Composed of Discrete Cytoarchitectonic Units." *Brain Research* 17 (2): 205–42.

Xie, Yicheng, Allen W. Chan, Alexander McGirr, Songchao Xue, Dongsheng Xiao, Hongkui Zeng, and Timothy H. Murphy. 2016. "Resolution of High-Frequency Mesoscale Intracortical Maps Using the Genetically Encoded Glutamate Sensor iGluSnFR." *The Journal of Neuroscience: The Official Journal of the Society for Neuroscience* 36 (4): 1261–72.

Yamashita, Takayuki, and Carl Ch Petersen. 2016. "Target-Specific Membrane Potential Dynamics of Neocortical Projection Neurons during Goal-Directed Behavior." *eLife* 5 (June). https://doi.org/10.7554/eLife.15798.

Yeomans, John S., Liang Li, Brian W. Scott, and Paul W. Frankland. 2002. "Tactile, Acoustic and Vestibular Systems Sum to Elicit the Startle Reflex." *Neuroscience and Biobehavioral Reviews* 26 (1): 1–11.

Yoshida, Keitaro, Yu Mimura, Ryosuke Ishihara, Hiroshi Nishida, Yuji Komaki, Tomohito Minakuchi, Tomokazu Tsurugizawa, et al. 2016. "Physiological Effects of a Habituation Procedure for Functional MRI in Awake Mice Using a Cryogenic Radiofrequency Probe." *Journal of Neuroscience Methods* 274 (December): 38–48.

Young, Nicole, Iwona Stepniewska, and Jon Kaas. 2012. "Motor Cortex." In *The Mouse Nervous System*, 528–38.

Zemelman, Boris V., Georgia A. Lee, Minna Ng, and Gero Miesenböck. 2002. "Selective Photostimulation of Genetically chARGed Neurons." *Neuron* 33 (1): 15–22.

Zhao, Xinyu, Mingna Liu, and Jianhua Cang. 2014. "Visual Cortex Modulates the Magnitude but Not the Selectivity of Looming-Evoked Responses in the Superior Colliculus of Awake Mice." *Neuron* 84 (1): 202–13.

Zhuang, Jun, Lydia Ng, Derric Williams, Matthew Valley, Yang Li, Marina Garrett, and Jack Waters. 2017. "An Extended Retinotopic Map of Mouse Cortex." *eLife* 6 (January). https://doi.org/10.7554/eLife.18372.

Zucker, E., and W. I. Welker. 1969. "Coding of Somatic Sensory Input by Vibrissae Neurons in the Rat's Trigeminal Ganglion." *Brain Research* 12 (1): 138–56.

Curriculum Vitae

Matthieu AUFFRET

Chemin des Perrettes 1
1024 Ecublens

+41 76 740 67 67

matthieu.auffret@gmail.com

linkedin.com/in/auffret-matthieu-91b124b5

PROGRAMMING SKILLS

JAVA	●●●○○
PYTHON	●●●○○
GIT	●●●○○
MATLAB	●●●●●
C++	●●●●○
CSS HTML	●●●●○

MANAGEMENT SKILLS

MENTORING AND TEACHING
PROJECTS SUPERVISION
ROADMAP DEFINITION
TEAM COORDINATION
PROJECTS REVIEW
SCIENTIFIC PUBLICATIONS

BIOLOGY

BENCH WORK
ANIMAL EXPERIMENTATION
SAMPLE AND MOUSE MANAGE-
MENT WITH SLIMS
DATA ACQUISITION SOFTWARE
DEVELOPMENT
IMAGE PROCESSING

LANGUAGES

FRENCH	●●●●●
ENGLISH	●●●●○
GERMAN	●●●○○

INTERESTS

EDUCATION

2013 - 2018 ● PhD in Neurosciences
EPFL - École Polytechnique Fédérale de Lausanne

PhD project: "Optical sensory and motor mapping of mouse dorsal cortex"

2011-2013 ● Master in Bioengineering
EPFL / Harvard University – MGH/HST Martinos Center for Biomedical Imaging

Master project: "Detection of free radicals with a very low field open access MRI scanner"

2008-2011 ● Bachelor in Life Sciences and Technology | SV
EPFL - École Polytechnique Fédérale de Lausanne

EXPERIENCES

2018 ● Federal program for startup founders
Innosuisse Start-up Training: Business Concept

Content: Market analysis & value proposition, IP technology transfer, Financing, Product market fit, Presentation skill

2012
2 months ● Carl Zeiss – Munich

Objective: to develop a protocol for combining confocal-microscopy and electro-macroscopy, and to show the performance and possibilities of the microscopes designed by Carl Zeiss to different potential customers

2011
1 month ● Centre d'Imagerie BioMédicale – CIBM, EPFL

Objective: to generate MRI brain images from ex-vivo rat brain to create a high spatial resolution brain atlas for a collaboration with the Blue Brain Project

2010
1 month ● Institut Suisse de Recherche Expérimentale sur le Cancer – ISREC, EPFL

Objective: to evaluate gene expression of the signaling pathway of planar cell polarity in the pancreas of mice

Papers

Auffret M, Samim I, Lepore M, Gruetter R, Just N. 2016. "Quantitative activity-induced manganese-dependent MRI for characterizing cortical layers in the primary somatosensory cortex of the rat." Brain Struct Funct. 221(2):695-707. doi: 10.1007/s00429-014-0933-3.

Kyriakatos A, Sadashivaiah V, Zhang Y, Motta A, Auffret M, Petersen CC. 2016. "Voltage-sensitive dye imaging of mouse neocortex during a whisker detection task." Neurophotonics. 4(3):031204.

Auffret M, Ravano VL, Rossi GMC, Hankov N, Petersen MFA, Petersen CCH. 2018. "Optogenetic stimulation of cortex to map evoked whisker movements in awake head-restrained mice." Neuroscience. 368:199-213. doi: 10.1016/j.neuroscience.2017.04.004.

Conferences

Auffret M, Petersen CCH, Ipek O, Gruetter R, Just N. 2014. "Physiology and sensitivity of BOLD fMRI in mice." Poster 3 at National Competence Center for Biomedical Imaging (NCCBI) Annual Meeting.

Auffret M, Kyriakatos A, Just N, Gruetter R, Petersen CCH. 2015. "Functional mapping of mouse cortex." Poster 8 at National Competence Center for Biomedical Imaging (NCCBI) Annual Meeting.

Auffret M, Esmaeili V, Petersen CCH. 2016. "Multimodal detection task during wide-field calcium imaging of mouse neocortex." Poster 92 at Lemanic Neuroscience Annual Meeting (LNAM).

Auffret M, El Boustani S, Mayrhofer JM, Daigle T, Zeng H, Petersen CCH. 2017. "Optical mapping of large-scale cortical sensorimotor activity in awake head-restrained mice." Poster 680.04/DD18 at Society for Neurosciences (SfN).